The Effects of Transgressions and Regressions on Coastal and Offshore Groundwater

A case study of Suriname and generic studies into groundwater flow systems, salinity patterns and paleogroundwater.

Koos Groen

2002

Vrije Universiteit

Photograph front cover: Corryenne and Joshua, children of the author, playing at the beach in Katwijk, The Netherlands.

This study is carried out at the Faculty of Earth- and Life Sciences of the Vrije Universiteit Amsterdam. Part of the study is a contribution to the NEESDI program, funded by the Netherlands Organisation for Scientific Research (NWO)

The full text of this thesis is available at: http://www.geo.vu.nl/grok/

Groen, Jacobus

The effects of transgressions and regressions on coastal and offshore groundwater. A case study of Suriname and generic studies into groundwater flow systems, salinity patterns and paleogroundwater. - Doctoral Thesis Vrije Universiteit Amsterdam – With ref. – With summary in Dutch

ISBN 90-9016211-9

Subject headings: hydrology, groundwater / coastal plain / regression / transgression / paleogroundwater / solute transport / hydrogeochemistry / isotope hydrology / groundwater salinity / submarine groundwater / Suriname / South America.

Printed by: PrintPartners Ipskamp, Enschede, The Netherlands

VRIJE UNIVERSITEIT

The Effects of Transgressions and Regressions on Coastal and Offshore Groundwater

A case study of Suriname and generic studies of groundwater flow systems, salinity patterns and paleogroundwater

ACADEMISCH PROEFSCHRIFT

ter verkrijging van de graad van doctor aan
de Vrije Universiteit Amsterdam,
op gezag van de rector magnificus
prof.dr T. Sminia,
in het openbaar te verdedigen
ten overstaan van de promotiecommissie
van de faculteit der Aard- en Levenswetenschappen
op dinsdag 8 oktober 2002 om 15.45 uur
in de aula van de universiteit,
De Boelelaan 1105

door

Jacobus Groen

geboren te Katwijk aan Zee

promotor: prof.dr. J.J. de Vries
copromotor: dr. H. Kooi

Soli Deo Gloria

Contents

Voorwoord

Waarom en hoe is dit proefschrift tot stand gekomen? Een goed antwoord zou een ware biografie vereisen, omdat dit werk het resultaat is van een lange keten van gebeurtenissen en ontmoetingen, ver teruggaand in de tijd: hier en daar wat bewuste keuzes, wat overtuigingskracht van anderen, maar vooral toevallige mogelijkheden en onmogelijkheden. Dit maakt dat ik nu in vrolijke verwondering en dankbaarheid omzie. Ik wil daarom beginnen om mijn ouders, Corrie en Huig Groen, te bedanken voor hun aanhoudende steun. In mijn jeugd stimuleerden zij en ook anderen, zoals wijlen opa Groen en meester Varkevisser, mijn leergierigheid en lieten mij – zonder dat ik het besefte - afdwalen van een bijna voorbestemd leven als visser.

Na mijn studie hydrologie aan de VU in Amsterdam (1972 tot 1980), heb ik gewerkt bij het adviesbureau IWACO (1980-1994), zowel in Nederland als het verre buitenland. Deze periodes waren natuurlijk ook van grote invloed. De mensen en belevenissen uit die periodes draag ik met me mee en maken me tot wat ik ben.

Pas in 1994 kreeg ik de kans om bij de universiteit te gaan werken. Ik dank daarom mijn promotor prof. Co de Vries voor zijn vertrouwen, toen hij mij - als wetenschappelijke outsider - aantrok bij de vakgroep hydrologie en stimuleerde tot dit promotieonderzoek. Na lang denken over een geschikt onderwerp begon ik in de zomer van 1995 met het onderzoek in Suriname, waar ik al eerder als consultant had gewerkt. Afgezien van mooie en intrigerende hydrologische gegevens uit dat land, had ik inmiddels een minstens zo mooie en intrigerende Surinaamse vrouw. De motieven waren dus niet zuiver wetenschappelijk. Maar zijn ze dat ooit ?.

Terugkijkend op de periode van de promotiestudie, ben ik vooral veel dank verschuldigd aan Henk Kooi, mijn copromotor. Dat geldt voor zijn kritische geest, het werk aan de modelexperimenten, maar vooral voor het aanstekelijke enthousiasme in onze discussies, dat voortdurend nieuwe wegen opende. Henk, laten we zo doorgaan! Ook de hulp van studenten, middels hun afstudeeronderzoeken, was onmisbaar. Ik denk dan aan Jouke Velstra voor zijn kartering van de zoutgehaltes van het grondwater, zijn hulp in Suriname en de geochemische en isotopenanalyses; aan Vincent Post voor de berekeningen met het grondwatermodel; aan Tibor Stigter voor het verzamelem en interpreteren van de hydrogeochemische gegevens en aan Kyrian van Vliet voor het uitvoeren en interpreteren van isotopenanalyses. Jongens, bedankt, zeker ook voor de gezelligheid. Dank gaat ook uit naar VU collega-'s voor hulp bij berekeningen, literatuuronderzoek, tekstcorrecties en logistieke ondersteuning, met name Antoon Meesters, Ersin Seyhan, Sampurno Bruynzeel, Kick Hemker, Michel Groen, Vincent Post, Boris van Breukelen, Ian Simmers en Tony Appelo.

Zonder hulp uit Suriname zou het ook niet zo ver zijn gekomen. In de eerste plaats dank ik Theo Goedhart, directeur van de Surinaamsche Waterleidingmaatschappij (SWM), die mij op alle mogelijke manieren logistiek heeft ondersteund bij het veldwerk, het verzamelen van gegevens en met introducties bij andere organisaties. "Je hoort gewoon bij de SWM", zei hij laatst. En zo is het. Gedurende mijn vele bezoeken sinds 1990 ben ik me thuis gaan voelen daar aan de Gravenstraat in Paramaribo. Die dank geldt ook voor andere SWM'ers, zoals Rudy Pawiro, Anand Gobind en Carolien Ligeon. Ook de Dienst Watervoorziening in Suriname ben ik dank verschuldigd in de personen van de heer Tsai Meu Chong, de wandelende database van de waterboringen – may he live forever - en Jerrol Ferrier. Goede herinneringen bewaar ik ook aan Siela en Pieter Teunissen voor hun gastvrijheid. Ik heb ook dankbaar gebruik gemaakt van Pieter's uitgebreide kennis van vegetatie, bodem en landschap van Suriname en zijn uitgebreide netwerk van contacten voor het vergaren van informatie. Cruciale boorgegevens zijn afkomstig van Staatsolie Maatschappij Suriname, waarvoor ik de directeur, de heer Jahrap, Ferry Nieuwland en Joan Telgt erkentelijk ben. Dat geldt ook voor de bauxietmaatschappijen Billiton Maatschappij Suriname en SURALCO, welke in de personen van, respectievelijk, Henk Morroy en Jan Vandenberge, behulpzaam waren met verlenen van gegevens en bij het veldwerk. Onder de dankbetuigingen noem ik verder de heer Coleridge van Consulting Services voor het uitvoeren van de pulsboringen en, last but not least, mijn voormalige werkgever IWACO, nu RoyalHaskoning, voor logistieke hulp.

Ik wil verder enkele personen noemen die mij geholpen hebben met laboratorium analyses. Dat zijn: Hetty Schafer van het hydrochemisch laboratorium van de VU; Gareth Davies van het isotopenlaboratorium van de VU; Harro Meijer, Harm-Jan Streurman, Bert Kers, en Hans van der Plicht van het Centrum voor Isotopenonderzoek in Groningen; Arnold van Dijk van het geochemisch laboratorium van de RUU in Utrecht; Sjerry van der Gaast van het NIOZ in Den Helder; Frank Wesselingh van het museum Naturalis in Leiden. Ik heb ook dankbaar gebruik gemaakt van gegevens, ter beschikking gesteld door SHELL (boorgatmetingen via Huib van der Brink), Leen Krook (mineralogische beschrijvingen sedimenten Suriname) en Theo Levelt (geochemische analyses). Beste mensen, sommigen van jullie zien dat ik (nog) niet alle gegevens heb gebruikt, maar dat doet niets af van mijn dankbaarheid voor jullie inzet.

Verder ben ik de leden van de leescommissie, prof. dr. H.A.J. Meijer, dr. ir. T.N. Oltshoorn, prof. dr. A. Leijnse, prof. dr. Th.E. Wong, prof. dr. W. Roeleveld en dr A.J. van Loon erkentelijk voor het beoordelen en becommentariëren van het proefsehrift. Ik wil in het bijzonder Tom van Loon bedanken voor zijn zeer grondige correctie van de tekst. Tenslotte dank ik Henry Sion en Nico Schaefers van de afdeling fotografie en vormgeving van onze faculteit voor het teken- en opmaakwerk van het proefschrift.

Gedurende de gehele onderzoeksperiode kreeg ik indireete, maar niet minder belangrijke, steun in het huishouden van mijn familie, met name van schoonmoeder Gisela Blackman, tante Lygia Hardy en schoonvader Oscar Stewart. Grantangi, lieve mensen. Naast een proefschrift hebben de afgelopen jaren mij ook twee beeldschone kinderen opgeleverd, Corryenne en Joshua. Schatjes, jullie hebben me vooral van mijn werk afgehouden en daar ben ik jullie eeuwig dankbaar voor. En dan mijn vrouw Jacintba. Ik kan hier niet opsommen, wat je allemaal voor me hebt gedaan. Ik volsta met te zeggen dat ik zonder jou niet eens was begonnen aan deze klus. Indachtig een Surinaams gezegde, ben jij voor mij het water waarin ik zwem. "Lek' fa wan fisi no man libi sondro watra, so mi no man libi sondro yu".

Tenslotte, het onderzoek duurde lang, maar er waren genoeg spannende en plezierige momenten van ontdekkingen - vaak samen met anderen - die het enthousiasme erin hielden. Wat dat betreft is er weinig verschil tussen aardwetenschappers en kinderen die spelenderwijs hun omgeving ontdekken, zoals de omslag van dit boek laat zien. Het gaat om de verwondering, kinderlijke verwondering over alles wat er te zien en te beleven is in de natuur, Gods eigen speeltuin.

Koos Groen

Samenvatting

De effecten van transgressies en regressies op grondwater in kustvlakten en onder de zeebodem

Inleiding

Dit proefschrift gaat in op de vraag hoe mariene transgressies en regressies grondwater in kustgebieden beïnvloeden wat betreft stromingssystemen en processen als verzilting en verzoeting. Deze vraag komt voort uit het feit dat zoutgehalten van grondwater in kustgebieden vaak een – op het eerste gezicht - onlogisch patroon vertonen: ver in binnenland kan men soms brak grondwater vinden, terwijl onder de zeebodem zoet grondwater wordt aangetroffen. De wezenlijke oorzaak ligt in de grote geologische dynamiek van het kustmilieu. Het grondwatersysteem moet zich steeds aanpassen aan soms abrupte gebeurtenissen als transgressie, regressie, sedimentatie en erosie. De hiermee gepaard gaande verzilting dan wel verzoeting van de sedimenten voltrekt zich traag en is vaak nog niet voltooid, wanneer het stromingssysteem in het kustgebied alweer verandert.

In dit proefschrift is getracht een beter begrip te krijgen van deze processen door middel van een case studie van de Surinaamse kustvlakte (Part I) en observaties uit andere delen van de wereld en algemene modelexperimenten (Part II). De case studie wordt beschreven in de drie volgende paragrafen van deze samenvatting: de algemene studies in de voorlaatste paragraaf.

Het kust- en offshore gebied van Suriname

De kustvlakte bij Paramaribo vormt een laaggelegen en, van nature, moerassig gebied, waar Kwartaire mariene afzettingen, grotendeels bestaande uit kleilagen (5 tot 35 m dikte), aan het oppervlak liggen (Figuur 3.1 en 3.5). Ten zuiden daarvan dagzomen Pliocene zanden in de hoger gelegen savannegordel. De Tertiaire afzettingen bestaan voornamelijk uit ongeconsolideerde zand- en kleilagen en hebben een totale dikte van enkele meters in de savannagordel tot 300 m in het noordelijke Holocene deel van de kustvlakte. De Tertiaire afzettingen, waarin zich de belangrijkste aquifers bevinden, rusten op kristallijne gesteentes (in savannegordel en Pleistocene kustvlakte) of op Krijtafzettingen (in Holocene kustvlakte).

Het zoutgehalte van het grondwater in de Tertiaire aquifers, in mg/l chloride, varieert van 6 tot 2000 mg/l. Hogere gehalten worden aangetroffen in de slecht doorlatende Krijtafzettingen en in de Kwartaire kleilagen van de Holocene kustvlakte (Figuur 3.5). Op een aantal pompstations wordt zoet grondwater (< 250 mg/l chloride) gewonnen uit de Tertiaire aquifers op diepten van 15 tot 180 m. Voor de aanvang van de grootschalige grondwaterwinning (1958 AD), was het grondwater in de kustvlakte min of meer stagnant. De aquifers werden en worden nauwelijks aangevuld, mede vanwege de zeer hoge hydraulische weerstand van het Kwartaire kleipakket. Een uitzondering vormt een hoger gelegen gebied rond het dorp Lelydorp. Grondwater kan wel infiltreren in de Pliocene zanden van de savannagordel, maar wordt geheel gedraineerd door de lokale kreken.

Uit olieboringen blijkt dat grondwater in het offshore gebied relatief zoet is (Figuur 3.5): tot 90 km afstand van de kust wordt nog grondwater met een chloridegehalte lager dan 2000 mg/l aangetroffen (zeewater heeft een chlorideconcentratie van ca 20000 mg/l). Dit

matig brakke grondwater is duidelijk van meteorische oorsprong en moet zijn gevormd door een ander stromingssysteem dan de huidige en wordt daarom aangeduid als paleogrondwater.

Verzoeting van sedimenten in het kust- en offshore gebied van Suriname tijdens de Weichsel regressie

^{14}C-leeftijden duiden erop dat het grondwater in de kustvlakte is gevormd tijdens het Laatste Glaciale Maximum of LGM (25 tot 12 ka BP) en Vroege Holoceen (12 tot 8 ka BP). In die periode en mogelijk daarvoor (De Weichsel regressie duurde van 115 tot 12 ka BP) moet er aanzienlijke grondwateraanvulling hebben plaatsgevonden teneinde de enorme hoeveelheid paleogrondwater in het kust- en offshore gebied te kunnen verklaren. Toch was de neerslag gedurende het LGM ongeveer 50 % van huidige neerslag, die 2200 mm/jaar bedraagt. Uit de signatuur van de stabiele waterisotopen ($\delta^{18}O$ en $\delta^{2}H$) in het Pleistocene grondwater blijkt dat de neerslag waarschijnlijk beperkt was tot het seizoen van april tot en met juli. In dit koelere en drogere klimaat bedekten uitgestrekte grassavannes de kustvlakte. Dit laatste kon worden afgeleid uit de stabiele koolstof isotopen in het grondwater ($\delta^{13}C$). De relatief hoge $\delta^{13}C$ waarden wijzen erop, dat dit grondwater is geïnfiltreerd onder een begroeiing met voornamelijk planten, die een C4-fotosynthese volgen, welke typisch is voor tropische grassen.

Gedurende het LGM stond de zeespiegel 100 tot 130 m lager dan nu en lag de kustlijn 140 km noordwaarts van de huidige ligging. Na 12 ka BP begon de zeespiegel te stijgen en bereikte rond 6 ka BP het huidige niveau. De kustlijn lag toen ongeveer 20 km landinwaarts van de huidige positie. Gedurende het Laat Holoceen begon de kustvlakte zich weer uit te breiden door de voortdurende afzetting van sediment, aangevoerd uit de Amazone. Boringen in de kustvlakte toonden aan, dat de rivieren en kreken diep waren ingesneden (10 tot 30 m) gedurende het LGM en Vroege Holoceen.

Grondwaterstijghoogten in de Tertiaire aquifers moeten veel lager zijn geweest dan de huidige vanwege de diep ingesneden dalen en de lagere zeespiegel. Daarentegen mag worden aangenomen dat de freatische grondwaterstanden op de slecht gedraineerde kleiplateaus dicht aan maaiveld bleven. Hieruit werd afgeleid, dat door het grote stijghoogteverschil er aanzienlijke grondwateraanvulling van de aquifers kon optreden in deze periode (Figuur 4.3). Een numeriek grondwatermodel, dat deze situatie simuleerde, toonde inderdaad aan dat er overal op de kleiplateaus van de kustvlakte grondwateraanvulling van enkele tientallen millimeters per jaar bestond. Uit berekende verblijftijden van het grondwater kan verder worden afgeleid dat de periode, waarin het systeem actief was, lang genoeg duurde om al het brakke en zoute grondwater van voorlaatste transgresie (Eemien) uit te spoelen, ook in het gebied dat nu ver offshore is gelegen (90 km uit de kust). Dat laatste bleek niet mogelijk te zijn in modelsimulaties van een vlakke kustvlakte zonder een erosierelief.

Het bestaan van stroming en grondwateraanvulling in de kustvlakte werd bevestigd door hydrogeochemische modellering van stoftransport en cationuitwisseling in de Pleistocene kleilaag. Modelsimulaties lieten zien, dat alleen bij neerwaartse stroming gedurende de Weichsel regressie, de uitwisselbare Na^{+}-ionen van de voormalige zoute klei kon worden gespoeld en de waargenomen dominantie van uitwisselbare Mg^{2+}- en Ca^{2+}-ionen kon ontstaan. In simulaties met alleen diffusief stoftransport - het momenteel heersende proces in de Kwartaire klei - werd dit niet bereikt.

Verzilting van sedimenten in het kust- en offshore gebied van Suriname tijdens de Holocene transgressie

Gedurende en na de Holocene transgressie, toen ook het erosierelief grotendeels is verdwenen door sedimentatie, zijn de stromingssystemen in het kust- en offshore gebied tot stilstand gekomen. Tijdens de snelle transgressie kwam relatief zout en zwaar grondwater op het stagnante meteorische grondwater te liggen. Dit vormt een potentieel instabiele situatie, die kan leiden tot convectieve dichtheidsstromen (fingering) en snelle verzilting van de onderliggende sedimenten, zoals in het Nederlandse kustgebied is gebeurd. In de dikke, slecht doorlatende Kwartaire kleilagen van Suriname gebeurde dit niet (geen overschrijding van het kritische Rayleigh getal) en verliep de verzilting veel trager volgens diffusief stoftransport.

Neerwaartse diffusieve verzilting is ook aangetoond met behulp van waargenomen profielen van chlorideconcentraties en chloorisotopenverhoudingen ($\delta^{37}Cl$). Deze profielen zijn vergeleken met de resultaten van een diffusie-sedimentatie model. Hieruit kon worden geconcludeerd dat de zouten in de bovenste 125 m van de formaties het gevolg zijn van neerwaartse diffusie uit de mariene Holocene sedimenten. Dit impliceerde dat de opgeloste zouten op grotere diepten afkomstig zijn uit een andere bron. Vermoedelijk bestaat deze bron uit de Krijtafzettingen op een diepte van ca 300 m, waaruit zout door opwaartse diffusie en laterale dispersie in de Tertiaire formaties zijn gedrongen.

Aanvullend bewijs voor de verschillende oorsprong van de zouten is gevonden in de cationconcentraties van het grondwater in de Tertiaire aquifers. Grondwater in de bovenste aquifers, ondieper dan 125 m, heeft een overschot aan Mg^{2+}- en Ca^{2+}-ionen (ten opzichte van conservatieve menging). Dit overschot is in balans met een Na^{+}-tekort en duidt op verzilting, gepaard gaande met cation uitwisseling. Een chromatografisch patroon in de cationensamenstelling, zoals elders vaak is waargenomen bij verzilting, ontbreekt hier. Het patroon kon redelijk goed worden gereproduceerd in hydrogeochemische modelsimulaties van een-dimensionaal diffusief stoftransport en cationuitwisseling. De simulaties lieten verder zien dat de cationuitwisseling voornamelijk in de Kwartaire klei plaatsvindt.

Het zoete en brakke grondwater op diepten groter dan 125 m heeft een geheel andere chemische compositie en wijst op een andere herkomst.

Algemene studies

Het voorkomen van onderzees meteorisch grondwater ver uit de kust in Suriname is niet uniek. Een inventarisatie van waarnemingen en studies elders (Verenigde Staten, Indonesië, China, Nigeria, Nederland) laat zien dat het verschijnsel eerder regel is dan uitzondering. Men kan onderscheid maken tussen twee typen offshore meteorisch water: (i) water dat deel uitmaakt van een actief stromingsysteem, waarbij grondwater aan land wordt aangevuld en uitstroomt op de zeebodem als diffuse kwel of in de vorm van onderzeese bron en (ii) paleogrondwater, dat niet langer wordt aangevuld en dus langzaam verdwijnt, zoals voor de kust van Suriname.

Simulaties met een simpel analytisch grondwatermodel (semi-confined aquifer met een scherp zoet/zout grensvlak) tonen aan dat actieve stromingssystemen, tot maximaal 50 km offshore kunnen reiken. Een hierop gebaseerd "approximate" analytisch model laat zien dat alleen het kustnabije gedeelte van dit stromingssysteem (tot maximaal 5 km uit de kust) zoet grondwater bevat. De lengte van de zoetwatertong wordt bepaald door de afstand uit de

kust, waar de opwaartse onderzeese uitstroming zo laag is, dat zout water door neerwaartse diffusie toch de aquifer bereikt en daar convectieve dichtheidsstroming veroorzaakt.

Tenslotte zijn in deze studie een groot aantal simulaties uitgevoerd met numerieke grondwatermodellen voor variabele dichtheid met het doel grondwaterverzilting in zijn algemeenheid te bestuderen tijdens een mariene transgressie. Transgressies zijn onderzocht in een model bestaande uit een aquifer onder een kleilaag met een hellend oppervlak. Dit model kan vergeleken worden met een kustvlakte of continentaal plat met een flauwe regionale helling. De simulaties lieten zien dat de transgressies in het algemeen zo snel verlopen, dat het zoet/zout front de landwaarts schuivende kustlijn niet kan "volgen". Verzilting na transgressie vindt voornamelijk plaats door neerwaarts transport via diffusie en convectieve dichtheidsstroming. Meestal treden deze twee processen tegelijkertijd op: diffusie in de klei en convectieve dichtheidsstroming in de aquifer. De dikte van de afdekkende kleilaag blijkt van groot belang te zijn voor de integrale verziltingssnelheid.

Gesuperponeerd op de regionaal hellende kustvlakte van het LGM kenden veel gebieden zoals Suriname en Nederland een erosielandsschap. Daarom zijn ook transgressiesimulaties uitgevoerd met een model van zo'n erosielandschap, bestaande uit een aquifer onder een kleilaag waarin een rivier is ingesneden. Uit de simulaties bleek dat het meteorische stromingssysteem zich nog lang handhaaft na inundatie van het dal. De opwaartse kwel in het dal, of beter estuarium, verhindert de verzilting. Pas na volledige inundatie draait de stroming om en dringt zout water naar binnen onder het dal en wordt het zoete grondwater uitgedreven door opwaartse stroming naar de zeebodem via de kleilaag. Het meteorische grondwater blijkt zich lang te kunnen handhaven tussen de rivierdalen.

Slotopmerkingen

Het grootste gedeelte van de wereldbevolking woont langs de kust, vaak in megacities. In veel van deze gebieden vormt de watervoorziening een probleem, dat alleen nog maar zal toenemen in de toekomst. Er is te weinig grondwater of er vindt al overexploitatie plaats en soms is het grondwater niet meer bruikbaar vanwege verontreinigingen. De voorraden matig brak meteorisch grondwater in offshore- en kustgebieden kunnen mogelijk alternatieve bronnen vormen in combinatie met nieuwe en goedkopere ontziltingstechnieken. In het geval van paleogrondwater is er weliswaar sprake van eindige hoeveelheden, maar die zijn van een zodanig grote omvang, dat winning nauwelijks als niet-duurzaam kan worden bestempeld. Bovendien zouden deze voorraden toch langzaam verdwijnen door diffusieve verzilting.

Verder onderzoek naar offshore meteorisch grondwater is daarom gewenst. Met een beter begrip van de omstandigheden, waaronder dit water kan ontstaan, is het mogelijk prognoses te geven over het voorkomen op bepaalde locaties. Het voorkomen is, zoals reeds gezegd, eerder regel dan uitzondering met name in ondiepe zeeen (< 70 m), waar de eerste 300 m onder de zeebodem bestaan uit afwisselend zand- en kleipakketten.

Voor de exploratie is het zinvol om geofysische detectiemethoden te ontwikkelen, zoals de combinatie van transient domain electromagnetics en hoge resolutie seismiek.

Chapter 1.

Introduction

1.1. Background

Before joining the - then - Faculty of Earth Sciences of the Vrije Universiteit Amsterdam in 1994, I worked 14 years in several countries as a consulting hydrogeologist. Many of the projects were carried out in coastal plains, among others those of the Netherlands, Mozambique, Arabian Gulf and Suriname. In these areas I often observed groundwater salinity patterns and flow systems that did not comply with the classic concepts on coastal hydrogeology. Notably in Suriname, where I worked from 1990 to 1994, I was confronted with enigmatic phenomena like unexplainable artesian heads, stagnant bodies of fresh groundwater in deep aquifers near the shore, but also saline groundwater bodies far inland (UNDP/WHO, 1972; Groen, 1998; IWACO/F.R. Harris, 1991). Lack of understanding of these phenomena complicated groundwater exploration and management and led to overlooking of valuable fresh groundwater resources and unexpected salinization of wells.

In the course of time, the impression grew on me that the main reason for anomalous observations is that classical hydrogeological concepts of coastal plains do not account for geological events operating on large scales of time and space. This refers specifically to climatic changes and marine regressions and transgressions during the last hundreds of thousands of years. The effects of these events are still reflected in the present hydrogeological state. Stated differently: the ever changing geological conditions of climate, topography and sea level appear to have produced hydrogeochemical, isotopic and even hydraulic head patterns in coastal groundwater, which are not in equilibrium with present-day boundary conditions because of the large relaxation times. In that respect we find ourselves at a very specific point in geological history, as a major sea level rise of more than 100 m took place a relatively short time ago (12000 to 6000 years BP).

After joining the university, I proposed to initiate a Ph.D. study into these matter. The coastal plain around the capital of Paramaribo in Suriname (South America) seemed to be a suitable case study because of the availability of data. Many earth scientists and engineers investigated the coastal plain around the capital of Paramaribo especially during Dutch colonial times (Wong et al., 1998a; Groen, 1998). Also water supply, mining and oil companies in Suriname were very cooperative in supplying well data and providing assistance in the field. Investigations started in 1995 after promotor prof. dr J.J. de Vries, head of the hydrology department of the Faculty of Earth Sciences, had accepted the proposal. Dr. H. Kooi took on the role of copromotor.

1.2. Objective and scope of the study

During the final stage of a PhD study it may be customary to write down objectives that fit the results. This may give the thesis a straightforward and "scientific" appearance. It is, however, not realistic to suggest that objectives and scope remained unaltered during this

7-year study. In my opinion it is essential in science to show how the work took place and how and why objectives and scope changed.

Initially, the objective of the PhD study was to unravel the relationship between the anomalous salinity, age and flow patterns in coastal groundwater in Suriname and the geological and paleogeographical development during the Last Glacial Maximum (LGM) and the Holocene. The methodology consisted of conceptualising the paleogeographical and paleohydrological development using existing geological proxy data and new chemical and isotopic groundwater data. Subsequently, these concepts and hypotheses were tested by numerical simulation models.

The study area encompassed the 70 km wide sedimentary belt between the Suriname and Saramacca Rivers (see Figure 3.1). Though initially investigations were restricted to the coastal plain, I soon became intrigued by data from offshore exploration wells in Suriname showing a body of low salinity groundwater (< 200 mg/l) extending 90 km into the offshore sediments! I suspected that present and past onshore processes are intimately coupled to those in the offshore domain and that, consequently, the latter had to be included in this study.

Related to this, a larger time frame of about 120,000 years, including the end of the previous Sangamonian (Eemian) transgression and the entire Wisconsinan regression and Holocene transgression, appeared to be more suitable. An even longer period would be needed in order to answer questions about the genesis of deep groundwater(> 300 m). However, I refrained from considering earlier time intervals because of the many uncertainties regarding the Early Pleistocene and Pliocene paleogeography.

After I had acquired a basic understanding of the hydrogeological characteristics of the Suriname coastal plain, I wanted to know how exceptional this case actually was. Thus, I started to review data and reports from other coastal plains, especially concerning the presence of fresh or low-salinity offshore groundwater. There appeared to be striking similarities with the Suriname coast, but also dissimilarities. It was there that my research took a more generic turn. The review study motivated my colleague Henk Kooi and myself to develop mathematical models in order to define the generic conditions, which control the presence or absence of offshore low salinity groundwater and the salinization process in general.

1.3. Structure of the thesis

Chapter 2 discusses some general concepts and definitions related to coastal hydrogeology, which will be used in the following chapters. The remaining part of the thesis is divided into two parts in accordance with the objectives described above. Part I (Chapters 3-7) deals with observations and interpretations related to hydrogeological processes in the coastal plain of Suriname, whereas Part II (Chapters 8-10) is concerned with generic processes in coastal plains. Stated in other words: Part I represents mainly the inductive phase and Part II the deductive phase of this research project.

Part I starts in Chapter 3 with a description of the present hydrological and hydrogeological conditions in the coastal plain around Paramaribo. Chapter 4 presents a reconstruction of the paleogeography and paleohydrology during the last Wisconsinan (Weichselian) glacial and the Holocene, mainly based on previous studies and proxy data. A conceptual model explains how saline groundwater from the previous Sangamonian (Eemian) transgression has been flushed from the coastal and offshore sediments in Suriname. This process is quantitatively evaluated by numerical groundwater modelling. Chapter 5 deals with the salinization process of the coastal sediments during the Holocene transgression. The concept of the diffusive salinization process, derived from chloride concentration and chlorine isotope patterns, is verified by mathematical modelling. In Chapter 6 the hydrogeochemistry of the coastal sediments is investigated to provide additional clues for the freshening and salinization processes during the Wisconsinan and Holocene, respectively. Special attention is given to cation-exchange processes. Also in this chapter concepts derived from analyses are evaluated by mathematical hydrogeochemical models. Chapter 7 discusses the isotopic composition of groundwater. The groundwater isotopes shed more light on the paleogeographic conditions in the coastal plain of Suriname, notably that of climate, vegetation and groundwater flow during the Last Glacial Maximum (LGM) and the Early Holocene.

Part II starts in Chapter 8 with an overview of the worldwide occurrence of offshore groundwater of low salinity (meteoric groundwater). Then, in Chapter 9, a model is presented to calculate the offshore extension of meteoric groundwater driven by coastal flow systems. This model helps to discriminate between "recent" submarine meteoric groundwater belonging to active flow systems and to fossil groundwater bodies formed during glacial low stands (paleogroundwater). In Chapter 10, a variable density flow model is used to study salinity patterns in time and space for situations in which saline water of high density overlies fresh water of low density. The model is applied to (i) "steady state" conditions, arising when fresh groundwater is driven by coastal flow systems into the offshore and discharged as submarine seepage, and (ii) unsteady-state conditions created by a sea encroaching a coastal plain.

Chapter 2.

Some concepts and definitions related to coastal hydrogeology

2.1. Groundwater origin and salinity

The salinity of groundwater is expressed in total dissolved solids (TDS) in mg/l and chloride concentration in mg/l or mmol/l. The first is useful as it is directly related to the water density; the second is appropriate because chloride, as a conservative compound, is a better tracer for the origin of groundwater and the degree of mixing. Definition of salinity classes and groundwater origins are not consistent in literature. This study uses the classification shown below in Table 2.1.

Salinity class	Origin	TDS in mg/l	Chloride in mg/l
Fresh	Pristine meteoric		< 50
Fresh	Meteoric	0 – 1000	0 – 250
Moderately brackish	Meteoric	1000 – 12,000	250 – 7,000
Brackish		12,000 – 24,000	7,000 – 14,000
Saline	Marine	24,000 – 34,000	14,000 - 20,000
Hypersaline		> 34,000	> 20,000

Table 2.1. Groundwater salinity classes

Meteoric groundwater is groundwater originated from precipitation that has infiltrated in the soil, either directly or indirectly from surface water. In this study fresh meteoric groundwater, which only contains salts from aerosol dissolution and normal rock/water interaction, is defined as pristine meteoric groundwater. As a rule of thumb groundwater with salinities less than 50 mg/l of chloride can be considered pristine in most coastal areas. Meteoric groundwater in coastal plains with higher chloride contents has generally been influenced by diffusive and dispersive mixing with saline groundwater. Because groundwater looses its meteoric signature with increasing salinity, this study has, somewhat arbitrarily, defined meteoric groundwater as groundwater having a salinity less than 1/3 of that of seawater or less than 7000 mg/l of chloride. According to the definitions used here (Table 2.1) meteoric groundwater can be fresh to moderately brackish. Marine groundwater is saline water defined as water with chlorinities between 14,000 and 20,000 mg/l. Note that processes like evaporation (sabkhas) and dissolution of evaporitic rocks may also increase the salinity of meteoric and marine waters. This implies that some saline and hypersaline waters may be of meteoric and not of marine origin. These processes are not considered here.

2.2. Flow systems

This study adheres to the flow system concept described in Toth (1963, 1995), De Vries (1974) and Engelen and Kloosterman (1996). According to this concept the sedimentary basin forms a hydraulic continuum in which coastal topography and climate invoke a com-

plex pattern of groundwater flow paths from recharge to discharge areas. In this pattern a hierarchy of nested flow systems can be discerned (Figure 2.1). With increasing depth, flow systems increase in length, have larger groundwater residence times and become controlled by lower-order (regional) relief features. Generally the concept of flow systems is restricted to topography-driven flow and applied for steady-state flow. For this study the flow-systems concept is expanded to include the realms in the deeper and offshore part of the coastal sediments where density-driven and compaction-driven flow dominates (Bethke et al., 1988; Harrison and Summa, 1991; Kooi, 1999). In addition it is noted that not so much the present flow systems but rather the changes in these systems through time have to be understood to explain the characteristics of coastal groundwater.

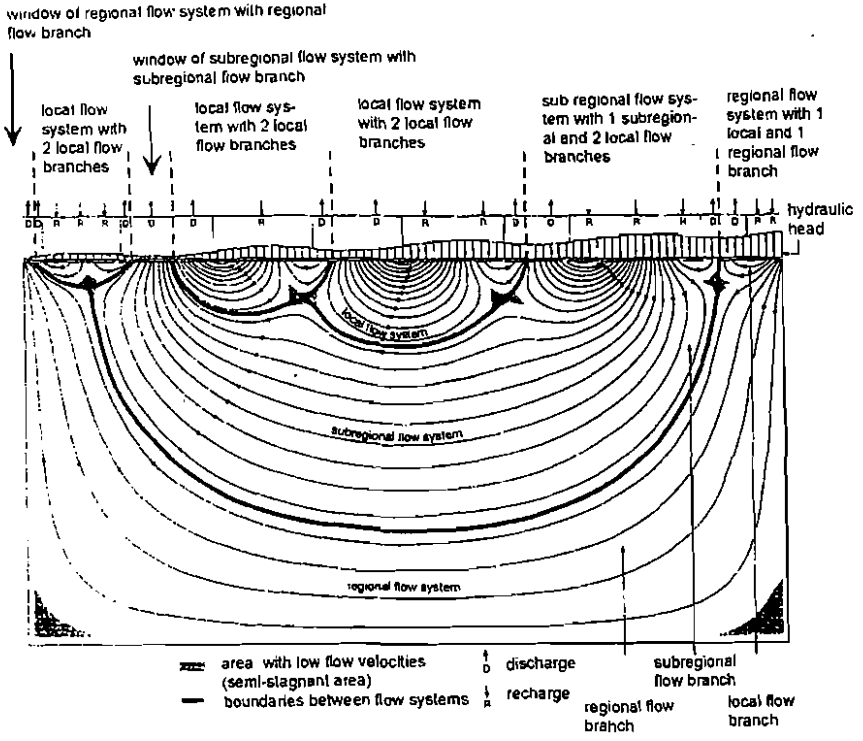

Figure 2.1. Groundwater flow systems (after Engelen and Kloosterman, 1996)

2.3. Fresh/saline interface

Topography-driven flow systems in coastal plains generally form fresh groundwater bodies "floating" on deeper saline groundwater. This is explicitly expressed in the equations of Badon Ghijben (1888), Herzberg (1901) and Hubbert (1940), which relate the depth of the fresh/saline interface position to groundwater heads in the meteoric groundwater body. These

relations assume steady-state fresh groundwater flow over an immiscible and stagnant body of saline groundwater. In reality, the interface is not sharp but forms a mixing zone caused by transverse dispersion of flow along the interface (Verruijt, 1971; Meinardi, 1991; De Josselin de Jong and van Duijn, 1986). The fresh/saline interface is an undulating surface, which arches upward below discharge zones like rivers and wells. Along the coastline the fresh/saline interface reaches the land surface or the seafloor. Near discharge areas the brackish transition zone may become relatively wide and the sharp interface approximation can no be longer maintained (Souza and Voss, 1987). In a sedimentary environment comprising several aquifers separated by semi-pervious clay layers, the fresh/saline interface forms a staggered line with fresh water protruding below the clay layers. This is well documented for the Long Island coast near New York, USA (Lusczynski and Swarzenski, 1966). Observations (Kohout, 1964) and analytical models (Bear and Dagan, 1964; Glover, 1959) show that the discharge zone of a phreatic aquifer extends several meters to hundreds of meters offshore. In a semi-confined aquifer the steady-state interface may extend many kilometers into the offshore zone as is shown by analytical models (Edelman, 1972; Mualem and Bear, 1974).

In the dispersion zone around the fresh/saline interface, topography-driven flow drags saline water from the underlying saline groundwater body and discharges brackish groundwater in the sea or inland seepage areas, like the polders in the Netherlands. Cooper (1964) reasoned that in a steady-state situation these salts have to be replenished by saline groundwater from the sea. Henry (1964) confirmed this hypothesis mathematically and found out that a convective flow pattern is induced in the saline groundwater body near the interface. The loss of salts from the dispersion zone may also be supplied by upward flow of salt water driven from deep sediments (compaction-driven flow).

In parts of sedimentary basins with little flow, fresh/saline interfaces are often absent and groundwater is mainly brackish. This cannot be explained by steady-state flow systems, but must the result of incomplete processes triggered by geological events in the past. This aspect is essentially the subject of this thesis.

2.4. Paleogroundwater

The more or less stagnant brackish groundwater bodies, mentioned above, in the deeper part of coastal sediments are generally old, often of Pleistocene age. Examples in various parts of the world are those found in Suriname (Groen, 1998), Jakarta, Indonesia (Geyh and Söfner, 1989), Belgium/Netherlands (Walraevens, 1990) and Bangkok, Thailand (Sanford and Buapeng, 1996). This groundwater dates from a period when the topography-driven flow systems had another and generally larger domain due to lower sea levels or higher relief. In the present study these "fossil" groundwater bodies are denoted as paleogroundwater. By comparison, in the isotope-hydrology literature, paleogroundwater is loosely defined as meteoric water originated in the distant past, when other climatic conditions prevailed and left their marks in the isotopic composition of groundwater (IAEA, 1981; 1983). I prefer the former definition, because in the dynamic coastal zone groundwater flow systems do not change so much because of climate change, but rather because of changes in topography and sea level. Therefore, paleogroundwater is defined in this study as meteoric groundwater formed by an old flow system that was controlled by conditions of sea level, topography or climate different from today. Another, simpler, definition is the following: paleogroundwater is meteoric groundwater that cannot be explained by the present flow systems.

Part I.

Case study of (paleo)groundwater in the coastal plain and continental shelf of Suriname

Chapter 3.

Hydrology of the coastal plain and continental shelf of Suriname

3.1. Introduction

Suriname is situated in South America, between 1° NL and 6° NL, and is bordered by Guyana in the West, French Guiana in the East and Brazil in the South (Figure 3.1). The Atlantic coast has a length of 350 km. Suriname has been a Dutch colony: it gained inde-

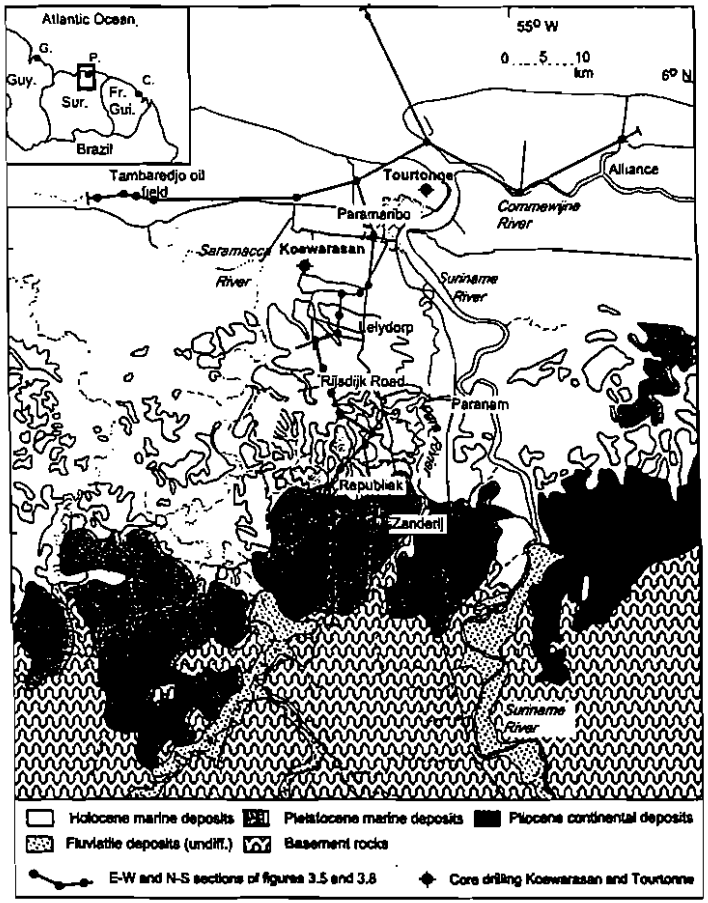

Figure 3.1. The coastal plain around Paramaribo, Suriname.

pendence in 1975. During colonial times the physical environment has been studied extensively because of the mineral resources (gold, bauxite and oil) and the high agricultural production of the coastal plain (Wong et al., 1998a). The population is about 400,000, of which 200,000 are living in and around Paramaribo. The capital always relied on the groundwater as a resource for drinking-water supply because of saline water intrusion in the coastal rivers. Groen (1998) reviewed the hydrogeological investigations that were carried out in the coastal plain during the last century. An important theme in these investigations was the complicated groundwater salinity pattern in the coastal aquifers. This chapter presents an outline of the geology, the present climate and hydrology and the basic hydrogeological characteristics, as observed today.

3.2. Climate

Suriname has a wet tropical climate with an average annual temperature of 27.1 °C and a total rainfall of 2200 mm at Paramaribo. Seasonal temperature variation is small: the maximum difference of monthly averages is 2 °C. Daily temperature fluctuates between an average daily maximum of 30.5 °C and an average daily minimum of 22.8 °C. Seasons are marked by the rainfall pattern shown in Figure 3.2. There is a long rainy season from April to mid-August followed by a long dry season until December. Less predictable both in timing and amount of rain are the short rainy season in December and January and the short dry season in February and March. Dry has a relative meaning, because even during the long dry season, rainfall at Paramaribo is generally higher than 70 mm/month.

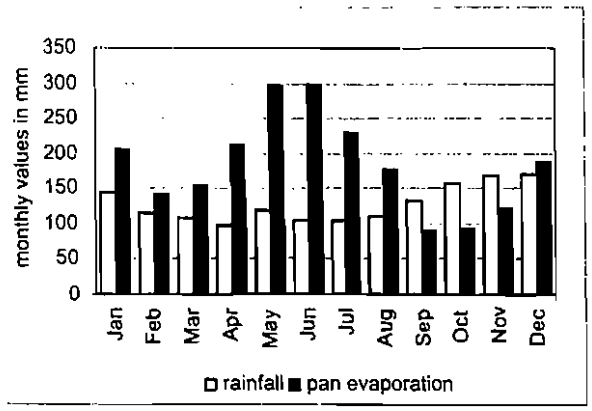

Figure 3.2. Rainfall and pan evaporation at Zanderij airport, Suriname.

The rainy seasons are related to the shifting Inter-Tropical Convergence Zone (ITCZ). The ITCZ, the average position of which is at 5° NL, the meteorological equator, passes Suriname twice a year. During the long dry season from August until December, the ITCZ is at its most northern limit and southeast trade winds prevail. During the rest of the year the ITCZ lies over, or just south of the study area, and northeast trade winds prevail. Pan evaporation at Paramaribo varies from 100 mm/month during the long rainy season to 170 mm in the long dry season (Figure 3.2).

3.3. Landscape

The major part of Suriname is underlain by the crystalline rocks of the Guiana Shield forming a hilly landscape with tropical rainforest. In the north of the country a belt of clastic sediments stretches along the Atlantic coast, having a width of 70 km in the study area near Paramaribo. Many earth scientists and biologists have investigated the sedimentary landscape in detail (Cohen and Van der Eyk, 1953; Van der Eyk, 1954, 1957; Zonneveld, 1955; Lindeman and Moolenaar, 1959; Brinkman and Pons, 1968; Veen, 1970 and Teunissen, 1978). The sedimentary landscape can be divided into three geomorphological units: the savannah belt, the "old" or Pleistocene coastal plain and the "young" or Holocene coastal plain.

The 20 km wide savannah belt in the South forms an undulating landscape on Pliocene sands (Figure 3.1). Elevations vary from + 10 m (relative to mean sea level) in the North to + 50 m in the south. Despite its name only 30 % of the savannah belt in the project area is covered by typical open savannahs with grasses, sedges and low bushes (Teunissen, 1978). Most vegetation consists of xeromorphie dry-land forest and savannah woodlands. Characteristie blaek water creeks, bordered by swamp and gallery forests, dissect the savannah belt. Apart from Zanderij airport, human impact is small in this sparsely populated area. Despite the tropical climate, savannah vegetation can persist because of the low moisture retention capacity and nutrient content of the coarse sandy soils and the regular burnings by the Amerindian population.

The actual coastal plain north of the savannah belt is much different: the flat marine plain is primarily underlain by clays with elongated East-West running beach barrier deposits ("ritsen") as the main morphological features. The Pleistocene part of the coastal plain is a 25 km wide zone between Zanderij airport and Lelydorp with elevations between +3 to +10 m (Figure 3.1). The plain is an assembly of clay plates ("schollen") dissected by numerous swamps and creeks filled with Holocene clay and peat. The plain was probably formed during the Sangamonian transgression and later dissected during the Wisconsinan regression (Veen, 1970). Between Lelydorp and Rijsdijk road, Pleistocene beach barrier deposits have coalesced into an elevated complex (+6 to +10 m), called the Lelydorp sands (Figure 3.1). Swamp grasses and swamp forests cover the inaccessible and marshy parts, mainly in the south, while dry-land forest is found on the better-drained parts. In the rest of the area, and especially on the Leldyorp sands, the original dry-land forests have disappeared by settlements and activities like agriculture, forestry and cattle breeding. Most of the old plantations have been abandoned and are presently overgrown by secondary vegetation. In the area between the Rijsdijk road and Paranam, the landscape has been strongly affected by the large and deep bauxite mines and the bauxite refinery at Paranam. Nowadays the abandoned mines form large lakes.

The Holocene plain, elevated at +1 to +3 m, has a width of about 25 km. Locally it penetrates deeply southward along the valleys of the Suriname and Saramacca rivers (Figure 3.1). This part of the coastal plain has lost most of its original character because of agricultural activities, settlements and especially the expanding city of Paramaribo. The vegetation was formerly marked by dry-land forests on the beach barriers and better drained parts of

the clayey plain, and by swamp forests on the low-lying parts. Grasses and shrubs dominate the recently formed land (after 1 ka BP) North of the line Groningen-Paramaribo-Commewijne River, where soils still contain brackish water.

The continental shelf slopes with a gradient of about 1:2,000 to a depth of 50 m about 100 km offshore (Figure 3.3 and 4.4). Then the gradient increases to 1:800 until it reaches the shelf break at a depth of 100 m about 140 km offshore, where the gradient increases to about 1:20 to 1:100. Remarkable morphological features are remnants of the Pleistocene paleochannels of the major rivers like the Marowijne (Nota, 1971) and old coastlines and coral reefs related to interruptions of the Holocene transgression (Nota, 1958, 1971).

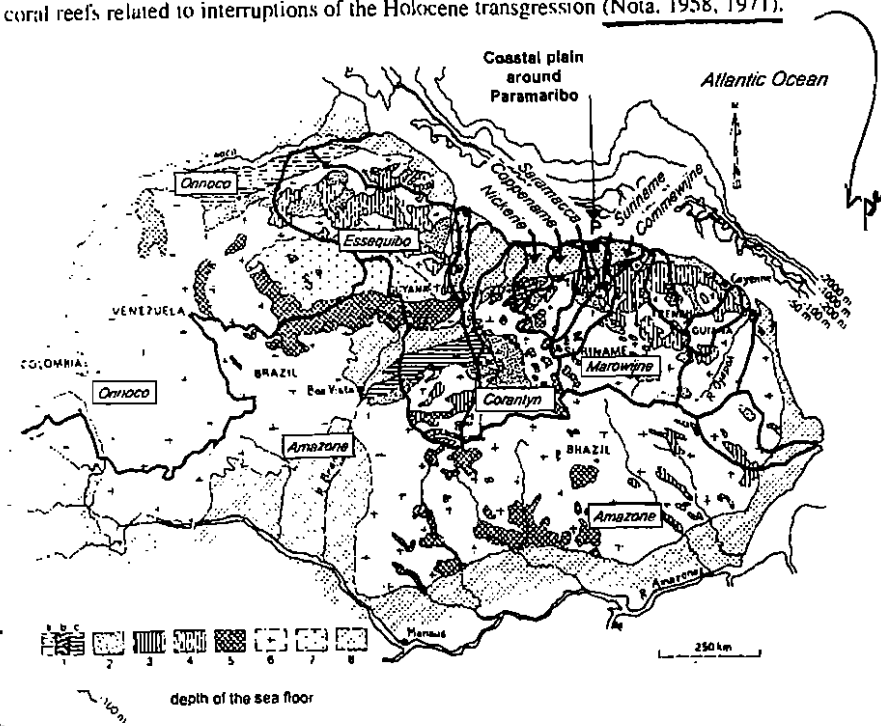

Figure 3.3. Geology and catchments of major rivers along the Guiana coast (after Bosma et al., 1983). (1) Granulite belts; (2) Amphibolite facies of 1; (3) Low-grade metasediments; (4) Greenstone belts; (5) Acid-intermediate metavolcanics; (6) Granitoid rocks; (7) Roraima sandstones (Precambrian); (8) Phanerozoic sediments

3.4. Geology

3.4.1. General

The crystalline basement of Suriname is part of the Guiana shield (Figure 3.3) and consists mainly of granitoid and metamorphic rocks (De Vletter et al., 1998). Metamorphic rocks (Marowijne Group) underlie the northern part of the catchments of the Saramacca and

Suriname rivers (Figure 3.3) and are also encountered in boreholes in the coastal sedimentary zone. The clastic Mesozoic and Cenozoic sediments in the coastal zone and the continental shelf are part of the Guiana Basin, which extends from the Waini River in Guyana to the Marowijne River in eastern Suriname (Figure 3.3). The sediments are described in more detail in Annex I (see also D'Audretsch (1953), Brinkman and Pons, (1968), Veen, (1970), Krook, (1979), Hanou (1981) and Wong (1984, 1989). Sedimentation in the Guiana Basin started in Late Jurassic to Early Cretaceous times, when the African and South American shields began to drift away (Wong 1976).

The stratigraphy (Figure 3.4) consists of a series of formations increasing in thickness and depth towards the north and onlapping the basement rocks or older sediments (Figure 3.5). The thickness of the sediment wedge increases from a few meters in the savannah belt to 750 m along the coastline and finally to 10,000 m about 140 km offshore (Wong et al, 1998b; Figure 3.6). The material for the subsiding basin was derived from the continuously

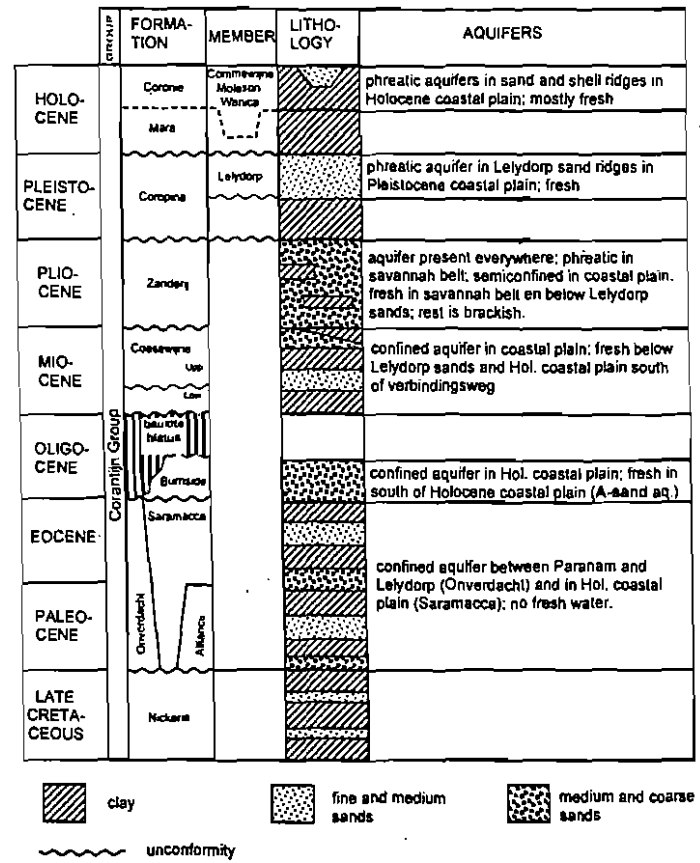

Figure 3.4. Stratigraphy of the coastal plain of Suriname

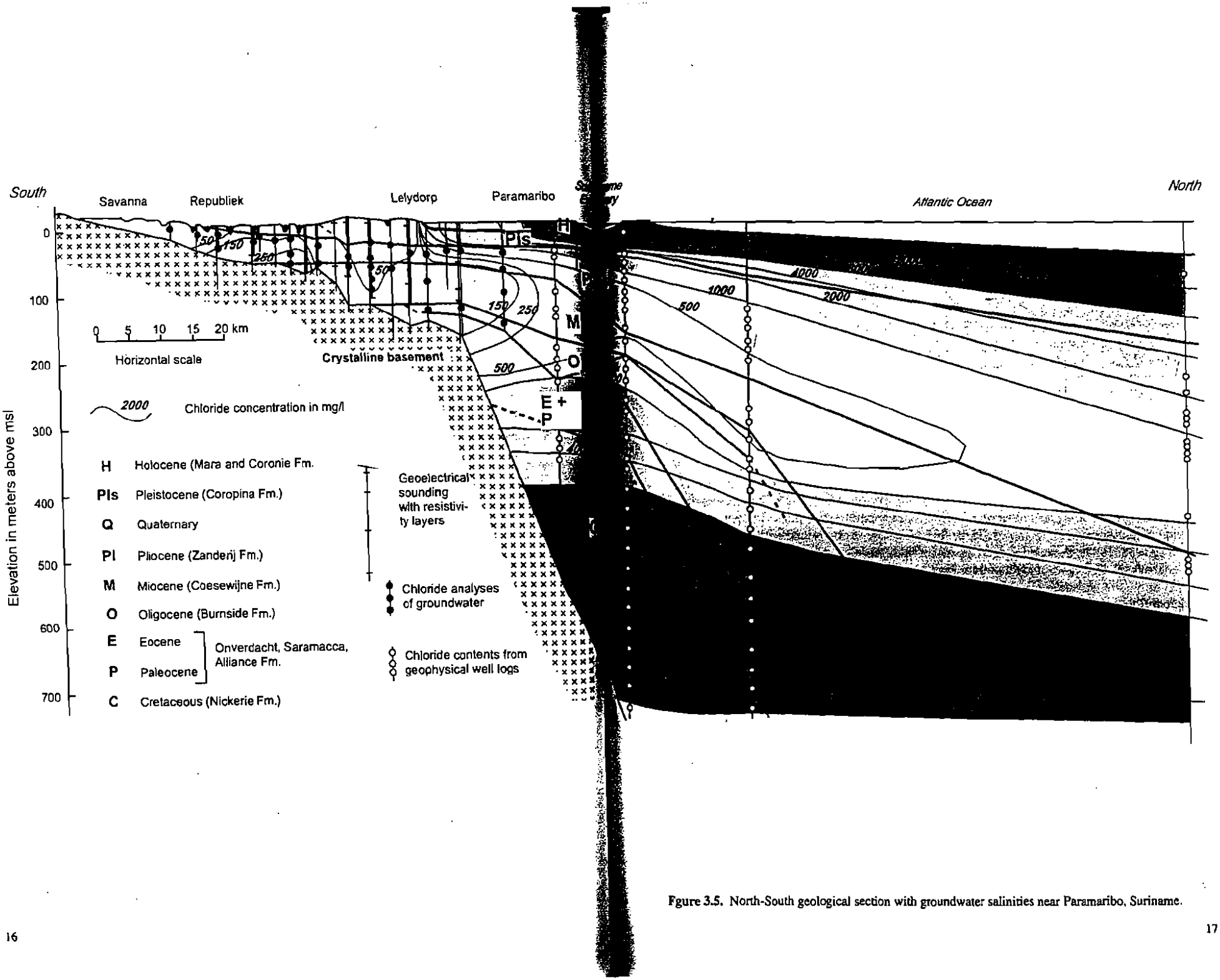

Figure 3.5. North-South geological section with groundwater salinities near Paramaribo, Suriname.

rising crystalline basement, south of the basin (Krook, 1994). After the Early Miocene the Amazon River became a more important source of supply (Wong, 1976, Krook, 1979). Before that time, when the Andes Mountains were not yet formed, drainage on the South American continent was directed towards the West (Krook, 1979).

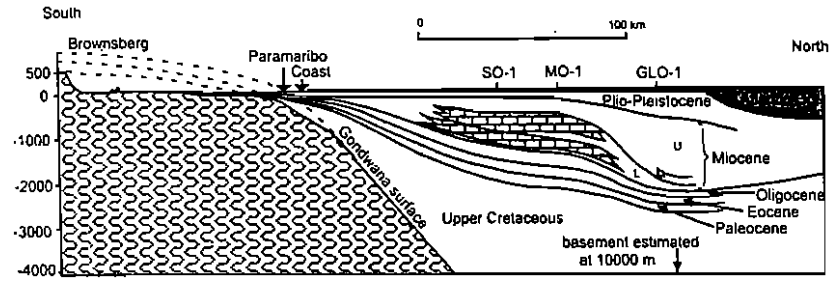

Figure 3.6. Offshore geology (after Wong et al., 1998b).

3.4.2. *Cretaceous and Tertiary*

The Cretaceous sediments in the coastal plain consist of terrestrial unconsolidated and consolidated fine to very coarse sands and kaolinitic claystones of the *Nickerie Formation*.

During the Paleocene and Eocene mainly shallow marine deposits were deposited during several transgressive phases. Three formations are distinguished with different facies (Wong, 1986, 1989): the continental 1 to 40 m thick *Onverdacht Formation* is characterized by coarse kaolinitic sands and kaolinitic clays deposited on alluvial fans and in braided rivers during the Paleocene, and in floodplains and coastal swamps during the more humid tropical Eocene. In the study area, the formation can be found as isolated buried "hills" capped by bauxite and laterite in a 10 km wide small zone around Onverdacht and further eastward. The Onverdacht Formation passes northward into *Saramacca Formation*, found between the Groningen-Lelydorp line and the coastline (Hanou, 1981). The formation consists of alternating quartz sands and kaolinitic clays, forming depositional cycles with alternating marine and continental environments. The formation contains thick and continuous sand units, which enable deep groundwater circulation. Oil in the Tambaredjo oil field is recovered from one of the lower sand units (T-sands), which is confined by an impermeable clay layer. The top of the formation is found at a depth of about -140 m (below msl) just North of Lelydorp and slopes to -220 m along the coastline West of Paramaribo. Further North the Saramacca Formation changes facies and passes into the marine *Alliance Formation*. This formation, consisting of silty marls, clays, calcareous sands and lignites, is much less permeable. Weathering during a prolonged recession in the Oligocene led to bauxite formation on the Onverdacht formation and crystalline basement rocks. Erosion products were deposited as braided-river and alluvial-fan deposits forming the *Burnside Formation* (A-sand aquifer). In Suriname the formation is found in some northeast-southwest oriented tectonic basins along the coast, like that of Paramaribo (Hanou, 1981). The Burnside Formation has been encountered just North of Lelydorp at a depth of -130 m.

North of Paramaribo near the coastline the top of the formation is found at -180 m. The coarse permeable sands of Burnside Formation vary in thickness from 5 to 80 m in a depositional centre 10 to 15 km West of Paramaribo.

During the Early Miocene two major trangressions led to deposition of clays, sandy clays and sands with glauconite and lignite layers (*Coesewijne Formation*). Compared to the older formations the deposits of this formation contain much more clay (40-80 %), originating from the proto-Amazon catchment. The lower, more clayey part of the Coesewijne Formation is found only in the Holocene coastal plain at a depth of around -95 m. The upper more sandy part extends as far south as the Rijsdijk Road in the Pleistocene coastal plain, though it is absent on the buried bauxite hills around Onverdacht. The depth of the top of the Coesewijne Formation varies from -60 m in the south to -75 m. On the continental shelf the facies of the Coesewijne Formation changes into a shallow-marine carbonate platform.

The Pliocene sediments, exposed in the savannah belt, consist of coarse, white and brown, kaolinitic sands with interbedded kaolinite clays and were deposited in braided streams and alluvial fans (Krook, 1979, Van Voorthuysen, 1969). Intensive weathering and leaching gave the savannah sands their characteristic bright-white appearance. North of the savannah belt the Zanderij Formation is covered by Quaternary clays with a thickness of 4 m at Republiek to 35 m along the coastline.

3.4.3. *Quaternary*

During a Pleistocene, probably the Sangamonian, transgression tidal lagoon clays interspersed with sand barriers were deposited. These sediments form the *Coropina Formation* and are found in the Pleistocene coastal plain between Republiek and Lelydorp. The sand barriers, found mainly in the northern part of the Pleistocene coastal plain, form now a more or less continuous blanket of sands. The Wisconsinan regression led to erosion of the Pleistocene surface in the coastal plain and the present offshore zone. Veen (1970) and Roeleveld and Van Loon (1979) found several gullies in the Pleistocene plain filled with Holocene deposits to depths of 10 m below the present surface. The present author found evidence that the paleochannel of the Suriname River near Paramaribo was deeper than 30 m. This is based on the results of two boreholes drilled for this study (Chapter 5) and on some unpublished well logs and cone-penetration tests. The Pleistocene clays show signs of deep weathering during the Wiseonsinan regression (Veen, 1970, Levelt and Quakernaat, 1968).

During the Early Holocene from 12 to 6 ka BP, the sea level rose from a depth of more than 100 m to the present level (Roeleveld and van Loon, 1979; Fairbanks, 1989; Figure 4.2). Marine deposition resumed and obliterated most of the Pleistocene erosion topography. Beeause the Holocene transgression did not reach the level of the previous Sangamonian transgression, the Pleistocene coastal plain in the south was preserved, though the gullies were filled with the peaty clays of the *Mara Formation* and can still be recognized as swamps. After sea-level rise slowed down between 6 and 7 ka BP coastal aggradation began and extensive tidal flat clays alternating with beach barriers with sands and shells were deposited in the Holocene coastal plain (*Coronie Formation*). Brinkman and Pons (1968) discerned three distinctive phases in the coastal aggradation: the Wanica phase from 6 to 3 ka BP, the Moleson phase from 2.5 to 1.3 ka BP and the Commewijne phase from 1 ka BP to present. The main part of the Holocene coastal plain in the study area dates from the Wanica phase. Only North of the road Paramaribo-Groningen and the Commewijne River

recent deposits of the Commewijne phase are found. Coastal aggradation is still going on: in the littoral zone rapid sedimentation is taking place on moving mud banks (Augustinus, 1978; Augustinus et al., 1989). Oceanographic surveys show that these Holocene mud deposits are found on the sea floor up to 30 km offshore and have a maximum thickness of 20 m (Nota, 1958, 1969).

3.5. Runoff and recharge

3.5.1. The savannah belt

Rainfall runoff processes have been investigated by Poels (1987) and Brouwer (1996) in small catchments in the savannah belt. Poels (1987) studied a catchment near Kabo west of the study area and Brouwer (1996) a savannah catchment in Guyana. Both authors report that, despite the frequent high-intensity rainstorms, surface runoff is a small component of total runoff (< 10 %), because of the sandy subsoil and the low surface gradients. Rainfall leaves the catchment mainly via evapotranspiration, while the rest is drained by perennial and ephemeral creeks (Table 3.1). Rainfall is transformed in river flow by (i) fast runoff just below or on the surface, here called interflow and (ii) slow runoff by groundwater, which is equal to groundwater recharge. Chemical analyses of peak flows indicate that fast runoff is not much affected by evapotranspiration. On the basis of simple water and chloride mass balances, using average data of these catchment studies, recharge values can be estimated:

$$P - E = Q \tag{3.1}$$

$$Q = R_{rech.} + R_{int} \tag{3.2}$$

$$P \cdot Cl_{rain} = R_{rech.} \cdot Cl_{groundw.} + R_{int.} \cdot Cl_{rain} \tag{3.3}$$

where P = precipitation, E = actual evapotranspiration, Q = creek discharge, $R_{rech.}$ = groundwater recharge and R_{int} = interflow. All these fluxes are in mm/a. Cl_{rain} and $Cl_{groundw.}$ are the chloride concentrations of rainfall (and interflow) and groundwater recharge, respectively. Equations (3.1), (3.2) and (3.3) lead to the following relation, where groundwater recharge is expressed as a function of measurable variables:

$$R_{rech.} = (P - Q) \left(\frac{Cl_{groundw.}}{Cl_{rain}} - 1 \right) \tag{3.4}$$

The results for fast and slow runoff are presented in Table 3.1. For verification Cl_{river} can be calculated and compared with the average measured value according to:

$$Cl_{river} = \frac{R_{rech.}}{Q} . Cl_{groundw.} + \frac{R_{int.}}{Q} . Cl_{rain} \tag{3.5}$$

Variables	Kabo (Sur.) (1980-1982)	Mabura Hill (Guy.) (1991-1992)
Measured:		
P (mm/a)	2200	2480
Q (mm/a)	590	1040
Cl_{rain} (mmol/l)	0.025	0.023
$Cl_{groundw.}$ (mmol/l)	0.156	0.093
Cl_{river} (mmol/l)	0.100	0.073
Calculated:		
$R_{int.}$ (mm/a)	290	570
$R_{rech.}$ (mm/a)	300	470
Cl_{river} (mmol/l)	0.092	0.055

Table 3.1. Water balances of catchments in the savannah belt based on chloride mass balances. Data for Kabo are from Poels (1987) and data for Maburo Hill from Brouwer (1996).

The results (Table 3.1) show that groundwater recharge varies between 300 and 500 mm/a. Because the savannah belt in the study area has a relatively large percentage grasses and shrub vegetation, a value of 500 mm/a seems more likely and has been used for groundwater modelling. According to Poels (1987) and Brouwer (1996), catchment losses by deep groundwater flow are negligible. This implies that the recharge in the savannah belt does not feed the Tertiary aquifers in the coastal plain. This is corroborated by a groundwater modelling study by Post (1996). Groundwater recharge appears to take place mainly during the long rainy season: observations of phreatic groundwater levels in the savannah belt (Weyerman, 1930; Heyligers, 1963; UNDP/WHO, 1972) show large fluctuations (2.5 to 3 m) with maximum levels at the end of the long wet season and minimum levels at the end of the long dry season. Effective rainfall, which is equal to rainfall minus actual evapotranspiration, is positive only during the long rainy season. This can be inferred from Figure 3.2, where monthly rainfall and pan evaporation are shown. It is noted that actual evapotranspiration in the wet tropics is close to potential evapotranspiration (Bruijnzeel, 1990).

3.5.2. The coastal plain

Catchments in the flat coastal plain are not as well defined as in the savannah belt. Effective rainfall on clayey terrain is mainly discharged via overland flow and interflow to swamps, creeks and man-made drainage channels. Typical for the clay terrain is the "kaw-foetoe" surface consisting of little hummocks (0.1 to 0.3 m²) separated by small drainage channels (0.1 to 0.2 m wide). Even with small topographic gradients, such a terrain enables fast overland drainage during heavy rainstorms. Phreatic groundwater flow systems cannot develop because of the low permeability and flat topography. The more permeable and slightly elevated beach barriers have higher infiltration capacities and sustain small groundwater flow systems. Relatively large phreatic flow systems are found in the Lelydorp sands, where drainage density is much smaller than in the rest of the coastal plain.

3.6. Groundwater

3.6.1. Aquifers and aquitards

Only a general description of aquifers and aquitards in the coastal plain of Suriname is given (Annex I provides a more detailed description). The most important aquifers are found in the Tertiary formations. The deep Eocene and Paleocene Saramacca Formation in the Holocene coastal plain around Paramaribo have not been investigated much in earlier hydrogeological studies (Figure 3.5). Oil exploration drillings show that this formation contains thick sand units, but these are saturated with brackish groundwater. The coarse sands of the Oligocene Burnside Formation form a well-defined and interconnected unit and have good aquifer properties. Groundwater in this aquifer is recovered by pumping stations in Paramaribo for drinking water supply (Table 3.2). In hydrogeological literature this aquifer is also known as the A-sand aquifer. The massive Coesewijne Formation consists of alternating clays and sand layers. Sometimes, a distinction is made between upper and lower Coesewijne aquifers, though the aquifers are not well defined. The sands of the upper Coeswijne Formation, which have the best aquifer properties, extend southward into the Pleistocene coastal plain, where they link with the overlying Zanderij Formation (Figure 3.5). The Coesewijne sands are also exploited in some small pumping stations in and around Paramaribo (Figure 3.1 and Table 3.2). The Zanderij Formation contains mainly sands and forms a good aquifer, which is present in the entire study area. Sand barriers (ritsen) in the Coropina and Coronie Formations form shallow phreatic aquifers of local extent.

The fined-grained, compacted Cretaceous deposits act as an aquitard. Modern and paleoflow systems were not able to flush saline groundwater from these deposits (Section 5.4.2). The clays between the Burnside and Coesewijne aquifers probably form another important aquitard, as is derived from the originally artesian groundwater heads (Section 3.6.3.). Also clays below the Burnside Formation are believed to have a high hydraulic resistance, as the salinity of pumped water in the well fields only slowly increases due to lateral advection rather than by upward flow from the more saline deeper strata. The Quaternary marine clays exposed in the coastal plain form an aquitard with a high hydraulic resistance, as was observed in pumping tests (Mente, 1990a; IWACO/F.R. Harris, 1991; Terracon Anguilla Ltd).

3.6.2. Groundwater salinity

The salinity pattern in the coastal sediments has been studied before in exploration studies for the drinking water supply (Groen, 1998; IWACO/F.R.Harris, 1991; UNDP/WHO, 1972). Figure 3.7 (from Groen, 1998) shows only the extent of fresh groundwater (chloride content < 200 mg/l) in the various aquifers. Therefore a more detailed survey has been carried out (Groen et al., 2000a) to delineate the salinity contour lines in a North-South and East-West section (Figure 3.5 and Figure 3.8, respectively). These salinities, expressed in mg/l of chloride, are based on laboratory analyses of water samples from observation and pumping wells and stem tests (exploration drilling) and estimated concentrations from vertical geophysical soundings and geophysical borehole logs.

In the Holocene coastal plain, brackish and saline groundwater with chloride concentrations exceeding 2,000 mg/l is found in the upper 30 to 100 m of the coastal sediments and shows a deepening trend towards the north. Saline pore water in the upper part of the

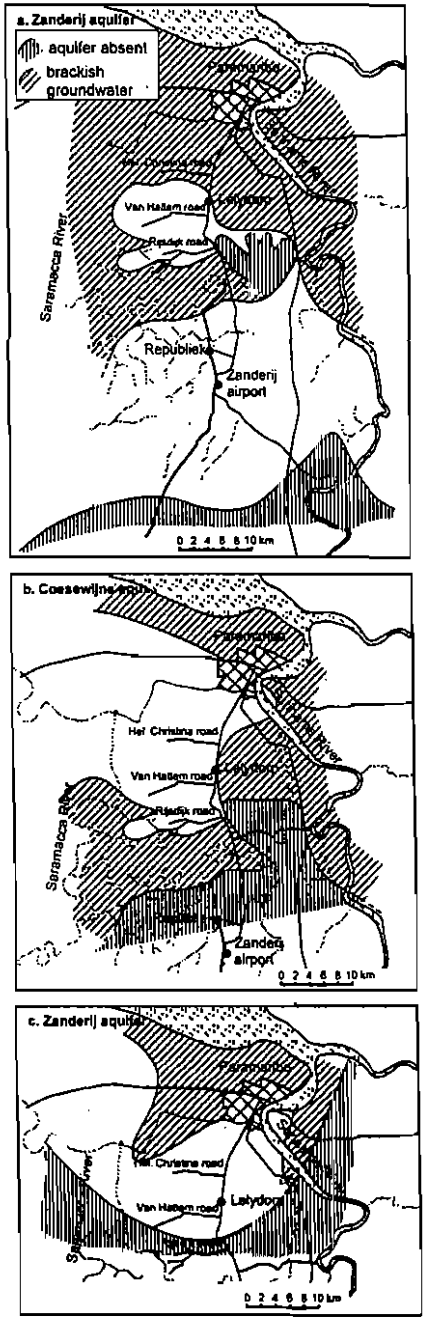

Figure 3.7. Fresh groundwater in the coastal aquifers of Suriname around Paramaribo (from Groen, 1998)

Holocene coastal plain salinity has been partly flushed. The depth of freshening depends on the time of retreat of the sea (Brinkman and Pons, 1968) and the permeability. The sandy beach barriers, in particular, contain fresh groundwater lenses, which were exploited by open wells before public water supply was established in 1933.

The Tertiary sediments contain relatively fresh groundwater of meteoric origin. The North-South section of Figure 3.5 shows that an actual interface between fresh and saline groundwater does not exist near the coastline, as hydrogeologists feared in the past (Groen, 1998) . Groundwater increases only very gradually in the seaward direction. Groundwater with low chloride content (< 2.000 mg/l) extends even 90 km into offshore shelf deposits. Fresh potable water with chloride concentrations below 250 mg/l is found South of Paramaribo, though the pattern differs for the various aquifers (Figure 3.7). In the far South of the coastal plain pockets with brackish groundwater are found. These are probably related to the short incursion of the sea in the incised Pleistocene valleys around 6 to 8 ka BP, when also the Mara deposits were formed (Roeleveld and Van Loon, 1979; Groen, 1998). Pristine groundwater, not affected by salinization (Cl < 50 mg/l) is found below the active recharge areas of the savannah belt and the Lelydorp sands (Figure 3.5).

Highly mineralised brackish and saline water is also found in the Cretaceous sediments in the lower part of the sedimentary wedge at depths of about 300 m (Figures 3.5 and 3.8).

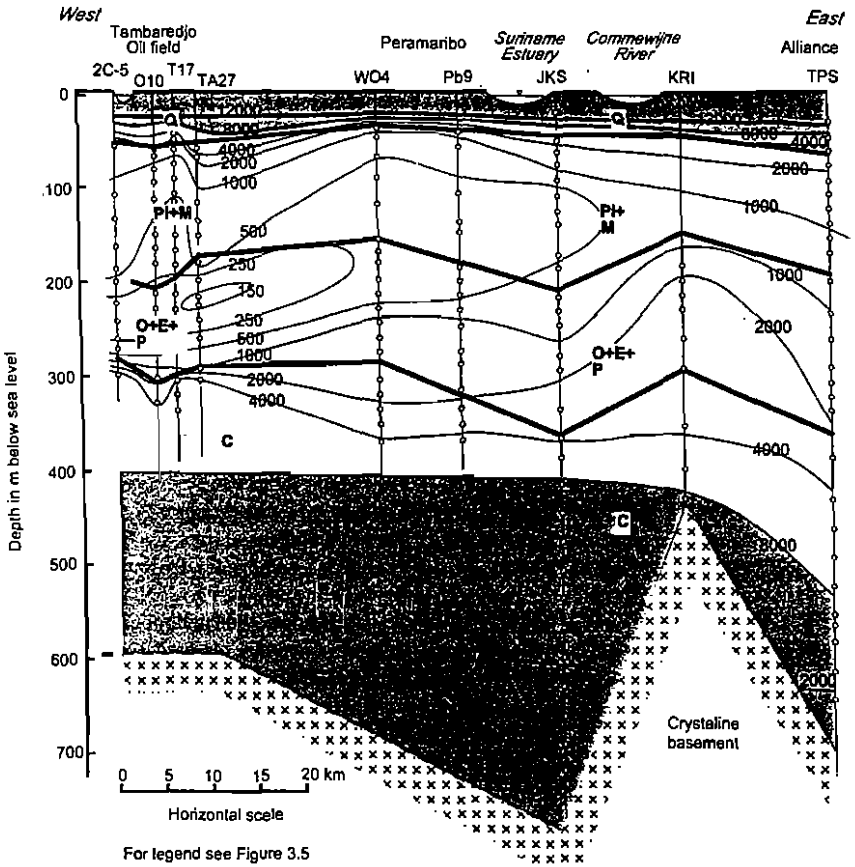

Figure 3.8. East-West geological section with groundwater salinities near Paramaribo, Suriname.

3.6.3. *Groundwater flow systems in the Tertiary formations*

The groundwater flow systems in the Pliocene sands of the savannah belt are local systems, as discussed above. Groundwater from this zone does not reach the Tertiary aquifers in the coastal plain. Also in the coastal plain local groundwater flow systems do not extend into the Tertiary formations either, because of the high hydraulic resistance of the Quaternary clays. Moreover, sub-recent heads in the Tertiary aquifers were equal to, or higher than, the phreatic water levels (Figure 3.9). An exception is the broad complex of sand barriers near Lelydorp. The elevated terrain and low drainage density there lead to relatively high groundwater levels, even higher than the heads in the Pliocene (Zanderij) aquifer (Figure 3.9). Given the hydraulic resistance of the Quaternary clays, a downward flux or recharge of 10 to 30 mm/a is estimated. In this area a flow system has developed in the Pliocene aquifer. Groundwater modelling (Post, 1996; Groen, 1998) showed, however, that this groundwater is discharged locally by seepage into the bordering creeks and swamps.

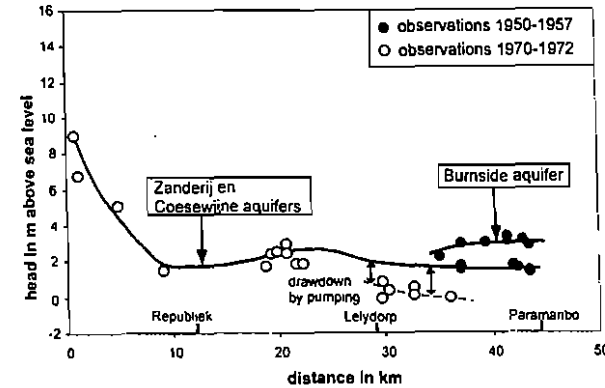

Figure 3.9. North-south section with groundwater heads before the sub-recent or pre-pumping period (after UNDP/WHO, 1972).

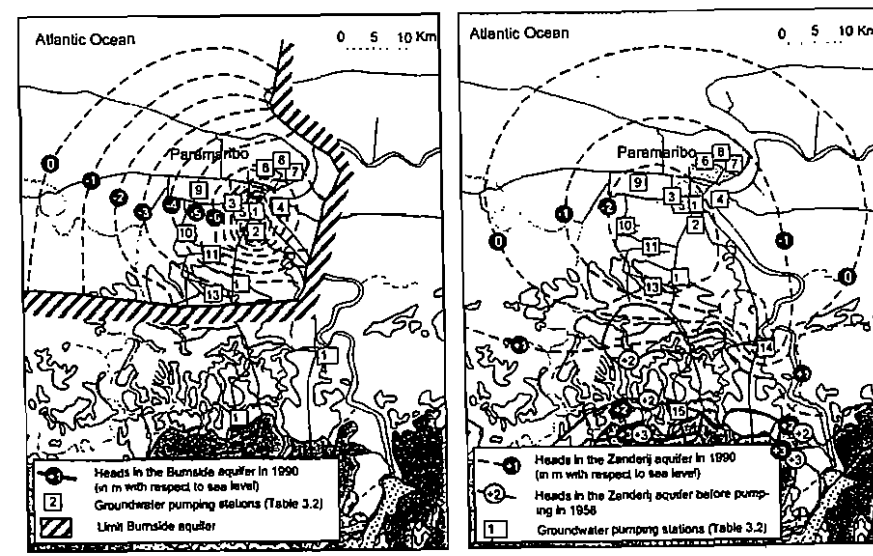

Figure 3.10. Piezometric heads in Zanderij aquifer in 1990 and 1950.

Sub-recent groundwater heads (Figure 3.9) and groundwater modelling results (Figure 3.10; Groen, 1998; Post, 1996) showed that the remaining part of the groundwater in the Tertiary formations was essentially stagnant before large-scale pumping started. The present natural flow systems cannot explain the genesis of this stagnant and more mineralised part of the groundwater, which therefore is denoted as paleogroundwater. Indeed, earlier studies (UNDP/WHO, 1972; Verleur, 1991) showed that this groundwater dates from the Last Glacial Maximum to Early Holocene (30 to 8 ka BP. In the next chapter a more detailed

account is given of the past flow systems, which to the formation of paleogroundwater.

Pumping by well fields in and around Paramaribo during the last 40 years has led to large declines in regional groundwater heads (up to 25 m), and dominates the entire flow field in the coastal plain.

Sub-recent heads in the deep Oligocene Burnside aquifer were artesian (+ 3.5 m), a condition also found in other parts of the coastal plain like Nickerie, Suriname (UNDP/WHO, 1972) and the coastal plain of Guyana (Ramsahoye, 1959; Arad, 1983; Groen, 1998). This phenomenon cannot be explained easily, as the aquifer has no outcrop and groundwater advection from the elevated savannah recharge area is impossible given the gradients in the aquifers (Figure 3.9) "Ocean loading", suggested by Dixon (1971), does not hold either, as the wedge of high-density seawater cannot create such an overpressure. It is more likely that the artesian heads are the result of the rapid Holocene sedimentation. Instantaneous "sediment loading" initially evokes increased pore-water pressures and intergranular pressures. The first normally quickly dissipate by upward seepage. In this case, however, the overlying Coesewijne clays must have a very high hydraulic resistivity, which has retarded this process. Heads in the Saramacca Formation are probably even higher than those of the Burnside Formation. A study of the oil reservoirs in Suriname by Noorthoorn van der Kruijff (1970) reports that the fluids in the Saramacca Formation are over-pressurized with respect to hydrostatic pressure.

3.6.4. Groundwater recovery

Groundwater recovery for the public water supply started in 1933 with the Republiek production station, some 45 km south of Paramaribo (Figure 3.1). This well field, which is still operational, pumps groundwater of excellent quality at shallow depths from the Zanderij aquifer. Earlier (in 1903), an exploration well revealed the presence of potable water in the Coesewijne and Burnside aquifers in the very heart of Paramaribo. Because groundwater in these aquifers had relatively high chloride contents (170 mg/l), the Dutch water-supply engineers thought that saline groundwater was close to the wells and feared imminent salinization of the wells (Groen, 1998). This fear was fed by the serious problem of salt-water intrusion in coastal wells in the Netherlands at that time.

Only in 1958 the first well field was established at the W.K. Plein in Paramaribo, to be followed by several others in and around Paramaribo during the 20 years thereafter (Groen, 1998). Table 3.2 displays a list of all pumping stations with their 1990 extractions, which were used for the numerical groundwater model (Section 4.3.2.). Most groundwater is pumped from the Coesewijne and Burnside aquifers. Since 1997 a large pumping station at the Van Hattemweg has become operational, which extracts groundwater from the Zanderij aquifer.

Nr	Station name	Aquifer	Production in m^3/h in 1991 (model)
1	Benie	Burnside	50
2	Flora	Burnside	100
3	Helena Christina	Burnside	70
		Coesewijne	260
		Zanderij	70
4	Paranam	Zanderij	830
5	Koewarasan	Burnside	80
		Coesewijne	140
		Zanderij	70
6	Leiding 9a	Coesewijne	460
7	Leysweg	Burnside	150
		Coesewijne	375
8	Livorno	Burnside	450
9	W.K. Plein	Burnside	700
		Coesewijne	40
10	Meerzorg	Burnside	100
11	Lelydorp	Zanderij	250
12	Republiek	Zanderij	375
13	Tourtonne	Coesewijne	60
14	Blauwgrond	Coesewijne	60
15	Van Hattemweg	Zanderij	1000 (after 1997)

Table 3.2. Pumping stations in and around Paramaribo. (Numbers refer to location in Figure 3.10)

Chlorinities of produced groundwater at these well fields vary from 150 to 400 mg/l and display a very slowly rising trend with time. This can be explained from the chlorinity pattern in the Tertiary aquifers described above, which shows only a very gradual increase towards the North (Figure 3.5). Another problem are the steadily declining piezometric heads in the aquifers. At the W.K. Plein regional heads in the Burnside aquifer declined from +3.5 m (artesian) to -25 m. Obviously, groundwater recovery from the Burnside and Coesewijne aquifers has not induced much recharge and is, in fact, mining. Groundwater levels and also the regional flow pattern in the coastal plain became completely controlled by the extractions, even in the Zanderij aquifer (Figure 3.10.). Apart from increasing pumping costs, the declining groundwater heads may over time lead to land subsidence, a problem not uncommon in coastal plains with overexploitation of groundwater, like those near Bangkok and Jakarta.

In the seventies a quest for more sustainable groundwater exploitation started (Groen, 1998). It appeared that sustainability can only be guaranteed in the far south near Republiek, where there is ample recharge (UNDP/WHO, 1972; IWACO/F.R.Harris, 1991). However, exploitation there appeared not feasible financially, because of the distance and the presence of extensive swamps. Bank infiltration along the major Saramacca and Suriname rivers has also been contemplated, but salt-water tongues extend far upstream in these rivers. Finally, in 1997, a new large well field has been put in operation along the Van Hattem road, South of Lelydorp. This well field exploits a large isolated body of groundwater of low chloride content (< 50 mg/l) (IWACO/F.R.Harris, 1991). Active recharge is taking place here (see above), but it does not balance the pumping rate. Nevertheless, the present production could be doubled and still last for about 100 years. At this moment there is still a serious water supply shortage. If everlasting sustainability is not required, there is still ample scope for groundwater recovery from the Coesewijne and Burnside aquifers south and southwest of Paramaribo, using properly designed well fields. The well fields in and close to Paramaribo should be abandoned in the course of time.

3.7. Conclusions

The main aquifers in the coastal sedimentary zone of Suriname consist of sand layers in the Tertiary formations. Recharge is only taking place in the savannah belt (Pliocene

sands) in the south and on the Lelydorp sands in the coastal plain. This recharge participates in small groundwater flow systems and is locally drained. Until recently most groundwater in the Tertiary formations of the coastal plain was more or less stagnant. The (former) body of stagnant groundwater is fresh to moderately brackish and extends 90 km into the offshore groundwater, where chloride contents are still below 2000 mg/l. Saline groundwater is present in the upper 30 m of Holocene and Pleistocene clays and in the fine-grained Cretaceous sediments below 300 m. The groundwater extractions, realized around Paramaribo after 1958, created a man-made regional flow pattern in the coastal plain. Natural recharge does not balance the extractions and therefore groundwater mining leads to large declines in groundwater levels and salt-water intrusion. The latter problem is not as severe as suspected, because salinity variations in the aquifers are very gradual.

Chapter 4.

Freshening of the coastal and offshore sediments during the Wisconsinan regression: a reconstruction of paleogeography and groundwater flow systems

4.1. Introduction

The Suriname data (Chapter 3) showed that paleogroundwater of low salinity (< 2,000 mg/l) in the Tertiary sediments extends about 90 km into the offshore zone. The stagnant conditions and the high age indicate that this groundwater has been formed by extinct flow systems of Wisconsin and Early Holocene age. Note that, at the end of the preceding Sangamonian transgression, the sea level had reached a level even higher than today. At that time the coastal and offshore Tertiary sediments were probably saturated with saline and brackish groundwater. This assumption is based on the fact that during the early stages of the Sangamonian transgression, these sediments were not yet protected against saline intrusion by the Coropina clays (Chapters 5 and 10). Freshening during the Wisconsinan spans a period of 100 ka. However, the meteoric groundwater, found more than 90 km offshore, must have been formed during a much shorter period: these remote parts of the shelf were only exposed during the Last Glacial Maximum (25 to 15 ka BP), when sea-level was more than 100 m below present level (Figure 4.1; Linsley, 1996). As recharge appears to be very limited at present, the question now arises what kind of flow systems could have created this vast body of meteoric groundwater in the past.

In order to address this question in this chapter special attention is being paid to the paleogeographical development. After the sea has retracted during a regression, topography-driven flow systems expand downward and seaward, and saline groundwater in their domains is driven out. This does not take place via a simple push-through mechanism. Because of macro-dispersion at a regional scale, meteoric groundwater has to pass several times through the flow domains before salinities reach a steady-state (Domenico and

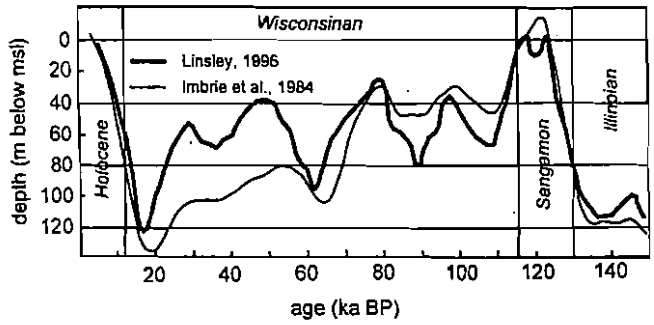

Figure 4.1. Sea level during the last 150 ka (after Imbrie et al., 1984 and Linsley, 1996)

Robbins, 1985). Freshening of deep aquifers in the domain of primary flow systems requires relatively long periods. In fact, residence times in these flow systems may even be longer than the lifetime of the system itself. On the other hand, sediments in the domain of secondary and tertiary flow systems with small residence times are flushed more rapidly. These flow systems are related to erosional or sedimentary relief forms superimposed on the regional slope (Toth, 1963, 1995; Engelen and Kloosterman, 1996; De Vries, 1974). Examples of the sedimentary forms are beach barriers and dunes in aggrading Holocene coastal plains, like the coastal dunes in the Netherlands, where underlying sediments have been freshened to depths of 40 to 60 m in a period of about 800 years (Stuyfzand, 1993). Erosional relief in coastal plains is not so common in present marine coastal plains, but may have been important after a relative fall of sea level during the Wisconsinan glacial.

A reconstruction of the paleogeographical conditions of the coastal plain and shelf of Suriname is presented in the following. Based on these reconstructions, paleoflow systems are conceptualized and investigated by numerical groundwater models for their efficiency in causing extensive freshening. Some results from this study have been published earlier in (Groen et al., 2000b).

4.2. Paleogeography of the Suriname coastal plain

4.2.1. Sea level and coastlines

During the early and middle part of the Wisconsinan, sea level varied between 40 to 65 m below present sea-level (Linsley, 1996). Taking into account 20 m of Holocene sedimentation in the southern part of the shelf, the coastline must have been located 40 to 85 km further northward. During the last glacial maximum between 25 and 15 ka BP, sea-level declined to values around - 100 m (below present sea level) with minimum of -130 m at 18 ka BP (Linsley, 1996; Fairbanks, 1989). During this period the coastline was located even 130 to 150 km north of the present coastline. After the steep rise at the beginning of the Holocene (12 ka BP) the level reached its present level at 6.5 ka BP (Figure 4.2; Roeleveld and Van Loon, 1979; Fairbanks, 1989). Given an average gradient of 1 : 1500 for the Pleistocene surface and a rate of sea-level rise varying between 9 and 22 mm/a, the coastline must have moved landward over the shelf at a rate of 13.5 to 33 m/yr. The sea penetrated first the incised fluvial paleochannels, forming a ria coast until the sea-level rise slowed down after 7 ka BP and coastal aggradation started. Submarine terraces and coral reefs at depths of 20 to 25 m on the Guiana coast indicate that around 8 ka BP (Nota, 1958) or 9 ka BP (Van der Hammen, 1963) sea-level rise temporarily halted.

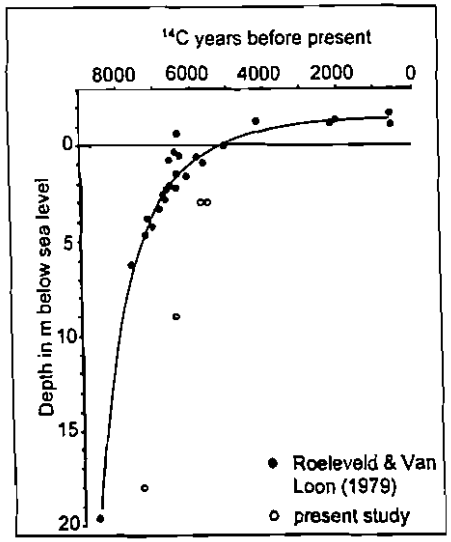

Figure 4.2. Sea level rise along the Suriname coast (after Roeleveld and Van Loon, 1979).

The data from this study do not fall on the sea level curve of Roeleveld and Van Loon (1979) (Figure 4.2). This is because radiocarbon dating has been carried out on organic material and shells in the Holocene clays, which were deposited in a shallow sea. Roeleveld and Van Loon carried out dating on peat deposits, which were formed close to sea level.

4.2.2. Topography

During the Wisconsinan regression fluviatile erosion dissected the flat Sangamonian landscape (Tricart, 1985; Clapperton, 1993; Thomas and Thorp, 1996). The Amazon and Orinoco rivers created deep paleochannels on the continent and the shelf (up to 100 m), which were filled up later with Holocene deposits. Erosion also took place in the coastal plain and on the shelf of Suriname (Brinkman and Pons, 1968; Roeleveld, 1969; Veen, 1970; Roeleveld and Van Loon, 1979; Wong, 1986) found several deep gullies (up to 10 m) in the Pleistocene coastal plain filled with Holocene Mara deposits. The drainage pattern of these former creeks can still be recognized on the Pleistocene coastal plain in the present meandering swamps and creeks. The drainage density varied between 0.3 to 1 km/km^2. Also the large Suriname and Saramacca rivers must have eroded into the sediments of the coastal plain and continental shelf. Bathymetric and seismic surveys on the Suriname shelf revealed paleochannels related to the Marowijne and Coppename rivers, respectively west and east of the study area (Nota, 1971, Frappa and Pujos, 1994). Core drilling for this study (Chapter 4) and unpublished data from existing boreholes and cone penetration tests show that near Paramaribo the bottom of the paleochannel of the Suriname River was about -35 m (below msl).

4.2.3. Vegetation

Palynological records demonstrate that extensive grass savannahs with *Curatella* and *Byrsonima* shrubs covered the coastal plain of Suriname and Guyana during certain periods of the Wisconsinan regression (LGM) and earlier regressions (Van der Hammen, 1974). This corresponds remarkably well with the floristic composition of "Welgelegen", or clay savannahs, we find nowadays on some well drained clay and silt soils in the Pleistocene coastal plain (Van Donselaar, 1965). This particular type of savannah may have been much more common during the last glacial. Though the Holocene climate change set in at about 12 ka BP, the savannahs disappeared only after 9 ka BP (Markgraf, 1993). The present grass and woodland savannahs are relicts of the vast Wisconsinan savannahs and could only persist because of the poor soil conditions and burning by the Amerindian population (Jansma, 1994).

4.2.4. Climate

Van der Hammen and Absy (1994) and Van der Hammen (1974) estimate that precipitation during the LGM must have been about 500 to 1,000 mm/a to sustain a natural grass savannah or 1,000 to 1,500 mm/a for a mixed grass/woodland savannah. They also state that the rainfall regime was more seasonal with a prolonged dry season. This agrees with predic-

tions of 750 to 1500 mm/a for the LGM by global climate models (Kutzbach et al., 1998).

During the Early Holocene precipitation increased (Markgraf, 1993). Global climate model (GCM) simulations show that rainfall still was concentrated in the summer monsoon. This may explain the persistence of the savannahs during the Early Holocene. Palynological studies (Van der Hammen and Absy, 1994), GCM simulations (Kutzbach et al., 1998) and noble-gas studies of groundwater in Brazil and New Mexico (Stute et al., 1995; Stute and Bonani; 1995) all show that the average yearly temperature was about 5 to 6 °C lower than today during the LGM. According to (Kutzbach et al., 1998) yearly actual evapotranspiration was 15 % lower than today, which leads to a figure of 1300 mm/a in Suriname.

4.2.5. Hydrology during the LGM

The paleogeographical conditions described in the preceding sections enables us to define a conceptual model of the hydrological processes during the last glacial and the LGM in particular. In following chapters this concept will be quantified and refined using isotopic and hydrogeochemical data and simulation models.

Because of the lower and more seasonal rainfall runoff during the last glacial has been smaller than today, but also more variable. Nevertheless, the Saramacca and Suriname rivers, with their large catchments, would still have had a substantial base flow during the entire year. Water levels of these rivers were probably not much higher than the base of the incised paleochannels.

In the savannah belt, runoff processes during the last glacial were not much different from today, though recharge must have been lower and the smaller creeks probably had a more ephemeral character. Despite the large uncertainties in the paleoclimate, we may conclude that in the savannah belt recharge to the Tertiary aquifers was lower than 200 mm/a during the LGM, which is much less that the present amount of 500 mm/a (Section 3.5.1.).

Estimating recharge in the coastal plain is more difficult, as it depends mainly on the heads in the Zanderij aquifer below the Quaternary clays (see next section). Conditions on the Pleistocene surface in the present coastal plain and continental shelf were much different (up to 140 km offshore during the LGM). This surface had a relatively flat sloping primary topography and a secondary topography of incised creeks. The interfluvial areas formed clay plateaus, which are preserved as the "schollen" landscape in the present Pleistocene coastal plain (Section 3.3.). Most rainfall on the clay plateaus was drained by overland flow, similar to what we observe today in the coastal plain. Most likely, the incised creeks between the plateaus only carried water during the monsoon season. Because of the low permeability of the subsoil and the low drainage density, base flows were very low. If there were any seepage into the creek valleys, it would have been entirely consumed by the vegetation in the gallery forests in the valleys. This situation can now be observed in some regions in West and South Africa with little rainfall or a strong seasonality in rainfall. On the flat clay plateaus marshy conditions must have existed during the summer monsoon, with phreatic groundwater levels close to the surface. Groundwater heads in the Pliocene sands below the clays must have been much lower, as they were controlled by the water levels of the South-North running Suriname and Saramacca rivers, which were deeply incised into the Pliocene Zanderij formation. The relatively low heads induced downward seepage and recharge to the Tertiary aquifers (Figure 4.3). This recharge, though small per unit surface area, acted on the entire coastal plain and continental shelf and may have been greater than the recharge in the

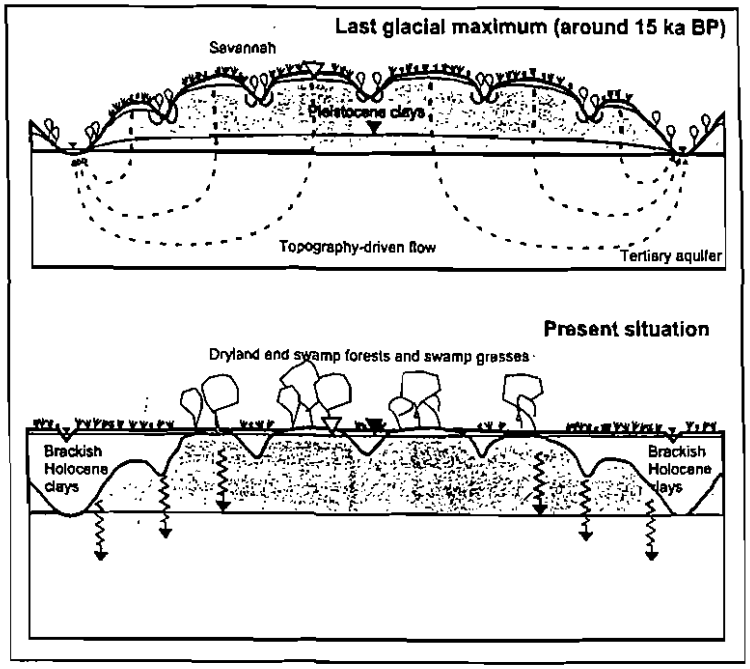

Figure 4.3 Present and paleohydrological conditions on the surface and in the Quaternary clays.

Zanderij aquifer outcrop. The recharge and the resulting flow systems in the Tertiary aquifers were halted by the encroaching sea in the Holocene, but probably persisted in the present coastal plain to 9 ka or even 7 ka BP. In this period the sea intruded the paleochannels of the Suriname and Saramacca rivers and the grass and shrub savannahs disappeared (Markgraf, 1993). River erosion may even have increased during the Early Holocene, as rainfall increased, while retaining its strong seasonality (Markgraf, 1993; Kutzbach et al., 1998).

The next section deals with the question, whether this hypothesized recharge mechanism and the resulting flow systems were sufficient to flush all brackish and saline groundwater from the Tertiary sediments up to the outer part of the continental shelf during the last glacial.

4.3. Paleohydrological modeling

4.3.1. Introduction

The hypothesis from the preceding section - i.e. that flow systems related to the primary and secondary erosion topography of the Pleistocene surface were responsible for the formation of onshore and offshore paleogroundwater in Suriname - has been verified with a

numerical groundwater model. For this purpose, first a steady-state groundwater model of the sub-recent situation was constructed (Model A) and calibrated with groundwater heads from this period. Next, a non-steady-state model was made for the present (1990) situation (Model B), and calibrated with present groundwater heads. Finally, the model was adapted to the paleohydrological situation during the LGM (Models C and D). This paleomodeling study has been reported in greater detail in Groen et al. (2000b).

4.3.2. Recent and sub-recent modelling

For the groundwater simulations, a model for the Paramaribo coastal plain was constructed based on the MICROFEM code (Diodato, 1997). The MICROFEM code is a finite element code for simulation of quasi three-dimensional, non-stationary groundwater flow in a system of aquifers separated by semi-permeable layers. For the construction of this model, earlier groundwater modelling studies of the Pliocene and Miocene aquifers (IWACO/F.R. Harris, 1991) and the Oligocene aquifer (Hutchinson, 1990) have been consulted. The model comprises the following five aquifers (Figures 3.4 and 3.5): (i) Zanderij (Pliocene), (ii) Upper Coesewijne (Miocene), (iii) Lower Coesewijne (Miocene), (iv) Burnside (Oligocene) and (v) Saramacca (Eocene and Paleocene). The first version of this groundwater model was made by Post (1996). The modelled area is shown in Figure 4.4.

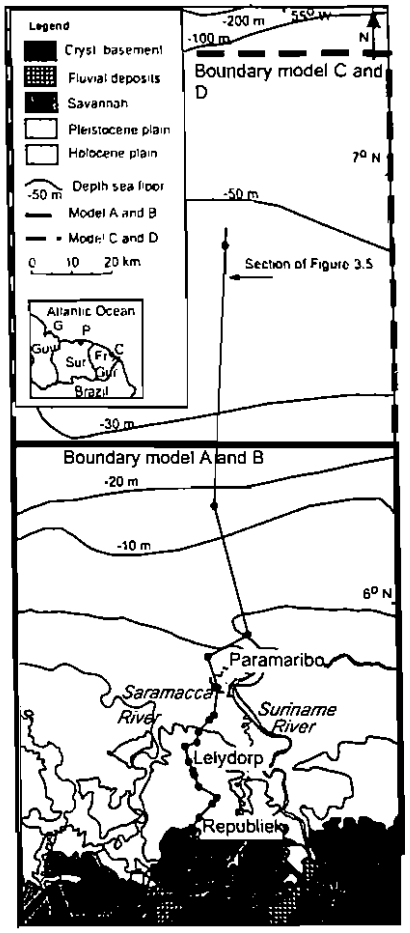

Figure 4.4.
Boundaries of numerical groundwater models.

A large modelling area was chosen to account for the large leakage factor caused by the high hydraulic resistances of the clay layers. The southern border is a no-flow boundary coinciding with the basement outcrops south of the savannah belt. Also the western and eastern boundaries are no-flow boundaries, which are assumed to follow the general South-North flow paths. The northern boundary of the models simulating recent (1990) and sub-recent (1957) conditions, model B and A respectively, is located 40 km offshore in the Atlantic Ocean and contains fixed fresh-water heads in all aquifers. In the coastal plain and offshore, fixed heads were assigned to the nodes of a top system: in the coastal plain they represent the level of phreatic groundwater in the Quaternary clays; offshore the heads correspond to fresh-water heads, calculated from the offshore wedge of seawater and saline groundwater. These heads are generally +1 to +2 m except for the elevated Lelydorp sand barriers, where heads of +4 m are maintained. For the outcrop of the Pliocene Zanderij aquifer in the savannah belt, a fixed recharge of 500 mm/a is imposed on the nodes. Model A (1957 situation) was run in steady-state and calibrated with the data from the 1950-1957 period. Then the non-steady-state run was made by introducing the various abstractions in the period between 1958 and 1990. The final situation in 1990 (model B) was calibrated with heads measured in the period 1987-1990. The procedure was repeated several times until a reasonable fit was reached. The average difference between measured and calculated heads in the Zanderij and Coesewijne aquifers for the 1990 situation was 0.49 m and equal to the modelling study of IWACO/F.R. Harris (1991). Comparing measured and calculated heads for the Burnside aquifer was more difficult because most observations were done within the cones of depressions around the pumping station. Differences varied from 0.25 to 2.00 m just as in the study of Hutchinson (1990). In Figure 4.5 groundwater heads in the Zanderij and Burnside aquifer are shown calculated by model A (1957 AD) and model B (1990 AD). The contour maps show that groundwater flow in the coastal plain in 1990 is completely controlled by groundwater extractions, while before 1958 almost stagnant conditions prevailed.

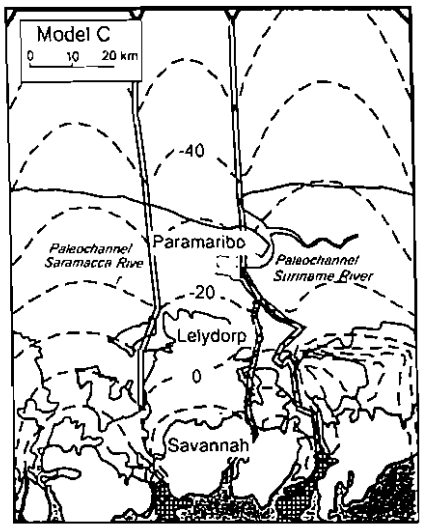

Figure 4.5. Simulated heads in the Zanderij aquifer during the LGM

4.3.3. Modelling the paleohydrology of the Late Glacial Maximum

In order to study the groundwater flow systems during the LGM and the role of the erosional relief, paleohydrological models (model C and D) were constructed on the basis of model A. These models have only experimental value as the offshore permeability distribution is largely unknown apart from a general trend of decreasing permeabilities as sediments becomes finer towards the North. During the LGM the coastline was located close to the shelf break, 140 km north of the present coastline (Figure 4.4). Therefore, the northern boundary of the models was extended to the shelf break, where no-flow conditions were imposed in all aquifers.

In model C, fixed heads along the Suriname and Saramacca Rivers were set equal to the bottom of the paleochannels, which grades from the present river bottom at the edge of the crystalline basement in the south to a depth of 30 m relative to the Pleistocene surface at Paramaribo and finally to an assumed depth of 15 m below the Pleistocene surface (seafloor) at the shelf break. Recharge on the Zanderij outcrop (present savannah belt) was lowered from 500 to 200 mm/a (see Section 2.5.). In model C the top system in the coastal plain was turned into a phreatic system with fixed recharge. Also, a drainage level of 10 m below the Pleistocene surface (depth of the creeks) and a drainage resistance of $5 \cdot 10^5$ days were assig-

ned to all nodes. The drainage resistance, calculated by relations given by De Vries (1974), is quite high because of the low permeability of the clays and the large spacing of the creeks. By trial and error, the recharge rates on the coastal plain were varied until groundwater levels were close to the Pleistocene surface. This was based on the assumption that marshy conditions prevailed on the flat and badly drained clay plateaus. For verification a second paleohydrological model (model D) was made without incised paleochannels in order to investigate the effect of the erosional relief. In this case, all nodes on the coastal plain were assigned fixed heads equal to the Pleistocene surface.

Simulations with model C showed that infiltration occurs everywhere on the clay plateaus in the Pleistocene coastal plain. Recharge varies between 44 and 56 mm. Because of the high drainage resistance only a small part (< 2 %) of this amount exfiltrates in the incised creeks on the clay plateaus. Most part of the infiltrated groundwater seeps downward to the underlying Pliocene Zanderij aquifer. This aquifer is drained by the deeply incised Suriname and Saramacca rivers, as is shown in Figure 4.5. This flow system is called a secondary flow system as it is controlled by the secondary topography created by erosion of the major Suriname and Saramacca rivers. Heads in the deeper aquifers are less controlled by the major rivers and indicate a more regional pattern with recharge on the clay plateaus in the southern part of coastal plain (present coastal plain and southern part of the shelf) and discharge in the floodplains of the Saramacca and Suriname rivers in the north (northern part of the shelf). In Figure 4.6 groundwater age zones in the aquifers are presented. Note that these ages refer to time elapsed after recharge. In the upper Zanderij aquifer groundwater is relatively young (< 0.5 ka) throughout the coastal plain, because of the rapid circulation in the secondary flow systems. Clearly, saline groundwater in the domain of these secondary flow systems could have been flushed entirely, even in the outer part of the shelf, which was exposed only during the LGM. The deeper aquifers belong to the domain of the primary and regional flow system. In this domain groundwater ages vary from a few hundred years in the southern to 20 ka in the northern and outer part of the shelf. This implies that saline water in the primary flow domain could not have been flushed from the outer part of the shelf

In model D, without the erosion topography, only a primary groundwater flow system exists. Recharge occurs in the southern part of the exposed shelf, up to 25 km offshore from the present coast. Upward seepage dominates in the outer part of the shelf. Groundwater

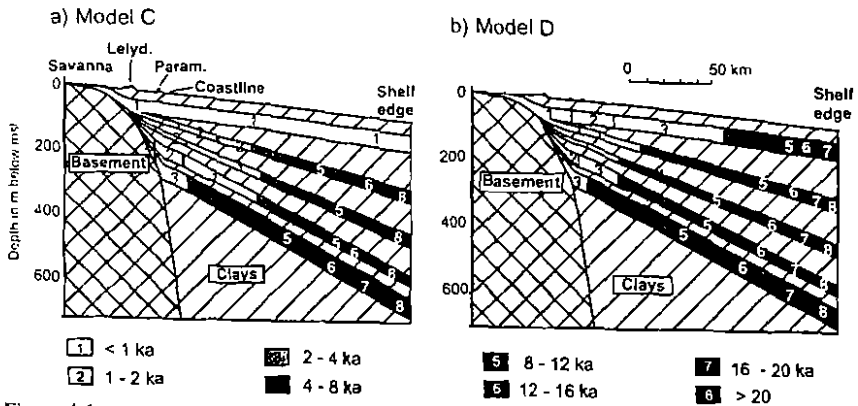

Figure 4.6. Groundwater ages calculated by paleohydrological models C and D.

recharge varies from 5 to 13 mm/a in the zone coinciding with the present Holocene coastal plain and 20 to 50 mm/a in the present Pleistocene coastal plain. Highest values are found in the zone between Rijsdijk Road to Republiek, where the Pleistocene clay layer (Coropina Formation) is relatively thin. Groundwater ages in the deep aquifers are about equal to those in model C. Only in the outer northern part of the shelf, ages are higher than in model C. According to model D saline groundwater could not have been flushed from the outer part of the shelf.

4.4. Discussion and conclusions

The stagnant body of fresh and moderately brackish groundwater, extending from the coastal plain to more than 90 km offshore, cannot have been produced by the present flow systems (Chapter 3). This paleogroundwater has been formed by different groundwater flow systems during the Wisconsinan regression (115 ka to 12 ka BP). During this period sea level was much lower and large parts of the continental shelves were exposed. During the LGM (25 to 15 ka BP) sea level dropped more than 100 m with respect to the present level. In that period the coastline was located 140 km further north. Climate was colder (5 °C difference), dryer (50 %) and had a more seasonal rainfall pattern (boreal summer monsoon). Grass and shrub savannahs covered the Pleistocene surface. Rivers and creeks eroded the surface and created a landscape of clay plateaus and incised valleys (10 to 30 m deep). Perennial runoff only occurred in the large Suriname and Saramacca rivers. Because of the incised rivers groundwater heads in the Zanderij aquifers were much lower than today, which induced widespread recharge. The larger recharge and the erosion relief created secondary flow systems superposed on a primary and regional flow system (Figure 4.7). Paleohydrological groundwater models showed that the primary flow system could not have led to freshening of the outer part of the shelf within the short period of the LGM. Only the residence times in the secondary flow systems were short enough to allow several flushings of the upper aquifers. The conclusion is that during the Wisconsinan regression secondary flow systems existed, related to an erosion topopgraphy, which is now obscured by Holocene sediments. These systems played an essential role in freshening the upper Tertiary sediments.

Paleohydrological modeling, using these quasi-3D hydraulic groundwater models, is useful for qualitative interpretation and the creation of conceptual ideas, as described above. In the first place, there are too many unknown hydrogeological parameters, especially in the offshore zone, for a realistic simulation. In the second place, the applied code is not suitable to study the actual process of freshening, as it does not take into account solute transport and variable-density flow. It would be interesting to use variable-density flow codes, like the one presented in the last chapter, to study the dynamics of freshening on large temporal and spatial scales.

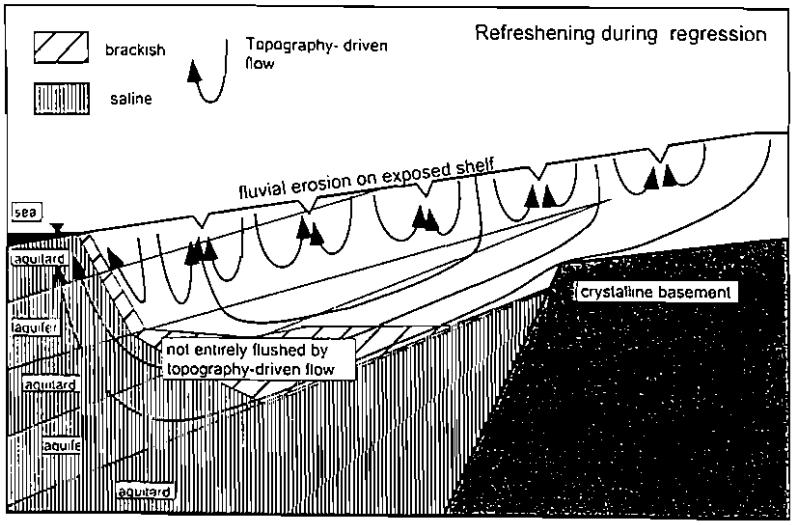

Figure 4.7. Freshening of the coastal and offshore deposits during a transgression by primary and secondary flow systems.

Chapter 5.

Salinization of the coastal and offshore sediments during the Holocene transgression: a study of diffusive solute transport

5.1. Introduction

In the coastal and offshore Tertiary sediments of Suriname a large stagnant body of fresh to moderately brackish groundwater is present (Chapter 3; Figure 3.5). It was motivated in Chapter 4 that this groundwater was formed by extinct flow systems, that were active during the Wisconsinan regression. This meteoric groundwater is, therefore, denoted as paleogroundwater according to the definition proposed in Section 2.4. Pristine groundwater (section 2.1) with chlorinities less than 50 mg/l occurs only in the present recharge areas of the savannah belt and the Lelydorp sands (Figure 3.5; Sections 3.6.2. and 3.6.3.). The remaining and major part of meteoric groundwater in the Tertiary formations, the actual paleogroundwater, is more mineralised with chlorinities up to 2,000 mg/l (Figures 3.5 and 3.8), though originally, the chloride content of this groundwater must have been lower and comparable to present pristine groundwater. It is most likely that salinization of the paleogroundwater started after the marine submersion of the shelf during the Holocene. In this chapter we will have a closer look at the salinization process, which is related to horizontal advection or vertical transport from the overlying and underlying saline sediments (Figure 3.5 and 3.8).

Horizontal advection takes place, when the shoreline advances landward during a transgression and the fresh/saline interface moves along with it, driven by density differences in groundwater. Meisler et al., (1984) studied the dynamics of a fresh/saline interface in a confined aquifer 90 km offshore from New Jersey (Hathaway et al., 1979), where conditions are comparable to those in Suriname. Using a numerical groundwater model, they found out that the interface there is moving landward with a speed of 0.03 m/a under influence of the Holocene transgression. Essaid (1990) carried out a similar study in Monterey Bay, California and reported values of 0.05 to 0.2 m/a. On the other hand shorelines migrated landward with a speed varying between 3 and 180 m/a during this time, based on rates of sea level rise of 10 to 30 mm/a (Cronin, 1983) and shelf slopes of 1/6000 to 1/300. Comparison of these figures shows that the fresh/saline interface in groundwater lags behind the advancing Holocene shorelines and that salinization of former meteoric groundwater is mainly the result of vertical transport. This applies to Suriname but is probably of more general significance, as will be discussed in chapter 10.

Salinization by vertical salt transport may take place as convective density-driven flow. Under certain critical conditions, density currents, in the form of downward protruding fingers of saline water, arise in groundwater with an inverse density stratification (Wooding et al., 1997a, 1997b). In this case, the reverse stratification relates to saline groundwater, deposited by the encroaching sea, on top of fresh groundwater. Van der Molen (1958, 1989) and Gieske (1991) believe that convective density flows may have been responsible for the rapid salinization of the mainly sandy formations in the coastal plain of the Netherlands. They calculated the approximate velocity of downward moving fingers of saline water and concluded that in a period of less than 200 years more than 200 m of sandy sediments could have been

become brackish or saline. The fact that paleogroundwater is still well preserved in the Suriname case, is an indication that this process has not played an important role. This will be substantiated further in Section 5.3.1.

In the absence of convective density currents, slow downward diffusion of salts after the Holocene transgression becomes the dominant salinization process of the paleogroundwaters in the upper Quaternary and Tertiary formations. Below a certain point brackish groundwater may contain salts from a much earlier marine transgression. This zone is part of the dispersive transition layer existing before the Holocene transgression. Upward diffusion from this zone is not considered here as it proceeds much slower than downward diffusion: concentration gradients in the deep dispersive transition layer are a lot smaller than those in the sharp transition layer above the paleogroundwater, created after the transgression.

A new diffusion-sedimentation model is developed for this case; subsequently, chloride concentrations and isotope ratios, simulated with the model, are compared with observations.

This chapter is based on an earlier published article by Groen et al., (2000a).

5.2. Data

For this study numerous chloride analyses of groundwater samples from existing wells, geoelectrical soundings and geophysical logs of oil wells were available (Velstra, 1966). These formed the basis of the chlorinity patterns displayed in Figures 3.5 and 3.8. Chlorine-isotope ratios were determined for 16 samples from existing wells.

At two sites on the coastal plain, clay samples have been recovered from Holocene and underlying Pleistocene clays in order to study shallow salinity gradients. The sites at Koewarasan and Tourtonne are located near Paramaribo, about 20 and 3 km from the coastline, respectively (Figure 3.1; Annex II). Drilling was carried out according to the Ackerman method: boreholes were drilled with normal cable tool technique, while at certain depths cores were recovered by pushing a stainless casing into the borehole bottom (45 cm length and 6.5 cm diameter). The drilling logs are shown in Figure 5.1. Some shells and peat particles were dated with ^{14}C analyses (Figure 5.1). The upper 5.5 m at Koewarasan consist of grey, plastic clay and is of Holocene age. The underlying Pleistocene clays are very stiff and show distinct red, yellow and olive-green mottling. According to Veen (1970), the Pleistocene clays have been deposited during the Sangamonian transgression (130 ka to 115 ka BP). At the final depth of 19 m fine sand was found. At Tourtonne, only very plastic, grey-blue Holocene clay was encountered down to the final depth of 25 m. In both drillings, shell layers were found between 4 and 5 m.

Pore water was squeezed from 22 clay samples (9 from Koewarasan and 13 from Tourtonne) and was analysed on chloride and all major ions (Velstra, 1997). Chlorine-isotope ratios were measured on 9 pore water samples (3 from Koewarasan and 6 from Tourtonne). Isotope measurements were carried out according to analytical procedures described by Eggenkamp (1994). The chlorine isotopic ratios ^{37}R (ratio of rare isotope ^{37}Cl to abundant isotope ^{35}Cl) are reported as differences in ‰ from Standard Mean Ocean Chloride (SMOC):

$$\partial^{37}Cl = \frac{{}^{37}R_{sample} - {}^{37}R_{SMOC}}{{}^{37}R_{SMOC}} * 1000 \qquad (5.1)$$

All water samples from core drillings and wells were analysed twice. The average difference between each pair of $\delta^{37}Cl$-analyses (n= 24) was 0.07 ‰ with standard deviation 0.07 ‰.

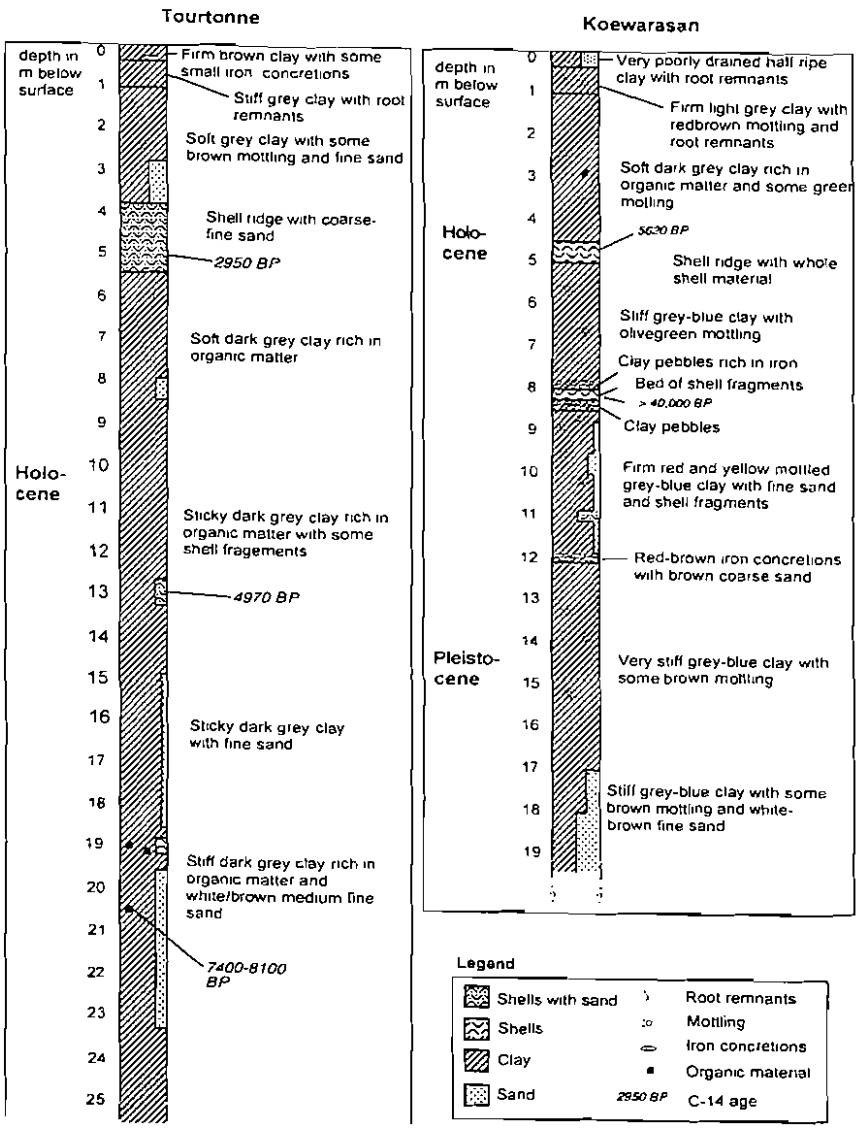

Figure 5.1. Drilling logs at Koewarasan and Tourtonne (locations shown in Figure 3.1 and Annex II).

5.3. Solute transport and fractionation

5.3.1. Downward convective solute transport

The critical conditions, under which convective density currents arise in groundwater with a reverse and linear density stratification, are attained when the Raleigh number, *Ra* exceeds $4\pi^2$ (Paschke and Hoopes, 1984; Schincariol and Schwartz, 1990), with:

$$Ra = \frac{(\Delta\rho)g\kappa H}{\mu D_e} \tag{5.2}$$

where $\Delta\rho$ is the density difference between top and bottom of the sediment layer (kg/m³), g the acceleration due to gravity (m/s²), μ the dynamic viscosity (Pa·s), κ the intrinsic permeability of the sediment (m²), H the thickness of the sediment layer (m) and D_e the effective diffusion coefficient (m²/s). Permeability, density difference and thickness are the determining factors in the Rayleigh number. As μ ($\approx 10^{-3}$), g (≈ 10) and D_e ($\approx 10^{-10}$) do not vary much and k, the hydraulic conductivity in m/day, is equal to $\kappa\rho g/\mu$ ($\rho g/\mu \approx 10^{7}$), Eq. 5.2 can be simplified to:

$$Ra = 10^{7}(\Delta\rho)kH \tag{5.3}$$

Eq. 5.3 has been applied to the Quaternary clays of Suriname with a hydraulic conductivity less than 10^{-4} m/day, a thickness larger than 20 m and a maximum density difference of 25 kg/m³ between seawater and fresh water. This results in Rayleigh numbers far less than the critical value of $4\pi^2$, indicating that diffusion is the dominating process in the Quaternary clays.

5.3.2. Diffusion

Diffusion of molecules in a liquid is a mass transport process due to random thermal (Brownian) motion of the molecules. Fick's first law describes the diffusion process as:

$$F = -D_{aq}\frac{\partial C}{\partial z} \tag{5.4}$$

where F is the flux of molecules (mol/s/m²), C the concentration of molecules (mol/m³) and D_{aq} the diffusion coefficient in water (m²/s). Combining Fick's first law with the law of conservation of mass yields Fick's second law:

$$\frac{\partial C}{\partial t} = D_{aq}\frac{\partial^2 C}{\partial z^2} \tag{5.5}$$

The equation can be solved for various boundary conditions. The most appropriate case is a semi-infinite porous medium filled with water with concentration C_0, which at the finite end is suddenly exposed to a solution with a constant concentration, C_s. With boundary conditions: $C_{z,t} = C_0$ for $z > 0$ and $t = 0$; $C_{z,t} = C_0$ for $z = \infty$ and $t \geq 0$; and $C_{z,t} = C_s$ for $z = 0$ and $t \geq 0$, the following analytical expression can be derived (Carslaw and Jaeger, 1959):

$$C_{z,t} = C_0 + (C_s - C_0)\,\mathrm{erfc}\left(\frac{z}{2\sqrt{D_e t}}\right) \tag{5.6}$$

Note that D_{aq} is replaced by D_e the effective diffusion coefficient in a porous medium (see below). If advective groundwater flow also contributes to mass transport, Equation (5.5) is expanded with a flow term to:

$$\frac{\partial C}{\partial t} = D_e\frac{\partial^2 C}{\partial z^2} - v_z\frac{\partial C}{\partial z} \tag{5.7}$$

where v_z is the flow velocity of water.

For the case of a fluid with salt concentration C_s entering a semi-infinite porous medium with water of salt concentration C_0 at a flow velocity v_z, Eq. 5.7 can be solved with the same boundary conditions as for Eq. 5.5. Ogata and Banks (1961) found the following analytical expression:

$$C_{z,t} = C_0 + \frac{(C_s - C_0)}{2}\left[\mathrm{erfc}\left(\frac{z - v_z t}{2\sqrt{D_e t}}\right) + \exp\left(\frac{v_z z}{D_e}\right)\mathrm{erfc}\left(\frac{z + v_z t}{2\sqrt{D_e t}}\right)\right] \tag{5.8}$$

5.3.3. Diffusion coefficients

Diffusion coefficients of solutes in water are a function of temperature and molecular or atomic mass. Based on the Stokes-Einstein equation, Woreh (1993) (in Gratwohl, 1998) derived the following relationship for uncharged molecules, like gases:

$$D_{aq} = \frac{3.595\cdot 10^{-7} T}{\mu m_s^{0.53}} \tag{5.9}$$

where T = temperature (K), μ = dynamic viscosity (Pas [1.002×10^{-3}]) and m_s = molecular mass (g/mol) for a certain solute.

According to Gratwohl (1998) this equation works also well for non-dissociated organic substances. However, for charged ions this relation does not apply, because the ions cannot diffuse in isolation; electrostatic forces mutually influence the mobility of the ions. The result of this complicated coupled diffusion process is that differences in diffusion coefficients are much smaller than expected from their molecular weight. Experiments show that diffusion coefficients of the major ions in water vary from 1×10^{-9} to 2×10^{-9} m²/s at 25 °C. Robinson and Stokes (1965) and Li and Gregory (1974) report a value of 1.2×10^{-9} m²/s for seawater diffusing into distilled water; the self-diffusion coefficient of water molecules is 2.7×10^{-9} m²/s (Wang et al., 1953).

Diffusion in pore water of saturated sediments is slowed down by obstruction of the grains and by the tortuosity of the pore channels. Various empirical relations have been def-

ined between the effective diffusion coefficient (D_e) and textural properties such as the effective transport-trough porosity (part of porosity acting as transport channels), tortuosity of the pore channels and pore constrictivity (Grathwohl, 1998). In practice, these parameters are unknown and only the bulk porosity (φ) of sediments is determined. Most authors use the empirical relation:

$$D_e = D_{aq}\varphi^m \qquad (5.10)$$

Field and laboratory studies yield a wide variation of values of m, which also seem to be a function of porosity. In shales and compacted clays m is relatively high. Remenda et al. (1996) investigated diffusion of $\delta^{18}O$ in a clay-rich till and found a value of about 0.1 for the ratio D_e/D_{aq}, which corresponds to about $m = 2$ with clay porosities varying between 0.3 and 0.35. Lerman (1979) in Ranganathan and Hanor (1987) found values of 2.5 to 5.4 for shales. For younger, less consolidated clays and sands, m is closer to 1 (Appelo and Postma, 1993).

Studies by Desaulniers et al. (1981), Beekman (1991), Volker and Van der Molen (1991) and Eggenkamp et al. (1994) resulted in values for D_e varying from 5×10^{-10} to 13×10^{-10} m²/s. As the conditions of these studies are comparable to those reported here, diffusion coefficients are expected to fall in the same range.

5.3.4. Fractionation of chlorine-isotopes by diffusive transport

Chloride ions are chemically inert in underground environments and are therefore the most appropriate ions for studying diffusion processes. Measuring chlorine-isotopes ^{35}Cl and ^{37}Cl gives valuable extra information, as diffusive transport creates fractionation of concentrations. The difference in atomic mass of the isotopes brings about differences in mobility and diffusion coefficients (Eq. 5.9). The heavier isotope is slower and therefore the solution becomes relatively depleted in heavy isotopes at the diffusion front and relatively enriched near the source. The ratio of effective diffusion coefficients for both isotopes is equal to the fractionation factor, α:

$$\alpha = \frac{D_{e\ ^{35}Cl}}{D_{e\ ^{37}Cl}} \qquad (5.11)$$

This factor cannot be derived theoretically as for gases, because hydration of chloride ions in the solution moderates the effect of the mass difference between the two chloride isotopes. Fractionation factors derived from isotope measurements in comparable environments - shallow sediments affected by recent transgressions and regressions - vary from 1.0012 to 1.0030 (Desaulniers et al., 1981; Beekman, 1991; Eggenkamp et al., 1994).

Fractionation of chlorine-isotopes as a result of diffusion can be simulated by separately calculating the ^{35}Cl and ^{37}Cl concentrations using Eq. 5.8 or 5.13. Initial concentrations are based on the chloride concentrations and the chlorine-isotope ratios (^{37}R) of seawater and fresh groundwater. For the present study, the ^{37}R of these waters were considered to be equal to a $^{37}R_{SMOC}$ of 0.31978 (Eggenkamp, 1994).

5.3.5. Diffusion-sedimentation model simulating transgression followed by regression

The downward diffusion process in the Suriname coastal plain is more complicated than the simple analytical model of Eq. 5.8. Firstly, exposure to the sea was temporary and, secondly, marine sedimentation took place during the transgressive phase. Eggenkamp (1994) found a solution for the sedimentation problem by letting the origin ($z = 0$) move along with the rising sea floor during sedimentation and regarding the salinization process as a downward flow of salt water in the underlying sediments with diffusion at the salt front. If sedimentation is constant, Eq. 5.8 is valid with v_z equal to the sedimentation rate. However, the transgressive phase and the sedimentation are of finite duration and are followed by a regressive phase and exposure to fresh water at the top. Beekman (1991) used a finite difference scheme to simulate these conditions. Here another solution is proposed, analogous to that for the heat-flow problem described by Carslaw and Jaeger (1959, p. 58). In order to apply this solution the semi-infinite concentration profile at the start of the regression is made infinite using:

$$C_{-z,t_r} = 2C_{fresh} - C_{z,t_r} \qquad (5.12)$$

where t_r is the time elapsed between Holocene transgression and regression, $C_{z,tr}$ is the chloride concentration according to Eq. 5.8 and C_{fresh} is the chloride concentration of fresh groundwater at the surface. $C_{-z,tr}$ is the imaginary chloride profile extending infinitely upward from the surface. The evolution of the subsurface part ($z \geq 0$) of this infinite profile according to the diffusion equation is exactly the same as the evolution of the semi-infinite profile with boundary condition $C_{0,t} = C_{fresh}$. After the regression ($t \geq t_r$) the evolution of the chloride content until present can be determined by convolution of the initial profile (at the start of the regression) with Green's function. The convolution integral has the following form:

$$C_{z,t_r} = \frac{1}{2\sqrt{\pi D_e t_p}}\left[\int_0^{\infty} C_{-z',t_r}\, e^{\frac{(z-z')^2}{4D_e t_p}}\, dz' + \int_{-\infty}^{0} (2C_{fresh} - C_{-z',t_r})\, e^{\frac{(z-z')^2}{4D_e t_p}}\, dz'\right] \qquad (5.13)$$

where t_p is elapsed time between the Holocene regression and the present.

A straightforward analytical expression does not exist for this equation. The function has to be made discrete by calculating a large number (N) of concentrations at certain depths with spacing Δz, before the convolution is applied. Because the integration has to be carried between certain limits along z, $N\Delta z$ must be large enough to include the area of influence of the diffusion process. The calculations were performed using the mathematical MATLAB computation program (The Math Works Inc., Natick, USA); accuracy was tested by varying the spacing and N. Results indicated that the final concentration values did not change for $\Delta z < 0.25$ m nor for $N > 600$.

Applying Eq. 5.8 and 5.13 in the actual field situation is only valid if the aquifers and the Pleistocene clays contained pristine meteoric water ($C_{z,t} = C_0$ for $z > 0$ and $t = 0$) at the onset of the Holocene transgression. The Pleistocene clays from the Sangamonian transgression contained seawater. However, it can be readily shown with a simple diffusion model that during 100 ka of the Wisconsinan regression all salts from the Sangamonian transgres-

sion have diffused out of the clays to the phreatic surface and to the fresh underlying aquifers. Further evidence is given by Levelt and Quakernaat (1968), who reported dilute pore water in the Pleistocene clays in the southern part of the coastal plain. Freshening of the clays during the Wisconsinan regression was probably enhanced by downward seepage, induced by the deeply incised rivers and creeks (Chapter 3).

5.4. Results

5.4.1. Downward diffusion

Quaternary clays

In the absence of convective density flow, discussed in Section 5.3.1., the diffusion-sedimentation model can be applied to the Quaternary clays. Figure 5.2 displays depth profiles of chloride concentrations and the $\delta^{37}Cl$ values for pore water from the clay cores at Koewarasan and Tourtonne. Maximum concentrations are about 3,000 mg/l (or 85 mmol/l) at Koewarasan and 18,000 mg/l (or 500 mmol/l) at Tourtonne. Towards the top and bottom of the clay formations, water becomes fresher. The high salinity at Tourtonne marks a recent retreat of the sea at this site. Koewarasan has experienced a longer period of freshening. $\delta^{37}Cl$ values deviate from the SMOC value (0 ‰), indicating a diffusion effect in the process of freshening. The $\delta^{37}Cl$ values at Tourtonne decrease down profile from positive to negative. This indicates downward diffusion with isotopic enrichment at the peak concentrations and depletion closer to the diffusion front. The $\delta^{37}Cl$ values at Koewarasan, where only three analyses have been carried out, are distinctly more positive. Apparently a longer period of diffusion has resulted in a relatively large enrichment throughout the entire clay layer.

It would be impossible to calibrate all parameters of the diffusion model (Eq. 5.8 and 5.13) with the analyses of chloride contents and chlorine-isotope ratios. However, for some parameters reliable assumptions can be made. The time of transgression can be derived from local sea level curves (Brinkman and Pons, 1968; Roeleveld and Van Loon, 1979). Transgression at Koewarasan and Tourtonne is estimated at 6 ka BP and 10 ka BP, respectively. This time is equal to the sum of t_r and t_p in Eq. 5.13. Holocene sedimentation rates (v_s) at Koewarasan and Tourtonne have been derived from ^{14}C dates of shells and organic material in the clays (Figure 5.1); the rates are 2.9 and 2.6 mm/year respectively. The chloride concentrations of fresh meteoric groundwater before the transgression (C_0 and $C_{w,t}$) and at the surface after the transgression (C_{fresh}) are 25 mg/l or 0.7 mmol/l. This value is the average concentration of groundwater in the Tertiary formations below the recharge area of the Lelydorp sands. Seawater chloride concentration is assumed to be 20,000 mg/l or 566 mmol/l (Appelo and Postma, 1993). The isotopic ratio of seawater chloride ($^{37}R_{SMOC}$) is equal to 0.31978 (Eggenkamp, 1994). We may assume that in coastal areas, like Suriname, chloride in rainfall and in fresh meteoric groundwater is of marine origin (Appelo and Postma, 1993; Drever, 1997). Evaporitic rocks, which may release chloride, do not occur in this area. Moreover, Krook (1979) states that only the most stable silicates in the Tertiary sediments of Suriname have survived intensive weathering. Consequently, fresh meteoric groundwater must have the same isotopic chlorine ratio as seawater, which is expressed as $\delta^{37}Cl$ is equal to 0 ‰. With the assumptions on concentrations and isotopic ratios, the initial concentrations of ^{35}Cl and ^{37}Cl are known.

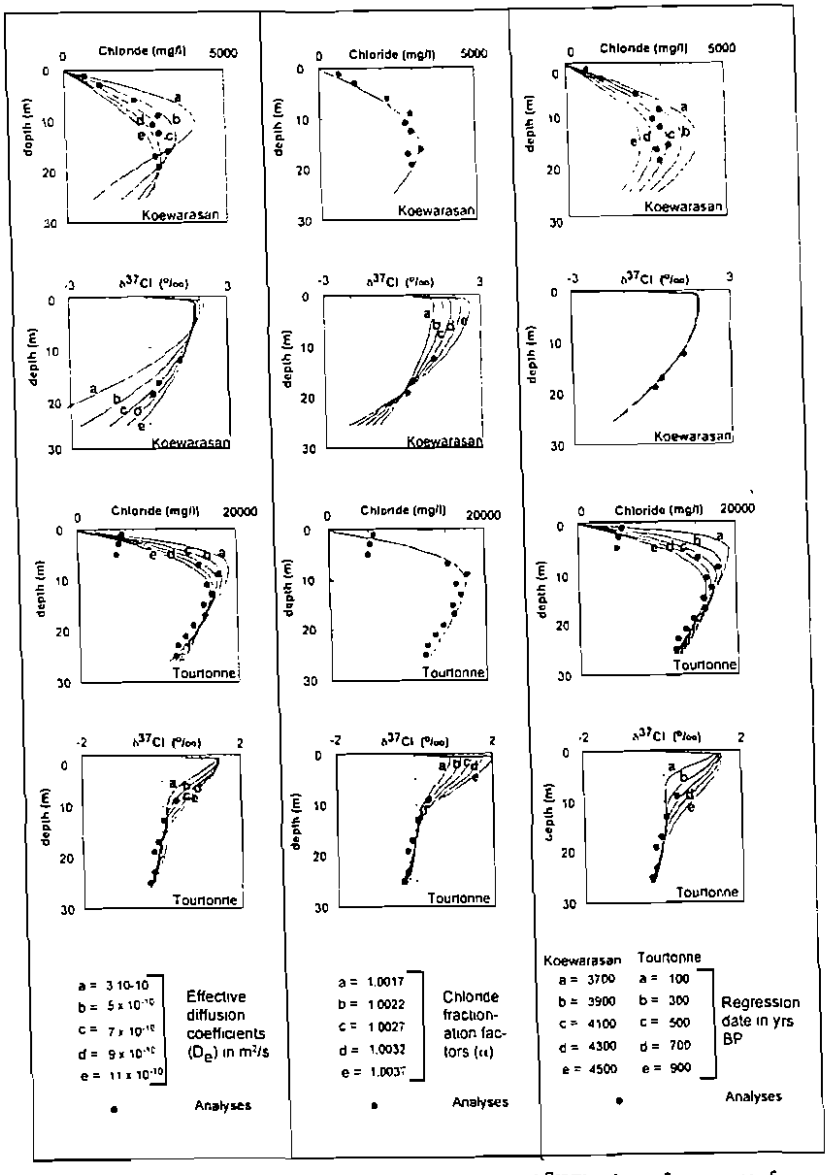

Figure 5.2. Measured and simulated chloride concentrations and $\delta^{37}Cl$ values of pore water from the Quaternary clays at Koewarasan and Tourtonne. Curve fitting resulted in an optimum effective diffusion coefficient and chlorine-isotope fractionation of 7 x 10^{-10} m^2/s and 1.0027, respectively. With curve fitting, regression at Koewarasan and Tourtonne was dated at 4.1 ka BP and 0.5 ka BP respectively, leading to sedimentation rates of 2.9 mm/year and 2.6 mm/year respectively. The assumed transgression at both sites at 6 ka and 10 ka BP, respectively, was previously based on ^{14}C-analyses.

Three unknown parameters are left in the diffusion model: t_r = period between regression and present ($t_r + t_p$ is known); D_e = effective diffusion coefficient of the abundant ^{35}Cl isotope; α = fractionation factor between the ^{35}Cl and ^{37}Cl isotopes. The model parameters D_e and α were optimised by trial and error until the calculated profiles of the chloride concentration and $\delta^{37}Cl$ fitted the laboratory measurements (Figure 5.2). As an extra constraint to this procedure, values for D_e and α for both sites were set equal to ensure the reproducibility of the assumed diffusion process. For D_e a value of 7 x 10^{-10} m^2/s was found, which lies within the range of values reported above. The same holds true for the value of 1.0027 found for α. The resulting regression dates are 4.1 ka BP and 0.5 ka BP for Koewarasan and Tourtonne respectively.

Figure 5.2 displays the sensitivity of the model for variations in parameters values. Parameter c in each subfigure represents the optimised value. It is interesting to note that the modelled $\delta^{37}Cl$ at Koewarasan is not very sensitive to variation of the regression date. This is because the ratio of the transgressive period to the regressive period does not differ much within the range of regression dates. At Tourtonne regression took place only a few hundred years ago. Therefore, varying the regression date with the same order of magnitude has more effect at this site. It goes without saying that variation of the fractionation factor has no visible effect on the total chloride concentration.

Given the maximum values for the density difference of pore water in the clays (5 kg/m^3), the hydraulic conductivities (4 x 10^{-4} m/day) and the thickness (30 m) of the Quaternary clays, the Rayleigh number calculated with Eq. 5.2 appears to be smaller than 1. This is well below the stability criterion of $4\pi^2$ and, therefore, we may conclude that convective density flows will not occur.

Tertiary formations

Figure 5.3 shows the simulation results for chloride concentrations and $\delta^{37}Cl$ values of groundwater over a greater depth range in the Tertiary formations at Koewarasan and Tourtonne. Model parameters are equal to those described above. Implicitly, it is assumed that also in these formations diffusion controls salt transport, which may not be true for the sand layers. There are no vertical series of analyses in the Tertiary formations at the Koewarasan and Tourtonne sites. Therefore chloride concentrations from nearby wells are shown in Figure 5.3. The chlorine-isotope ratios in Figure 5.3 are from various wells from all parts of the coastal plain and cannot be compared with the simulations. Figure 5.3 shows that the simulated chloride concentrations at both sites decrease rapidly downward, which is in agreement with the analyses from nearby wells (see also Figures 3.5, 3.8 and 5.4). At Tourtonne concentrations in nearby wells are lower than predicted by the model. Unlike the Tourtonne borehole, these wells are probably located outside the paleochannel of the Suriname River, where transgression and salinization started relatively early.

According to the model, the diffusion front has not penetrated deeper than 60 and 90 m at Koewarasan and Tourtonne, respectively. The diffusion front is arbitrarily defined as the zone where chloride concentrations have increased to twice the average background concentration of 25 mg/l. The thus defined value of 50 mg/l is approximately the concentration at which groundwater is detectably affected by salinization. Sensitivity analyses using the parameter variation above demonstrate that the depth of the diffusion front varies with 30 m.

Conspicuous are the modelled negative peaks in $\delta^{37}Cl$ at 50 and 80 m at Koewarasan and Tourtonne, respectively, just above the diffusion fronts. The fractionation effect normally increases along the diffusion path, but decreases again near the diffusion front. Near the

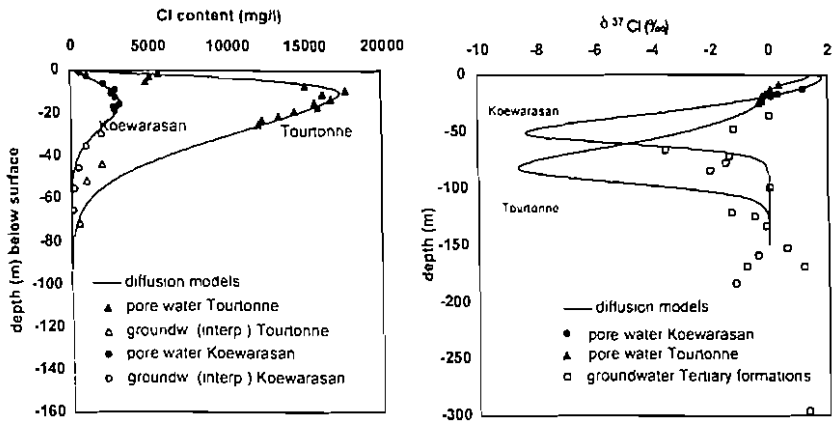

Figure 5.3. Measured chloride concentration and $\delta^{37}Cl$ values of groundwater from Tertiary formations and values simulated with the diffusion-sedimentation model for Koewarasan and Tourtonne.

front, chloride concentrations are low and the isotopic composition is dominated by the composition of the initial fresh groundwater. Sensitivity analyses show that the magnitude of the peaks varies between –5 and –12 ‰ and depends mainly on the fractionation factor. The depth of the peaks depends on the diffusion coefficient and varies within a range of 30 m around the depths stated above. Also, the initial chloride concentration is of influence: if the initial chloride concentration is increased tenfold, the peak reduces to half its value. The $\delta^{37}Cl$ analyses in Figure 5.3 are from wells located far from each other and with different diffusion histories, which does not allow a meaningful comparison with modelled $\delta^{37}Cl$ values. Yet, the pattern of negative values ranging between –4 and 0 above a depth of -125 m and values between –1.3 and +1.3 below that depth may reflect the simulated $\delta^{37}Cl$ peaks.

We expect that, if water samples from the Tertiary sediments at the two sites were obtained and analysed, it would be difficult to reproduce the analyses with the diffusion simulations for several reasons. First of all, the model does not account for upward salt transport from deep saline groundwater, which may be of influence in the fresh and moderately brackish zone below a depth of -40 m. Secondly the assumption of negligible advective transport, which seems appropriate for the Quaternary clays, may not hold for the Tertiary sands. Advection may be related to regional compaction and density-driven flow as discussed in section 3 or flow caused by pumping. More important is the advection caused by free convective density flows (mixing), which may arise in the Pliocene aquifer if the stability criterion of $4\pi^2$ for the Rayleigh number is exceeded (Eq. 5.2. With estimates for density difference $\Delta\rho$ (0.9 - 3.6 kg/m3), hydraulic conductivity k (10 - 30 m/day) and aquifer thickness H (15 - 30 m), the Rayleigh number varies between 1,350 and 32,400. This suggests that free convection is an effective mixing process in the upper Pliocene aquifer, which will reduce the modelled concentration gradient and the peak of the chlorine-isotope ratio (Figure 5.3). In the aquifers deeper than 70 m below the surface density differences are probably too small to create density flows.

5.4.2. *Upward transport of saline and brackish groundwater*

The saline groundwater in the Cretaceous sediments is not connate. Contact with fresh meteoric groundwater during long regressive periods in the Late Cretaceous and Oligocene would have drawn much of the original salt from the sediments by diffusion. The high concentrations found in the lower part of Cretaceous deposits may be the result of salinization during later transgressions. As the sediments are not very permeable, salinization by downward diffusive transport requires a prolonged period of marine submersion, suggesting a Miocene age for this deep saline water. Another explanation is that saline groundwater from the deep and seaward part of the Guiana basin has migrated upslope and landward. Noorthoorn van der Kruijff (1970) proposed this mechanism of compaction-driven flow to explain the presence of oil in the Lower Tertiary, west of Paramaribo.

The chlorinity profiles in Figure 5.4 indicate an upward flux of salts from the Cretaceous sediments. The flux, that persisted during a long time in the Neogene, is controlled by diffusive transport and lateral dispersion, related to meteoric groundwater flow in the Tertiary sediments during regression phases (Meinardi, 1991). This transport process has been going on for a long time during the Neogene and is not only controlled by diffusion. During periods of low sea level, groundwater flow in the permeable Tertiary formations enhanced upward transport by lateral dispersion. These meteoric flow systems have been arrested and reactivated several times during the Neogene. Uncertainty on these boundary conditions makes simulations of upward salt transport from the Cretaceous sediments less meaningful than those of downward transport described earlier. Nevertheless, chloride concentrations in Figure 5.4 and the $\delta^{37}Cl$ values in Figure 5.3 in the deeper part of the Tertiary formations still permit some qualitative conclusions. Geophysical logs from the eastern

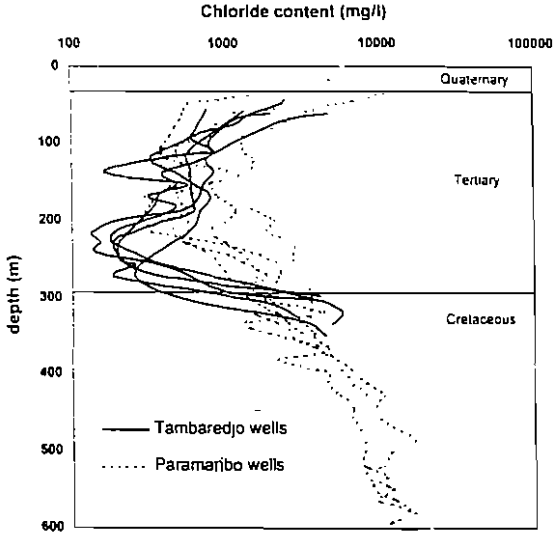

Figure 5.4. Chloride profiles in oil exploration wells based on geophysical borehole logs.

wells near Paramaribo show a gradual increase in chlorinity from a minimum of 600-800 mg/l at depths between 100 and 200 m to almost seawater quality below 500 m. In the Tambaredjo wells, minimum chloride concentrations attain relatively low values of about 200 mg/l at depths between 200 and 250 m. Below this depth a sharp increase in chloride concentration is observed. This seems to be related to the clay layer above the basal Tertiary sand layer that also forms the host rock for the oil of the Tambaredjo field. The presence of oil implies that the clay must be very impermeable and has protected the lower deposits against flushing by meteoric groundwater flow during regressions. Otherwise, the oil would have been dispersed and microbiologically degraded as a result of mixing with meteoric water. We believe that the steep chlorinity gradient below the clay seal reflects upward diffusive transport of salts in stagnant formation water. East of the Tambaredjo oil field the clay is absent or less continuous, which enabled groundwater flow systems to extend to the top of the Cretaceous sediments during regressions. Meinardi (1991) points out that in such a situation lateral dispersion along the interface of fresh and brackish groundwater enhances the upward solute transport. As a result, larger and more gradual transition zones are found in the eastern wells compared to those in the western Tambaredjo wells (Figure 5.4).

It is concluded from the simulations of downward diffusion that groundwater below a depth of 100 to 125 m could not have been influenced by Holocene salinization. Nevertheless, groundwater from the Paleogene formations is marked by chlorine-isotope fractionation: $\delta^{37}Cl$ values vary from -1.3 ‰ to $+1.3$ ‰ below a depth of about -125 m (Figure 5.3). It is believed that the $\delta^{37}Cl$ variations are indicative of diffusive processes. However, a more profound interpretation of vertical solute transport in deep groundwater based on the available $\delta^{37}Cl$ data is impossible, as the values are from different wells (Figure 5.3). Moreover, borehole logs of these wells were not available.

5.5. Discussion and conclusions

Salinization of sediments with fresh groundwater following a transgression can take place through several processes, as depicted in Figure 5.5. In the case of Suriname diffusive transport is the dominant process.

A diffusion-sedimentation model has been set up that simulates chloride diffusion and chlorine-isotope fractionation in sediments that have been exposed to marine inundation and sedimentation during a finite period. The simulated chloride concentrations and $\delta^{37}Cl$-values were in good agreement with analyses of pore water from two sites in the coastal plain. Values found for the effective groundwater diffusion coefficient of chloride and the fractionation factor for the chlorine-isotopes are 7×10^{-10} m^2/s and 1.0027, respectively. These values are supported by previous studies (Desaulniers et al., 1981; Beekman, 1991; Volker and Van der Molen, 1991; Eggenkamp et al., 1994).

Chloride concentrations and chlorine-isotope ratios, as well as the diffusion model show that salts from the Holocene transgression have penetrated to a maximum depth of 100 to 125 m in the underlying Tertiary sediments (Figure 5.3 and 5.4).

The model could even be used as a marker for the marine transgression and regression during the Holocene at the two sites. Transgression at Tourtonne and Koewarasan, located more inland, took place at 10 ka and 6 ka BP, respectively. Regression occurred at 0.5 ka BP and 4.1 ka BP, respectively. These dates are in line with results from earlier studies in the Suriname coastal plain based on ^{14}C-dating (Brinkman and Pons, 1968; Roeleveld and Van Loon, 1979).

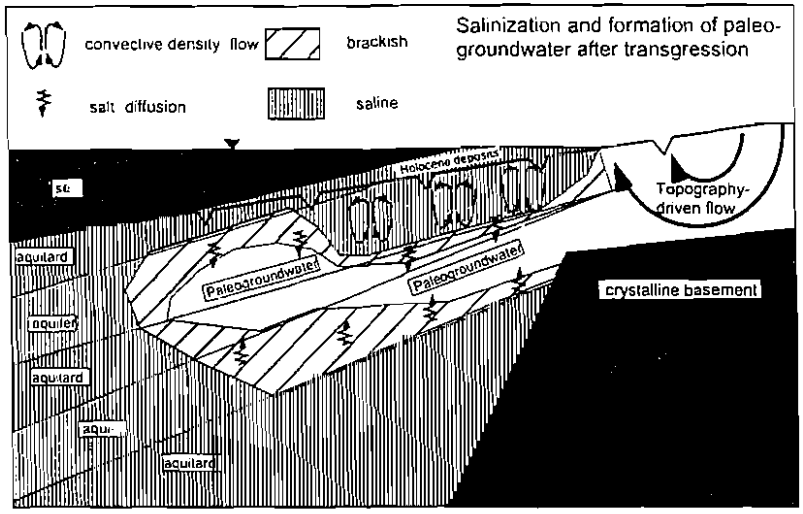

Figure 5.5. Salinization in offshore and coastal sediments after a transgression.

Salts below depths of about 125 m belong to the pre-exiting dispersive fresh/saline transition zone and originate from the Cretaceous. The thickness of this zone depends on the presence of impermeable clays at the base of the Tertiary (Figure 3.8). In the clay layer sealing the Tambaredjo oil reservoir diffusive transport dominates, whereas groundwater above the clay is continually flushed by meteoric flow systems during regressions. In the Paramariho area the clay is lacking, which allowed more lateral dispersive mixing at the Tertiary/Cretaceous boundary, resulting in more gradational salinity profiles (Figure 3.8). In fact, the chloride profile in the upper 250 m may be used as a proxy to detect the presence of clay seals and perhaps shallow oil reservoirs in the Guiana Basin.

Reconstruction of the upward transport of salts from the Cretaceous sediments was not possible due to lack of data. In addition, modelling is meaningless as boundary conditions related to the various transgressions and regressions are unknown.

This study and earlier studies (Beekman, 1991; Eggenkamp et al., 1994) show that the approach of combining chloride and $\delta^{37}Cl$ analyses and salt transport modelling is successful in reconstructing paleohydrological events in coastal areas. These techniques may also be applied to study diffusion in low-permeability environments around deep disposal sites of nuclear waste and landfills.

Further work focuses on combination of chlorine-isotope analyses with 2- and 3-dimensional modelling of water and solute transport of variable densities.

Chapter 6.

Hydrogeochemical signals of the hydrology and paleohydrology in the coastal plain of Suriname

6.1. Introduction

This chapter deals with the hydrochemical composition of groundwater with the objective to provide new evidence on the hydrology and paleohydrology of the coastal plain of Suriname, and to substantiate results derived at in earlier chapters. Attention is given in particular to processes of cation-exchange. This process accompanied freshening during the last glacial, when the body of stagnant meteoric groundwater in the coastal and offshore Tertiary sediments was formed (Chapter 4). It also occurred, in a reverse order, during the subsequent salinization after the Holocene transgression. Cation-exchange between soluble and adsorbed phases is of particular interest, as it provides a signal with a long memory. Cation-exchange occurs when groundwater with a hydrochemical composition different from the residing groundwater penetrates a formation (Appelo and Postma, 1993). The exchange process for saline water (dominated by Na^+) flowing in a formerly fresh aquifer (with exchangers dominated by Ca^{2+}) can be described by:

$$Na^{+} + {}^{1}/_{2}(Ca \cdot X_2) \Leftrightarrow (Na \cdot X) + {}^{1}/_{2}Ca^{2+} \qquad (6.1)$$

In which X represents the exchange sites on charged surfaces like clays. The equilibrium condition according to the Gaines Thomas convention (Appelo and Postma, 1993) is expressed as:

$$K_{Na/Ca} = \frac{[Na-X]^2[Ca^{2+}]}{[Ca-X_2][Na^+]^2} \qquad (6.2)$$

The coefficient $K_{Na/Ca}$ is not a true constant, but depends on the salinity of the pore-water. The selectivity of an exchanger differs for various species, but decreases in the following order: Ca, Mg, K, NH_4 to Na. Because exchange reactions are fast with respect to advective and diffusive transport, continuous chemical equilibrium may be assumed between dissolved and adsorbed phases. Because of the continuous release of cations from a relatively large pool of adsorbed ions on the exchangers, the cation composition in pore-water at a particular point requires some time (several flushings) before it assumes the composition at the source. In the front zone of a water type moving or diffusing into another water type, exchange effects can be noticed in the cation composition. This has been reported in many studies dealing with freshening of coastal aquifers (Appelo and Postma, 1993). Due to exchange processes, the front zone of fresh groundwater flushing a saline aquifer is often enriched in sodium or magnesium with respect to conservative mixing (based on conservative tracers like chloride). Calcium, the principal cation in fresh water, is then exchanged for sodium and magnesium, which dominated the exchange complex during the former marine conditions. Sometimes even a chromatographic pattern of groundwater facies with Na-Cl, Na-HCO_3, Mg-HCO_3 to Ca-HCO_3 watertypes is observed (Edmunds and Walton, 1983;

Walraevens and Lehbe, 1989; Stuyfzand, 1993; Appelo, 1994). Freshening and the accompanying cation-exchange may take place in young flow systems developed below dunes and beach barriers in aggrading Holocene plains. It can also be observed in much older and often deep flow systems, that have been active during the last glacial or even earlier, but have not entirely flushed the formations because of low flow velocities. Salinization of formations resulting from a marine transgression evokes the reverse exchange process and leads to a relative surplus of calcium or magnesium. However, this process is hard to recognize in the field as the large sodium concentrations in the passing saline groundwater result in rapid equilibration between the dissolved and absorbed phases (Appelo and Postma, 1993). Ca-Cl and Mg-Cl water types are only observed near relatively recent saline groundwater intrusions near wells (Stuyfzand, 1993) and polders (Geirnaert, 1969).

6.2. Data

For the present study hydrochemical analyses have been used from previous studies (UNDP/WHO, 1972; IWACO, 1983; Ho Len Fat, 1986; Poels, 1987; Planning and Research Corporation, 1988; Mente, 1990a, 1990b; IWACO/F.R.Harris, 1991) and unpublished analyses of water supply companies. In addition analyses were carried out on 95 samples collected by the author in the period from 1995 to 1998. Most water samples were tapped from running production wells or were pumped from observation wells with centrifugal suction pumps or small diameter submersible pumps (Annex II and III). A special group are the water samples squeezed from clay samples, retrieved for this study from two percussion drillings (Velstra, 1997) in the Holocene coastal plain at Tourtonne and at Koewarasan (Figure 3.1). The percussion drillings have been discussed in more detail in Chapter 4.

Most water samples originate from the Quaternary and Tertiary formations in the coastal plain around Paramaribo. Two groups of analyses from outside the study area (Annex II and Figure 3.1.) have been analysed as well: these are groundwater analyses from the Paleocene oil bearing sand layer of the Tambaredjo oil field, 40 km west of Paramaribo (Ho Len Fat, 1986) and analyses of shallow phreatic groundwater from the savannah belt near Kabo, 60 km southwest of Zanderij airport (Poels, 1987). The samples from the study area are not evenly distributed over the various formations. Because most samples were taken from pumping wells and observations wells of water-supply agencies, the sample density is relatively high in the zones containing fresh groundwater with chloride contents less than 250 mg/l.

The sampling and laboratory procedures of the archived samples are unknown. The samples taken for this study were analysed in the laboratory of the Vrije Universiteit in Amsterdam. Samples were filtered in the field and stored in acidified and non-acidified bottles. In the field pH, electrical conductivity, temperature and, in some cases, alkalinity were measured. The soil samples were retrieved from the borehole in stainless steel tubes, which were sealed and cooled during transport to the Netherlands. Pore-water was squeezed from the clay samples in the laboratory of the Earth Sciences Faculty of the University of Utrecht.

Stigter (1996) compiled the initial hydrochemical dataset. The final dataset for this study consists of 221 analyses of all prineipal chemical components with an electro-neutrality imbalance of less than 10 % (Annex III). The chosen electro-neutrality imbalance is higher than the usual 5 % in order to include analyses from zones with a low sample density. For this data, also dissolved total inorganic carbon (TIC) has been calculated with the PHREEQC code. Annex III also includes incomplete analyses (59) and analyses (47) with an electro-neutrality imbalance higher than 10 %. In some qualitative interpretations of hydrochemical and isotopic patterns also incomplete analyses have been used.

Information on the mineralogy and geochemistry of the Quaternary and Tertiary formations has been found in studies of D'Audretsch (1953), Brinkman and Pons (1968), Levelt and Quakernaat (1968), Hartman (1969), Veen (1970), Eisma and Van der Marel (1971), UNDP/WHO (1972), Krook (1979), Wong (1983, 1989) and Poels (1987). For this study the composition of elements on all Quaternary clays samples from the percussion drilling was studied by X-ray fluorescence (XRF).

For this study also cation-exchange capacities (CEC) have been determined on 22 bulk soil samples from the two percussion drillings (7 on Pleistocene clays and 15 on Holocene clays). In this procedure exchangers were saturated first with ammonium by rinsing with an ammonium-acetate solution; subsequently the absorbed ammonium was displaced by sodium by flushing with a sodium-chloride solution; CEC equals the total amount of liberated ammonium (Velstra, 1997).

Existing CEC analyses of Pleistocene clays (51) and Pliocene sands (17) were available from other studies (Levelt and Quakernaat, 1968; Veen, 1970; Poels, 1987). These analyses were carried out on the clay fraction only (< 2 µm).

6.3. Hydrogeochemical evolution of meteoric groundwater in the coastal plain

6.3.1. Rainfall and evapotranspiration

Analyses of rainwater at Kabo by Poels (1987) demonstrate the dominant influence of marine aerosols, though calcium and potassium are significantly enriched (Figure 6.1). This enrichment is probably the result of dissolution of pyrogenic organic aerosols (Crutzen and Andreae, 1990) advected from the African continent (Prospero et al., 1981). On its way through the canopy and the upper soil zone, rainwater becomes more concentrated by evapotranspiration. Chloride contents in groundwater at Kabo (Poels, 1987) indicate that rainwater has been concentrated by a factor of 6.4 (Figure 6.1). Concentration factors for calcium and potassium are much lower, because they are largely filtered out in the root mat (Bruijnzeel, 1990; Forti and Neal, 1992; Grimaldi, 1988). As discussed above, the reactivity of the Pliocene and Pleistocene sediments is quite low. Therefore groundwater below the present recharge areas of the savannah belt and the Lelydorp sands has retained the marine hydrochemical signature of the aerosols (Figure 6.1). This groundwater is denoted here as pristine meteoric groundwater, marked by chloride concentrations of less than 50 mg/l. This distinction is necessary as groundwater with higher chloride contents has a marine signature caused by salt intrusion (Chapter 3 and 4). The average chloride concentration of pristine groundwater in the Pliocene aquifer in the savannah belt ranges from 2 to 16 mg/l. This groundwater is very young as it contains high tritium concentrations (Chapter 7; UNDP/WHO, 1972). Pristine groundwater in the Pliocene aquifer below the Lelydorp sands contains more chloride (15 to 45 mg/l), which may be due to the proximity of the ocean at the time of infiltration (2 to 8 ka BP, Chapter 7), higher evapotranspiration or leaching of salts from the overlying Pleistocene clays.

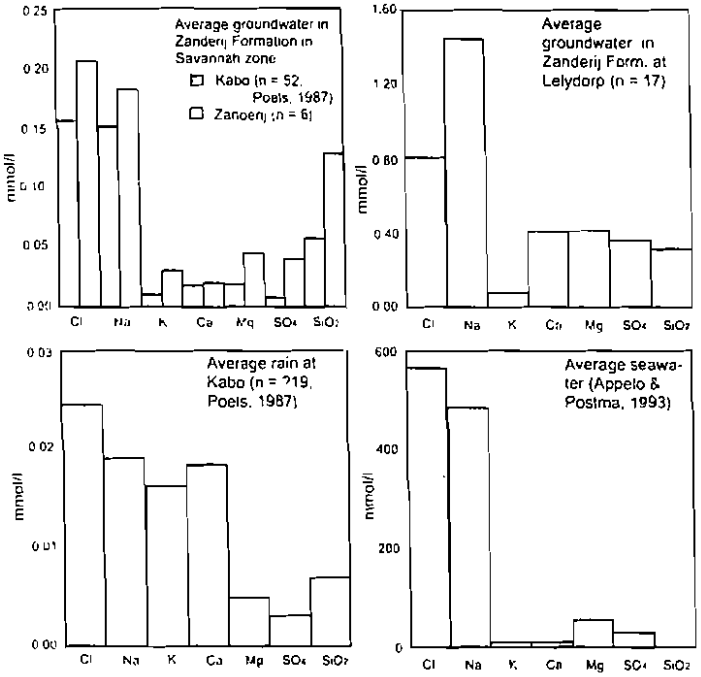

Figure 6.1. Hydrochemical composition of rain, pristine meteoric groundwater and seawater in Suriname.

6.3.2. Dissolution of carbon in the soil zone

Acid conditions (pH < 5) prevail in the soils and shallow phreatic groundwater in the coastal plain (Brinkman and Pons, 1968; Levelt and Quakernaat, 1968; Veen, 1970; Poels, 1987). They result from dissolution in the soil zone of carbon-dioxide gas and organic acids. The latter give the strongest acid reactions. McKnight et al. (1985) report that these acids, a complex of humic and fulvic acids, typically buffer solutions around a pH of 4.5, as is also the case in the study area. The presence of organic acids is also apparent in the numerous "black water" creeks in the savannah belt and the Pleistocene coastal plain.

In order to understand other hydrogeochemical and isotopic processes (Chapter 7) it is important to estimate the initial content of dissolved carbon in the recharging groundwater. According to a compilation by Brook et al. (1983) and to a study by Davidson and Trumbore (1995) in Brazil, soil carbon-dioxide pressures in tropical soils may vary between 10^{-2} to $10^{-1.4}$ atm. (10,000 to 40,000 ppmV). Given this pressure range, speciation calculations with PHREEQC showed that the initial inorganic carbon content of groundwater varies between 0.84 and 1.67 mmol/l. According to analyses by Poels (1987) organic carbon contents in savannah groundwater vary from 0 to 0.9 mmol/l (average of 0.17 mmol/l). Therefore the total amount of initial carbon of groundwater is expected to be in the range of 1 to 2 mmol/l.

Shallow phreatic groundwater analyses from the present study and earlier investigations (Poels, 1987; UNDP/WHO, 1972), represent mainly the savannah belt and hardly the coastal plain with its more dense and different vegetation. The early hydrochemical development of groundwater, described above, may therefore be biased. However, conditions in the savannah belt are of particular interest: most of the deeper groundwater has been recharged during the LGM and Early Holocene (Chapters 3 and 6), when the entire coastal plain was covered by grass and shrub savannahs comparable to that of the present savannah belt (Chapter 3; Van der Hammen, 1974).

6.3.3. Mineral dissolution

Low feldspar contents and the absence of calcite and aragonite in the Tertiary sediments are signs of prolonged leaching by groundwater flow (Krook, 1979). Krook also believes that the mostly kaolinitic Tertiary clays (of marine origin) originally had a higher content of smectites and illites and that they were later transformed as a result of weathering and leaching. Despite the low reactivity of the sediments weathering of detrital silicates has led to enrichment in cations, as can be observed in the pristine groundwater of the recharge areas (Fig 6.1.). Cation/chloride ratios are higher than those of rain, which is characterized mainly by dissolved marine aerosols. Outside the pristine groundwater the influence of weathering on the groundwater chemistry is masked by salt intrusion. Stability diagrams in Figure 6.2 show that kaolinite is the stable silicate phase in most circumstances, which agrees with the hypothesis of Krook (1979) that most kaolinite in the Tertiary sediments consists of transformed marine illites or smectites. In saline environments like those in which Holocene clays were deposited, smectites form the stable silicate phase. Carbonate dissolution hardly takes place in the Tertiary sediments. Most groundwater samples, inclu-

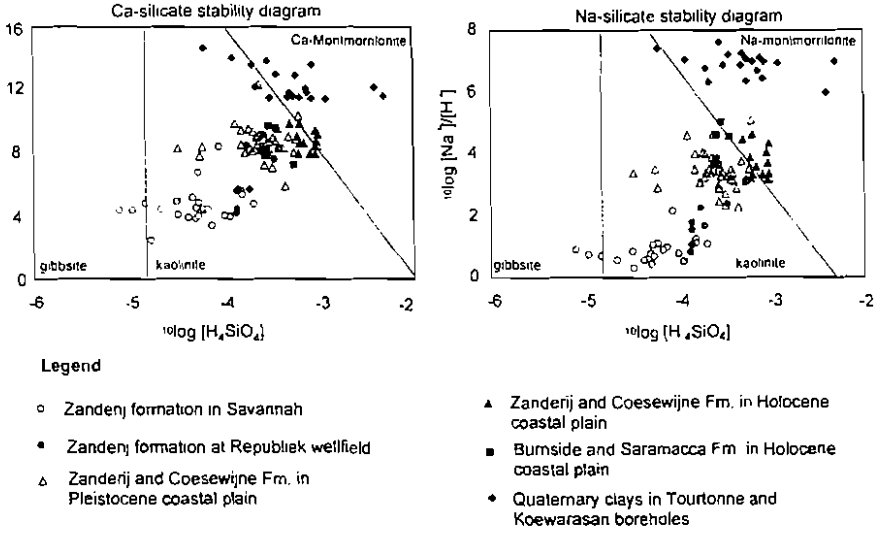

Figure 6.2. Stability diagrams of silicate minerals with respect to the groundwater analyses from the coastal plain of Suriname.

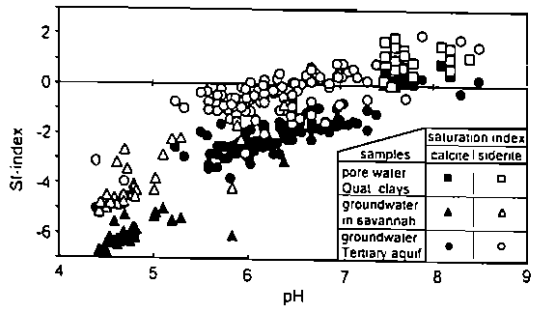

Figure 6.3. Saturation indices for calcite and siderite for groundwater in the coastal plain of Suriname.

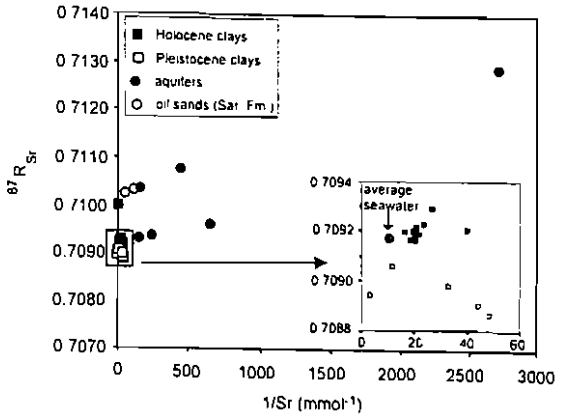

Figure 6.4. Strontium isotopes ratios against strontium concentrations in groundwater from the coastal plain of Suriname.

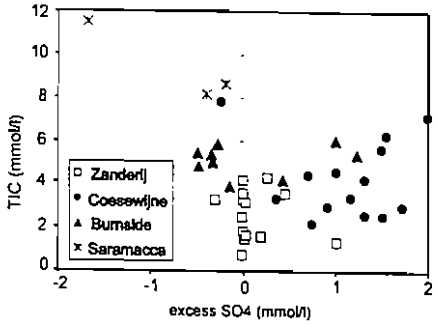

Figure 6.5. Excess sulphate against total inorganic carbon (TIC) for groundwater in the coastal plain of Suriname. TIC has been calculated with PHREEQC.

ding those influenced by salinization, are under-saturated with respect to calcite and have pH values lower than 6.5 (Figure 6.3). Strontium-isotope ratios provide information on the provenance of dissolved calcium, as the chemically familiar element occurs concomitantly with calcium in most minerals (Faure, 1986; Bierman et al., 1998). $^{87}Sr/^{86}Sr$ isotopes ratios in groundwater samples (Figure 6.4), measured at the VU isotope laboratory, proved to be much higher than the ratios for strontium in seawater and marine carbonates (Burke et al., 1982). These relatively high $^{87}Sr/^{86}Sr$ ratios are typical for strontium in the plutonic crystalline rocks of the Guiana shield (Priem et al., 1980; Vonhof et al., 1998). Therefore, dissolved strontium and calcium most probably originated form detrital silicates in the Tertiary sediments.

6.3.4. Redox processes

Calculated TIC contents of groundwater in the Tertiary formations range from 2 to 8 mmol/l. However, the estimated initial amount of carbon, which is dissolved in groundwater in the savannah belt at present, varies between 1 and 2 mmol/l. It is assumed that, at the time of recharge during the LGM and Early Holocene, the initial TIC content of groundwater did not much differ from these values. It follows that, in absence of carbonate dissolution, oxidation of sediment organic matter (SOM) must have led to the enrichment in dissolved carbon. In the Pliocene and Miocene formations, SOM oxidation is probably coupled with iron reduction, as groundwater contains relatively high contents of ferric iron but also sulphate. It is likely that the liberated ferric iron has precipitated as siderite, as many samples indicate saturation with respect to siderite (Figure 6.3). This corresponds with the observations by Krook (1979), who reported that these formations in particular contain amorphous iron hydroxides and authigenic siderite, while in the lower formations the more stable hematite and goethite dominate. High TIC and low sulphate contents (Figure 6.5) and enriched $\delta^{13}C_{TIC}$ values (Chapter 6) in groundwater of the deeper Paleogene (Oligocene, Eocene and Paleocene) formations give evidence of sulphate reduction and methanogenesis. The saline reactive Holocene clays form a completely different hydrogeochemical environment: groundwater is generally saturated with respect to calcite, which is present as allogenic and authigenic minerals in the sediments; pyrite and TIC contents are high because of sulphate reduction and methanogenesis (Figures 6.6 and 6.7, Groen, unpublished data). The same holds for the Cretaceous, the source rock of the oil that is found in several place in the coastal plain. This can be derived from groundwater samples from the oil-bearing sands at the bottom of the Tertiary at Saramacca.

6.4. Cation-exchange and freshening in the Pleistocene clays during the Wisconsinan regression

6.4.1. Introduction

During the 100 ka of the Wisconsinan regression, meteoric flow systems in the coastal plain have flushed all saline groundwater, formed during the preceding Sangamonian transgression. It is expected that cation exchange has long reached equilibrium. If there were any cation-exchange signals left, they would be expected in the clays, because of the high cation-exchange capacities (see next section). This applies in particular to Pleistocene clays (Coropina Formation) in the southern part of the coastal plain, which have not been affected by the Holocene transgression. The following sections are mainly based on data from Levelt and

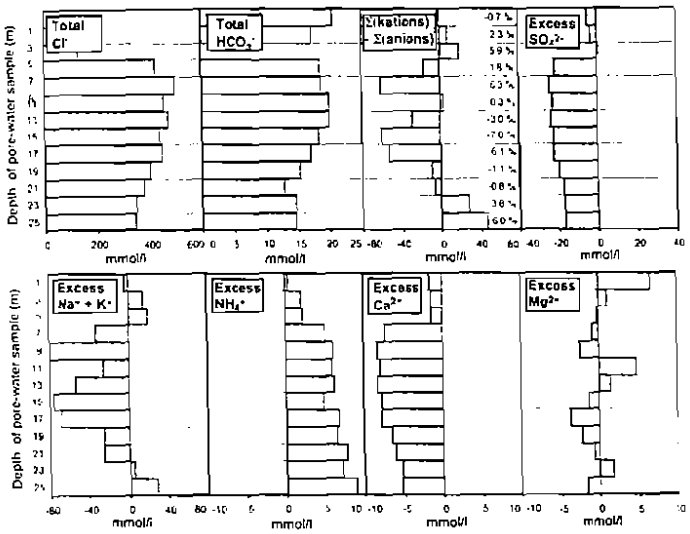

Figure 6.6. Chemistry of pore-water squeezed from Holocene clay samples retrieved at Tourtonne. Cl- and HCO_3-contents are total concentrations. Na-, K-, Ca-, Mg-, NH_4- and SO_4-contents are expressed as excesses with respect to conservative mixing of seawater and fresh groundwater. Σ(kations) - Σ(anions) imbalance is given in mmol/l and also as percentages.

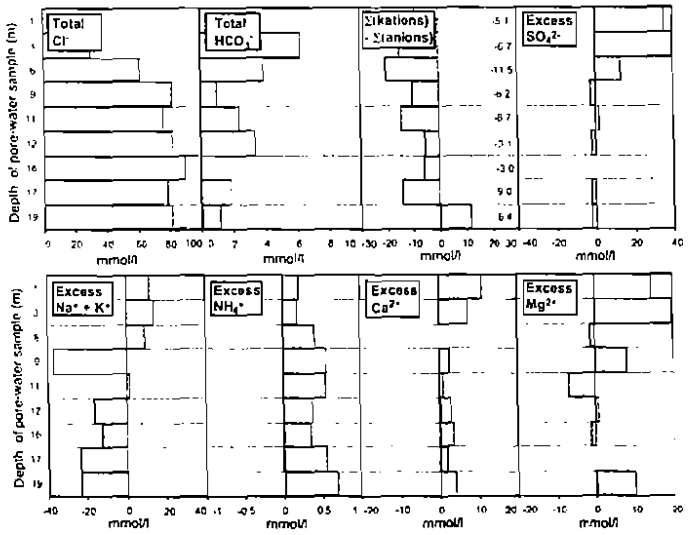

Figure 6.7. Chemistry of pore-water squeezed from Holocene and Pleistocene clay samples retrieved at Koewarasan. Cl- and HCO_3-contents are total concentrations. Na-, K-, Ca-, Mg-, NH_4- and SO_4-contents are expressed as excesses with respect to conservative mixing of seawater and fresh groundwater. Σ(kations)-Σ(anions) imbalance is given in mmol/l and also as percentages.

Quakernaat (1968) and Veen (1970), who carried out physical and chemical analyses on clays in this area.

6.4.2. Observations

Cation-exchange effects in the Pleistoeene clays are expected to be large beeause of the high CEC. CEC's of 7 samples from the Koewarasan borchole vary from 16 to 29 meq/100 g of dry soil, with an average of 24 meq/100 g. The CEC's of 51 samples from the studies in the southern part of the coastal plain (Levelt and Quakernaat, 1968; Veen, 1970), are considerably lower (average of 12 meq/100 g). This may be due to the higher silt fraction in that part of the coastal plain. Also these CEC were calculated on the basis of analyses of clay fraetions only, whieh may introduce errors. Average base saturation for the samples from the boreholes is about 34 %. The low base saturation is normal for the present day acid conditions, but in more mineralised and less acid groundwater, base saturation would probably be higher.

A typical depth profile of the cation composition on the exchange sites of the Coropina clays is shown in Figure 6.8. Magnesium appeared to be the dominant cation adsorbed to the exchange sites, followed by calcium. In the first instanee one is tempted to attribute the high magnesium content of the exchange sites to the marine origin of the clays, which would imply that the cation-exchange process has not been completed. This would be in accordance with the suggestion, made in Section 5.4.1, that the higher chloride contents of pristine groundwater below the clays may be the result of leaching of residual salts from the Sangamonian clays. On the other hand, the currently infiltrating water is not very mineralised and has a low calcium concentration (Section 6.3.). Also Levelt and Quakernaat (1968) report very dilute porewaters. This raises the question of whether the observed cation composition of the exchange sites is in equilibrium with the infiltrating water. These questions will be addressed by cation-exchange modelling in the next section.

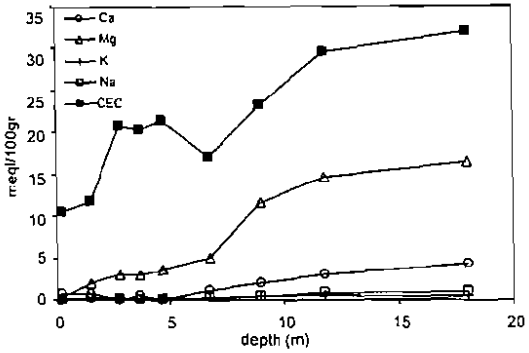

Figure 6.8. Exchangeable cations and exchange capacity of Pleistocene clays in the southern part of the coastal plain of Suriname (unpublished data from Levelt and Quakernaat, 1968)

6.4.3. Cation-exchange simulations

Model set-up

Cation-exchange occurring along with freshening of the Pleistocene clays has been simulated with the PHREEQC code for hydrogeochemical modelling (Parkhurst and Appelo, 1999). Simulations are restricted to processes of one-dimensional advective and diffusive solute transport and cation-exchange. The results are compared with observed cation compo-

sitions of the exchange sites of the clays in the southern part of the coastal plain (Levelt and Quakernaat, 1968).

In the reference model, a vertical column of 12 cells with lengths of 1 m each represents the clayey Pleistocene Formation. This corresponds to an average thickness of the formation varying from 2 to 20 m. In the model, an effective CEC of 600 mmol/l was applied (based on the average CEC of 25 mg/l/100 g of dry soil, bulk density of 1.8 gr/cm^3, porosity of 0.3 and an estimated base saturation of 40 %). For the diffusion coefficient a value of 7 x 10^{-10} m^2/s was used, based on the chlorine isotope study (Chapter 4). The exchange coefficients $K_{Na/Ca}$ and $K_{Na/Mg}$ (Equation 5.2) of 0.4 and 0.5 are average values based on a compilation by Appelo and Postma (1973). Other hydrogeochemical processes, like oxidation of pyrites and sediment organic matter and calcite dissolution have not been accounted for, because (i) the lower part of the Pleistocene clays had already been intensively oxidized during an early regression phase in the Sangamonian or even during the Illinoian (Saalien) regression (Veen, 1970) and (ii) it is assumed that during the prolonged Wisconsinan regression the clays quickly lost their reactivity and cation-exchange became the dominant process. The simulations cover a period of 105 ka from the end of the Sangamonian (around 115 ka BP) transgression to the Holocene transgression (around 10 ka BP). In each simulation exchange sites are first equilibrated with seawater, representing the situation during the Sangamonian transgression. As a result, exchange sites become filled mainly by sodium and magnesium. Freshening by diffusive transport during the Wisconsinan is controlled by fixed ion concentrations of fresh groundwater at the top and the bottom of the column. With respect to the latter boundary condition it is assumed that during the Wisconsinan the underlying Pliocene formation was rapidly flushed by meteoric groundwater. For the fresh groundwater at the bottom, the composition of average Lelydorp groundwater was chosen. At the top, fresh water with a theoretical composition was imposed: chloride concentration was set equal to the average of groundwater below Lelydorp and cations concentrations were proportional to that of chloride, as in seawater (Figure 6.9). For simulations of freshening by advective transport, the latter water type was used to flush the column. The flow rate through the column was based on a recharge of 30 mm/a and an effective porosity of 30 %. Estimated dispersivity for advective transport was set at 0.1 m.

The sensitivity of the diffusive and advective freshening models has been tested by varying model parameters between reasonable end member values. In Table 6.1 the parameters used for the various simulations are listed. Simulations 1 and 11 are the reference models for diffusive and advective salt transport, respectively. Also the chemical composition of water at the top boundary condition was varied: instead of the theoretical fresh water composition with a marine signature (dilute marine) also runs were made with average Lelydorp groundwater at the top (100 % Lelydorp) and a water type forming a mixture of average Lelydorp groundwater and the diluted marine water (50 % Lelydorp).

Results

The most interesting results of the simulations are shown in Figure 6.9. The concentrations of dissolved and exchangeable cations are plotted against depth. Simulation 1 demonstrates that diffusion alone is not able to drive out all sodium from the exchange sites (Figure 6.9a). This also applies to other simulations under conditions that enhance the exchange, like small layer thickness (simulation 2), maximum and minimum selectivity for magnesium and calcium, respectively (in simulation 4), small effective CEC (300 mmol/l in simulation 5) and high diffusivity (10 x 10^{-10} m^2/s in simulation 10). Figure 6.9a shows that

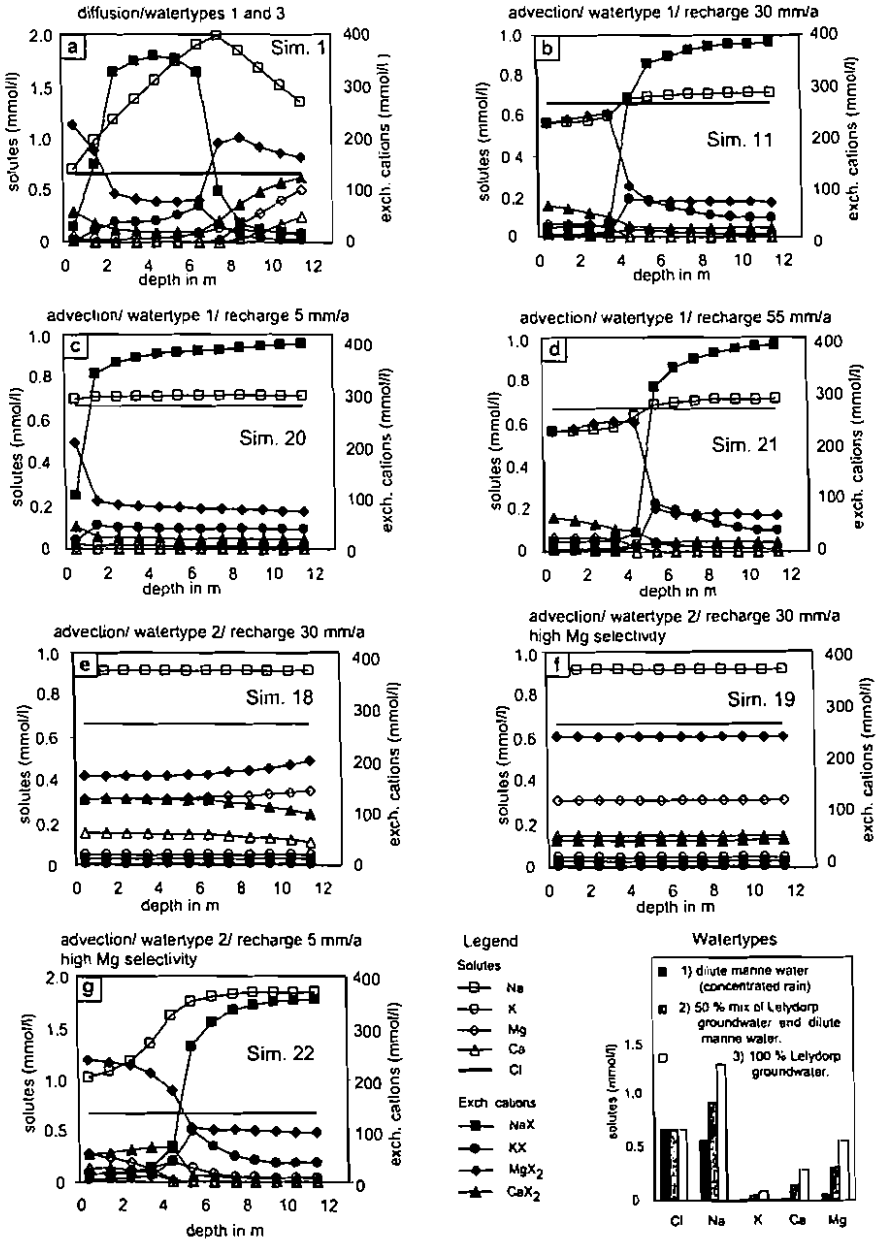

Figure 6.9. Simulated concentrations of dissolved and exchangeable cations and chloride in Pleistocene clays after 105 ka of freshening during the Wisconsinan regression. PHREEQC models simulate freshening by vertical diffusive and advective solute transport (recharge) and cation-exchange (see Table 6.1).

the release of sodium takes place more quickly at the bottom of the Pleistocene clays. This is caused by the relatively high cation concentrations of the bottom boundary condition (100 % Lelydorp groundwater). Simulation 7, with 100 % Lelydorp groundwater as top boundary condition, results in a faster equilibration at the top part, but sodium is still not driven out. Though diffusion may not have led to complete cation-exchange, the process itself is fast enough to drive out the chloride and other conservative solutes from the original saline pore-water: it appears that after 35 ka (one-third of simulation period) the total concentration (meq/l) in pore-water has almost reached the total concentration of the solutions at the boundaries.

Freshening by advective transport with the reference model (simulation 11) is also not sufficient to reach equilibrium between the solute infiltrating at the top and the exchange sites (Figure 6.9b). Varying parameters such as the recharge rates (5 mm/a in simulation 20 and 55 mm/a in simulation 21) has some effect, though the "exchange equilibrium front" does not reach the bottom of the clays (Figures 6.9c and 6.9d). Raising the cation concentrations in the infiltrating groundwater has a much larger effect, as the quantities exchanged between dissolved and adsorbed cations are larger. If 100 % Lelydorp groundwater is allowed to infiltrate (simulation 17), the entire clay column reaches equilibrium with the infiltrating water. If 50 % Lelydorp groundwater is used (simulation 18) the bottom part is not completely equilibrated with the infiltrating water (Figure 6.9e). The equilibrium MgX/CaX ratio is about 1.3, which is still lower than the observed ratio of 4 (Levelt and Quakernaat, 1968). In simulation 19 the same mixed water type was used together with a maximum selectivity for magnesium ($K_{Na/Ca} = 0.6$ and $K_{Na/Mg} = 0.4$). Equilibrium is reached everywhere with this model with a MgX/CaX ratio of about 6 (Figure 6.9f). In simulation 22, which combines simulation model 19 with a low recharge rate of 5 mm/a, the exchange front did not reach the bottom (Figure 6.9g). This indicates that relatively high recharge rates (> 30 mm/a) during the Wisconsinan are likely, as was concluded in Chapter 4, based on the paleohydrological model with the incised palcovalleys.

6.5. Cation-exchange and salinization in the Quaternary and Tertiary formations during the Holocene transgression

6.5.1 Introduction

When the sea inundated the present coastal plain during the Early Holocene, fresh groundwater in the Tertiary aquifers stopped flowing and became subjected to salinization from above and below, mainly by diffusive solute transport (Chapter 3 and 5). It was demonstrated in Chapter 5 that downward diffusive transport in the coastal plain reached a maximum depth of –125 m. Deeper salts have been transported from below by diffusion and lateral dispersion during regression periods with deep groundwater flow. In the next sections cation-exchange is studied occurring during the downward diffusive salt transport. This study is mainly based on analyses of pore-water recovered from clay samples from two boreholes at Koewarasan and Tourtonne and analyses of water from existing wells.

6.5.2.Observations

Because of the high smectite contents of the Holocene clays CEC's of 15 samples from the Koewarasan and Tourtonne boreholes are relatively high, varying between 18 and 32 meq/100 g, with an average of 25 meq/100 g. CEC values for the Pliocene sands vary from 0.1 to 1 meq/100 g dry soil, with an average of 0.6 meq/100 g. Base saturation of the acid savannah sands is less than 20 %.

Holocene clays (Coronie Fm.)

The pore-water analyses from the Tourtonne and Koewarasan boreholes are displayed in Figures 6.6. and 6.7. In these figures cation and sulphate concentrations are expressed as excesses and deficits with respect to mixing of fresh water and seawater based on chloride content. At Tourtonne a 25 m thick succession of Holocene clays is found, covering a period of about 10 ka. In the reactive Holocene sediments the original seawater composition has been transformed by sulphate reduction, which produced large quantities of bicarbonate, and, consequently, by precipitation of calcite and pyrite (Velstra, 1997). Because the sea withdrew from this area only 500 years ago, the chloride concentrations are still close to those in seawater (Section 5.4.1.). The loss of dissolved calcium is partly compensated by desorption of calcium from the exchange sites coupled with adsorption of sodium and ammonium. The net result of these processes is a deficit for dissolved sodium as well as calcium. These processes are best illustrated by sample T21 (Figure 6.6). The other samples have a relatively large imbalance in ion electro neutrality, mainly caused by inaccuracies in the sodium analyses.

At Koewarasan, where marine influence lasted from about 6 to 4 ka BP, only the upper 6 m consist of Holocene sediments. Pore-water salinities are much lower than at Tourtonne (Chapter 4). Here the reverse process becomes apparent (Figure 6.7): pyrites, formed during and shortly after deposition, have already been oxidized, leading to acid soils, high sulphate contents in pore-water and dissolution of carbonates (Velstra, 1997).

Pleistocene clays (Coropina Fm.)

Pleistocene clays have lost most of their reactivity due to prolonged weathering during the last glacial (Veen 1970; Levelt and Quakernaat, 1968; Section 1.6. in Annex I). As a result salinization by diffusion from the overlying Holocene sediments results only in cation-exchange, as can be observed by the calcium excess and sodium deficit of pore-water in Figure 6.7. The magnesium excesses or deficits display a more erratic pattern.

Neogene formations

Cation-exchange patterns in the Neogene formations should be studied along the vertical diffusion path, just as in the Quaternary clays. However, this was not possible, since samples were taken from different wells far apart. Therefore, instead, the chloride concentration was used to mark the advancement of the diffusion process (Chapter 5). In Figure 6.10 excess cation concentrations of all wells in the coastal plain have been plotted against chloride concentrations in mmol/l. Ion excesses (and deficits) have been determined with respect to mixing of seawater and fresh pristine groundwater below the Lelydorp sands (Figure 6.1). The latter is supposed to be the dominant groundwater type in the formations before the Holocene transgression. Samples affected by salinization (Cl > 50 mg/l or 1.4 mmol/l) have sodium deficits balanced in milliequivalents by calcium and magnesium excesses. This is a sign of cation-exchange, in this case related to diffusive salinization. Figure 6.10 further shows that cation deficits and excesses increase linearly with chloride contents. This is not expected because of the non-linear relation between selectivity coefficients and concentra-

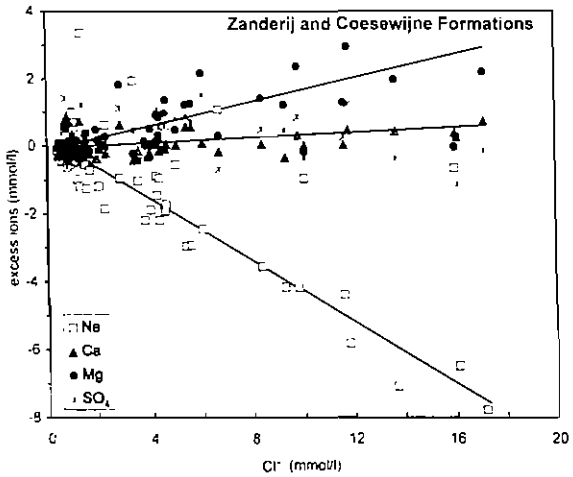

Figure 6.10. Excess ions contents in the Pliocene and Miocene formations (Zanderij and Coesewijne Fm.) against chloride contents. Excess ions concentrations are expressed as excesses relative to the expected concentration from conservative mixing of fresh groundwater (groundwater in Pliocene formations, recharged below the Lelydorp sands) and seawater. Mixing ratios are based on chloride contents.

tion (Equation 5.2) and the chromatographic order of cation release from the exchangers. This suggests that in the Tertiary formations, which have low CEC's, cation-exchange is negligible. Therefore, the observed cation-exchange signature of groundwater in the Neogene formations has probably been formed in the overlying Pleistocene clays.

Stigter (1996) plotted the cation excesses of some samples against the distance to the coastline. This gives essentially the same result, since chloride concentrations generally increase towards the north, where diffusion started earlier on the sloping Pleistocene surface.

Groundwater also displays sulphate excesses with respect to mixing, which cannot be explained easily. Pyrite oxidation has probably taken place, but the deeper part of the Holocene clays, the source of the salts, is strongly reduced and has low sulphate contents.

Paleogene formations

Figures 6.11 and 6.12 show the data for the Oligocene (Burnside) and Eocene/Paleocene (Saramacca) formations. Here a completely different pattern emerges. Sodium concentrations are in excess, while calcium and magnesium do not exhibit clear excesses or deficits. This pattern is most outspoken for the samples of the Paleocene formation (T-sands) from the Tambaredjo oil field. Most of the sulphate is reduced. The low contents of dissolved iron, which has precipitated as pyrite, are probably related to this. As has been discussed in Chapter 5, the solutes at these depths most likely originate from the saline Cretaceous (Figure 3.5). Due to lack of sufficient information on hydraulic and hydrogeochemical processes at these depths, no attempt has been made to analyse these observations in more detail.

6.5.3. *Cation-exchange simulations*

Model set-up

In this section the hypotheses regarding the salinization of the Pleistocene and Neogene formations (Section 4.5 and Chapter 4) are verified by PHREEQC modelling. Simulations in this case are restricted to diffusive solute transport (Chapter 4) and cation-exchange. The results are compared with the groundwater chemistry of the Neogene formations.

The reference model consists of a column with 12 cells at the top representing the Pleistocene clays followed by 113 cells for the Tertiary sediments. All cells have lengths of 1 m. The effective CEC of the Tertiary is quite low 14.4 mmol/l and is based on the average CEC from studies by Poels (1987) and Level and Quakernaat (1968) of sands of the Pliocene Zanderij formation. Diffusion and exchange coefficients and CEC for the clays are equal to those of the previous freshening model (Table 6.1). For the CEC of the Tertiary sediments in the reference model a value of 14 meq/l is used. The downward diffusion process was allowed to continue for a period of 10 ka, which corresponds to the length of time after the sea had reached the present coastal plain in the Early Holocene.

In all simulations pore-water in the cells has the composition of average Lelydorp groundwater prior to the Holoeene inundation. The initial cation composition of the exchange sites of the Pleistocene clays was derived from the findings of Levelt and Quakernaat (1968) and Veen (1970). The initial cation compositions of the exchange sites of the Tertiary formations were determined

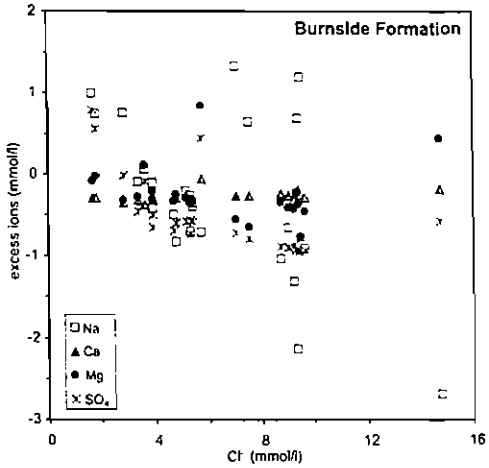

Figure 6.11. Excess ions contents in the Oligocene Formation (Burnside Fm.) against chloride contents. Excess ions concentrations are expressed as excesses relative to the expected concentration from conservative mixing of fresh groundwater (groundwater in Pliocene formations, recharged below the Lelydorp sands) and seawater. Mixing ratios are based on chloride contents.

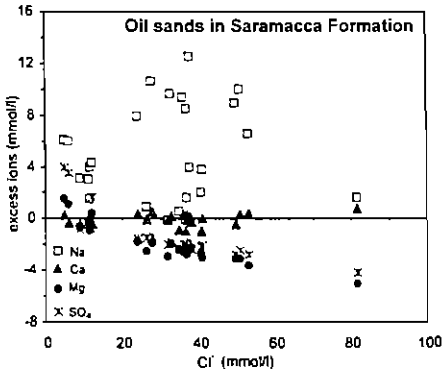

Figure 6.12. Excess ions contents in the oils sands at the base of the Paleocene (Saramacca Fm.) against chloride contents. Excess ions concentrations are expressed as excesses relative to the expected concentration from conservative mixing of fresh groundwater (groundwater in Pliocene formations, recharged below the Lelydorp sands) and seawater. Mixing ratios are based on chloride contents.

by PHREEQC, assuming equilibrium with pore-water. For the diffusion, fixed concentrations of saline water are imposed at the top of the column. These concentrations are derived from pore-water analyses of the Holocene clays at the bottom of Tourtonne borehole (sample T21). The regression and the subsequent upward diffusion are not taken into account, as in chapter 4. The sensitivity of the model was tested for the range of parameters listed in Table 6.2. For the chemical boundary condition at the top also pure seawater was used and the composition of pore-water sample K3 from the Holocene clay in the Koewarasan borehole. This sample has a relatively low salinity and is influenced by pyrite oxidation.

Results

In Figures 6.13a and 6.13b the total concentrations are shown for solutes and the exchangeable cations, respectively, against depth, according to the reference model (simulation 1). In Figures 6.13c and 6.14a excess concentrations of cations have been plotted against depth and chloride concentration, respectively. Excess concentration is defined as the excess (or deficit) with respect to mixing between seawater and average Lelydorp groundwater. Plotting excesses against chloride allows comparison with the analyses shown in Figure 6.10. Figure 6.13a shows how the simulated chloride concentrations decrease rapidly downward, approaching the background value of Lelydorp groundwater at 75 m below the top of the Pleistocene Coropina Formation. This is in agreement with the measurements and analytical simulations of Chapter 4. It should be noted, however, that the PHREEQC model does not take into account the effects of Holocene sedimentation and regression. Figures 6.13c and 6.14a show that diffusion of salts is accompanied by cation-exchange. This process leads to sodium deficits and calcium and magnesium excesses with respect to conservative mixing. Clearly, exchange has not reached equilibrium. The exchange takes place mainly in the Pleistocene clay with its large pool of exchangeable cations.

In the Tertiary formations there is little exchange, as can be seen in Figure 6.14a, which shows the quasi-linear relationship between chloride and cation excesses. The simulation results compare favorably with the chemical analyses, shown in Figure 6.10, though the Mg_{excess}/Ca_{excess} ratio of 2 in the Tertiary formations is lower than the ratios derived from the analyses (3 to 6). Nevertheless, the results suggest that the hydrochemistry of the Tertiary formations is largely defined by conservative mixing of old Pleistocene water and downward diffusing salts, which has acquired its composition by cation-exchange in the Pleistocene clays. The high Mg excess is explained by the dominance of Mg on the exchange sites in these clays prior to the transgression, as measured by Levelt and Quakernaat (1968) and Veen (1970). Most of the sensitivity tests show more or less the same results.

The maximum selectivity for magnesium used in simulation 4 is not likely as it leads to almost equal magnesium and calcium excesses (Figure 6.14b). In this simulation less magnesium and more calcium is released from the clays initially. Simulation 13 with maximum effective CEC (1200 meq/l) for the Pleistocene clays and minimum effective CEC for the Tertiary formations (2 meq/l) resulted in Mg_{excess}/Ca_{excess} ratio of 3.5 and provided the best match with the analyses (Figure 6.14c).

6.6. Discussion and conclusions

Most groundwater in the coastal formations is mineralised because of salt intrusion (Figure 3.5). Pristine groundwater is only found in the savannah belt and below the Lelydorp sands.

This water, even the relatively old pristine water at Lelydorp (> 1 ka BP) has retained a rainwater composition because of the low reactivity of the sediments. The Pleistocene and Tertiary formations contain hardly any calcite and weatherable silicates (Krook, 1979; Sections I.4, I.5, I.6 in Annex I), which is a sign that the coastal formations experienced intensive flushing by meteoric water during protracted regressions (Chapter 4). The present stagnant flow conditions in the coastal plain (Chapter 3) are the exception rather than the rule considered on a geological time scale.

Most groundwater is acid (pH less than 6.5) and undersaturated with respect to calcite.

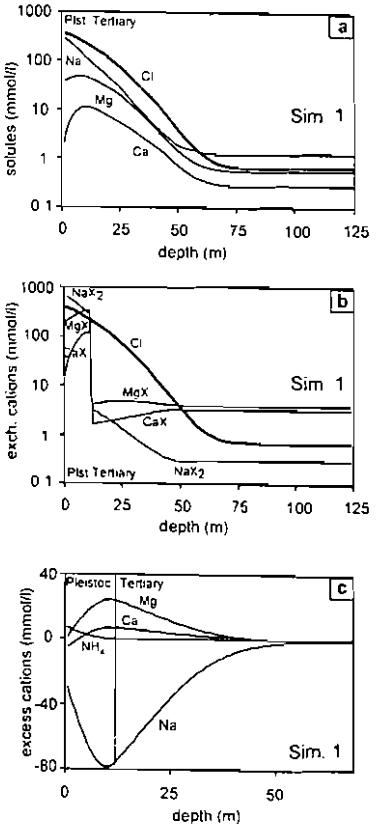

Figure 6.13. Simulated concentrations of dissolved and exchangeable cations and chloride in the Pleistocene and Neogene formations after 8 ka of salinization during the Holocene transgression. PHREEQC models simulate vertical diffusive solute transport and cation-exchange. Saline source is pore-water from Holocene clays (Simulation 1 in Table 6.2).

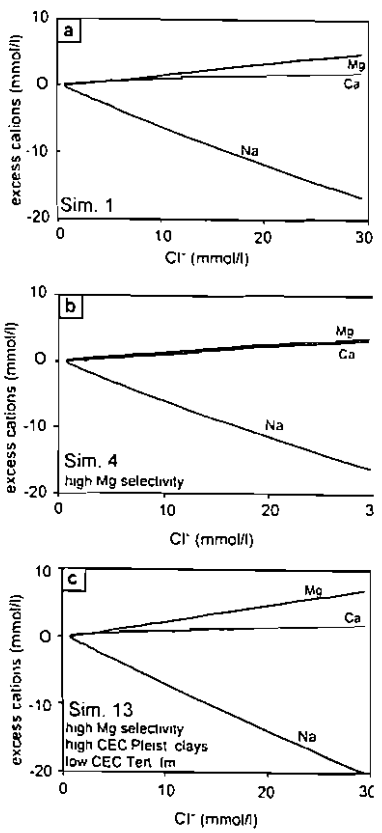

Figure 6.14. Simulated concentrations of dissolved and exchangeable cations in the Pleistocene and Neogene formations after 8 ka of salinization, plotted against chloride concentration. PHREEQC models simulate vertical diffusive solute transport and cation-exchange. Saline source is pore-water from Holocene clays (see Table 6.2). Three different simulations are shown (Simulation 1, 4 and 13 in Table 6.2)

In the deeper formations below a depth of 150 m, and in the Holocene clays, sulphate reduction and methanogenesis has taken place.

The Pleistocene clays in the southern part of the coastal plain contain fresh pore-water now, while the exchange sites of the clays are mainly occupied by magnesium ions. Simulations with the PHREEQC hydrogeochemical code show that this cannot be explained by diffusive solute transport during the Wisconsinan regression. Advective transport corresponding to a recharge of more than 5 mm/a is required to account for this effect. This is in agreement with the findings of the numerical paleohydrological model, which showed that a relatively high and widespread recharge must have persisted during the Wisconsinan.

Groundwater in the Pleistocene and Neogene (Zanderij and Coesewijne) formations, in the northern and Holocene part of the coastal plain is affected by diffusive downward salinization (Chapter 5). Cation-exchange, associated with the salinization, is recognized by the sodium deficits and magnesium and calcium excesses with respect to conservative mixing of fresh water and seawater. Diffusion and cation-exchange simulations with the PHREEQC code concur with this, showing a good correspondence between observed and calculated cation deficits and excesses. The cation-exchange appears to have taken place mainly in the Pleistocene clays; CEC's in the Tertiary formations are very low and salts from the overlying Quaternary clays have mixed conservatively with the fresh paleogroundwater. This explains the uniform ratios of cation deficits and excesses in the Neogene formations.

In the Paleogene (Burnside and Saramacca Formations), groundwater generally has sodium excesses. Salinization and cation-exchange processes in these deep formations cannot be reconstructed.

Sim. nr.	Chem.comp. Top	Chem. comp. bottom	Column length (m)	CEC (mmol/l)	$K_{Na/Ca}$	$K_{Na/Mg}$	Diffusion coeffic. (m^2/s)	Recharge rate (mm/a)	Longit. dispers. (m)
1	diluted marine	100% Lelydorp	12	600	0.4	0.5	7×10^{-10}	-	-
2	diluted marine	100% Lelydorp	6	600	0.4	0.5	7×10^{-10}	-	-
3	diluted marine	100% Lelydorp	24	600	0.4	0.5	7×10^{-10}	-	-
4	diluted marine	100% Lelydorp	12	600	0.6	0.4	7×10^{-10}	-	-
5	diluted marine	100% Lelydorp	12	300	0.4	0.5	7×10^{-10}	-	-
6	diluted marine	100% Lelydorp	12	1200	0.4	0.5	7×10^{-10}	-	-
7	100% Lelydorp	100% Lelydorp	12	600	0.4	0.5	7×10^{-10}	-	-
8	diluted marine	diluted marine	12	600	0.4	0.5	7×10^{-10}	-	-
9	diluted marine	100% Lelydorp	12	600	0.4	0.5	4×10^{-10}	-	-
10	diluted marine	100% Lelydorp	12	600	0.4	0.5	10×10^{-10}	-	-
11	diluted marine	-	12	600	0.4	0.5	7×10^{-10}	30	0.1
12	diluted marine	-	6	600	0.4	0.5	7×10^{-10}	30	0.1
13	diluted marine	-	24	600	0.4	0.5	7×10^{-10}	30	0.1
14	diluted marine	-	12	600	0.6	0.4	7×10^{-10}	30	0.1
15	diluted marine	-	12	300	0.4	0.5	7×10^{-10}	30	0.1
16	diluted marine	-	12	1200	0.4	0.5	7×10^{-10}	30	0.1
17	100% Lelydorp	-	12	600	0.4	0.5	7×10^{-10}	30	0.1
18	50% Lelydorp	-	12	600	0.4	0.5	7×10^{-10}	30	0.1
19	50% Lelydorp	-	12	600	0.6	0.4	7×10^{-10}	30	0.1
20	diluted marine	-	12	600	0.4	0.5	7×10^{-10}	5	0.1
21	diluted marine	-	12	600	0.4	0.5	7×10^{-10}	55	0.1
22	50% Lelydorp	-	12	600	0.6	0.4	7×10^{-10}	5	0.1

Table 6.1. Simulation parameters for modeling cation-exchange in a column of originally saline Pleistocene clays in Suriname as a result of freshening during the Wisconsinan

Sim. Nr.	Chem.comp. top	Chem. comp. bottom	Column length (m)		CEC (mmol)		$K_{Na/Ca}$	$K_{Na/Mg}$	Diffusion coeffic. (m^2/s)
			Pleist.	Tertiary	Pleist.	Tertiary			
1	saline T21	100% Lelydorp	12	113	14	600	0.4	0.5	7×10^{-10}
2	saline T21	100% Lelydorp	6	113	14	600	0.4	0.5	7×10^{-10}
3	saline T21	100% Lelydorp	24	113	14	600	0.4	0.5	7×10^{-10}
4	saline T21	100% Lelydorp	12	113	14	600	0.6	0.4	7×10^{-10}
5	saline T21	100% Lelydorp	12	113	14	300	0.4	0.5	7×10^{-10}
6	saline T21	100% Lelydorp	12	113	14	1200	0.4	0.5	7×10^{-10}
7	brackish K3	100% Lelydorp	12	113	14	600	0.4	0.5	7×10^{-10}
8	saline T21	100% Lelydorp	12	113	2	600	0.4	0.5	7×10^{-10}
9	saline T21	100% Lelydorp	12	113	24	600	0.4	0.5	7×10^{-10}
10	seawater	100% Lelydorp	12	113	14	600	0.4	0.5	7×10^{-10}
11	saline T21	100% Lelydorp	12	113	14	600	0.4	0.5	4×10^{-10}
12	saline T21	100% Lelydorp	12	113	14	600	0.4	0.5	10×10^{-10}
13	saline T21	100% Lelydorp	12	113	2	1200	0.4	0.5	7×10^{-10}

Table 6.2. Simulation parameters for modelling cation-exchange in a column of Pleistocene and Neogene formations in Suriname as a result of salinization during the Holocene transgression.

Chapter 7.

Isotopic signals of the hydrology and paleohydrology in the coastal plain of Suriname

7.1. Introduction

In this chapter the isotopic parameters (^{2}H, ^{3}H, ^{13}C, ^{14}C and ^{18}O) in groundwater are studied. They may add new information on the paleohydrological conditions in the coastal plain of Suriname. There is abundant literature on the application of these isotopes to determine various aspects of groundwater like origin, mixing, flow system, age and recharge, but also of (paleo)temperatures, vegetation and rainfall patterns (Clark and Fritz, 1997; Kendall and McDonnell, 1998; Cook and Herczeg, 2000; Mook, 2000a)

In Chapter 4 a reconstruction was presented of the LGM landscape, based mainly on earlier studies: the flat Pleistocene surface of the coastal plain and the continental shelf had been dissected by fluvial erosion during the Wisconsinan low stand; rainfall was about half the present-day value and more concentrated in the long rainy season, while temperatures were about 4 to 5 °C lower than today; the elevated interfluves were covered by grass and shrub savannahs, while the incised valleys were bordered by gallery forests. The Saramacca and Suriname rivers, running through deep (> 30 m) valleys, were probably perennial, while the tributaries had an ephemeral character. In this chapter I will use isotopic information mainly to define groundwater ages and flow patterns and to obtain more insight in vegetation and rainfall patterns

7.2. Data

7.2.1. New analyses

^{14}C-isotopes

For this study 30 groundwater samples were gathered. They were analyzed on ^{14}C isotopes by the laboratory of the Center for Isotope Research (CIO) of the Groningen University (the Netherlands). For these analyses groundwater samples of 30 liters were collected in plastic containers. In Suriname all CO_2 gas was expelled from the containers by adding acid and injecting air. The gas was led through a tube and released in bottle with a NaOH solution, where the gas dissolved as carbonate and bicarbonate. The ^{14}C isotope radioactivity was determined by measuring β decay events in a low background proportional counter, filled with the purified sample CO_2.

The ^{14}C content is expressed as a percentage of the measured activity (a_m) to the activity of oxalic acid from 1950 (a_O), the standard for modern atmospheric carbon. The accuracy of ^{14}C analyses of this study is about 1 % (standard deviation). The accuracy is dependent on counting time and counter volume. For groundwater samples an accuracy of 1% (standard deviation) is normally sufficient.

Groundwater samples have become slightly depleted in ^{14}C isotopes by CO_2 loss during transport (see next section), but the effect on ^{14}C content expressed as a percentage of modern carbon is negligible.

^{13}C-isotopes

$^{13}C/^{12}C$ isotopic ratios were analyzed by CIO on 44 groundwater samples. To avoid biological reactions and fractionation an I_2-KI solution was added to the samples. The ratios are measured on CO_2 gas, expelled from the water by orthophosphoric acid. Ratios are expressed as $\delta^{13}C$ values. These are deviations in per mill of the measured $^{13}C/^{12}C$ ratio of the sample with that of the international "VPDB" calibration material. Accuracy of $\delta^{13}C$ measurements is 0.1 ‰. It appeared that many measured $\delta^{13}C$ values of dissolved total inorganic carbon (TIC) were influenced by loss of CO_2 gas in the period between sampling and analysis. Loss of CO2, which is isotopically light with respect to bicarbonate, leads to higher $\delta^{13}C_{TIC}$ values and higher pH. The latter was observed in the difference between laboratory pH and field pH of most samples. For most samples, CO_2 loss could be estimated by substracting the amount of TIC, measured at the CIO laboratory, from the original TIC. The original TIC was calculated with the PHREEQC code (Parkhurst and Appelo, 1999) on the basis of field pH and hydrochemical composition. Subsequently, the effect of CO_2 loss on $\delta^{13}C_{TIC}$ was calculated with a Raleigh distillation model using the equilibrium fractionation factors reported by Mook (2000b). In the calculations, it was assumed that alkalinity did not change during CO_2 escape and that dissolved carbon species remained in isotopic equilibrium. Calculations showed that the analyses needed negative corrections of 1 to 4 ‰.

^{3}H-isotopes

7 Groundwater samples were analyzed on ^{3}H content (tritium) by β-radiation counting in the CIO laboratory. Prior to measuring H_2 was extracted from water in a mg-oven and combined with tritium-free ethene gas to form ethane gas. The tritium content is determined by relating the measured activity to the activity of a laboratory reference of known TU. TU is the tritium unit and equal to one ^{3}H atom per 10^{18} hydrogen atoms. Samples with low tritium content (< 20 TU), like those from Suriname, are artificially enriched by electrolysis before measurement. Measurement accuracy of enriched water of the new analyses is 0.2 TU.

^{18}O- and ^{2}H-isotopes

47 Samples were analyzed at the CIO laboratory on $^{18}O/^{16}O$ and $^{2}H/^{1}H$ ratios. The ^{18}O-ratios are determined by isotope ratio mass spectrometry (IRMS) on CO_2 gas, which is equilibrated with the water sample. $^{2}H/^{1}H$ ratios are measured with a mass spectrometer on H_2 gas formed from water by directing water vapor over hot uranium. Ratios are expressed in $\delta^{18}O$ and $\delta^{2}H$ as differences with the international calibration material, Vienna Standard Mean Ocean Water (VSMOW). Accuracy of the $\delta^{18}O$ and $\delta^{2}H$ measurements is 0.1 and 2 ‰, respectively.

7.2.2. Analyses from existing isotope studies

In earlier hydrogeological studies isotope analyses have been carried on groundwater samples from the coastal plain of Suriname (UNDP/WHO, 1972; Verleur, 1991). These analyses on ^{14}C (23), ^{3}H (39), ^{18}O (64), 2H (11) and ^{13}C (19) are combined with those carried out for the present study. These analyses have been carried out by CIO in Groningen, The

Netherlands, and the International Atomic Energy Agency (IAEA) in Vienna. Accuracies of existing analyses are comparable to those mentioned above for the new analyses carried out for this study.

In order to relate the isotopic characteristics of groundwater with those of rainfall, data were used from the meteorological stations of Cayenne (French Guiana) and Belem (Brazil). These stations are located 350 km east and 1100 km southeast from the study area, respectively. The data were retrieved from the IAEA GNIP database (Global Network for Isotopes in Precipitation) (http://isohis.iaea.org/). The database contains $\delta^{18}O$ en $\delta^{2}H$ analyses of monthly precipitation totals. The Cayenne dataset comprises 79 records (31 records lack deuterium analyses) from the 1962 to 1976 period. The Belem database covers the 1965 to 1988 period and contains 233 records (32 records without deuterium analyses).

Apart from the GNIP data, also precipitation analyses from other studies were used. Negrel at al. (1997) studied isotopic and hydrochemical composition of monthly rainfall samples from Cayenne in 1995. Important for the present study were also the data from Matsui et al. (1983), who carried out $\delta^{18}O$ analyses on more than 400 daily samples from Belem in the 1978 to 1980 period.

Van Vliet (1998) gathered all existing and new isotopic data. Her report also presents isotopic data of pore water squeezed from samples of the Koewarasan and Tourtonne core drillings (Velstra, 1997). These will be discussed in future publications.

7.3. Identification of hydrogeochemical processes and paleovegetation with $\delta^{13}C$ of dissolved inorganic carbon

7.3.1. Introduction

$\delta^{13}C$ isotope ratios of dissolved total inorganic carbon (TIC) can provide valuable information regarding the carbon sources and sinks along the groundwater pathway. As soon as groundwater enters the soil, carbon-dioxide gas is taken up because of the relatively high partial pressure caused by root respiration and oxidation of soil organic matter. The $\delta^{13}C$ value of this gas ($\delta^{13}C_{CO2(pl)}$) depends on the photosynthetic process of the vegetation (O'Leary, 1988). Most plants have a Calvin or C3 photosynthetic pathway and produce carbon with $\delta^{13}C$ values of –22 to –33 ‰, with an average of -27 ‰ (Vogel, 1993). This figure is also representative for soil organic matter produced by forests in Brazil (Martinelli et al., 1996). Carbon from plants with a Hatch-Slack or C4 photosynthetic pathway is characterized by $\delta^{13}C_{CO2(pl)}$ values varying between from –10 to –16 ‰ with an average of –13 ‰ (Vogel, 1993). Plants operating according to the CAM pathway have intermediate $\delta^{13}C$ values. Most C4 plants are found among the family of monocotyledonous grasses and sedges. C4 plants thrive particularly well in semi arid and hot climates and low atmospheric CO_2 content (Ehleringer et al., 1997). This is why C4 plants were much more abundant during the LGM, when the atmospheric CO_2 content was 180 ppmV (Cole and Monger, 1994). During the Holocene, atmospheric CO_2 content increased to a preindustial value of 275 ppmV and currently to 370 ppmV as a result of fossil-fuel combustion during the last century.

Because of diffusion and mixing with atmospheric carbon-dioxide gas ($\delta^{13}C_{CO2(atm)}$ at present is –8 ‰ and in preindustrial Holocene –6.5 ‰), the actual isotopic composition of carbon-dioxide gas ($\delta^{13}C_{CO2(so)}$) is higher than $\delta^{13}C_{CO2(pl)}$. Cerling (1984) and Cerling et al. (1991) showed that a minimal enrichment of 4.4 ‰ could be expected below the root zone

in soils with a high partial carbon-dioxide pressure (> 10^{-2} atm), like we find in Suriname (Section 6.3.2). Carbon-dioxide gas dissolved in the percolating groundwater ($\delta^{13}C_{CO2(aq)}$) is depleted by 1‰ with respect to $\delta^{13}C_{CO2(soil)}$ at the average soil temperature of 27 °C in Suriname. It is therefore assumed that, in the tropical soils of Suriname, $\delta^{13}C_{CO2(aq)}$ will be about –9.5 under C4 vegetation and –23.5 under C3 vegetation. At present, the natural vegetation of the study area consists mainly of dry-land forests and marshland forests in the lower clayey parts of the coastal plain (Lindeman and Moolenaar, 1959; Teunissen, 1978). These vegetation types comprise mostly C3 plants.

Further along the flow path, carbon may be added to the groundwater by dissolution of minerals and sediment organic matter (SOM). These reactions do not take place in the deply weathered soils of the recharge areas in Suriname but at larger depth in the saturated zone (Section 6.3.4) under closed conditions (no interaction with soil gases). In that case, the $\delta^{13}C_{TIC}$ of total inorganic carbon in groundwater is a mixture of the original $\delta^{13}C_{CO2(aq)}$ and the isotopic composition of the added carbon, unless fractionation occurs due to precipitation or methanogenesis (Clark and Fritz, 1997).

Carbonate dissolution does not occur in the Tertiary sediments of the coastal plain, which was indicated by the under-saturation with respect to calcite and by the non-carbonate source of dissolved strontium (Section 6.3.3). Precipitation of siderite may take place in some parts (Section 6.3.4), which is accompanied by some fractionation. However, this effect will not be taken into account in this study.

Carbon is only added to the groundwater by liberalization of SOM, which is found frequently as lignite in the lower Pliocene and Miocene sediments (D'Audretsch, 1953). Palynological data (Wymstra, 1969) show this SOM consist mainly of C3 plant material (Rhizopora and Palmae). Analyses of Holocene peat with the same plant material show that $\delta^{13}C_{SOM}$ values vary from -25 to -31 ‰ (Roeleveld and Van Loon, 1979; Van Vliet, 1998). Tertiary SOM will probably be enriched relative to these values because of breakdown of the more reactive organic compounds. Martinelli et al. (1996) found an enrichment of about 2 ‰ for organic matter of Pleistocene age in Brazilian soils. Therefore, an average of –25 ‰ is assumed for SOM in the Tertiary formations.

Breakdown of SOM takes place mainly by iron and sulphate reduction in the Pliocene, Miocene and Oligocene formations and results in inorganic carbon with $\delta^{13}C$ equal to its source. In the more saline deeper formations and in the Holocene clays methanogenesis takes place and produces highly enriched inorganic carbon (> 5 ‰). As this signal obscures the other processes, the samples with salinities higher than 1000 mg/l have been left out.

7.3.2. Results

The range of $\delta^{13}C_{TIC}$ values of groundwater in the Tertiary formations is shown in Figure 7.1. The analyses have been subdivided in age categories expressed in ^{14}C activities. Though the samples cover a wide range of values between –26 and +2 ‰, almost half of the samples (47 %) fall in the range of –17 to –20 ‰. Note that no samples have been found in the ^{14}C activity class between 30 and 45 %.

All samples are enriched with respect to the initial soil carbon-dioxide formed under C3 vegetation, presently covering most of the study area. Dissolution of marine carbonates with $\delta^{13}C$ values between -3 to +3 ‰ (Clark and Fritz, 1997) is usually the cause for the enrichment, but is absent in this case (Section 6.3.3). Methanogenesis as a possible cause of enrichment is not likely either, because samples from the saline and mostly methanogenic zones have been left out. In a few samples the methanogenic cause for high $\delta^{13}C$ values (> -11 ‰) can be inferred from the anomalously high TIC contents. This leads to the hypothesis that the $\delta^{13}C_{TIC}$ value of soil carbon-dioxide may have been higher than at present. Two mechanisms may lead to the typical $\delta^{13}C_{TIC}$ values of –17 to –20 ‰:

1. Dissolution of carbon-dioxide gas in a soil under a vegetation with a mixture of C3 (-23.5 ‰) and C4 (-9.5 ‰) plants: it is noted that C3 and C4 plants do not necessarily have to be mixed within a single vegetation type; mixing in the aquifers of groundwater formed under different vegetations has the same effect.
2. Dissolution of carbon-dioxide in the soil under a C4 vegetation (-9.5 ‰) followed by dissolution of carbon from SOM (-25 ‰) under influence of iron and sulphate reduction. Mixing leads to the observed range between –17 to –20 ‰.

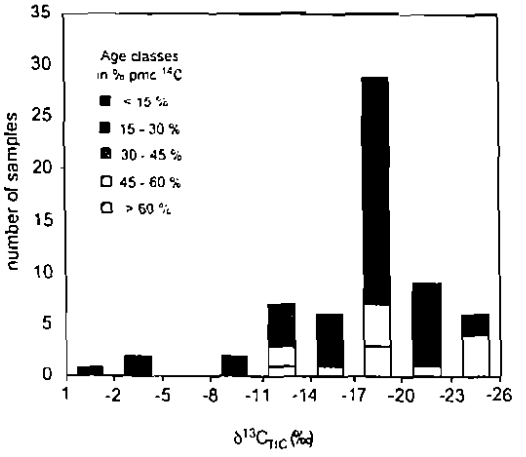

Figure 7.1. Frequency of $\delta^{13}C_{TIC}$ analyses for different radiocarbon activity classes expressed as % of modern ^{14}C activity (pmc).

The first mechanism implies that the contribution of C3 and C4 plants to soil carbon-dioxide is about equal and that no carbon from SOM is added further along the groundwater flow paths. This not likely as TIC of most groundwater samples ranges from 2 to 8 mmol/l, which exceeds the initial TIC of 1 to 2 mmol/l, estimated in Section 6.3.2. The second mechanism is more realistic, but requires a vegetation dominated by C4 plants.

In Chapter 4 it was conjectured on hydraulic grounds, that the major part of the groundwater was formed during the LGM and Early Holocene. At that time, extensive grass savannahs covered the study area (Van der Hammen, 1974; Markgraf, 1989; Van der Hammen and Absy, 1994). Relics of these grass savannahs are the present patches of open savannahs in the savannah zone and some isolated well-drained places in the Pleistocene coastal plain (Jansma, 1994). (In the study area open grass and shrub savannahs occupy only 30 % of the savannah zone). These grass savannah patches persist on the leached sandy and silty soils because of the low retention capacity for moisture and nutrients. Because the modern savannahs are believed to contain the same plant species as the old savannahs, their C3/C4 plants ratio was determined based on floristic studies of the modern savannahs (Heyligers, 1963; Van Donselaar, 1965; Jansma, 1994). For species with a dominance factor higher than 1 (surface coverage of more than 5 %), the photosynthetic pathways were determined by consulting plant databases (Dallwitz, 1980; Dallwitz et al., 1993 and onwards; Ehleringer et al., 1997). The results are presented in Annex IV. It appeared that 83 % of the dominant plant species, mostly grasses and sedges from the open grass savannahs, belong to the C4 group. By contrast, in the savannah bushes and forests less than 7 % of the dominant species have C4 photosynthetic pathways. For verification, plant tissue of the most

dominant grass (*Panicum micranthum*) and shrub (*Clusia fockeana*) from the grass savannah south of Zanderij was analyzed in the CIO laboratory of the Groningen University. The assumed C3 and C4 character of these plants was confirmed by the $\delta^{13}C$ values of -29.95 and -13.95 ‰, respectively. The general conclusion is that all grasses and sedges in the open savannah area belong to the C4 group, while all dicotyledonous plants belong to the C3 group. Therefore groundwater recharged in grass savannahs is expected to have relatively high $\delta^{13}C_{TIC}$ values. $\delta^{13}C_{TIC}$ values of shallow groundwater samples confirm this, though they are few in number: $\delta^{13}C_{TIC}$ values of 4 samples are lower than -23 ‰ (fully C3 vegetation), while one sample on the border of an open grass savannah has a $\delta^{13}C_{TIC}$ of -12 ‰ (more than 80 % C4 contribution).

The hypothesis is verified by determining the $^{13}C_{TIC}$ mass balance. Knowing the $\delta^{13}C$ values of dissolved soil carbon dioxide gas (-9.5 ‰) and mineralized SOM (-25 ‰) and the total TIC content and $\delta^{13}C$ value of a sample, the initial TIC content can be calculated. The outcome is a wide range of TIC values, averaging around a value of 1.8 mmol/l. Figure 7.2 shows the results of a reverse calculation, where measured and calculated $\delta^{13}C_{TIC}$ for groundwater are shown for an initial TIC of 1.8 mmol/l. Especially the large group with values between -17 and -20 ‰ seems to fit well. The amount of 1.8 mmol/l for initial TIC is close to upper limit of the range of 1 to 2 mmol/l estimated in Section 6.3.2.

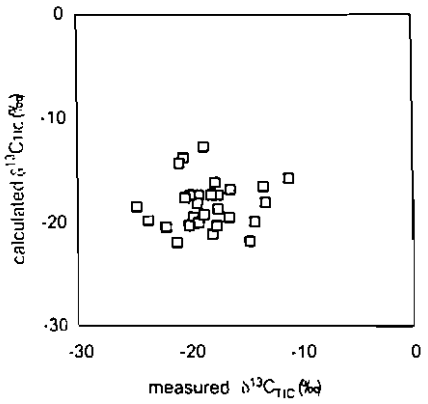

Figure 7.2. Measured and calculated $\delta^{13}C_{TIC}$ of groundwater, based on mixing of initial TIC (1.8 mmol/l) from dissolution of soil carbon-dioxide gas in recharge area under C4 vegetation (-10 ‰) with secondary TIC from oxidation of sediment organic matter (-25 ‰).

The idea that C4 species dominated the LGM savannahs is corroborated by $\delta^{13}C$ shifts in organic material in Brazilian soils (Martinelli et al., 1996). Shifts in $\delta^{13}C$ of soil carbonates in New Mexico were also related to change of C4 to C3 vegetation between 7 and 9 ka (radiocarbon) BP (Cole and Monger, 1994).

7.4. Groundwater dating with ^{14}C of dissolved inorganic carbon and ^{3}H of groundwater

7.4.1. Introduction

Groundwater dating, based on the exponential decay of radiogenic ^{14}C in dissolved inorganic carbon (TIC), may be complicated by admixture of other carbon sources as discussed above. In the study area, the situation is relatively simple. In the soil, groundwater takes up gaseous carbon-dioxide and therefore has an initial ^{14}C activity equal to atmospheric ^{14}C activity. The fractionation by gas diffusion and dissolution, as discussed above, has a negligible effect on the ^{14}C activity expressed as a percentage ratio to modern atmospheric carbon. Apart from soil carbon-dioxide dissolution, all other processes are assumed to take

place under closed conditions (see above). Without admixture from other sources, groundwater age can be determined according to:

$$t_{14} = -8267 \ln \frac{a_m}{a_0} \qquad (7.1)$$

where t_{14} = time since groundwater recharge (^{14}C age) and a_m and a_0 are the activities of the measured ^{14}C and atmospheric ^{14}C during recharge, expressed as pmc (percentages to modern carbon in 1950). As shown in Sections 6.3.3 and 6.3.4, organic material SOM from the Tertiary formations is dissolved along the groundwater pathway and carbonate dissolution is negligible. Since SOM is very old compared to the half life of ^{14}C, only "dead" carbon is added, which "dilutes" the ^{14}C content of the initial carbon from the soil zone. Under these conditions the corrected age t'_{14} becomes (Clark and Fritz, 1997):

$$t'_{14} = -8267 ln\left(\frac{a_m}{a_0} \cdot \frac{TIC_m}{TIC_{rec}}\right) \qquad (7.2)$$

where TIC_m is the measured TIC content of the sample and TIC_{rec} is the initial TIC content after recharge. TIC_m values of groundwater from the Tertiary formations were calculated with the PHREEQC code from measured pH and bicarbonate contents of the samples and ranged from 0.5 to 12 mmol/l (Annex III). Estimates for TIC_{rec} in the recharge area, based on soil CO_2 pressures, range from 1 tot 2 mmol/l (Section 6.3.2.). Interpretation of the $\delta^{13}C_{TIC}$ values of groundwater learned that TIC_{rec} was probably close to 1.8 mmol/l.

Outside the present recharge areas (savannah zone and the Lelydorp sands), groundwater is influenced to some degree by mixing with saline groundwaters from the Holocene formations above or the Early Tertiary and Cretaceous formations below. Because TIC and ^{14}C content of these saline sources are not well known, all samples with chloride concentrations higher than 1000 mg/l (more than 5 % seawater contribution) were, again, left out.

Apart from geochemical reactions, corrections may also be required for diffusive loss of ^{14}C (Sanford, 1997) or dispersion (Johnson and Depaolo, 1996). However, these corrections cannot be applied, unless present and previous flow paths can be reconstructed in some detail.

The initial atmospheric activity a_0 in (1) and (2) has not been a constant in time. Atmospheric ^{14}C content has decreased steadily from 150 % pmc at 20 ka BP to 100 % pmc in 1950 AD. This effect has been accounted for by correcting ^{14}C ages by means of an empirical relation based on calibration data from Stuiver et al. (1998).

$$t_{cal} = -4.10^{-10}\left(t'_{14c}\right)^3 + 2.10^{-5}\left(t'_{14c}\right)^2 + 1.0473\left(t'_{14c}\right) - 71.299 \qquad (7.3)$$

7.4.2. Results

In Figure 7.3 the uncorrected radiocarbon ages t_{14} (Equation 7.1) are plotted against the ages corrected for dead-carbon dissolution t'_{14} (Equation 7.2) and atmospheric ^{14}C activity t_{cal} (Equation 7.3). Most samples show a sizable reduction in age after dead-carbon correction. The correction for atmospheric ^{14}C activity (Equation 7.3) results in an increase in age for ages higher than 10 ka BP.

The radiocarbon ages are checked by plotting $\delta^{18}O$ of groundwater against the corrected radiocarbon age (Figure 7.4). The shift in $\delta^{18}O$ content, marking the climatic change at the beginning of the Holocene is found around a radiocarbon age of 10 ka BP, which corresponds with other groundwater dating studies in the tropics and subtropics (Kimmelman et al., 1989; Stute et al., 1995; Heaton et al., 1986; Stute and Talma, 1998). Although this does not "prove" that the applied corrections are correct, it does indicate that there is, given the uncertainties, no point to pursue further corrections. The errors introduced by field, laboratory and correction procedures create a large uncertainty in the final groundwater ages. Especially the errors related to the assumptions for the dead-carbon correction are very critical. These errors are most probably systematic and, therefore, relative groundwater ages and isochrones patterns are more significant rather than absolute ages.

Dead-carbon dissolution during passage through lignite layers in the Late Tertiary formations is accompanied by a rapid decrease of ^{14}C content and explains the lack of samples with ^{14}C activities between 30 and 45 % as was noted above. This is

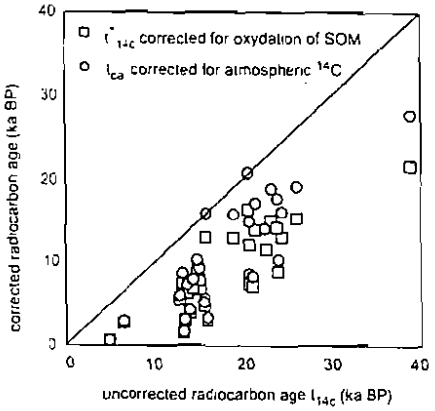

Figure 7.3. Radiocarbon ages for groundwater corrected for seawater mixing, oxidation of sediment organic matter (SOM) and atmospheric ^{14}C activity.

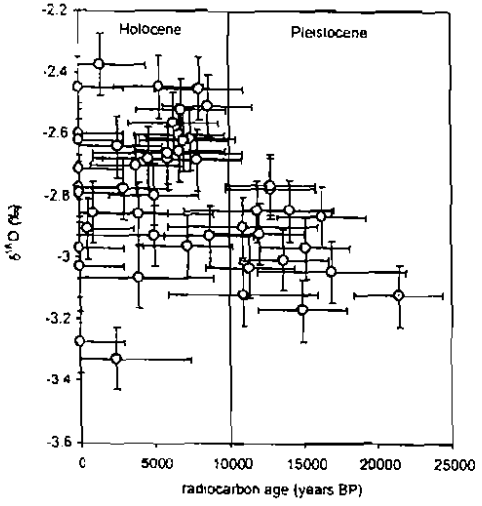

Figure 7.4. Relation of $\delta^{18}O$ and radiocarbon age of groundwater. Values have been corrected for dead-carbon dissolution by oxidation of organic matter.

consistent with Figure 7.5, which shows that samples low in ^{14}C activity generally have higher TIC contents.

Figure 7.6 shows the groundwater ages in a North-South transect in the coastal plain. The corrected and calibrated groundwater ages in the Young Coastal Plain range from 20 to 7 ka BP. These ages demonstrate that groundwater has been formed in a period before the sea invaded the present coastal plain, when there was still groundwater flow in the Tertiary formations (Chapter 4). Groundwater in the Holocene coastal plain, therefore, can be denoted as paleo-groundwater (definition in Section 2.4). As would be expected, younger groundwater is only found below the present recharge areas of the savannah zone and the Lelydorp sands, where groundwater has not been affected by salinization (Sections 3.6.2 and 5.6.1).

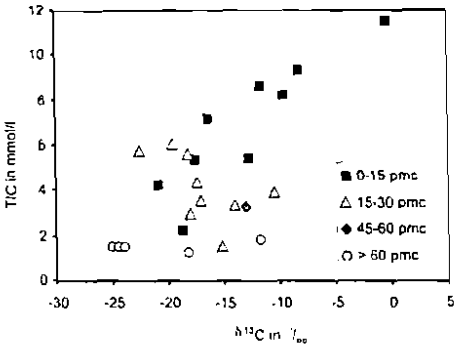

Figure 7.5. Total inorganic carbon contents and $\delta^{13}C_{TIC}$ of groundwater for different radiocarbon activity classes expressed as a percentage of modern ^{14}C activity (pmc).

Although there are not many data, the subhorizontal isochrones in the Holocene coastal plain indicate that, during the Late Wisconsinan, recharge to the Tertiary aquifers was more widespread, as was derived from the paleohydrological model discussed in Chapter 4: if paleorecharge would have been confined to the present recharge areas, the isochrones in the Holocene coastal plain would show a more oblique pattern.

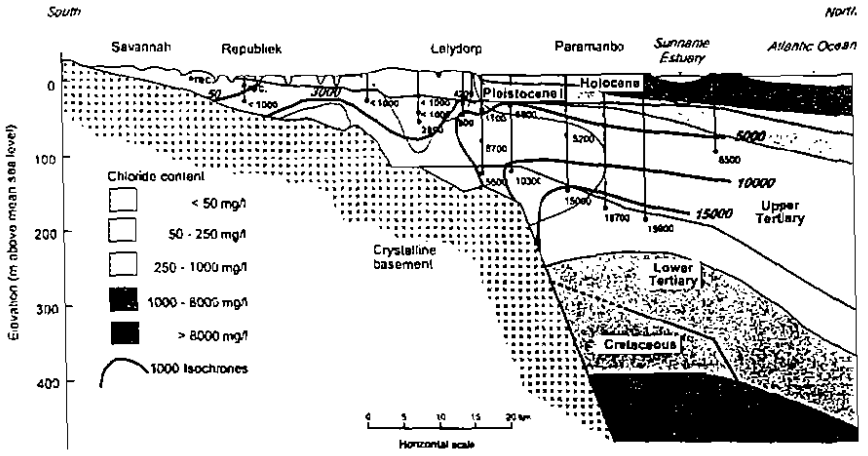

Figure 7.6. North-South geological section in the coastal plain of Suriname with groundwater ages and salinities

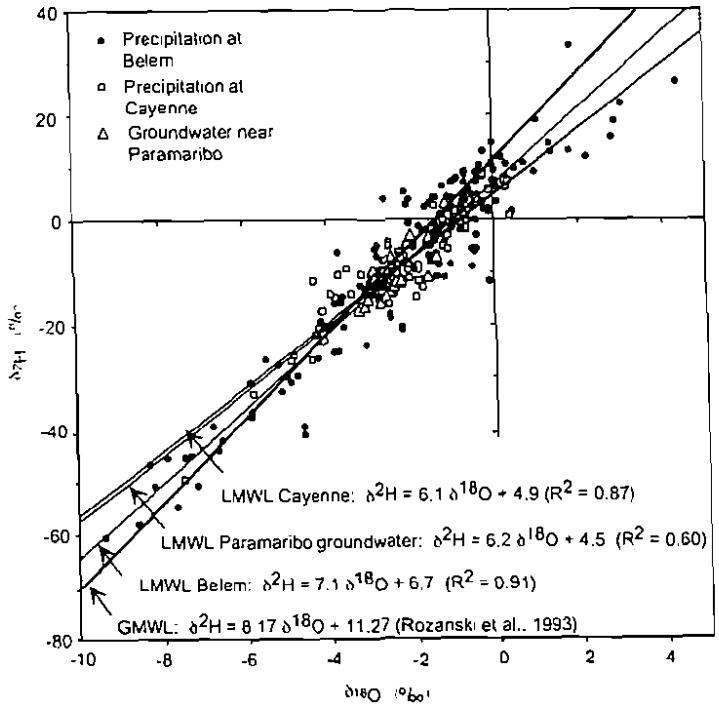

Figure 7.7. Weighted monthly averages of stable-isotope composition in rainfall at Cayenne, French Guiana (1962 to 1975) and Belem, Brazil (1965 - 1985) and in groundwater around Paramaribo, Suriname. Rainfall data are derived from the IAEA/WMO GNIP database.

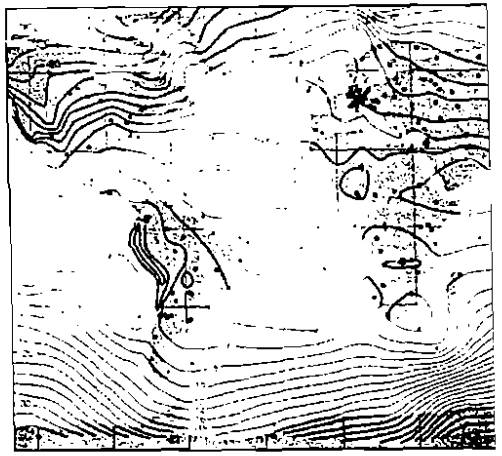

Figure 7.8. $\delta^{18}O$ pattern of average yearly rainfall over North and South America, Africa and Europe (After Rozanski et al., 1993)

7.5. Reconstruction the paleoclimate with stable $\delta^{18}O$ and $\delta^{2}H$ isotopes in rainfall and groundwater

7.5.1. Introduction

The stable $\delta^{18}O$ and $\delta^{2}H$ isotopes of groundwater may contain paleoclimatic information as they reflect the isotopic signature of precipitation at the time of recharge. First we will have a closer look at spatial and temporal stable-isotope patterns of tropical rainfall, as they are somewhat different from those at middle latitudes.

The relation between $\delta^{18}O$ and $\delta^{2}H$ of tropical rainfall deviates slightly from the Global Meteoric Water Line (GMWL) shown in Figure 7.7 (Rozanski et al., 1993):

$$\delta^{2}H = 8.17\,\delta^{18}O + 11.27 \qquad (7.4)$$

The slope of local meteoric water lines (LMWL) in the tropics is often smaller because of the "amount effect" (Dansgaard, 1964). Relatively light rains appear to be enriched in $d^{18}O$ and $d^{2}H$ in comparison to heavy rains. The overall effect is that the slope of the LMWL through the data points is smaller than 8. According to Dansgaard (1964), the main cause is evaporation and, hence, enrichment of raindrops of light rains. Other explanations for the difference between light and heavy rains proposed by him are: (i) exchange with "heavier" atmospheric moisture below the clouds, which tends to have more effect on light showers, and (ii) gradual depletion of the condensate during rain development resulting in low isotopic content in prolonged rain showers.

The average weighted $\delta^{18}O$-values of precipitation of various meteorological stations displays a worldwide spatial pattern (Figure 7.8), called the "latitude effect" (Dansgaard, 1964). Superposed on this pattern are "continental effects" and "mountain effects" (Dansgaard, 1964). These patterns result from Rayleigh distillation taking place during continuous condensation and rainout from water-vapor masses, which are moving from warm to colder regions (Merlivat and Jouzel, 1983; Van der Straaten and Mook 1983). Consequently, average weighted $\delta^{18}O$ of precipitation is linearly related to the average yearly temperature at the meteorogical station (Jouzel et al., 1994). The relation of spatial patterns with temperature does not exist in (sub)tropical regions with average temperatures above 20 °C. Relevant for Suriname is the study by Salati et al. (1979), who attributed the small east-west gradients in stable-isotopes of rainfall over Amazonia to recirculation of water by evapotranspiration from the rainforests.

Seasonal to secular time variations in the stable-isotope composition of precipitation are also related to temperature variations in middle and high latitudes (Rozanski et al., 1992, 1998). A $\Delta\delta^{18}O/\Delta T$ value of 0.6 is generally used to calculate the difference between the LGM and present temperatures. This value includes the correction of about 1.1 ‰ for the higher ^{18}O content of ocean water during the LGM (Shackleton, 1987; Jouzel et al., 1994). Just as the spatial relationship, the large-scale temporal relationship is absent in the tropics and subtropics according to Rozanski et al. (1992, 1998) and Stute et al. (1995). The reason is that distance and temperature difference between the tropical landmasses and the oceans (vapor source) are small, also during the LGM. Therefore, isotopic depletion of water vapor by Rayleigh distillation during rainout is limited and not much effected by global cooling.

Nevertheless, tropical and subtropical America and Africa were about 4 to 6 °C colder during the LGM (Heaton et al., 1986; Stute et al., 1992, 1995; Plummer, 1993; Dutton,

1995; Stute and Bonani, 1995; Clark et al., 1997, 1998; Stute and Talma, 1998). Some researchers still relate $\delta^{18}O$ depletion of old groundwater in the tropics to a lower LGM temperature, like Sanford and Buapeng (1996) for groundwater at Bangkok and Heaton et al. (1986) for groundwater at Uitenhage, South Africa. In most other areas depleted and even enriched $\delta^{18}O$ values of paleogroundwater are explained differently. In Windhoek and Saltblock in Namibia, Vogel and Van Urk (1975) discovered Late Pleistocene groundwater with $\delta^{18}O$ values depleted by 2.4 ‰ with respect to recent groundwater, which they attributed to recharge in distant and more elevated areas during that period. Stute and Talma (1998) reported isotopically enriched (1.3 ‰) groundwater of LGM age in the Stampriet aquifer also in Namibia. They suggested that this was caused by the advection of Atlantic moisture sources during the LGM. Also, the Floridan aquifer (southeastern USA) contains Pleistocene groundwater enriched in ^{18}O isotopes (2.3 ‰). Plummer (1993) attributed this to an intensification of summer tropical storms during the LGM. Clark et al. (1997) found groundwater in the same region, which (after correcting for the enriched glacial ocean) was slightly depleted with 0.6 ‰. They suggested that this was due to the larger distance to the coastline during the LGM (continental effect). Earlier, Love et al. (1994) proposed the same mechanism to explain the varying degree of ^{18}O depletion in Pleistocene groundwaters in the Otway Basin in Australia. Around Jakarta in Indonesia groundwater does not show any changes at all in $\delta^{18}O$ throughout the LGM and Holocene (Geyh and Söfner, 1989). In the Great Artesian Basin in Australia, groundwater with ages ranging from recent to 300 ka BP shows little variation in stable-isotopes (Airey et al., 1979). Though Stute et al. (1995) do not report $\delta^{18}O$ data in their paleotemperature study of northeastern Brazil, they state that stable-isotopes are not related to paleotemperature. Another study in the south of Brazil shows Pleistocene groundwater depleted in $\delta^{18}O$ by 2.5 ‰ (Kimmelman et al., 1989).

Care should be taken in using groundwater as an archive for the isotopic composition of past precipitation. The isotopic composition of groundwater may not be equal to the weighted average composition of precipitation if recharge is confined to a certain season, like Brinkmann et al. (1963) and Vogel and Van Urk (1975) inferred for the Rhine valley and Namibia, respectively. The stable-isotope composition of groundwater may also be affected by evaporation or isotopic exchange with the rock matrix, but these effects may be recognized as a departure from the GMWL or LMWL, provided one analyses both $\delta^{18}O$ and $\delta^{2}H$.

7.5.2. Results

In Figure 7.7 stable-isotope analyses of rainfall (monthly weighted average) at Belem and Cayenne and groundwater from study area around Paramaribo are presented. Groundwater and Cayenne rainfall analyses plot along a similar LMWL.

$$\delta^{2}H = 6.14\delta^{18}O + 4.87 \quad (R^2 = 0.87) \qquad (7.5)$$

Although the correlation coefficient for the groundwater samples is low (0.60) compared to that Cayenne rainfall (0.87), there is statistically no difference between the two populations. Therefore, it is reasonable to assume that the weather system at Cayenne is representative for the Paramaribo area. The LMWL of Belem rainfall differs slightly from the Cayenne/Paramaribo LMWL because of some extreme values, but the majority of the Belem data fall in the same domain as Cayenne and Paramaribo data (Figure 7.7). The "amount" effect, discussed above, can be recognized in the relatively low slope and low intercept as compared to the GMWL. This effect seems also apparent in Figure 7.9 showing the negative correlation between average monthly $\delta^{18}O$ values and average monthly rainfall amounts for Cayenne and Belem. (As discussed above, the pattern does not correlate with monthly temperature, which hardly varies anyway in this region) The supposed correlation with "amount" is much weaker if the isotopic composition of daily rainfall is analysed for data from Belem (Matsui et al., 1983). In Figure 7.10, the daily records are shown for the wet season (January to June) and the dry season. Rains in both seasons display a small amount effect. However, the seasonal difference is much stronger, as wet season and dry season rains of the same amount differ by about 2 ‰. Therefore, the monthly averages of $\delta^{18}O$ in Figure 7.9 are not so much related to "amount", but rather to seasonal differences in vapour origin, condensation process or ambient air humidity. Dansgaard (1964) studied daily rainfall data from Binza in Congo and concluded that air humidity has an important effect of the stable isotopic composition: lower air humidity causes stronger evaporation and fractionation of the raindrops.

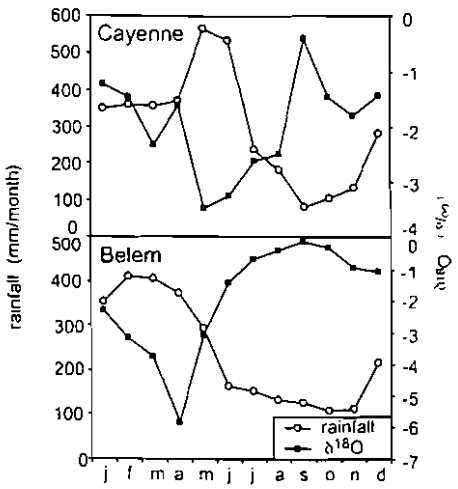

Figure 7.9. Average monthly rainfall and weighted monthly average of $\delta^{18}O$ in rainfall at Cayenne, French Guiana and Belem, Brazil. Basic data for Cayenne cover the years 1962-1975 (IAEA/WMO GNIP database) and 1995 (Negrel et al., 1997). For Belem data are from the years 1965-1985 (IAEA/WMO GNIP database).

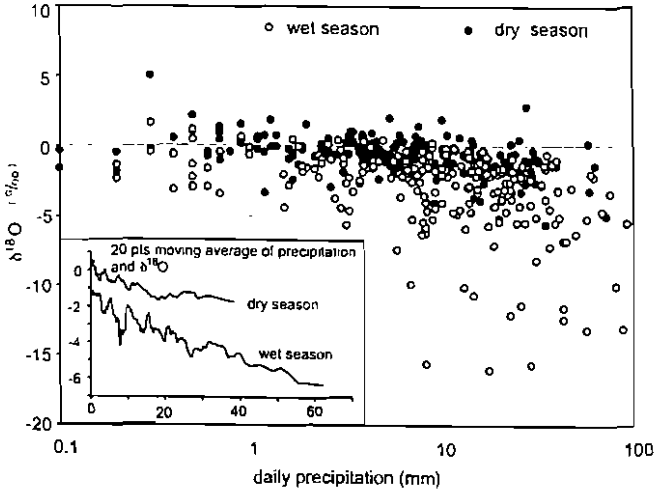

Figure 7.10. Daily rainfall amounts and $\delta^{18}O$ values of 400 daily rainfall samples at Belem from 1978 to 1980. (Data from Matsui et al., 1983). Rains from the relatively wet season (January to July) and relatively dry season (July tot December) are depicted separately. 20-point moving averages of $\delta^{18}O$ are calculated for daily rains in order of increasing magnitude.

As climatic conditions in the Guianas and northeastern Brazil are not essentially different, also the seasonal isotopic behaviour of rain at Cayenne and Paramaribo is related to seasonal weather conditions, rather than amount. Rainfall at Cayenne and Paramaribo is marked by two relatively wet and two relatively dry seasons, related to the passage of the ITCZ over this region twice a year. Figure 7.9 shows that, in particular, the rains from the long rainy season from April to July have depleted values below –2 ‰.

Rainfall during the long rainy season in Cayenne is higher than in the study area around Paramaribo (compare Figures 7.9 and 3.2). Therefore, the weighted yearly average of stable-isotopes in rainfall at Paramaribo will be different from that at Cayenne. The former has been calculated assuming that the monthly isotopic composition at Cayenne and Paramaribo are the same. This assumption is based on the observation that the isotopic composition in this region is related to season rather than amount. Calculations show that average rainfall at Paramaribo is slightly enriched with respect to that of Cayenne (Figure 7.11).

Most groundwater samples are depleted with respect to the average rainfall signature (Figure 7.11). The most probable explanation is that recharge mainly occurs during the months of the short and long rainy season, when rains are relatively depleted. This was already concluded in Section 3.5.1, on the basis of monthly rainfall and potential evaporation. Indeed the weighted average of modern recharge water, calculated from stable-isotopes of precipitation during the 8 wettest months, is close to the composition of average Holocene groundwater (Figure 7.11).

Groundwater of the LGM and Early Holocene is depleted in comparison to younger groundwater: average $\delta^{18}O$ of LGM and Holocene groundwater are –2.9 ‰ and –2.5 ‰ respectively. The actual difference is larger if the effect of the enriched glacial ocean (1.1 ‰) is included. The review in the introduction above made clear that the LGM/Holocene isotopic shift is not related to the temperature shift. Hypotheses related to different water-vapor sources and weather systems are not likely, as these have not essentially changed in

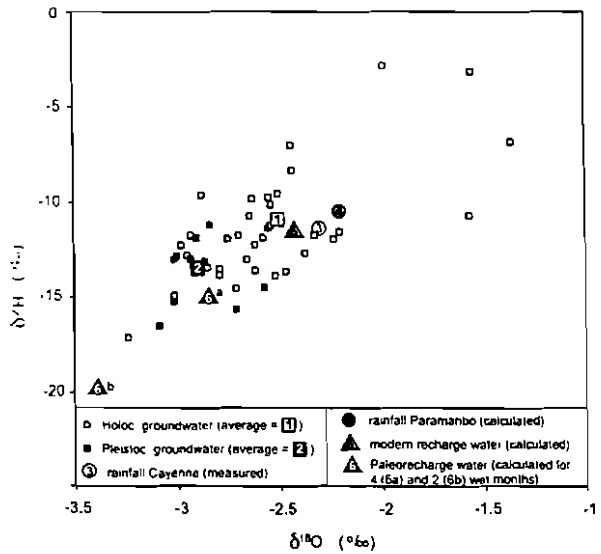

Figure 7.11. Yearly weighted averages of stable-isotope composition of rainfall at Cayenne and Paramaribo and stable-isotope composition of groundwater around Paramaribo.

this area. Larger distance to the LGM shoreline (about 100 km) does not explain the shift either, as $\delta^{18}O$ gradients in present rainfall over northern Amazonia are only 0.75 ‰ per 1000 km or less (Salati et al., 1979). In the present study the more seasonal rainfall pattern during the LGM is proposed as a possible cause. According to palynological studies (Van der Hammen, 1974) and global climate models (Kutzbach et al., 1998) rainfall during the LGM was about half of the present amount of 2200 mm/a and restricted to a single rainy season coinciding with the present long rainy season during April through July. Groundwater recharge during the LGM took place only during this rainy season with a stable-isotope composition comparable to that of present-day rainfall. The $\delta^{18}O$ of this paleorecharge water has been determined by calculating the weighted average from the four wettest months (scenario a) and the two wettest months (scenario b) of present-day rainfall. Figure 7.11 demonstrates that the paleorecharge water according to scenario a) is close to the average isotopic composition of Pleistocene groundwater. However, if the correction for the enriched ocean during the LGM (1.1 ‰) is applied, paleorecharge according to scenario b) is more likely.

7.6. Discussion and conclusions

$\delta^{13}C$ analyses in combination with hydrogeochemical information show that the dissolved inorganic carbon (TIC) results from dissolution of carbon-dioxide gas in the soil zone and mineralisation of sediment organic matter (SOM). The $d^{13}C$ mass balance demonstrates that in most samples in the coastal plain soil carbon-dioxide gas has been produced under a vegetation dominated by plants with a Hatch-Slack (C4) synthetic pathway (O'Leary, 1988). However, today C4 plants are not common in the natural vegetation types of the study area, consisting mainly of dicotyledonous plants (Lindeman and Moolenaar, 1959; Teunissen, 1978). Data from floristic studies revealed that C4 plants (grasses and edges) are currently dominant only in the open grass savannahs found in some isolated parts of the study area (Heyligers, 1963; Van Donselaar, 1965; Jansma, 1994). Since most groundwater dates from the LGM and Early Holocene, open grass savannahs must have covered the major part of the coastal plain during this interval. This was also concluded by Van der Hammen (1974) on the basis of palynological data. The present open grass savannahs in the savannah belt are supposed to be relics of these vast grass savannahs during the LGM (Teunissen, personal communication).

The $\delta^{13}C_{TIC}$ values appear to be influenced by loss of CO_2 during sampling and transport. For these acid waters, it is recommended to carry out pH and alkalinity tests both in the field and prior to processing in the laboratory in order to check, and if necessary, to correct measured $\delta^{13}C_{TIC}$.

Groundwater ages in the Tertiary formations of the coastal plain of Suriname vary from recent to 30 ka BP. The outcropping Pliocene sands in the savannah zone in the south contain recent groundwater: the high tritium contents (UNDP, 1972) indicate that the major part of the groundwater has been recharged after 1950. In the coastal plain northward of Republiek, groundwater ages are generally higher than 1000 years and more mineralised. Late Holocene groundwater (1 to 5 ka BP) is found in the upper part of the Pliocene formation. The recharge zone of the Lelydorp sands is marked by a downward protrusion of this relatively young groundwater. Groundwater in the major part of the coastal formations is of Early Holocene to LGM age. This supports the conclusion from Chapter 4 that the large body of stagnant groundwater in the coastal plain is paleogroundwater formed before the

marine inundation. In that period the lower and the more northward position of the coastline and the erosive relief of the coastal plain led to small, but more widespread, recharge in the entire coastal plain. Despite the low accuracy of the ages, the subhorizontal position of the isochrones suggests that groundwater recharge was not confined to the present recharge areas.

The amount effect can be observed in the weighted monthly averages of stable-isotope composition ($\delta^{18}O$ and $\delta^{2}H$) in rainfall at Belem and Cayenne, located 350 km east and 1100 km southeast of the study area. However, the amount effect largely disappears in the analyses of daily rainfall at Belem (Matsui et al., 1983). It is therefore concluded that the seasonal stable-isotope pattern is more related to specific weather systems related to the position of the Inter-Tropical Convergence Zone (ITCZ). The summer monsoon rain, falling during the northward passage of the ITCZ from April to August (long rainy season), has the most depleted values.

Average Holocene groundwater in the Suriname coastal plain is depleted with respect to average rainfall at Cayenne and Paramaribo. The depletion with respect to rainfall is attributed to the fact that recharge takes place mainly during the wet months of the short and long rainy seasons which has more depleted rains (see also Section 3.5.1). Average Pleistocene groundwater is even more depleted than Holocene groundwater, which in the tropics is not related to the colder climate. The low $\delta^{18}O$ and $\delta^{2}H$ values probably indicate that paleorecharge was restricted to a rainy season during boreal summer, similar to the present-day long rainy season, which is the wettest period with the most depleted rains. This is in agreement with other studies stating that rainfall during the LGM was lower and more seasonal than today (Van der Hammen, 1974; Markgraf 1989, 1993; Van der Hammen and Absy, 1994; Kutzbach et al., 1998). The different climatic pattern is probably related to the shifted position of the ITCZ during the LGM.

Part II.

Generic investigations into the origin of offshore meteoric groundwater

Chapter 8.

Worldwide observations of offshore meteoric groundwater

8.1. Introduction

The preceding chapters dealt with the paleohydrological processes that have led to the rather specific groundwater conditions of the Suriname coastal plain, notably the vast body of meteoric groundwater (defined in Section 2.1.) extending to more than 90 km offshore the Suriname coast. The question now arises, how abnormal is the Suriname case compared to other coastal plains worldwide? And can we state something in general about the origin of offshore groundwater? This is an important question as, in many classical concepts of coastal hydrology, the meteoric groundwater domain is still supposed to end somewhere near the coastline.

Although systematic surveys of offshore groundwater are rare, an attempt is made here to review a number of observations of offshore meteoric groundwater. In this case "offshore" means a distance of more than a few hundreds of meters from the coast, since the presence of meteoric groundwater in the very near-coastal zone would be considered "normal". The observations are divided into two groups: observations of submarine groundwater discharge and observations of groundwater in wells and boreholes.

8.2. Submarine groundwater discharge

Meteoric groundwater may discharge directly to the sea via submarine springs and as diffuse seepage through aquitards. This form of discharge of meteoric groundwater is a substantial part of the world hydrological balance. Zektser and Loaiciga (1993) estimate that total groundwater discharge is about 6 % of the river discharge to the oceans, while the dissolved solid discharge by groundwater is even 52 % of the discharge by rivers

8.2.1. Submarine springs

Submarine springs are well known all over the world. Their occurrence and functioning is described by several authors (Kohout, 1966; Stringfield and LeGrand, 1969, 1971; Zektzer et al., 1973; Custodio, 1987). The coasts of the Mediterranean, Black Sea, Persian Gulf, Florida, Yucatan (Mexico) and the Caribbean are well known for this phenomenon. Submarine springs are also reported from Hawaii, Samoa, Australia, Japan, Norway and Chile. Strabo and Plinius the elder, writers from the classical world already described this phenomenon (Kohout, 1966). The latter reports how groundwater from such a spring near Arvad, an island 4 km off the Syrian coast, was diverted by a lead bowl placed on the sea floor over the spring: the pressure, built up under the funnel, forced the water through a long leather hose to the sea surface (Figure 8.1). Spectacular is also the account by Williams (1946) of submarine springs around Bahrein in the Arabian Gulf. Until recently these springs were used by local water vendors, who dived down to the springs and filled deflated

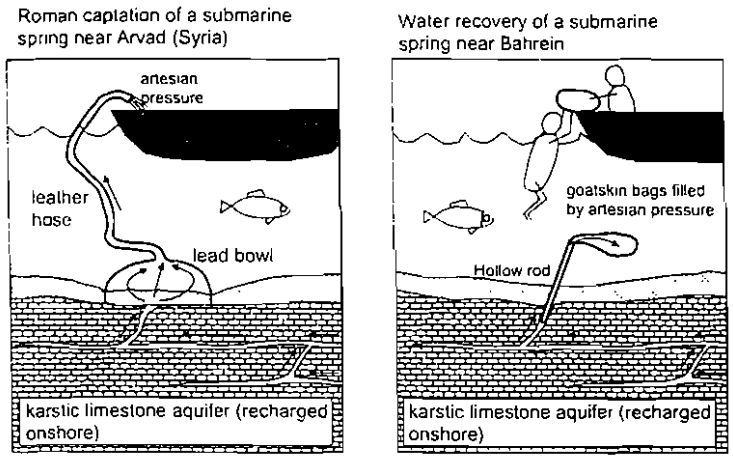

Figure 8.1. Captation of submarine springs at Syria and Bahrein

goatskin bags (Figure 8.1). Springs can be observed either by the eye at the sea surface as boils, different coloring of the water or slick and smooth sea surfaces, or by measuring salinity, electrical conductivity and temperature of seawater. Discharges can be quite high: based on salt mass-balance calculations, Kohout (1966) estimated a discharge of 42 m^3/s for a spring 4 km offshore from Crescent Beach, Florida.

Circumstantial evidence for the presence of springs is provided by geomorphological features at the sea bottom like karstic cavities (blue holes), slumps resulting from groundwater sapping in steep submarine canyons and "pockmarks", (circular depressions on the seafloor) (Johnson, 1939a, 1939b; Harrington, 1985; Robb, 1990). Indicative are also deposits of iron- and manganese-oxide precipitated on the sea floor from reduced groundwater entering the oxic ocean (Manheim, 1967).

Generally, the springs are related to discharge points of karstified aquifers of carbonate rocks or basalts, like the Mediterranean coasts (Zekster et al., 1973). Springs may also be related to stratigraphic, structural or erosive windows in aquicludes, where meteoric water emerges from underlying confined aquifers (Kohout, 1966). Most reported springs occur at water depths less than 40 m (Custodio, 1987) and within 5 km from the coastline. Custodio (1987) reasons that the submarine springs in carbonate terrain have been formed by karstic dissolution during low sea levels. Manheim and Horn (1968) report the existence of springs at much larger depths on the continental slopes, though their discharge may not be meteoric groundwater.

8.2.2. Diffuse submarine discharge

Submarine discharge by diffuse seepage is more difficult to ascertain than by springs, though according to Zekster et al. (1973) it accounts for the major part of groundwater discharge to the sea. Submarine seepage may be observed and quantified by means of salinity and hydraulic head patterns beneath the sea floor (Kohout, 1964), seepage meters (Lee, 1977; Simmons et al., 1992) or analyses of chemical and isotopic tracers in seawater like

salinity (Guglielmi and Prieur, 1997), radon (Cable et al., 1996a, 1996b), radium (Moore, 1996; Cable et al., 1997), methane (Cable et al., 1996a) and barium (Shaw et al., 1998). Benthic bioindicators like diatomes may also reveal seepage zones (Piekarek-Jankowska, 1996). Sometimes very high seepage rates are found with these methods (5 to 70 mm/day. The widths of the area over which these seepage rates have been calculated vary from 2 to 20 km, which implies that the aquifers must transmit large quantities of groundwater ranging from 20 to 1400 m^3/day per meter width of the coastline. These flows would require aquifers with extremely high transmissivities and also very large recharge areas. It is questionable whether these methods actually quantify the seepage of meteoric groundwater from the underlying aquifers: tracers may not be representative for meteoric groundwater or there is seepage of seawater circulating through the upper seafloor sediments.

Promising is the study of groundwater seepage based on concentration profiles of conservative tracers in pore waters of seafloor sediments. If seepage rates are low, the concentration reflects the competition of advective and diffusive solute transport. Post et al. (2000) used chloride concentrations, ^{18}O and ^{37}Cl isotope ratios for a site 50 km off the Dutch coast. They concluded that there was no upward seepage, but only downward salt diffusion. Piekarek-Jankowska (1996) determined chloride concentration, ^{18}O and ^{2}H isotope analyses in pore water from sediments in the Puck Bay near Gdansk, Poland. Groundwater seepage was not quantified with these data, but seepage rates of 0.4 mm/day are reported based on regional groundwater flow calculations.

8.3. Meteoric groundwater in offshore boreholes

Well log data from oil exploration and production wells could provide a wealth of information on offshore groundwater. However, data are often classified and in most cases the first few hundreds of meters are not logged. Nevertheless some interesting publications are reviewed below, indicating the presence of offshore meteoric groundwater. The locations are shown on the world map in Figures 8.2a to 8.2c.

8.3.1. Nantucket island (USA) – Atlantic Ocean

Kohout et al. (1977) describe a borehole at Nantucket Island, 70 km off the Atlantic coast at Cap Cod (USA) traversing a 457 m succession of Quaternary and Tertiary clastic sediments on basement rocks. Fresh groundwater (< 1.000 mg/l TDS) was found until a depth of 158 m below sea level, followed by a zone with alternating layers of brackish and saline water until 350 m. The basal sands layers below 350 m contained water of a relatively low salinity (< 2.000 mg/l TDS). As the piezometric head in the upper fresh water is 3.6 m above msl, it is concluded that this groundwater is a lens of recently formed fresh water floating on saline water. In the basal sands, however, a groundwater head of +7 m with respect to sea level exists, while the head has a landward gradient, as inferred from measurements in a well on a nearby island. Kohout et al. (1977) assume that groundwater in the basal sands was formed during the last glacial and is now being forced landward by the encroaching wedge of seawater on the continental shelf. They further state that the landward drive may be particularly strong because the aquifer is in direct hydraulic contact with the sea through outcrops on the shelf slope (Rona, 1969)

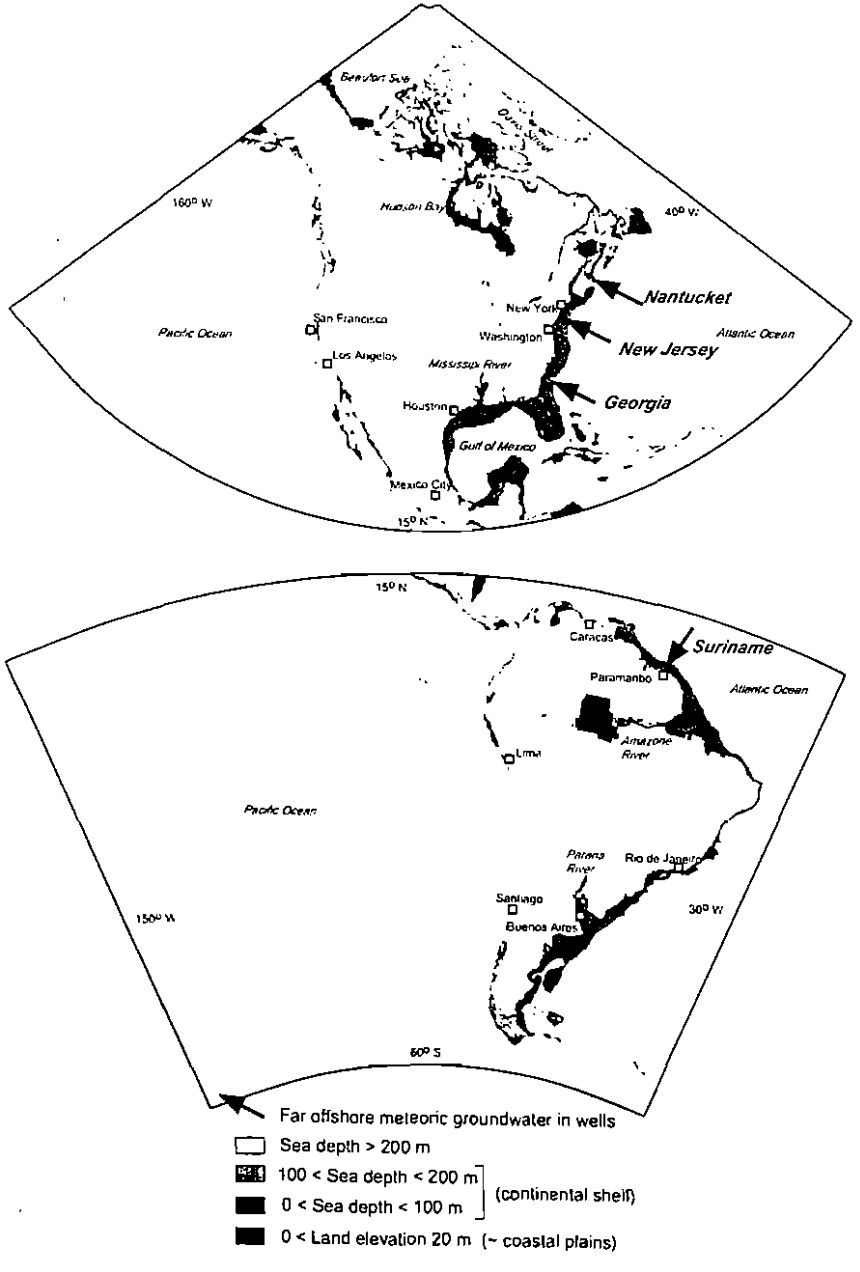

Figure 8.2a. Coastel plains and continental shelves of North and South America

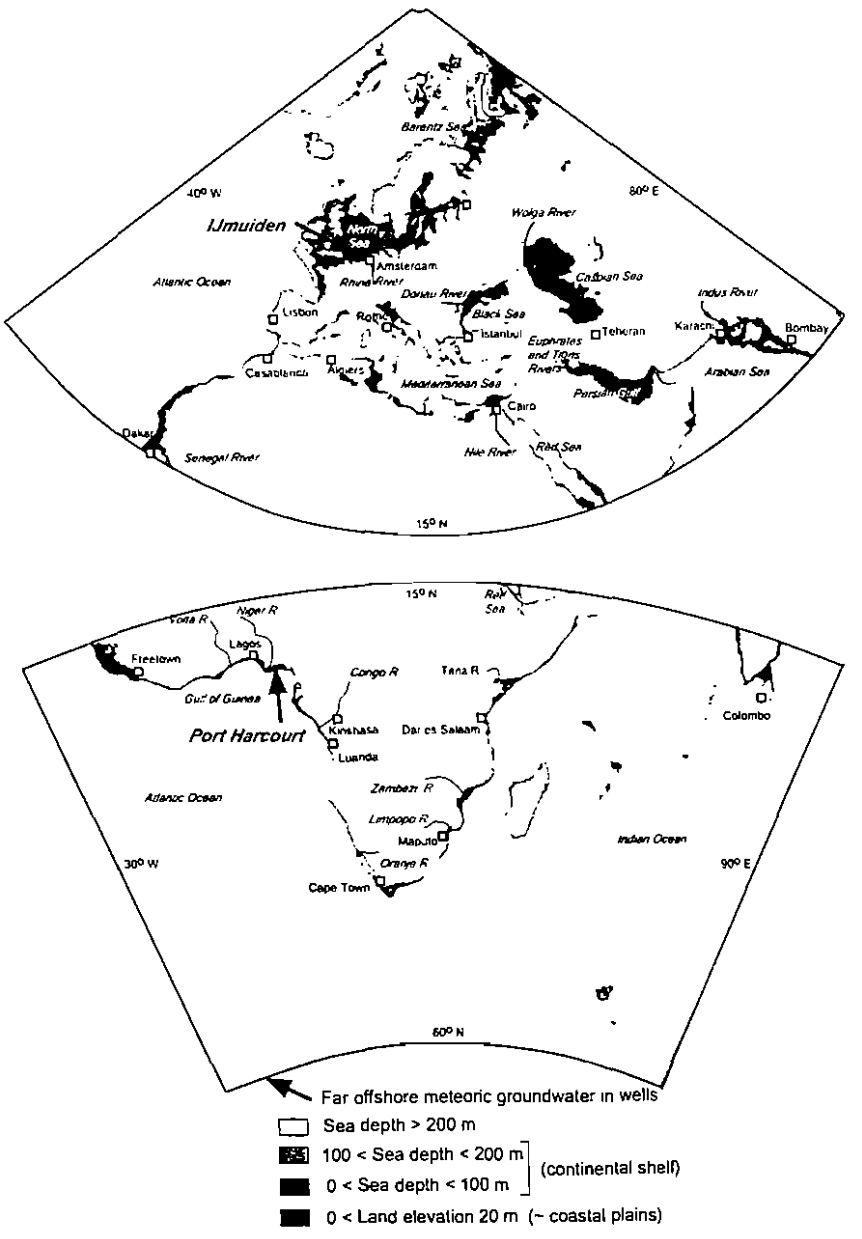

Figure 8.2b. Coastel plains and continental shelves of Europe, Middle East and Africa

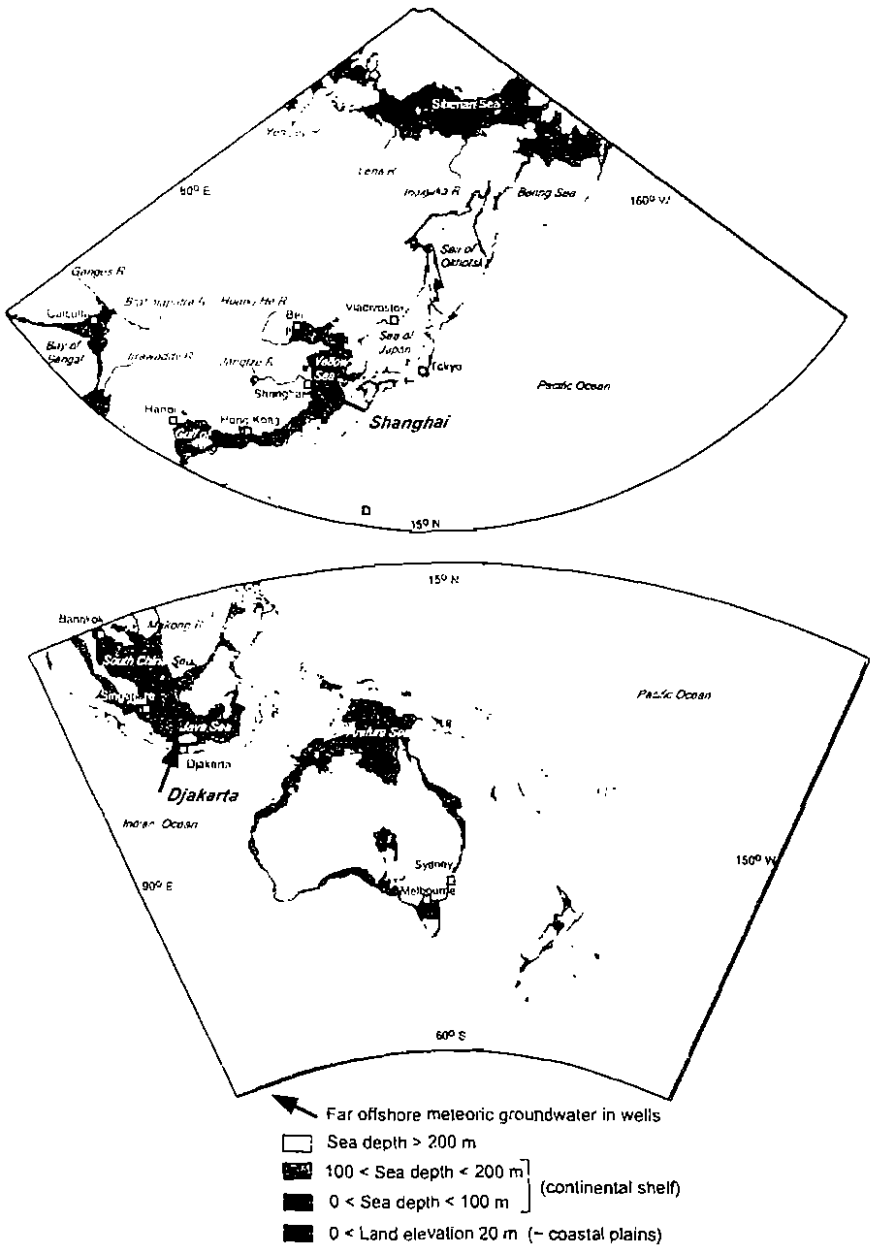

Figure 8.2c. Coastel plains and continental shelves of Asia and Australia

8.3.2. New Jersey and Maryland (USA) – Atlantic Ocean

In 1976, a series of boreholes were drilled for the (AMCOR) Atlantic Margin Coring Program (Hathaway et al., 1979). In this scientific program also pore water squeezed from sediment samples was studied. A transect of 5 boreholes perpendicular to the Atlantic coast of New Jersey (USA) showed that groundwater with salinities less than 5,000 mg/l TDS extends 100 km offshore (Figure 8.3). This meteoric groundwater is found between 100 and 300 m below m.s.l. in the Miocene (Kirkwood Formation) and in Pliocene formations (see Figure 8.3). In another AMCOR well further south, some 20 km offshore of Maryland, even fresh, potable groundwater was encountered. Along the eastern and bottom fringes of the meteoric water, very wide transition zones are found, while there is a sharp transition at the top.

The New Jersey transect was the basis for the paleohydrological modeling study by Meisler et al. (1984). The model showed that the offshore interface is now very slowly moving landward. They concluded that the high frequency of the Quaternary sea-level oscillations caused only small movements of the interface and that its position largely reflects the average sea level during the Quaternary. Meisler et al. (1984) concluded that the wide transition zone around the interface is the result of the larger periodicity of sea-level movements during the Miocene and Pliocene. A reflection of the to and fro movement is the hydrochemistry of the offshore groundwater. The more dilute meteoric groundwater shows a sodium surplus with respect to mixing of meteoric and marine waters, while more brackish and saline waters show a calcium surplus. Assuming that this pattern is caused by cation exchange, it suggests that closer to the coast freshening dominates, while in the transition zone salinization is taking place. Before groundwater development started in the last century, groundwater heads were artesian (Kohout et al., 1988), which indicates that, close to the shore, the meteoric groundwater body may belong to a topography-driven flow domain.

8.3.3. Georgia (USA) – Atlantic Ocean

A transect of JOIDES wells and two exploration wells offshore southeast Georgia (Figure 8.3) revealed a body of meteoric groundwater (Cl concentration < 2,000 mg/l) in the Eocene Ocala limestones extending 120 km offshore and almost reaching to the shelf slope (Manheim, 1967). Analyses were carried out on pore waters squeezed from sediment samples. Later a drill stem test on an oil exploration well, 85 km offshore and nearby the JOIDES transect, produced groundwater with a concentration less than 700 mg/l (Kohout, 1966). Also, the resistivity log of an oil exploration well at the shelf edge showed the presence of brackish water in the upper 900 m (Manheim and Paull, 1981). The top of the meteoric water body slopes from -50 m (with respect to sea-level) to -200 m at 120 km offshore. The base of the meteoric groundwater body ranges from 1,000 m at the coast to at least 600 m at the JOIDES well at 120 km offshore. During drilling, a hydraulic head of 9 m above m.s.l. was measured in the JOIDES well at 40 km offshore (Manheim, 1967). Stringfield (1966) reports onshore artesian heads in the prepumping period of +18 m with respect to sea level. He calculated that this head would be sufficient to force meteoric groundwater through the highly permeable Ocala aquifer to a submarine outlet at some 100 km offshore. Kohout et al., (1988) and Manheim (1967) assume therefore that, until recently, the offshore meteoric groundwater body was part of an active flow system with onshore recharge and submarine discharge on the shelf slope.

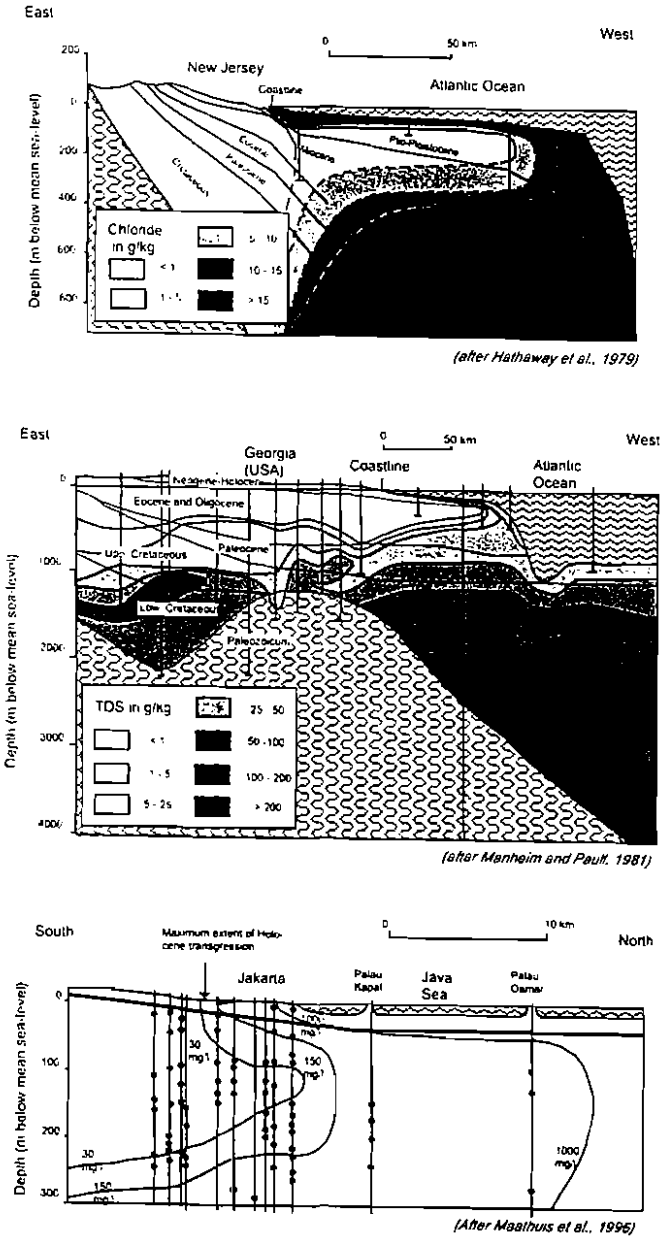

Figure 8.3. Sections of offshore meteoric groundwater at New Jersey (USA), Georgia (USA) and Java (Indonesia)

8.3.4. Georgia (USA) – Atlantic Ocean

Maathuis et al. (1996) report the presence of meteoric water in wells in the coastal plain near Jakarta and two coral-reef islands, Palau Kapal and Palau Damar, at 5 and 15 km offshore (Figure 8.3). Groundwater with chloride contents less than 1,000 mg/l is found between depths of 50 to 300 m. Hydraulic heads in the island wells are close to sea level. Therefore deep fresh groundwater in the island wells cannot be part of a recently formed lens recharged on the island itself. It must have been formed by another flow system. In the Jakarta coastal plain, the hydraulic heads of deep meteoric groundwater, measured before large-scale groundwater pumping started, range from 5 to10 m above m.s.l. ^{14}C data of this groundwater indicate Pleistocene ages exceeding 30 ka BP (Geyh and Söfner, 1989). This suggests that the offshore meteoric groundwater is formed by an old topography-driven flow system recharged in the hills south of the coastal plain. This flow system remained active during the Holocene, though gradients must have been reduced after the rise of the sea level (Geyh and Söfner, 1989).

8.3.5. Port Harcourt (Nigeria) - Atlantic Ocean

The resistivity logs of 12 oil wells 15 to 40 km offshore Port Harcourt in Nigeria indicate the presence of groundwater with concentrations of less than 1,000 mg/l chloride between depths of 120 to 450 m below sea-level (Shell, unpublished data).

8.3.6. IJmuiden (Netherlands) - North Sea

A shallow well drilled in the North Sea, 60 km offshore from IJmuiden on the Dutch coast, revealed the presence of brackish groundwater (Post et al., 2000). The well was drilled only 5.5 m into a clay layer (Brown Bank Formation) exposed at the seafloor. Pore-water samples squeezed from sediment samples showed that chloride concentration decreased from 20,000 mg/l at the sea floor to 9,000 mg/l a 5.5 m depth. Post et al. (2000) showed that the vertical decrease of chloride concentrations could be explained by salt diffusion from the sea into fresh groundwater starting 8500 years BP, when the sea submerged the southern North Sea.

8.3.7. Shanghai (China) - Chinese Sea

Meteoric groundwater was found in a well between depths of 150 to 320 m on one of the Holocene Shengsi islands, 50 km offshore in the Chinese Sea, near Shanghai (Wang, 1994). Groundwater deeper than 229 m appeared even to be potable. It is unlikely that this groundwater has been formed during recent times. Moreover, groundwater onshore at the same depths is of LGM age (Hua Aibing, 1998).

8.4. Discussion and conclusions

The observations show that meteoric groundwater, observed in wells 10 to 100 km offshore, is not restricted to Suriname, but occurs all over the world. Accounts of submarine discharge are even more numerous, though generally the discharge is located closer to the

shore, either as springs or as diffuse seepage. Despite the scanty and ill-documented observations, I conclude that the offshore meteoric groundwater can no longer be considered as an exceptional phenomenon.

Most observations do not make clear whether the meteoric groundwater belongs to an active topography-driven flow system with onshore recharge, or to paleogroundwater formed by extinct flow systems. The New Jersey coast is the only case, in which the distal offshore meteoric groundwater can be designated as paleogroundwater (Meisler et al., 1984). Submarine discharge will generally be a sign of an active flow system, but it may also be discharge of a very large paleogroundwater body, that is slowly squeezed out by density-driven forces after the Holocene transgression. Age is not always a diagnostic marker either, since very old groundwater may still belong to an active topography-driven flow system with a very long residence time. The same applies to salinity: in coastal and offshore discharge areas very wide dispersive transition zones exist (Sousa and Voss, 1987), where brackish groundwater is still part of the active flow domain. The next chapters will address this question in more detail.

This study and that of Meisler et al. (1984) show that a flat and shallow continental shelf and a thick, continuous formation of low permeability below the sea floor, together with climate and secondary topography, are the most important conditions for the formation of offshore paleogroundwater. A worldwide inventory of these conditions would be useful to predict the presence of offshore paleogroundwater, which may become an exploitable resource in future. The world map in Figures 8.2a to 8.2c shows extensive continental shelves and many inland seas with depths less than 100 m. These offshore areas were exposed during the LGM and favored paleogroundwater formation.

Chapter 9.

Prediction of the offshore continuation of coastal groundwater flow systems

9.1. Introduction

There are many observations of offshore meteoric groundwater, as discussed in Chapter 8. However, in many cases, the observations cannot conclusively indicate whether this groundwater is (i) paleogroundwater, formed by extinct flow systems or (ii) groundwater in a modern flow system with onshore recharge. This can only be established with a dense offshore observation network of heads or pressures, which is quite costly. Kohout (1964) carried out such a detailed survey of offshore groundwater close to the shoreline in Biscayne Bay, Florida. In this chapter the question about the origin of offshore meteoric groundwater is addressed indirectly: given the present conditions, how far could fresh and meteoric groundwater penetrate into the offshore?
Reilly and Goodman (1985), Custodio (1987) and Kooi and Groen (2001) reviewed a number of models and concepts defining the submarine extension of fresh groundwater.

Through time, the complexity of the models increased. Figure 9.1 schematically illustrates a number of classical studies that employed various levels of approximation in model calculations and various subsurface conditions. First analytical solutions were found for sharp-interface models in phreatic aquifers (Badon Ghijben, 1888; Glover, 1959) and semi-confined aquifers (Edelman, 1972; Mualem and Bear, 1974). Later numerical codes were developed for sharp-interface models to allow incorporation of spatial geological heterogeneity and non-stationary modelling (Essaid, 1986, 1990; Meisler et al., 1984). Diffusion and dispersion processes along the fresh/saline interface were studied analytically by Henry (1964) and later incorporated in numerical codes (Huyakorn et al., 1987; Voss and Sousa, 1987; Oude Essink, 1996). However, none of the above models accounted for the potential instability of an inverse salinity and density stratification in the top of the offshore meteoric groundwater body. Such instability leads to the development of convective density currents (when a critical Raleigh number is exceeded). Kooi and Groen (2001) devised an approximate model (AM), that determines the distance from the shore to the place where the inverse stratification in an aquifer becomes unstable, and where salinization by convective mixing takes place. This chapter, which is largely based on this article, discusses the results of a modified version of AM, the New Approximate Model (NAM).

9.2. The New Approximate Model

The approximate analytical model (NAM), presented here, combines two competing processes of solute transport in the offshore zone (Figure 9.2). The first process is the advection of salt by groundwater flow through the aquifer in combination with the upward seepage through an aquitard to the sea floor. The advection is based on the model of Edelman

(1972) for fresh groundwater flow in an offshore semi-confined aquifer with a sharp fresh/saline interface. The second process is the downward diffusion from the sea towards the underlying fresh groundwater through the aquitard, which is described by a one-dimensional diffusion-advection model.

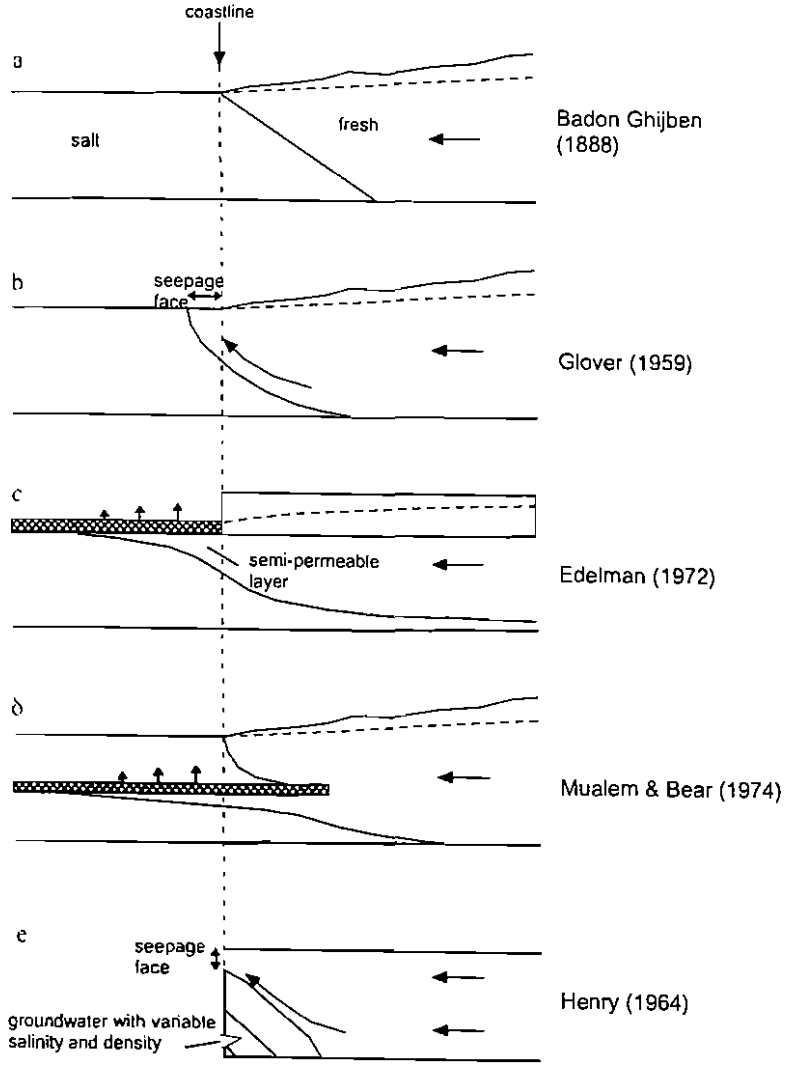

Figure 9.1. Conceptual models of coastal groundwater flow systems with fresh and saline groundwater according to some classical studies (from Kooi and Groen, 2001).

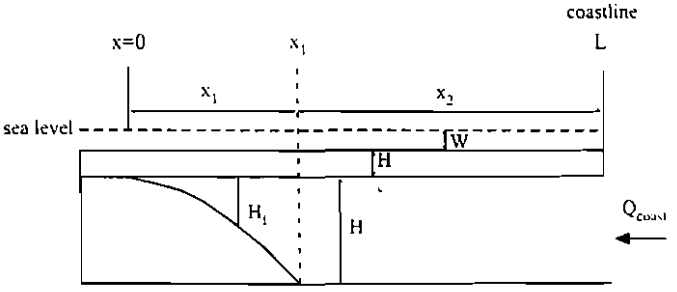

Figure 9.2. Schematic section showing groundwater flow according to the offshore sharp-interface model (SIM) and downward salt transport by diffusion and convection.

The NAM defines the distance from the coast, where the upward seepage become so small that downward diffusive transport reaches into the aquifer and creates instability and convective density currents. It is assumed that this distance is a good measure for the offshore limit of the fresh groundwater tongue.

Sharp-interface model

The geometry of the Sharp-Interface Model (SIM), based on the model of Edelman (1972) for offshore fresh groundwater flow, is shown in Figure 9.3. The salt water is assu-

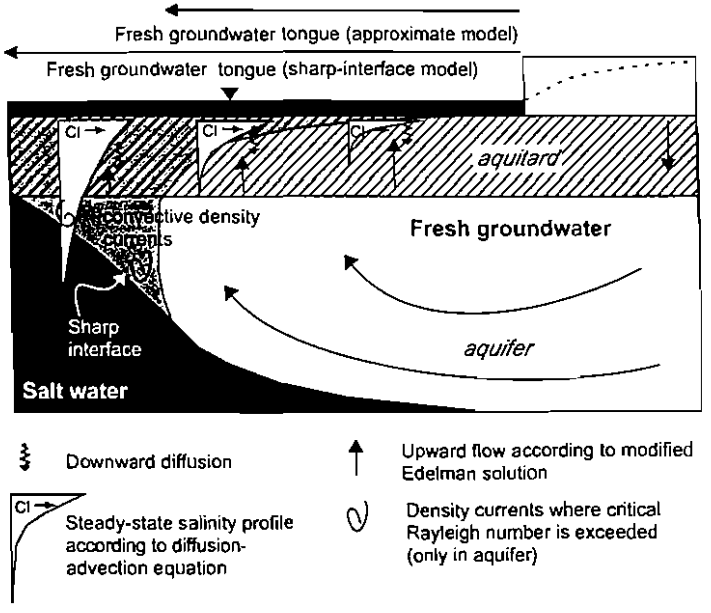

Figure 9.3. Schematic diagram of the sharp-interface model used to calculate the length L of a steady-state offshore fresh-water tongue (from Kooi and Groen, 2001).

med to be static, except for the water within the confining layer, because upward seepage through this layer into the overlying sea should be allowed. The Dupuit assumptions are applied, i.e. within the aquifer, fresh-water heads are assumed to be uniform with depth and within the confining layer above the fresh-water tongue, salt-water heads are assumed uniform in the horizontal. In contrast to Edelman (1972), the aquitard above the fresh-water lens is assumed fully saline to avoid having a finite fresh-water seepage rate at x = 0 (the seaward-most edge of the tongue where its thickness becomes nil). Independent variables of the system are the fresh-water discharge at the coast, Q_{coast}, the horizontal hydraulic conductivity and thickness of the aquifer, k, and, H, the vertical hydraulic conductivity and thickness of the confining (clay) layer, k_c, and H_c, and the local depth of the sea, W. Conductivities and thicknesses are not lumped into resistances and transmissivities, because in this as well as in the following section some of the dependent variables are functions of the separate parameters. The unknowns, which are to be solved, are measures of the offshore fresh-water length, L, and the fresh-water piezometric head at the shoreline, h_{coast}. The analytical solution for SIM, described in more detail in Kooi and Groen (2001), is separately derived for the part where fresh groundwater completely fills the aquifer, and for the part where the thickness of the fresh water is smaller than the aquifer thickness (Figure 9.3).

Diffusion-advection model

The downward diffusion of salts through the aquitard with a counteracting upward seepage can be written by the advection-dispersion equation as:

$$D_z \frac{d^2\omega}{dz^2} - q_z \frac{d\omega}{dz} = 0 \qquad (9.1)$$

where q_z is the vertical Darcy velocity, ω is the salt mass fraction, and D_z is the vertical component of the diffusion tensor (including effects of porosity and tortuosity). Eq. 9.1 implicitly assumes that D_z is constant. The Boussinesq approximation has been applied which assumes that spatial density variations can be neglected in the mass balance. These assumptions are reasonable for the level of accuracy required in the present analysis. Moreover, the difference in density between seawater and fresh water is about 2.5% only.

If effects of horizontal advection within the aquifer at the base of the confining layer are ignored, the solution to Eq. 9.1 is given by

$$\omega = \omega_{sea} e^{-z/\delta} \quad \text{with} \quad \delta = |D_z / q_z| \qquad (9.2)$$

where ω_{sea} is the salt mass fraction of sea water and δ is the characteristic thickness of the stationary exponential boundary layer that forms a transition zone between sea water and fresh water. In (9.2), z is taken positive downward from the seafloor. The upward seepage rate can be estimated from SIM by:

$$q_z = \frac{\gamma_s}{\gamma} \frac{k_c}{H_c} h_s' \qquad (9.3)$$

where γ_s and γ are the specific weights of seawater and fresh water, respectively, and h_s' is the salt-water head at the base of the aquitard.

Convective break-up and fingering of this boundary layer will take place when the boundary-layer Rayleigh number, Ra_δ, which is defined as

$$Ra_\delta = \frac{\Delta\rho k_z \delta}{\rho D_z} \qquad (9.4)$$

exceeds the critical value of about 10 (Wooding et al., 1997a). In practice, boundary layers in clayey sediments (aquitards) will be stable because of their low permeabilities. The permeabilities of sands and silts are several orders of magnitude higher. Therefore Ra_δ of the boundary layer in sandy and silty aquifers tends to be above the critical value even for small density contrasts and limited thicknesses. The onset of instability is defined to occur here at the location where the critical Raleigh number of the boundary layer within the aquifer is exceeded. This criterion is physically more realistic than the criterion in the AM model of Kooi and Groen (2001), where onset of instability was assumed when the thickness of the boundary layer as a whole exceeded the thickness of the clay.

9.3. Results

In the first series of calculations (Figure 9.4) the length of the fresh groundwater wedge was calculated with three different models SIM, AM and NAM. The lengths were calculated for varying values of aquitard thickness H_c (1 to 100 m, x-axis), aquitard hydraulic conductivity k_c (10^{-9} m/s, 10^{-8} m/s and 10^{-7} m/s) and coastal heads h_{coast} (+2 and +10 m above msl in left and right panels, respectively). The tongue lengths L, predicted by SIM are larger than the lengths of the approximate models L_d for the lower hydraulic conductivities $k_c = 10^{-9}$ m/s and $k_c = 10^{-8}$ m/s. This is the result of the predicted effect of instability, when the diffusive boundary layer reaches the aquifer. This is particularly true for the lowest aquitard permeability ($k_c = 10^{-9}$ m/s): maximum tongue lengths of 5 km and more than 100 km are predicted by NAM and SIM, respectively, for $h_{coast} = +10$ m above msl; for $h_{coast} = +2$ m above msl the tongue lengths are 0 m and more than 30 km, respectively. For the relatively high hydraulic conductivity $k_c = 10^{-7}$ m/s, the difference in tongue lengths is not very large between all models. Comparison of the two approximate models AM and NAM shows that NAM (Figure 9.4c) leads to smaller tongue lengths than AM (Figure 9.4b). Again the discrepancy is largest for the low hydraulic conductivity.

For high hydraulic heads at the coastline ($h_{coast} = +10$ m above msl), the tongue length increases with the thickness of the aquitard (Figure 9.4a to 9.4c, right panels). However, for low hydraulic heads ($h_{coast} = +2$ m above msl) the length initially increases but decreases at thickness of over 40 m (Figure 9.4a to 9.4c, left panels). This effect is primarily due to the fact that the increasing hydraulic resistance of the clay (H_c/k_c) eventually reduces the total outflow under this low hydraulic driving force. The maximum lengths for AM and NAM (Figures 9.4b en 9.4c, left panels) are found at smaller H_c than that for SIM (Figure 9.4a, left panel). This is due to the earlier onset of instability.

In the next series of calculations, the influence of aquifer parameters was tested. Figure 9.5a shows the results of NAM calculations with an aquifer transmissivity, Hk, of 4.5 x 10^{-3} m²/s (~ 400 m²/day) and a coastal head (h_{coast}) of +2 m above msl. In the left panel, aquifer thickness, H, and hydraulic conductivity, k, are 10 m and 4.5 x 10^{-4} m/s, respectively, and in the right panel 30 m and 1.5 x 10^{-4} m/s. In Figure 9.5b the transmissivity is 15 x 10^{-3} m²/s (~ 1300 m²/day), where in the left panel aquifer thickness and hydraulic conductivity are 100 m and 1.5 10^{-4} m/s, respectively, and in the right panel 10 and 1.5 x 10^{-3} m/s. The transmissivity in Figure 9.5b is 3 times as high as that of Figure 9.5a, but the lengths of the

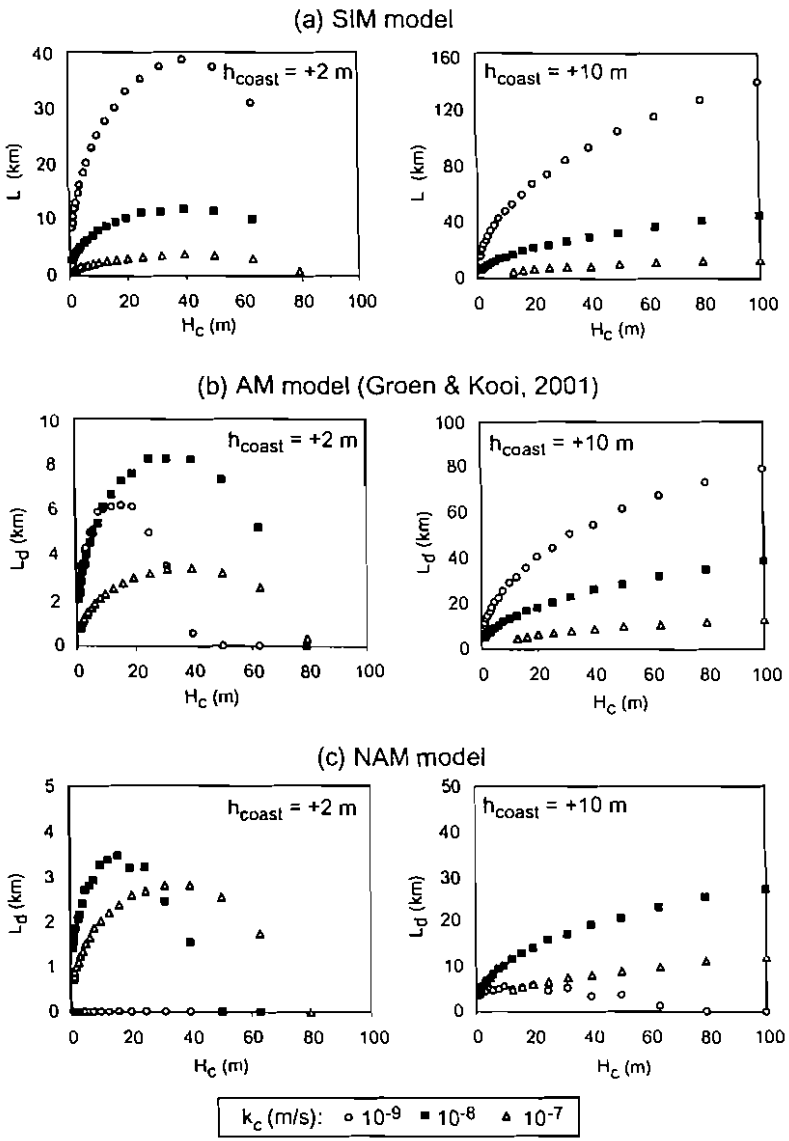

Figure 9.4. Submarine extension of fresh groundwater according to three different models: (a) sharp-interface model (SIM), (b) approximate model (AM) with downward diffusion and convection according to Kooi and Groen (2001) and (c) the new approximate model (NAM). The semi-confined aquifer has a thickness (H) of 100 m and a hydraulic conductivity (k) of 1.5 x 10^{-4} m/s. The thickness of the overlying clay layer (H_c) has been varied between 1 and 100 m. For the hydraulic conductivity of the clay (k_c) three different values have been chosen: 10^{-9} m/s, 10^{-8} m/s and 10^{-7} m/s. Coastal heads (h_{coast}) are +2 and +10 m above msl (left and right panels). Sea depth (W) is 0 m.

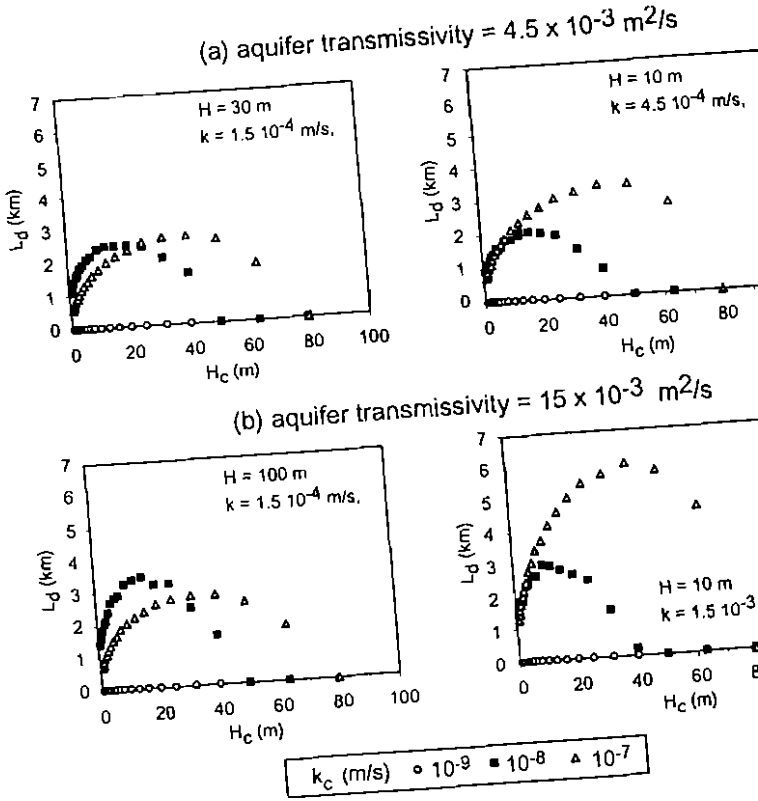

Figure 9.5. Submarine extension of fresh groundwater for different values of the aqu
and transmissivity and a coastal head (h_{coast}) of +2 m above msl.
Calculations have been carried out with the new approximate model (NAM): (a) in th
panels for a semi-confined aquifer with a transmissivity (Hk) of 4.5 x 10^{-3} m^2/s (~ 40
in the left panel aquifer thickness (H) and hydraulic conductivity (k) are 10 m and 4.
in the right panel 30 and 1.5 x 10^{-4} m/s, respectively; (b) in the lower panels the tran
10^{-3} m^2/s (~ 1300 m^2/day), where in the left panel aquifer thickness (H) and hydrauli
are 100 m and 1.5 x 10^{-4} m/s, and in the right panel 10 and 1.5. x 10^{-3} m/s, respectiv
of the overlying clay layer (H_c) has been varied between 1 and 100 m. For the hydra
of the clay (k_c), three different values have been chosen: 10^{-9} m/s, 10^{-8} m/s and 10^{-7}
(W) is 0 m.

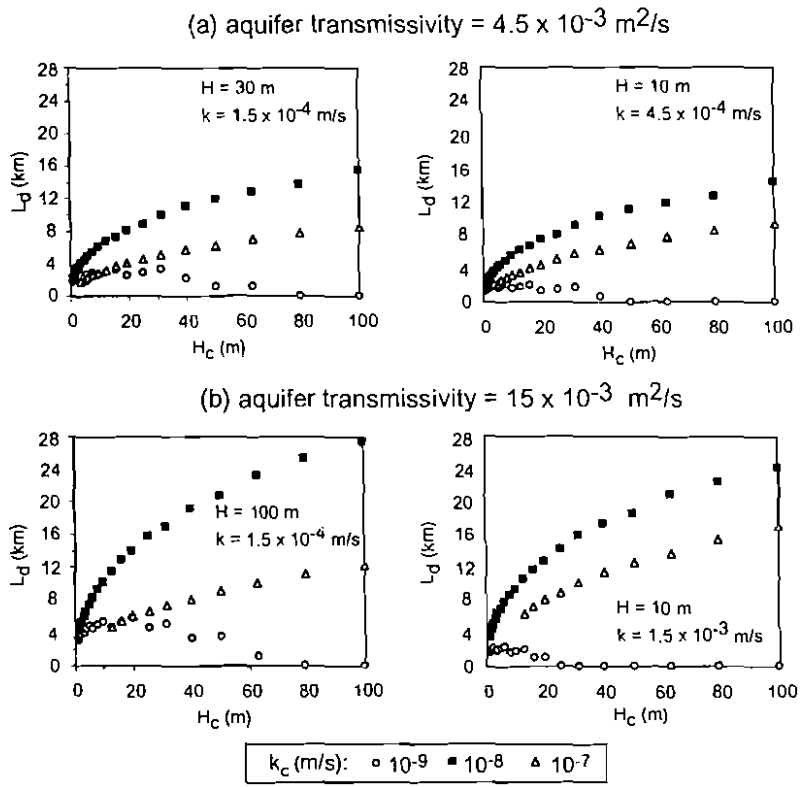

Figure 9.6. Submarine extension of fresh groundwater for different values of the aquifer thickness and transmissivity and a coastal head (h_{coast}) of 10 m above msl.
Calculations have been carried out with the new approximate model (NAM): (a) in the upper two panels for a semi-confined aquifer with a transmissivity (Hk) of 4.5 x 10^{-3} m²/s (~ 400 m²/day), where in the left panel aquifer thickness (H) and hydraulic conductivity (k) are 10 m and 4.5 x 10^{-4} m/s and in the right panel 30 and 1.5 x 10^{-4} m/s, respectively; (b) in the lower panels the transmissivity is 15 x 10^{-3} m²/s (~ 1300 m²/day), where in the left panel aquifer thickness (H) and hydraulic conductivity (k) are 100 m and 1.5 x 10^{-4} m/s, and in the right panel 10 and 1.5 x 10^{-3} m/s, respectively. The thickness of the overlying clay layer (H_c) has been varied between 1 and 100 m. For the hydraulic conductivity of the clay (k_c), three different values have been chosen: 10^{-9} m/s, 10^{-8} m/s and 10^{-7} m/s. Sea depth (W) is 0 m.

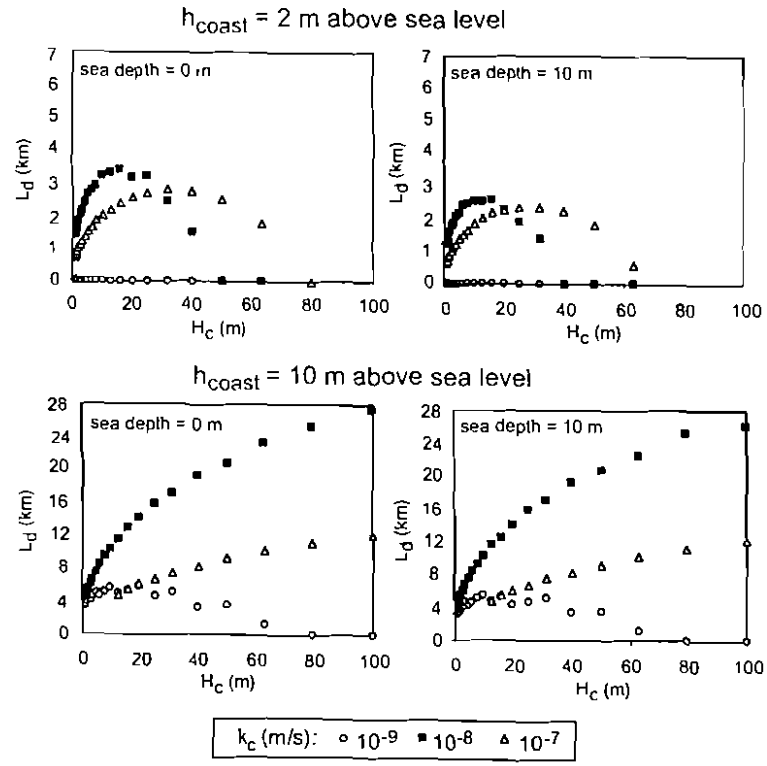

Figure 9.7. Submarine extension of fresh groundwater for different sea depths, calculated with the new approximate model (NAM): (a) in the upper panels for a coastal head (h_{coast}) of +2 m above msl and (b) in the lower panels for a coastal head (h_{coast}) of 10 m above msl. The semi-confined aquifer has a thickness (H) of 100 m and hydraulic conductivity (k) of 1.5 x 10^{-4} m/s. Sea depth (W) in the left and right panels is 0 and 10 m respectively. The thickness of the overlying clay layer (H_c) has been varied between 1 and 100 m. For the hydraulic conductivity of the clay (k_c), three different values have been chosen: 10^{-9} m/s, 10^{-8} m/s and 10^{-7} m/s.

fresh water tongues are only 5 to 50 % higher. Variation of aquifer thickness, H, and aquifer hydraulic conductivity, k, with the same transmissivity, (compare left and right panels) does not have much influence. Only calculations with the highest value for the hydraulic conductivity of the aquitard leads to considerably longer tongue lengths. Note that for the lowest hydraulic conductivity of the aquitard there is no submarine extension of fresh groundwater as was observed already in the discussion of Figure 9.4. In Figure 9.6 similar results are shown for a coastal head (h_{coast}) of +10 m above msl. Again the effects of varying aquifer parameters are less important than that of the aquitard.

In figure 9.7 the results are compared for calculations with a sea depth of 0 and 10 m (left and right panels, respectively). Varying sea depths appear to have only a minor effect on the tongue length. This is not surprising as it can be reasoned that extra seawater loading of 10 m is equivalent to a reduction of the coastal head with only 0.25 m.

Note that the markers in Figures 9.4, 9.5, 9.6 and 9.7 sometimes do not follow smooth curves. The reason is that the coastal heads for these data are not exactly +2 or +10 m above msl; in the calculations Q_{coast} is an independent variable, and h_{coast} is calculated by the model. Therefore a large number of calculations with varying Q_{coast} have been carried out, from which the h_{coast} closest to +2 and +10 above msl have been chosen.

9.4. Discussion and conclusions

Offshore extension of fresh groundwater in a semi-confined coastal aquifer with steady-state flow is smaller than calculated with a simple sharp-interface model (SIM). The submarine discharge decreases in an offshore direction until the diffusive boundary layer in the overlying aquitard eventually reaches the aquifer and creates instability and convective density currents.

The New Approximate Model (NAM), presented above, results in an earlier onset of instability and shorter fresh water tongues than the old Approximate Model of Kooi and Groen (2001) did. In general, both models lead to similar conclusions.

Sensitivity tests with NAM, which combines upward seepage and downward diffusion, show that increasing the hydraulic resistance, H_c/k_c, of the aquitard initially results in longer fresh water tongues. However, at very high resistances the lengths decrease again due to a combination of two effects: (i) total submarine groundwater outflow dimishes and (ii) the declining upward seepage (though becoming spread out over a larger distance) leads to instability closer to the coast.

The sensitivity tests with NAM further show that the fresh groundwater tongues do not extend more than 6 to 28 km offshore for coastal groundwater heads (h_{coast}) of +2 m and +10 m above msl, respectively. Leaving out the extreme cases ($H_c > 50$, $h_{coast} > +2$ m above msl), one may assume that fresh groundwater generally does not extend more than 5 km offshore.

Brackish groundwater, within a topography-driven flow domain, may extend further offshore. In this transition zone, the salinity will gradually rise as the seaward flowing meteoric groundwater mixes with downward transported salt. The outer limits of the transition zone, according to SIM, vary from 40 to 140 km for h_{coast} = +2 m to +10 m, respectively. After leaving out the extreme cases again, the outer limit in most cases will not exceed 50 km.

The NAM model is compared with two of the best-documented cases, the New Jersey coast of the USA and the coast of Suriname (Chapter 8). The model input values f New Jersey coast derived from the study by Meisler et al. (1984) were: H_c = 50 m x 10^{-6} m/s, H = 350 m, k = 1.7 x 10^{-5} m/s, W = 50 m and h_{coast} = +6 m above msl. responding lengths of the fresh groundwater, calculated with SIM (L) and NAM (and 0 km respectively. For the Suriname coast, the input values are: H_c = 25 m, k_c ^{9} m/s, H = 250 m, k = 1 x 10^{-4} m/s, W = 50 m and h_{coast} = +3.5 m above msl. The an L of 9 km and a L_d of 0 km. This makes clear that the offshore meteoric groun these two sites has been formed by different flow systems and can therefore deno ogroundwater.

The situation offshore the coast of Florida, where very high hydraulic heads above msl) prevailed until extensive pumping started in the last century, is differe meteoric groundwater beyond 100 km offshore may be fed by active flow system hore recharge.

It can be inferred from the sensitivity analysis and the comparison of model with observations that occurrences of moderately brackish meteoric groundwater the offshore are not in equilibrium with present-day onshore hydrological conditi independent measurements of sub-sea pressure head and groundwater age are ne ther ascertain that these waters are indeed relics from changing conditions at a g time scale, and to provide data for more detailed modelling (Chapter 10).

Flow and solute transport in the brackish transition zone will also be studie 10 with a model that incorporates variable density flow and transport, including ment of convective density currents.

Chapter 10.

Flow and salt transport in submarine meteoric groundwater in steady-state and transient systems

10.1. Introduction

In the preceding chapters, flow and solute transport processes have been studied based on single- or double-density density groundwater flow models (Chapters 4 and 9) and chemical and isotopic parameters (Chapters 5, 6 and 7). However, understanding of flow and solute transport in the coastal and offshore zone requires integration of topography-driven flow, density-driven flow, diffusion, dispersion and free convection in unstably stratified groundwaters. Especially the latter process is seldom accounted for in groundwater models, but it is very important in coastal and submarine groundwater where inverse salinity stratifications often arise. These processes are relevant in situations, where:

a) fresh groundwater, recharged onshore, flows into the offshore part of an aquifer;
b) a coastal landscape becomes submerged during a transgression.

The submarine outflow situation (a) forms a steady-state condition and has been investigated with the approximate model in the preceding chapter. The transgression situation (b) creates unsteady-state conditions, which have been discussed in Chapter 5. In the present chapter, the dynamics of these situations are studied in numerical experiments using models, that combine all relevant processes. Model 1 simulates the submarine outflow situation. Models 2 and 3 represent transgression situations over a flat continental shelf and a shelf with an erosive topography, respectively. Model 3 is relevant as investigations (Chapter 4) demonstrated that, during the last glacial, the exposed shelf was subjected to strong fluvial erosion. In such a landscape, salinization starts in valleys which are intruded by the sea in an early stage, while topography-driven systems continue to function on the interfluves. The contents of this chapter are partly based on articles, published earlier (Kooi et al., 2000; Kooi and Groen, 2001).

10.2. Experimental setup

10.2.1. Numerical code

The numerical experiments reported here were conducted with the finite-element, variable-density flow and transport code, METROPOL-3. For a detailed description of the code, the reader is referred to the works by Leijnse (1992), Sauter et al. (1993), Leijnse and Oostrom (1994) and Oostrom et al. (1994). The code solves two coupled partial differential equations in salt mass fraction, ω, and fluid pressure, p. The equations are nonlinear because the fluid density, ρ, dynamic viscosity, μ, depend on ω. The equations are coupled through q and ρ. Here we use a constant value for μ, because of the low salt mass fractions considered. For fluid density, $\rho = \rho_0 e^{\gamma\omega}$, is used, where ρ_0 is the fresh-water density, and $\gamma = 0.69$. The latter value gives fluid densities deviating less than 0.1% from experimental values for salt

ass fractions varying from $\omega = 0$ (fresh water) to $\omega = 0.26$ (saturated brine) (Leijnse, 992). Fluid and pore compressibilities are neglected, corresponding to zero specific storage. his is reasonable given that the changes in pressure boundary conditions occur only very owly.

The numerical scheme uses the Galerkin weighted residual finite-element method, fully plicit backward time stepping with automatic time step control based on convergence quirements. A consistent velocity formulation is used to represent Darcy velocities (Voss d Souza, 1987). METROPOL-3 has been compared with other codes for a number of nchmark problems in the HYDROCOIN project (Leijnse and Hassanisadeh, 1989a, 89b) and was found to give comparable results.

2.2. *Discretization*

The spatial and temporal scales that can be handled by variable-density flow simulators e limited because of strict requirements of grid/mesh resolution. This applies in particular the simulation of diffusion in the boundary layer below the sea floor and density-driven nvection in unstably stratified fluids.

In model 2 and 3 a time-dependent Dirichlet boundary condition is used for the top ndary, where ω suddenly jumps from 0 to ω_{sea} after the transgression. Strictly speaking, is method is physically not very realistic as, over time, salt is introduced in the top ele- nts of the finite-element mesh (because ω varies linearly within an element) which is not counted for by boundary fluxes. However, as long as the vertical mesh size, Δz, is small, "mass-balance error" is also small (moreover, its cause is known).

In order to achieve convergence in the calculations the condition $\Delta z < \delta_{cr}$ should be t, where δ_{cr} denotes the thickness of the saline boundary layer at the top of the domain at instant it becomes unstable and fingers start to develop, which occurs when the boundary er reaches a finite thickness. This implies that the Rayleigh number for a boundary layer th length (thickness) scale, Δz, has to be smaller than the critical boundary layer Rayleigh mber or:

$$\frac{\Delta\rho g \kappa \Delta z}{\mu D} < \left(Ra_{cr} = \frac{\Delta\rho g \kappa \delta_{cr}}{\mu D} \right) \qquad (10.1)$$

ere $\Delta\rho = \rho_{sea} - \rho_0$; g and κ are absolute values of gravitational acceleration and (isotro-) intrinsic permeability; D is the scalar value of an assumed isotropic dispersion tensor. fects of porosity, n, and tortuosity, τ, are accounted for in the way D is defined in the del as $D = nD'/\tau^2$, with D' as the diffusivity in water (mechanical dispersion ignored). If $> \delta_{cr}$, the boundary layer that is created numerically just below the seafloor is always stable (its Rayleigh number is larger than critical). Hence, under these circumstances, fin- ing starts too early in the model. More crucial, however, is that upward seepage of fresh ter into the sea tends to create a boundary layer of finite thickness, $\delta = D/q$, which is re compressed if the upflow is stronger (Wooding et al., 1997a). If the upflow is strong ugh, the boundary layer is compressed to such an extent that it remains stable at all es. Hence, under these conditions insufficient spatial discretization, $\Delta z > \delta_{cr}$, will create unstable boundary layer and fingering in the model unjustly. Wooding et al. (1997a) nd $Ra_{cr} \approx 10$ from both perturbation analyses and numerical and Hele-Shaw cell experi- nts.

Similarly, Δx has to be chosen such that the critical wavelength of boundary-layer instabilities, λ_{cr}, which controls the dimensions of finger instabilities, is resolved. Because $\lambda_{cr} \approx 15\delta_{cr}$ (Wooding et al., 1997a) the following is appropriate:

$$\Delta x < \left(\tfrac{1}{8}\lambda_{cr} \approx 2\delta_{cr} = 2Ra_{cr}\mu D / \Delta\rho g \kappa \right) \qquad (10.2)$$

The validity of the above conditions was corroborated for the "long-heater" Elder probler (Elder, 1968) (sea-water conditions along entire width of the top of the domain) with and without upflow. That is, numerical experiments were performed to test (1) grid/mesh con gence and (2) $Ra_{cr} \approx 10$. Without upflow, progressive refinement of the mesh, both in the horizontal and vertical direction and reduction of time stepping indeed resulted in conver solutions where the location of individual fingers varied, but their characteristic wavelen and growth rate became constant. Too coarse discretization led to a different timing of in bility development and finger dimensions that were too large. Insufficient horizontal disc tization was found to have a stabilizing effect, causing finger development to be delayed finger widths equal to the element size. Convergence was also achieved when upflow w imposed for the above problem. Stable boundary layers occurred for boundary layer Rayleigh numbers of 7 and smaller, consistent with the results of Wooding et al. (1997a) Too coarse vertical discretization here led unjustly to fingering and salinisation. The gric convergence shows that the dynamics of the numerical system is governed by physics a not by the particular realization of "noise" (in our case truncation errors in the code), w seeds boundary-layer instability. This contrasts with recent findings of Simmons et al. (1999) who suggest that, in applying the SUTRA code to Wooding et al.'s (1997a) salt-l problem, it is inappropriate to rely on round-off errors. The cause for this difference is unclear. Recently, Kolditz et al. (1998) showed grid convergence for the "short-heater" Elder problem, apparently also relying on round-off errors. The grid size for which the obtain a converged solution agrees with Eq. 10.1 and 10.2.

For the experiments in model 1 and 2, the mesh size was chosen to satisfy Eq. 1 and 10.2 with dispersion dominated by molecular diffusion (substitution of the paramet listed in Table 10.1, 10.2 and 10.3 in Eq. 10.1 and 10.2 and using $Ra_{cr} = 7$ yields $\Delta z <$ m and $\Delta x < 0.56$ m, respectively). This should ensure proper discretization with respec Peclet and Courant conditions.

In model 3, hydrodynamic dispersion has been introduced: longitudinal and trans dispersion lengths are $\alpha_L = 1$ m and $\alpha_T = 0.1$ m, respectively. Under these conditions maximum mesh size can be enlarged to $\Delta z = 1$ m and $\Delta x = 2$ m to fulfill Peclet and C conditions. The maximum mesh for the simulation of density currents will also be larg than in model 1 and 2, although Eq. 10.1 and 10.2 cannot be applied. Nevertheless, th sen dimensions are believed to ensure a proper representation of the density currents.

10.2.3. *Models and boundary conditions*

Model 1: stationary submarine groundwater and solute transport

Because of strict requirements of grid/mesh resolution, accurate simulation of fr water tongues that extend over a long distance into the offshore is not feasible. The e ments presented here were conducted on a 500 m long section and a 10 m thick aquif overlain by a 1 m thick confining layer (Figure 10.1). For the same reasons the aquif

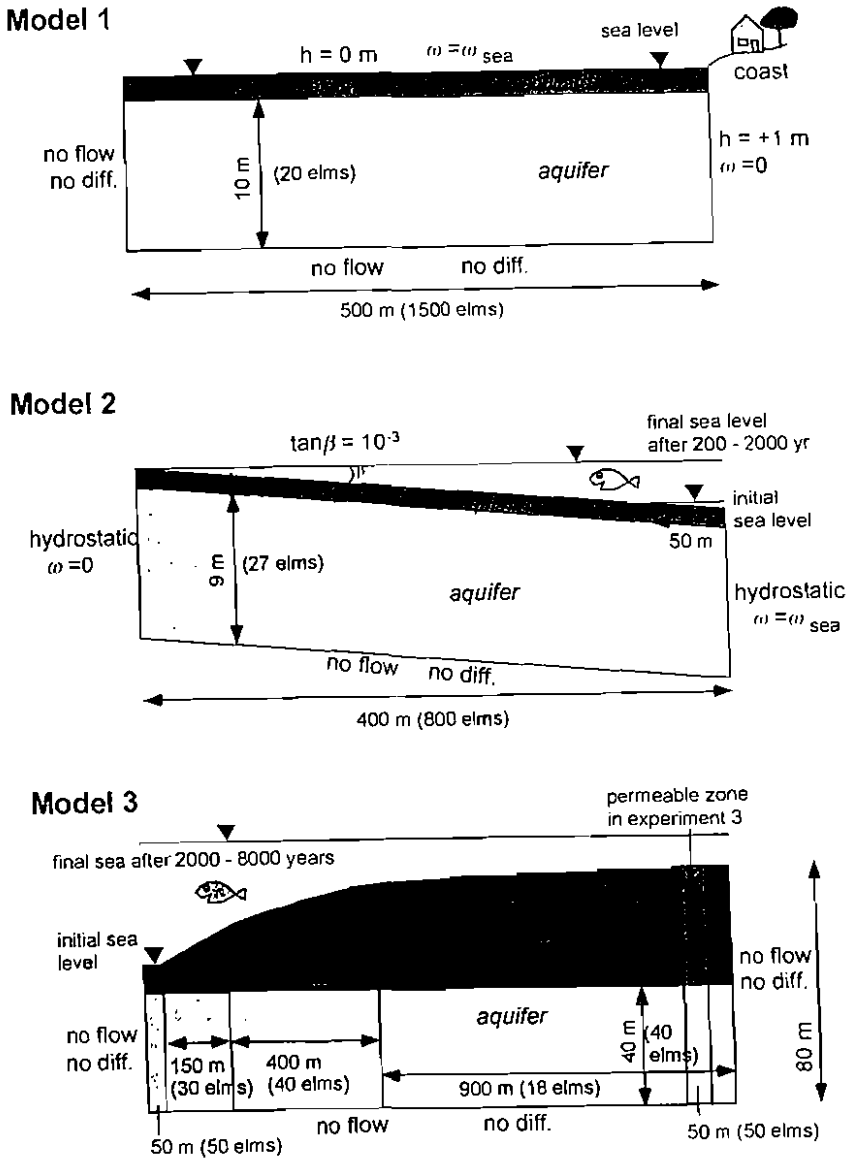

Figure 10.1. Schematic structures of three numerical models (elms = elements)

meability has to be assigned a relatively low value: $\kappa = 1.0 \times 10^{-13}$ m^2 or k (hydraulic conductivity) = 0.1 m/day. Fixed parameter values are listed in Table 10.1. Only the intrinsic permeability of the aquitard, κ_c, was varied in successive experiments. The finite-element mesh consists of 37,500 quadrilateral elements: 1500 in the horizontal and 25 in the vertical direction. The horizontal element size is uniform with $\Delta x = 0.5$ m. The vertical element size in the top 1 m of the section is $\Delta z = 0.2$ m; below this layer $\Delta z = 0.33$ m. Initially, the section was filled with seawater. Subsequently, each experiment was run until a steady-state salinity distribution was obtained. Most simulations only showed a quasi-steady solution because convective finger instabilities caused salinity values and the flow field to fluctuate around a constant mean. The dimensions and aquifer permeabilities did not correspond with the actual cases, where meteoric groundwater is found many kilometers offshore and to depths of several hundreds of meters (Chapter 8). The purpose of these experiments is to verify the assumptions and the results of the New Approximate Model (NAM) of Chapter 9.

Model 2: submarine groundwater and solute transport during transgressing over a flat seaward sloping land surface

Model experiments of the transgressing sea have been carried out on a two-dimensional vertical cross-section with a length of 400 m and an aquifer thickness of 10 m. Geometry and boundary conditions are depicted in Figure 10.1. The conditions at the top and right boundary are time dependent, depending on sea level. The right boundary is assigned hydrostatic pressure conditions and constant seawater salinity. The pressure part of the top-boundary condition is given by

$$p_b = \rho_{sea} g h(t) \quad | \quad h(t) \geq 0 \qquad \wedge \qquad p_b = 0 \quad | \quad h(t) < 0 \tag{10.3}$$

where p_b is the boundary fluid pressure and $h(t)$ is the local sea depth. Influence of tidal fluctuations is not taken into account. The section is assumed fully saturated such that the topographic gradient controls the onshore hydraulic pressure gradient. The gradient of the topographic surface in the experiments is $\beta = 1 \times 10^{-3}$, which is a typical mean value for continental shelves (100 m water depth at a the edge of a 100 km wide shelf). A time-dependent Dirichlet boundary condition is used for ω at the top boundary:

$$\omega_b = \omega_{sea} \quad | \quad h(t) \geq 0 \qquad \wedge \qquad \omega_b = 0 \quad | \quad h(t) < 0$$

Fixed parameter values are shown in Table 10.2, while parameters values varied in the various experiments are presented in Table 10.3.

The finite-element mesh consists of 29,600 quadrilateral elements: 800 in the horizontal and 37 in the vertical direction. The horizontal element size is uniform with $\Delta x = 0.5$ m. The vertical element size in the top 1 m of the section is $\Delta z = 0.1$ m, below this layer $\Delta z = 0.33$ m. The maximum time step employed is 1×10^7 s, which keeps Courant number smaller than 1 at all times. Each experiment started with the steady-state salinity distribution and flow field for a sea level of +0.05 m, which corresponds to a coastline location 50 m from the right boundary of the mesh. Model experiments simulated subsequent salinisation for a given rate of sea-level rise during a period of 200 to 2,000 years.

Again the dimensions of these experiments suffer from the same numerical limitations as in model 1. However, the basic styles of seawater intrusion that can develop are well illustrated, even at these reduced scales. Moreover, from the experiments and the discussion below, it can be understood how salinisation at larger space and time scales occurs.

In these experiments attention is given to the speed of the encroaching sea relative to advection of the fresh-saline interface. Earlier modelling studies by Meisler et al (1984) and

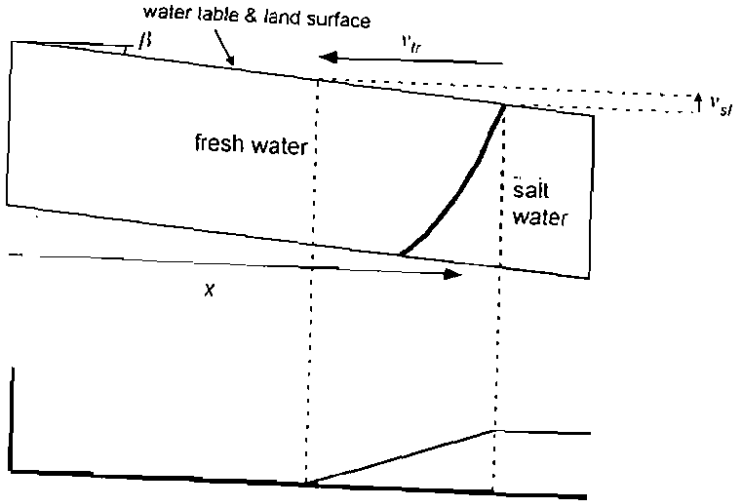

Figure 10.2. Density-driven force on the fresh/saline interface during transgression according to model 2.

Essaid (1990) showed that the interface reacts very slowly to the moving shoreline. The inland advection of the interface is primarily determined by the wedge of "heavy" seawater on the shelf, depicted in Figure 10.2 (Kooi and Groen, 2000):

$$v_{adv}^{max} = \frac{\kappa'}{n\mu} \rho_{sea} g \cdot \tan\beta \qquad (10.4)$$

where β is the landward dip of the shelf. The actual transgression speed, v_{tr}, is related to the sea level rise, v_{sl}, by:

$$v_{tr} = v_{sl} / \tan\beta$$

The transgression speed can be expressed in non-dimensional terms by:

$$\Gamma = v_{tr} / v_{adv}^{max} = \frac{n\mu v_{sl}}{\kappa \rho_{sea} g \cdot \tan^2\beta} \qquad (10.5)$$

where the critical value is expected at $\Gamma_{cr} = 1$. Eq. 10.5 shows that high values of Γ, which would favor the lagging behind of the salt-water wedge, tend to occur for large values of v_{sl}, low permeability (κ) and, in particular, low-gradient land surfaces ($\tan\beta$).

Model 3: submarine groundwater and solute transport during transgression over a dissected land surface

The effects of a rising sea level encroaching upon a continental shelf with valley topography has been studied with a two-dimensional model representing a vertical cross-section from a valley to a "water divide", as indicated in Figure 10.1. The length of the section is 1500 m. The aquifer thickness is 40 m, whereas the thickness of the clay layer on top varies from 10 m in the valley to 40 m at the water divide. Bottom, left and right bo are no-flow and no-diffusion boundaries. The hydraulic and concentration conditior open top boundary are time dependent, related to the rising sea level, as in model 2 experiment started with a steady-state situation with only fresh groundwater flow. T sea penetrated the valley and rose in 2,000 years to its final position, submerging th landscape. The water divide was then covered by 10 m of seawater Afterwards the nment was continued for another 6,000 years. This is a realistic scenario, reflecting ral Holocene sea level rise (Chapter 4): at 8 ka BP, the sea level was still rising tho below the present level, but at 6 ka BP it reached its present level.

Constant parameter values are shown in Table 10.4. The vertical and horizont abilities of the clay layer in experiment 1 are 10^{-16} and 10^{-15} m², respectively (or 1 ^{3} m/day in hydraulic conductivity). In the second experiment, the permeability has increased by a factor of 10 with respect to the first experiment. In the third experin permeabilities were equal to those in experiment 1, except for a 50 m wide zone n water divide, where they were increased by a factor of 100, relative to that of the f riment.

The finite-element mesh consists of 9660 quadrilateral elements: 138 in the h and 70 in the vertical direction. The horizontal element size varied from $\Delta x = 1$ m ley and gradually increased to $\Delta x = 50$ m at the water divide. The vertical element the aquifer equaled $\Delta z = 1$ m, while the element size in the clay varied from $\Delta z =$ the valley to $\Delta z = 1.33$ m at the water divide. For experiment 3, the horizontal gric the permeable zone was refined to $\Delta x = 1$ m to allow convective density currents.

10.3. Results

10.3.1. Model 1: stationary submarine groundwater and solute transport

Figure 10.3 displays the 'steady-state' salinity distribution for three experim which the permeability of the aquitard was progressively reduced from 7.4 x 10^{-1} x 10^{-17} m² to 1.5 x 10^{-17} m². The corresponding flow fields are depicted in Figure Three distinct zones can be distinguished: (i) a proximal stable zone closest to th where groundwater in the aquifer is fresh and high seepage rates restrain the diff dary layer to the clay layer; (ii) an intermediate instable zone where the diffusive layer reaches the aquifer and creates convection (density currents) and (iii) a dist zone where free convection is absent and salinities are high, though still less thar seawater.

In the first experiment seepage rates were high because of the relatively hig aquitard. A proximal stable zone of about 50 m developed. The length of this zo about equal to the length of the fresh-water tongue according to the New Approx Model (NAM) from Chapter 9 (indicated by an asterisk). Going further offshore rapidly diminished and the intermediate unstable zone commenced. Density cur clearly visible in Figure 10.4a. Beyond 100 m, the distal stable zone is found, w very little flow and salinities are high with very small vertical gradients. The lo second experiment led to a reduction of the upward seepage rate, but also to an the seepage zone into the offshore zone. In this case a wide intermediate unstab clearly visible from 100 to 250 m offshore (Figure 10.3b and 10.4b). The transi

proximal stable zone is not clear. The zone up to 100 m offshore looks stable, but it appears that from to time density currents develop reflecting the quasi-steady nature of the system. The instability can also be derived from the fact that Ra_L is exceeded in this zone (Figure 10.3b) and there is no submarine fresh-groundwater tongue according to the NAM model (Figure 10.3b). Apparently the instability is not very high as it takes a considerable time to develop fingers. Another possibility is that the small dispersion has a stabilizing effect on the boundary layer. Further reduction of κ_c in the third experiment did not change the general pattern, apart from the intermediate zone with frequent density currents, which moved closer to the shore. This is the result of the lower seepage rates allowing more salt intrusion into the aquifer.

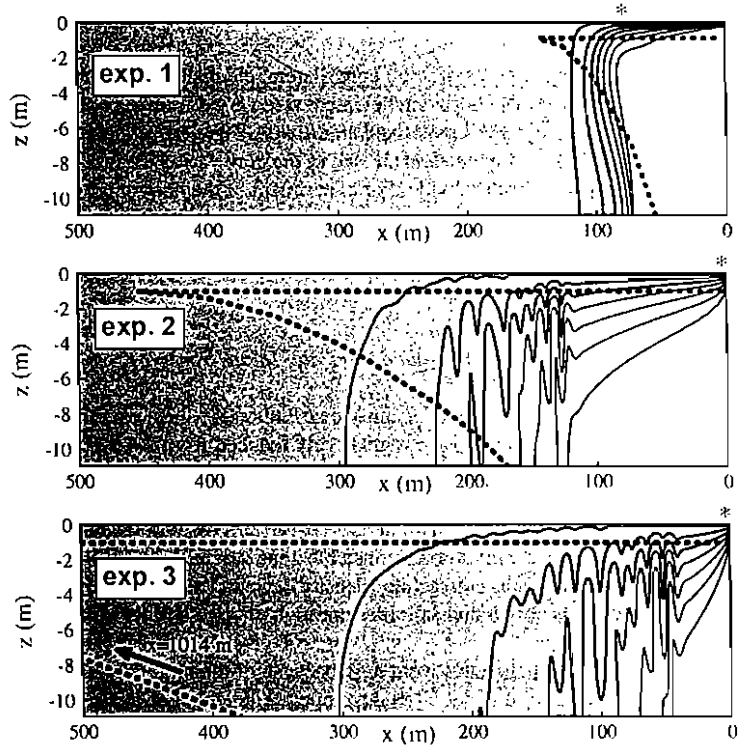

Figure 10.3. Variable-density flow and solute transport in experiments of model 1: steady-state submarine outflow of fresh groundwater; experiments 1 to 3 are results for κ_c equal to 7.4×10^{-16}, 7.4×10^{-17} and 1.5×10^{-17} m², respectively. Solid lines: contours of salt-mass fraction from $\omega = 0.005$ to $\omega = 0.035$ with contour interval 0.005. Shaded area: zone with $\omega > 0.020$. Heavy dashed lines: fresh/saline boundary according to sharp interface model. Asterisk above each panel: extent of fresh groundwater according to new approximate model.

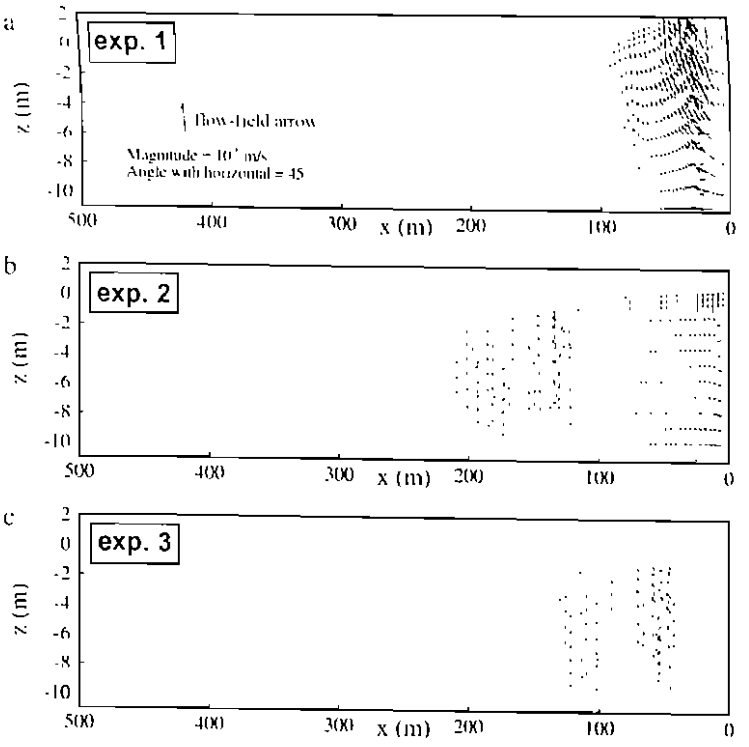

Figure 10.4. Visualization of the flow fields in experiments of model 1. True flow velocities are sho (Darcy velocity divided by porosity). The velocity is the same for the three panels and is indicated in upper panel.

Also shown for each of these experiments is the corresponding sharp-interface solutio according to the SIM model (Chapter 9) for the employed boundary condition for the coast groundwater head, $h_{coast} = 1$ m. The corresponding values of the submarine groundwater outflow Q_{coast} for the sharp-interface solutions are, respectively, 2.63×10^{-7}, 8.32×10^{-8} an 3.71×10^{-8} m²/s. Values of Q_{coast} inferred from the flow field of the numerical simulations are, respectively, 2.63×10^{-7}, 8.07×10^{-8} and 3.31×10^{-8} m²/s. The slightly lower values f the latter two numerical simulations as compared to the values for the sharp-interface approximations are caused by the density effect associated with the presence of more saline water in the aquifer close to the coast. Comparison of the results for the two types of mode shows that the sharp-interface approximations tend to overestimate the length of the fresh-water tongue, and that the discrepancy grows significantly with decreasing κ_c. The numerical experiments demonstrate that the downward salinization by convective density currents becomes progressively more dominant: that is, the fresh-water length initially increases, bu reaches a maximum value and then decreases upon further reduction of κ_c. For the hydroge ological conditions adopted in the experiments, this optimum approximately occurs for the

econd experiment.

Finally, an interesting feature of the predicted salinity patterns displayed in Figure 10.3 s that low-salinity waters extend farthest offshore near the base of the aquifer. This contrasts trongly with the results of sharp-interface models, which show fresh water to be progressi- ely confined to the top part of the aquifer when moving in a seaward direction.

0.3.2. *Model 2: submarine groundwater and solute transport during transgressing over a flat seaward sloping land surface*

The experiments that were conducted with the second model are summarized in Table 0.3. In the experiments the following parameters or conditions were varied:

- stratigraphy: (a) single sand layer (aquifer); (b) single clay layer (aquitard); (c) aquitard erlying an aquifer
- rate of sea-level rise, v_s
- clay permeability, κ_c, and
- longitudinal and transversal dispersivity, α_L and α_T.

Parameter values that were kept constant are given in Table 10.2. The term "sand" is ed here and in the following to denote sediments with permeabilities that are high relative clays. The permeability value listed in Table 10.2 corresponds to fine sand or silt. Using a gher permeability would imply a major increase in numerical cost, as explained in section 2.2. Γ_{sand} and Γ_{clay} denote the non-dimensional transgression rate of Eq. 10.5 substituting nd and clay permeability, respectively.

Experiments 1-7 constrain the critical transgression rate, Γ^{cr}, for a uniform sand sub- ate and very small hydrodynamic dispersion (more than 40 times smaller than molecular ffusion). Γ^{cr} was found to occur for this set of experiments between 5.58 and 6.51 (Table 3). Figure 10.5 displays the horizontal style of salinisation for experiment 1. It shows that transition zone quickly assumes a steeper and narrower geometry during its lateral gration in comparison with the initial steady-state situation. It was found that this effect is nger for higher rates of sea-level rise. The observed steepening is probably due to inhibi- outflow at the landward side of the transition zone and, therefore, enhanced input of salt he top of the transition zone. This steepening, in turn, enhances the clockwise vortex in flow field associated with the density distribution, which tends to flatten the transition e. Apparently, the two effects (input of salt at the seafloor and the enhanced clockwise tex) work together to: (1) maintain a constant shape of the transition zone and (2) provide echanism for lateral migration of the transition zone in addition to that due to the chan- e pressure boundary conditions at the land surface. The latter effect probably explains the experimentally determined value of Γ^{cr} of about 6 is larger than the value of 1 pre- ed in Section 10.2.3.

Figure 10.6 shows the salinisation history for experiment 7. In this experiment, the sition zone lags behind the migrating coastline and sea-water fingers emanated from a sive boundary layer which develops as a "moving wave" at the top of the aquifer as sea r overrode fresh groundwater (this boundary layer is seen more clearly in Figure 10.7, re it remained stable because of low permeability). Theoretically, fingering only started re this boundary layer reaches a critical thickness. In Figure 10.8 this occurred close to urrent shoreline because the critical thickness was very small; using Eq. 10.1 and adop- $Ra_{cr} = 7$ yields $\delta_{cr} = 0.28$ m. Sea-water fingers sank to the base of the aquifer and, in een, fresh water escaped upwards into the sea. As a result, a wide, high-salinity transi-

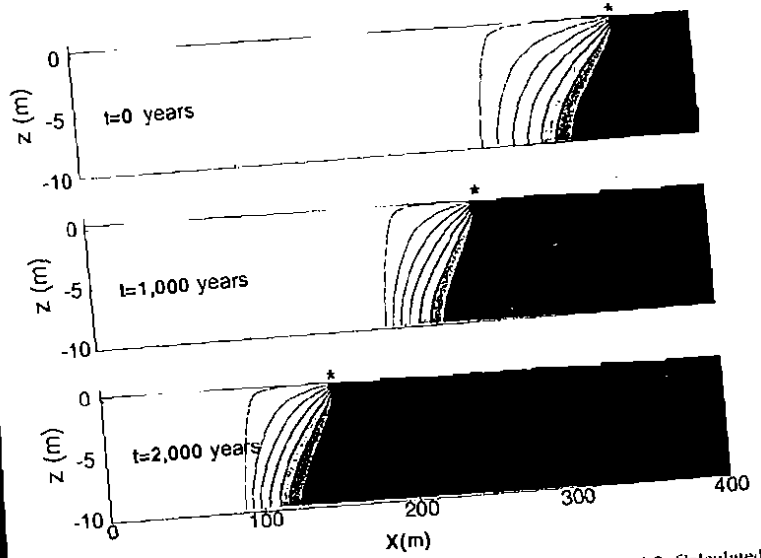

10.5. Variable-density flow and solute transport in experiment 1 of model 2. Calculated salinity ution at three time steps for a sandy substrate in combination with a sub-critical transgression rate. ass fraction increases with darkness of shading. Contours shown are from $\omega = 0.0005$ to 0.0355 form intervals. The current location of the shoreline is indicated by an asterisk. Details are given text.

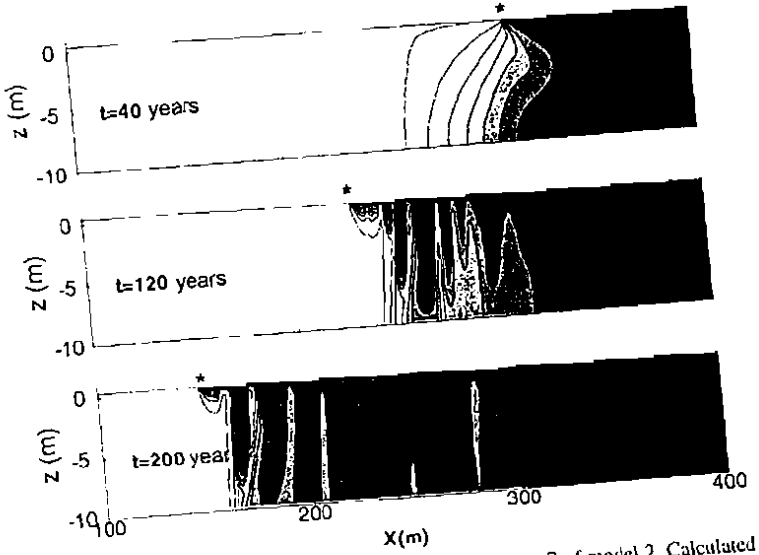

gure 10.6. Variable-density flow and solute transport in experiment 7 of model 2. Calculated salinity tribution at three time steps for a sandy substrate in combination with a supra-critical transgression te. Salt-mass fraction increases with darkness of shading. Contours shown are from $\omega = 0.0005$ to 0355 at uniform intervals. The current location of the shoreline is indicated by an asterisk. Left 100 m f model domain is not shown. Details are given in the text.

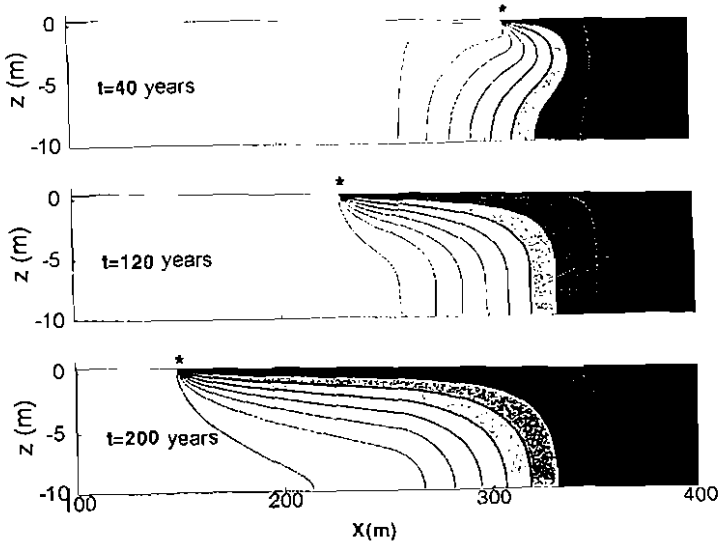

Figure 10.7. Variable-density flow and solute transport in experiment 13 of model 2. Calculated salinity distribution at three time steps for a clay substrate in combination with a supra-critical transgression rate. Salt-mass fraction increases with darkness of shading. Contours shown are from $\omega = 0.0005$ to 0.0355 at uniform intervals. An asterisk indicates the current location of the shoreline. Left 100 m of model domain is not shown. Details are given in the text.

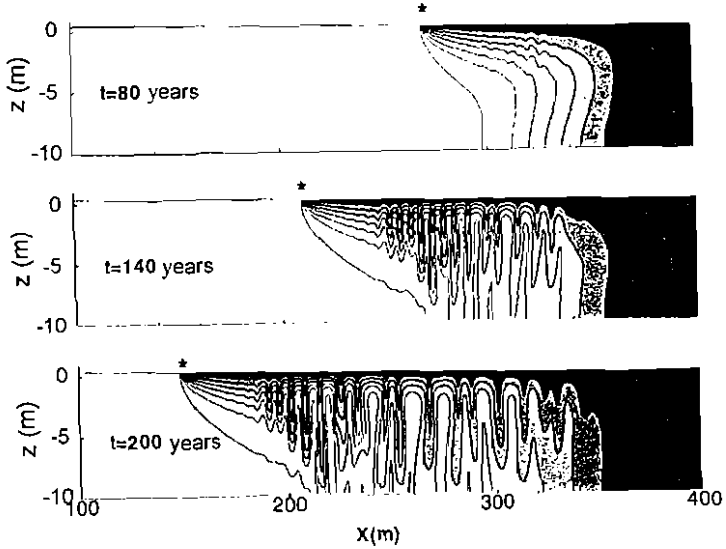

Figure 10.8. Variable-density flow and solute transport in experiment 17 of model 2. Calculated salinity distribution at three time steps for a sandy aquifer overlain by a 0.5 m thick clay layer in combination with a supra-critical transgression rate. Salt-mass fraction increases with darkness of shading. Contours shown are from $\omega = 0.0005$ to 0.0355 at uniform intervals. An asterisk indicates the current location of the shoreline. Left 100 m of model domain is not shown. Details are given in the text.

tion zone developed between the former and new coastline. Very little flow occurred in this zone once the fingers reached the base of the aquifer and, consequently, the subsequent development of this zone towards full sea-water quality was dominated by diffusion and, therefore, very slow. In Figure 10.6, the frontal fingers were deflected somewhat landward as they descended deeper into the aquifer.

In experiments 8-12, the role of hydrodynamic dispersion was investigated. Experiments 8 and 9 are the same as experiment 7 except for increased dispersivities. In experiment 9 with largest dispersivities, $\alpha_L = 1$ m and $\alpha_T = 0.1$ m, respectively, fingers emanated from a thicker saline boundary layer and finger dimensions were about three times larger than in experiment 7, but the basic style of sea-water intrusion was not altered. Experiments 10-12, which correspond with experiments 4-6, showed that hydrodynamic dispersion slightly increases Γ' to a value between 6.51 and 7.44.

Experiments 13 and 14 investigated salinisation of a uniform clay substrate. In these experiments vertical 'intrusion' by diffusion dominated. Figure 10.7 illustrates the "moving-wave behavior" of the diffusive boundary layer that developed below the sea floor for experiment 13. Due to the low permeability of the clay the boundary layer stayed intact. Not surprisingly, a seaward dipping fresh water wedge developed in the offshore.

The set of experiments 15-20 were conducted for a substrate in which a 0.5 m thick clay layer overlies a sandy aquifer. Figure 10.8 illustrates the salinisation history for experiment 17 which, apart from the 0.5 m thick clay layer, was the same as the experiment of Figure 10.6. The clay layer affects the results in several ways. First, because of its low permeability, the high salinity part of the diffusive boundary layer, which developed within the clay layer, is stable (see also Figure 10.7). Instabilities germinated beneath the clay layer where the diffusive boundary layer within the aquifer had reached a critical thickness. Second, this critical thickness was larger than for a uniform sandy substrate ($\delta_{cr} > 0.28$ m) because (i) the density contrast across the boundary layer within the aquifer was less than the fresh/sea-water density contrast, and (ii) flow into the top of the boundary was restricted relative to that in the experiment of Figure 10.6. The enhanced stability of the boundary layer is apparent in Figure 10.8 from the fact that instabilities appeared a finite distance from the current coastline. Third, once the instabilities have grown into macroscopic salt fingers, they do not sink as readily as in Figure 10.6 because of the small density contrast with the ambient groundwater and because of the greater resistance to drawing dense fluid from the overlying sea reservoir. Therefore, a wide low-salinity transition zone developed which is intermediate in nature relative to the experiments of Figures 10.6 and 10.7. It should be noted that a minimum thickness of the sandy layer is required for instabilities to arise.

Experiments 15 and 16 constrained the non-dimensional critical transgression rate to occur between $\Gamma_{sand} = 0.93$ and $\Gamma_{clay} = 1.86$, which is approximately 5 times lower than for a pure sand substrate. A greater thickness of the clay layer will probably further reduce the critical transgression rate and result in lower salinity pore waters in the underlying aquifer. However, this was not tested within the present set of experiments.

The effect of hydrodynamic dispersion was investigated in experiments 19 and 20. It was found that, similar to a uniform sand substrate, hydrodynamic dispersion increased the thickness of the boundary layer and the width of the fingers, but did not alter the mode of intrusion in a significant way.

10.3.3. *Model 3: submarine groundwater and solute transport during transgression over a dissected land surface*

Figure 10.9 shows the salinity distribution at four different stages after the sea has inundated the dissected landscape. After 1,000 year sea level has risen to 20 m above the valley bottom, but the interfluves have not been submerged yet. At this stage a ria-type coastline has been formed, as can still be observed along many coasts. Despite the inundation of the valley, salt-water intrusion does not occur. The reason for this behavior is that the groundwater system is still recharged on the interfluves and strong upward seepage below the valley is maintained, preventing downward diffusion into the aquifer. Only a thin stable diffusive boundary layer has developed in the top of the aquitard. This is shown by the vector field in Figure 10.9. When, after 1500 years, the entire landscape becomes submerged, the flow field dramatically changes. The meteoric flow system loses its drive and the fresh groundwater becomes subjected to diffusion and density-driven flow. The salt-water wedge in the drowned valley makes the fresh water flow in the reverse direction and drives it from the aquifer by upward seepage through the aquitard at the water divide. Below the valley, salts enter the aquifer by diffusive and advective transport and create instability and density currents. The expulsion and salinization of the meteoric groundwater body is a slow process: after 2,000 years, when the sea has level reached its final position, most of the aquifer is still fresh. Salinization takes place mainly by downward diffusion through the aquitard and density driven flow along the bottom of the aquifer. After 8,000 years (representing the present-day situation) groundwater in the aquifer is no longer fresh, though ω is still below 0.01 underneath the interfluves (chloride concentration < 6,000 mg/l).

Figure 10.10 displays the results of the second experiment, where the hydraulic conductivity of the aquitard has been increased by a factor of 10 with respect to experiment 1. Only the situation after 2,000 and 8,000 years is shown. It is clear that the higher conductivity of the aquitard has led to a larger flux of salt water into the aquifer below the valley. Also the upward seepage of fresh water further away from the valley has increased. Therefore, the diffusive boundary layer in this part is smaller than in the first experiment. Because of the larger flow rates, salinization proceeds more rapidly: after 8,000 years almost the entire system has become saline.

In the last experiment the effect of a relatively permeable zone in the aquitard has been studied. Parameters are equal to experiment 1, except for the 50 m wide zone, where hydraulic conductivities have been increased by a factor of 100. The salinities in this zone after 2,000 years in Figure 10.11 clearly show that a preferential flow path has developed here for the expulsion of the meteoric groundwater: the high outflow velocities compress the diffusive boundary layer to a thin zone. However, after 3,000 and 8,000 years saline intrusion by convective density currents can be observed in the permeable zone. Comparing the results after 8,000 years in experiments 1 and 3 shows that the aquifer in experiment 3 has a lower salinity. Apparently the two entrance zones resulted in lower groundwater flow velocities or even stagnant zones, which retarded the salinization process.

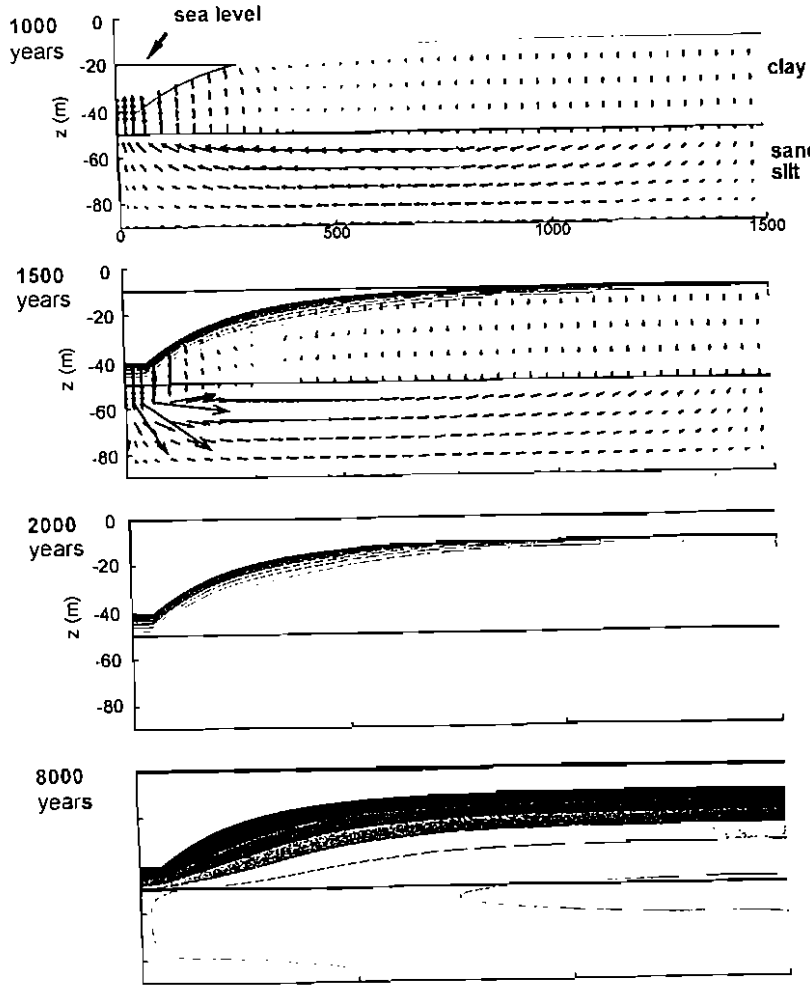

Figure 10.9. Variable-density flow and solute transport in experiment 1 of model 3. Calculated distribution at 1,000, 1,500, 2,000, and 8,000 years after transgression started in the valley. Valle ded in clay layer overlying a sandy aquifer. Vertical and horizontal clay permeabilities are $\kappa_z' =$ $\kappa_x = 10^{-15}$ m^2, respectively. Salt-mass fraction increases with darkness of shading. Contours sh from $\omega = 0.0005$ to 0.0355 at uniform intervals. For time step of 1,000 and 1,500 years flow l given.

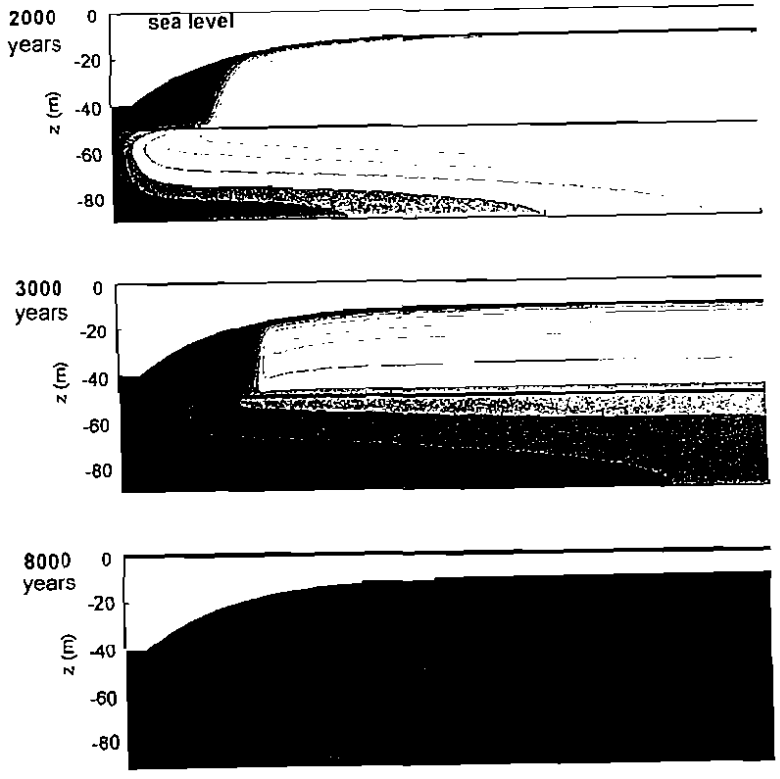

Figure 10.10. Variable-density flow and solute transport in experiment 2 of model 3. Calculated salinity distribution at 2,000, 3,000, and 8,000 years after transgression started in the valley. Valley is eroded in clay layer overlying a sandy aquifer. Vertical and horizontal clay permeabilities are $\kappa_z' = 10^{-15}$ and $\kappa_r = 10^{-14}$ m², respectively. Salt-mass fraction increases with darkness of shading. Contours shown are from $\omega = 0.0005$ to 0.0355 at uniform intervals.

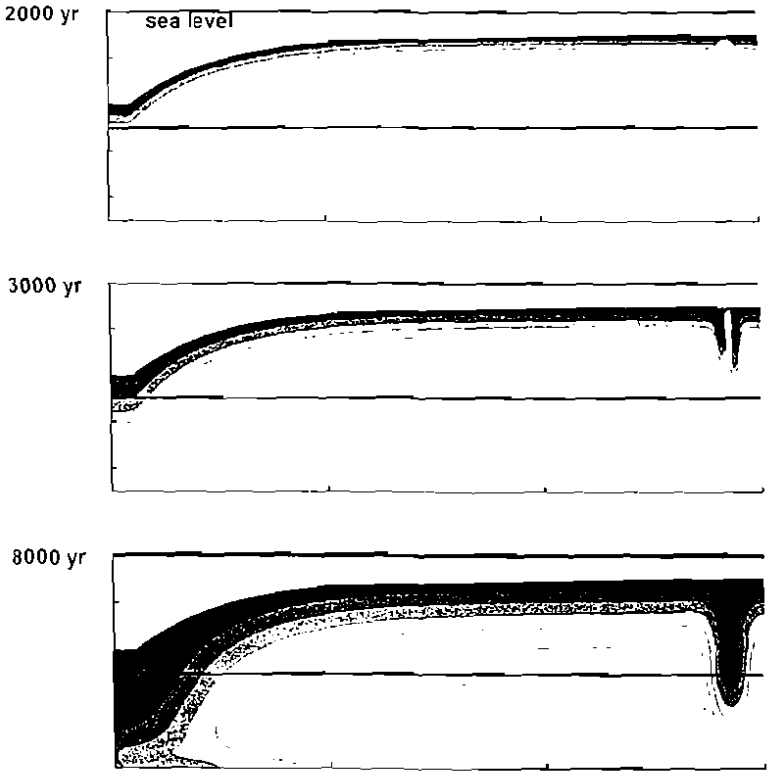

Figure 10.11. Variable-density flow and solute transport in experiment 3 of model 3. Calculated salinity distribution at 2,000, 3,000, and 8,000 years after transgression started in the valley. Valley is eroded in clay layer overlying a sandy aquifer. Vertical and horizontal clay permeabilities are $\kappa_z' = 10^{-16}$ and $\kappa_r = 10^{-15}$ m², respectively, as in experiment 1. Permeabilities in the permeable zone are 100 times higher. Salt-mass fraction increases with darkness of shading. Contours shown are from $\omega = 0.0005$ to 0.0355 at uniform intervals.

10.4. Discussion and conclusions

10.4.1. Model 1

The experiments show that the steady-state offshore outflow of coastal groundwater in semi-confined aquifers can result in extensive transition zones of low- to high-salinity groundwater (intermediate unstable and distal stable zone). In these zones relatively fresh pore water extends farthest into the offshore near the base of the aquifer. These transition zones result from convective mixing in the form of density currents. Fresh, unmixed offsho re groundwater is found in the near-shore zone only when the upward seepage is high enough to restrict the diffusive boundary layer to the clay layer and prevent instability (proximal stable zone). Note that fresh groundwater can also occur in the bottom of the aquifer in the intermediate unstable zone where density currents arise infrequently.

Although the present work was concerned with steady-state salinity distributions, the analysis does demonstrate that major modifications in offshore salinity patterns can occur as a result of relatively minor changes in coastal hydrological regime. As such changes are likely to have occurred in many coastal areas at time scales of thousands of years, the associated landward and seaward shifts of the fresh-water domain would have contributed to the development of wide transition zones. The inverted salinity distribution occurring within the confining layer and, to a lesser extent, in the aquifer as predicted by the variable-density flow modelling has been documented, for instance, for the North Sea (Post et al., 2000) and the Baltic Sea (Piekarek-Jankowska, 1996) and may have important implications for sediment diagenesis in such offshore environments. It may, therefore, be an interesting feature to consider in geochemical models of early diagenetic processes (Berner, 1980).

10.4.2. Model 2

Based on the findings of the second model simulating transgression on a flat sloping continental shelf, four modes of seawater intrusion are distinguished:

- Mode 1: Quasi-steady, "horizontal" seawater intrusion in the form of landward migration of a "narrow" transition zone closely following shoreline migration (Figure 10.5). This mode occurs for a sufficiently slow, sub-critical rate of transgression. An estimate of the critical trangression rate at which the transition to modes 2 or 3 occurs for uniform substrate conditions is given by Eq. 10.4. Experiments showed that Eq. 10.4 is accurate to one order of magnitude and tends to underestimate Γ_c. Referring to the recent Holocene transgression, this intrusion mode was not the dominant process in most of the offshore aquifers. The transgression speeds during the Early Holocene for many continental margins away from the major continental ice sheets of the last ice age were far higher (> 100 m/a) than critical transgression speeds.
- Mode 2: Vertical seawater intrusion by fingers of seawater (Figure 10.6). This mode occurs for supra-critical transgression rates and a relatively high-permeability substrate (sand/silt). A wide high-salinity transition zone develops. This rapid intrusion mode can keep up even with rapidly advancing shorelines. It explains, as an example, the presence of high-salinity groundwater in the exposed sandy aquifers in the western part of the Netherlands, which were inundated during the Early Holocene.
- Mode 3: Vertical seawater intrusion by diffusion (Figure 10.7). This mode occurs for supra-critical transgression rates, which can be very small, and for low-permeability substrate sediments (silt/clay) up to great depth. An extensive, seaward dipping fresh-water wedge develops below a thick, mainly vertically layered, transition zone. Salinization is mainly controlled by downward diffusion. This intrusion mode is restricted to shelf sediments with very thick clayey sediments below the sea floor.
- Mode 4: Vertical seawater intrusion by low-salinity fingers (Figure 10.8). This mode occurs for supra-critical transgression rates and a layer of low-permeability, sea-floor sediments (silt/clay) overlaying a relatively high-permeability aquifer. A wide, low-sa inity transition zone develops in the aquifer resulting from convective density current while in the overlaying low-permeability layer a relatively sharp diffusive boundary layer is present. This intrusion mode explains, just as the third mode, the temporary preservation of offshore meteoric groundwater. Although the dimensions of the mod are small, the same process explains the presence of vast bodies of meteoric groundw ter far offshore along the coast of Suriname, the Netherlands, Indonesia (Java Sea) a the eastern USA (Chapter 8).

The experiments are carried out for simple one- and two-layer systems. Most elastic continental shelves comprise a succession of alternating sand and clay layers. Therefore s ne intrusion may take place by superposition of various modes. For instance, rapid saliniz tion in a top sand layer takes place by convection in accordance to mode 2. The resulting high salinity in the sand aquifer may invoke diffusive salinization of a thick underlying c layer according to mode 3. In the subsequent sand layer, salinization may proceed as mo via convective density currents controlled by diffusion through the overlying clay.

10.4.3. Model 3

The transgression experiments with model 3 on a hilly landscape show that saliniz below valleys starts only after sea level has risen to a sufficiently high level. Intrusion s in when the discharge in the valley, related to the former meteoric flow system, declines disappears altogether. Note that in this case a wet climate is assumed with high groundw levels in a landscape underlain by a clay layer. Under more arid conditions (lower seep rates) and more permeable sediments under the valleys, salinization will start earlier. Th experiments show that after submersion of the landscape the flow system reverses. Fres and low-salinity groundwater is slowly expelled from the upland areas, where it was re ged before, either as diffuse discharge or via permeable pathways. The studied cases wi relatively low, but otherwise typical permeabilities show that meteoric submarine groun ter can be preserved for thousands of years after the submersion of the landscape. Thes paleowaters may form very large bodies, which slowly disappear either by expulsion o fusion.

Some observations of groundwater discharge, either as diffuse discharge, submari springs or based on geomorphological features, may be related to the expulsion of pale ters. This applies especially for observations far offshore, which cannot be related to a dy-state groundwater flow system with onshore recharge. The NAM model (Chapter 9 demonstrates that these systems under normal circumstances extend only several kilon into the offshore. In the experiments only a few parameters have been varied. The pur was not to show the various modes of salinization as in the experiments of model 2, b merely to show the possibility of preservation of offshore paleogroundwater.

10.4.4. Additional remarks

Incorporation of diurnal effects, such as tides, might affect details of the predicted salinity patterns. This would apply in particular to the relatively small spatial scale of the experiments presented here. However, it seems reasonable to assume that the results presented here provide insight into processes for much larger spatial scales (tens to hundreds of kilometers) and geological time scales for which the magnitude of sea-level change overwhelms that of diurnal processes.

Perhaps more important shortcomings of the modeling with respect to its applicability to natural systems are its 2-dimensional character and the absence of heterogeneity in subsurface conditions.

h_{coast}	=	+1	m
n	=	0.3	-
ω_{sea}	=	0.0357	-
ρ_o	=	10^3	$kg \cdot m^{-3}$
κ (aquifer)	=	10^{-13}	m^2
μ	=	10^{-3}	$Pa \cdot s$
G	=	10	$m \cdot s^{-2}$
D_m	=	10^{-9}	$m^2 \cdot s^{-1}$
α_L	=	0.2	m
α_T	=	0.02	m

Table 10.1. Constant parameter values for model 1

N	=	0.3	-
ω_{sea}	=	0.0357	-
ρ_o	=	10^3	$kg \cdot m^{-3}$
κ (sand)	=	10^{-13}	m^2
μ	=	10^{-3}	$Pa \cdot s$
G	=	10	$m \cdot s^{-2}$
D_m	=	10^{-9}	$m^2 \cdot s^{-1}$

Table 10.2. Constant parameter values for model 2

Experiment	Litholog y	v_{sl} (mm/a)	Γ_{sand}	Γ_{clay}	κ_{clay} (m^2)	α_L (m)	α_T (m)	intrusio n
1	sand	0.1	0.93	-	-	10^{-3}	10^{-3}	hor.
2	,,	0.2	1.86	-	-	10^{-3}	10^{-3}	hor.
3	,,	0.5	4.65	-	-	10^{-3}	10^{-3}	hor.
4	,,	0.6	5.58	-	-	10^{-3}	10^{-3}	hor.
5	,,	0.7	6.51	-	-	10^{-3}	10^{-3}	vert.
6	,,	0.8	7.44	-	-	10^{-3}	10^{-3}	vert.
7	,,	1.0	9.30	-	-	10^{-3}	10^{-3}	vert.
8	,,	1.0	9.30	-	-	10^{-4}	10^{-2}	vert.
9	,,	1.0	9.30	-	-	10^{0}	10^{-4}	vert.
10	,,	0.6	5.58	-	-	10^{0}	10^{-1}	hor.
11	,,	0.7	6.51	-	-	10^{0}	10^{-1}	hor.
12	,,	0.8	7.44	-	-	10^{0}	10^{-1}	vert.
13	clay	1.0	-	$9.3 \cdot 10^{4}$	10^{-17}	10^{-3}	10^{-3}	vert.
14	,,	1.0	-	$9.3 \cdot 10^{3}$	10^{-16}	10^{-3}	10^{-3}	vert.
15	sand/clay	0.1	0.93	$9.3 \cdot 10^{3}$	10^{-17}	10^{-3}	10^{-3}	hor.
16	,,	0.2	1.86	$1.9 \cdot 10^{4}$	10^{-17}	10^{-3}	10^{-3}	vert.
17	,,	1.0	9.30	$9.3 \cdot 10^{4}$	10^{-17}	10^{-3}	10^{-3}	vert.
18	,,	1.0	9.30	$9.3 \cdot 10^{3}$	10^{-16}	10^{-3}	10^{-3}	vert.
19	,,	1.0	9.30	$9.3 \cdot 10^{4}$	10^{-17}	10^{-1}	10^{-2}	vert.
20	,,	1.0	9.30	$9.3 \cdot 10^{4}$	10^{-17}	10^{0}	10^{-1}	vert.

Table 10.3. Variable parameter values for experiments of model 2

N	=	0.3	-
ω_{sea}	=	0.0357	-
ρ_o	=	10^3	$kg \cdot m^{-3}$
κ (aquifer)	=	10^{-13}	m^2
μ	=	10^{-3}	$Pa \cdot s$
G	=	10	$m \cdot s^{-2}$
D_m	=	10^{-9}	$m^2 \cdot s^{-1}$
α_L	=	0.2	m
α_T	=	0.02	m

Table 10.4. Constant parameter values for model 3

Chapter 11.

Summary and conclusions

Introduction

The objective of the work presented in this thesis is to shed more light on salinizatic and freshening of coastal groundwater at geological time scales, and on the origin of onsh re and offshore paleogroundwater. An essential approach to meet this objective is the rec struction of paleogeography and associated paleohydrology of coastal plains. The scope c the study encompasses groundwater in coastal plains and offshore.

In many cases the salinity distribution in groundwater in coastal plains and offshore aquifers is complex and does not comply with the classic concepts on coastal hydrogeolc The main reason for this incongruence is that these concepts do not account for geologic events like regressions, transgressions, sedimentation and landscape changes. These even have triggered processes that may not have reached steady state with respect to the salini concentrations of specific chemical components and even groundwater heads. This applic in particular, to groundwater salinization resulting from the Early Holocene transgressior and the subsequent freshening after coastal aggradation set in during the Late Holocene. Because flow systems change rapidly in the dynamic coastal and offshore zone, bodies o fresh to moderately brackish groundwater ($Cl^- < 7{,}000$ mg/l) occur that do not belong to present-day flow systems. These meteoric groundwaters have been formed by extinct systems and are designated as paleogroundwaters (Chapter 2.1).

Part I of this thesis comprises the results of a case study of the coastal plain around Paramaribo, the capital of Suriname, in South America, where peculiar salinity patterns paleogroundwaters were known to exist. Many researchers of various earth-scientific dis plines as well as consulting hydrogeologists have investigated the area. Existing informa from these studies, new hydrogeochemical and isotopic data, and mathematical simulati were used to explain the salinity patterns in the coastal plain and the offshore area.

Part II contains the results of general studies into the phenomenon of offshore met groundwater, as found in Suriname. Observations of other coasts were reviewed and exp ments with generic models were carried out to understand the genesis of offshore metec groundwater

Part I. Case study of the Suriname coast

Hydrology of the coastal plain (Chapter 3)

The coastal sedimentary zone in Suriname has a width of 70 km near the capital o Paramaribo (Figure 3.1). In the South, Pliocene sands are exposed forming a rolling la pe called the savannah belt because of the savannah-type vegetation. The low-lying ma coastal plain stretches northward of the savannah belt and is underlain by Pleistocene (South) and Holocene clays (North). Housing and agricultural activities are concentrat

the slightly elevated sand barriers in the coastal plain.

The stratigraphy comprises a wedge of mainly clastic formations of Late Cretaceous to Holocene age (Figure 3.5 and 3.6). Regional groundwater flow takes mainly place in the Tertiary sediments, forming an alternating succession of sand and clay layers. The Tertiary aquifers contain fresh to moderately brackish (meteoric) groundwater (Figures 3.5 and 3.8). Pristine meteoric groundwater (Cl< 50 mg/l) is only found below the recharge zones of the savannah belt and the Lelydorp sands in the Pleistocene coastal plain (Figure 3.1). Meteoric groundwater is sandwiched between saline groundwater in the Holocene clays and deep saline groundwater in the Cretaceous formations, and extends about 90 km into the offshore deposits.

Rainfall (2,200 mm/a) may occur all year round, but is most abundant during the short (Dec-Jan) and long (Apr-Jul) rainy season (Figure 3.2). Groundwater recharge rates in the sandy soils of the savannah belt are high, but this groundwater is discharged locally by creeks and does not feed the aquifers in the coastal plain. Direct recharge of the Tertiary aquifers is restricted in the coastal plain to the Lelydorp sands, where phreatic groundwater levels are relatively high. In the rest of the plain, the large hydraulic resistance and small vertical head gradient in the Quaternary clays prohibit recharge. In the period before large-scale groundwater pumping (before 1958) groundwater in the aquifers was almost stagnant (Figures 3.9 and 3.10). Nowadays, groundwater flow in completely controlled by the extractions in and around Paramaribo (Figure 3.10).

Interesting are the artesian heads in the Oligocene aquifer in the prepumping period (Figure 3.9). These heads cannot be related to an elevated recharge area, but are attributed to the rapid Holocene sedimentation. Most probably, the sediment loading caused an excess hydraulic pressure, which has not fully dissipated in this case. This effect may be more common than we think along other coasts with high sedimentation rates. However, it may be weakly developed in the absence of confining layers or obscured by regional coastal flow systems with submarine discharge.

Freshening during the Wisconsinan regression (Chapter 4).

Onshore and offshore meteoric groundwater in Suriname must have been formed by extinct flow systems acting under climate, landscape and sea level conditions different from today. During the Wisconsinan (Weichselian) glacial, sea level stood much lower, with a minimum of 130 m below present sea level during the last glacial maximum (LGM) from 25 ka to 15 ka BP (Figure 4.1). The Pleistocene surface was eroded and resulted in a topography of clay plateaus dissected by gullies and rivers. Climate during the LGM was colder and dryer. The large coastal plain of that time was covered by grass and shrub savannahs, similar to those in the present savannah. Recharge in the Pliocene sand outcrop (present savannah belt) is estimated at 200 mm/a (at present 500 mm/a). Paleohydrological conditions were much different In the coastal plain: the incised Saramacca and Suriname rivers (about 30 m incision near Paramaribo) lowered groundwater heads in the Pliocene aquifer inducing widespread recharge from the overlying clay plateaus (Figure 4.3).

The latter assumption was confirmed by simulating the paleohydrology with a groundwater model. The model shows that the secondary topography of the eroded river valleys created secondary flow systems superimposed on a regional primary flow system (Figure 4.7). Despite the large hydraulic resistance of the Pleistocene clays in the coastal plain (> 1 x 10^5 days) recharge rates reached values of 40 to 60 mm/a. The paleohydrological model showed that

groundwater residence times in the regional primary flow system was not sufficient to flush brackish or saline water from the aquifers (Figure 4.6). It appears that the more dynamic secondary systems with the smaller residence times, related to the erosion topography, are essential for explaining the present-day occurrence of meteoric groundwater far offshore.

Salinization during the Holocene transgression (Chapter 5).

During the Holocene transgression in Suriname the sea encroached the Pleistocene coastal plain with a speed of 3 to 180 m/a. The subvertical fresh/saline groundwater interface near the Pleistocene coastline also moved landward. However, earlier investigations showed that the density-driven horizontal displacement of the interface could not keep up with such a rapidly migrating coastline. When in such a situation, like in Suriname, saline groundwater overlies fresh groundwater, downward salinization takes place by convective density currents and diffusion (Figure 5.5). Because the former is a very rapid process and not in agreement with the presence of the offshore meteoric groundwater body, diffusive solute transport is assumed to be the main salinization process in the Suriname coastal plain. This hypothesis has been verified by studying chloride concentrations and chlorine-isotope ratios ($\delta^{37}Cl$) in groundwater from wells and in pore water from the Quaternary clays sampled at two sites in the coastal plain (Koewarasan and Tourtonne). The analyses were compared with simulations with a model that incorporated vertical diffusive solute transport related by the Early Holocene transgression and Late Holocene regression and Holocene sedimentation (Figure 5.2 and 5.3). Transgressions at 6 ka and 10 ka BP for Koewarasan and Tourtonne, respectively, as well as sedimentation rates of 2.9 and 2.6 mm/a were established on the basis of radiocarbon dating. Simulated vertical profiles are in good agreement with the analyses, when an effective chloride diffusion coefficient 7.10^{-10} m^2/s and a fractionation factor for the chlorine isotopes of 1.0027 were applied. These values are within the ranges reported in diffusion studies and support the hypothesis. The regression dates established by the diffusion model are also quite realistic: 4.1 ka BP at Koewarasan and 0.5 ka BP at Tourtonne.

Simulations and analyses indicate that diffusive salinization has penetrated to a maximum depth of 100 to 150 m (Figure 5.3). Below 125 m, concentrations of chloride increase gradually with depth (Figure 3.5, 3.8 and 5.4). These salts have risen upward from the Cretaceous sediments by diffusion and transversal dispersion, activated by deep regional flow systems during regressions. Clay seals above oil reservoir sands in Suriname, in the lower part of the Tertiary, obstructed transverse dispersion of meteoric groundwater flow. The anomalously low salinities above these clay seals and the steep salinity gradients in the clays (Figure 5.4) suggest that the salinity profiles may be used as proxies for the presence of clay seals, which may possibly act as stratigraphic traps for oil reservoirs.

Hydrogeochemical signals (Chapter 6)

The hydrochemistry of groundwater in the coastal plain of Suriname is mainly determined by the degree of diffusive mixing with salts or advective mixing with saline groundwater. Pristine meteoric groundwater in the Tertiary sediments (Cl^- content < 50 mg/l) is only found in the savannah belt and below the Lelydorp sands (Figure 3.5). Because of the low reactivity of the Tertiary formations, pristine groundwater basically has retained a rainwater composition, transformed mainly by evapotranspiration and uptake of carbon-dioxide in the soil zone (Figure 6.1). Consequently, most groundwater, also mixed types, is acid (pH < 6.5)

and under-saturated with respect to calcite. Oxidation of sediment organic mater (SOM) has raised the initial dissolved inorganic carbon content (TIC).

The Pleistocene clays in the southern part of the coastal plain, which remained outside the influence of the Holocene transgression, have very dilute pore waters and exchangeable cations, which are dominated by magnesium (Figure 6.8). This is an indication for cation exchange, since sodium was the dominant exchangeable cation at the time of deposition during the Sangamonian transgression. Simulations of vertical solute transport and cation exchange in these clays during 105 ka of the Wisconsinan regression showed that diffusive solute transport could not have driven out all sodium from the exchange sites (Figure 6.9). Only downward advective transport, related to a recharge of at least 5 mm/a, could have had this effect. This supports the conclusion from paleohydrological modeling (Chapter 4) that widespread recharge must have occurred during the Wisconsinan despite the hydraulic resistance of the clays. The high content of exchangeable magnesium is the result of the equilibration between exchange sites and very dilute infiltration water with relatively high magnesium content (rainwater signature).

Groundwater in the Pleistocene and Neogene sediments, which are influenced by salinization ($Cl^- > 50$ mg/l), is characterized by a sodium deficit balanced by calcium and magnesium excesses (Figure 6.10). This is clearly the result of cation exchange accompanying the diffusive salinization. Simulations of downward diffusive solute transport (salinization) and cation exchange from the saline Holocene reproduced the observed cation compositions (Figures 6.13 and 6.14). Cation exchange is taking place mainly in the Pleistocene clays, where cation exchange capacities are two orders of magnitude higher than in the Tertiary formations. In the Tertiary formations, mixing only occurs between the pre-existing groundwater (paleogroundwater) and downward diffusing salts. The Paleogene sediments at depths greater than -125 m contain groundwater with a sodium excess (Figure 6.11 and 6.12), which is a sign that the salts in these sediments have not been transported by diffusion from above, but that they probably originate from the deeper saline Cretaceous sediments. This supports the conclusion from chloride and chlorine-isotope modeling (Chapter 5).

Isotopic signals (Chapter 7)

High tritium contents indicate that groundwater in the Pliocene sands of the savannah belt is of recent age (after 1950) and circulates in systems with short residence times. Radiocarbon dating of groundwater - corrected for dead carbon dissolution (SOM) and temporal changes in atmospheric ^{14}C activity - shows that groundwater in the coastal plain is generally older than 1 ka BP (Figure 7.6). In the Pleistocene coastal plain, Late Holocene groundwater (1 to 5 ka BP) is found in the upper part of the Pliocene formation. Deeper groundwater dates from Early Holocene to Late Wisconsinan. The subhorizontal position of the isochrones suggests that paleorecharge was not confined to the present recharge areas of the savannah belt and the Lelydorp sands. The groundwater ages correspond well with the groundwater flow systems described in Chapter 3 and 4.

The $\delta^{13}C$ values of dissolved total inorganic carbon (TIC) in groundwater in the coastal plain fall in the range between -17 to -20 ‰. Simple mass-balance calculations, based on the hydrogeochemical processes described in Chapter 5, lead to the conclusion that $\delta^{13}C$ of dissolved carbon dioxide in infiltrating groundwater must have been relatively high (around −10 ‰) during Late Pleistocene and Early Holocene (Figure 7.2). This is attributed to a paleovegetation, consisting mainly of plants with a C4 photosynthetic pathway (mostly grasses and sedges), though C3 plants dominate the present natural vegetation in the coastal plain. The conc sion that grasses dominated the coastal plain during the LGM and Early Holocene is consist with the results of palynological studies. Relics of these old grass savannahs in the coastal plain have survived in the savannah belt. An inventory of all major plants species in the pres ent savannahs learned that almost all species, indeed, belong to the C4 group (Annex IV).

Monthly weighted averages of stable isotopes ($\delta^{18}O$ and $\delta^{2}H$) in rainfall in the nearb stations of Cayenne, French Guiana and Belem, Brazil are negatively correlated with mon ly rainfall (Figure 7.9). This relation is commonly known in the tropics as the "amount" effect. However, it seems to be an artifact in this case, as the relation largely disappears i analyses of daily rainfall at Belem (Figure 7.10). Isotopic variations are associated with s sonally changing weather systems and source regions of water vapor.

Average stable-isotope composition of Holocene groundwater in the coastal plain of Suriname is depleted with respect to the average composition of rainfall at Paramaribo (Figure 7.11). The depletion is attributed to groundwater recharge in wet months with rel vely low isotopic ratios. Groundwater of Pleistocene age is even more depleted with resp to Holocene groundwater and rainfall (Figure 7.11). The LGM was 5 °C colder than toda this region, but does not explain the isotopic depletion in paleoprecipitation. The spatial temporal relationship between stable isotopes of water and temperature, common at mid latitudes, is absent in the (sub)tropics according to many other studies. It is more likely t recharge then was restricted to the boreal summer monsoon (May to August) which had most depleted rains based on the present regime (Figures 7.9 and 7.11). Also palynologic studies and global climate modeling studies report that rainfall in this region was lower more seasonal at the end of the last glacial.

Part II. Generic investigations

Offshore meteoric groundwater (Chapter 8)

There are worldwide numerous accounts of fresh to moderately brackish submarin groundwater. These observations may be related to (i) large submarine springs often fou near coasts with karstic limestones, (ii) diffuse submarine discharge in clastic coasts (de ted by tracers) or (iii) offshore boreholes where pore-water analyses or resistivity loggi have been carried out (Figure 8.3).

Generally, the observations do not conclusively answer the question, whether offs meteoric groundwater belongs to an active topography-driven flow system with onshor recharge, or to paleogroundwater formed by extinct flow systems. Occurrence far offsh (> 50 km) may be a sign of paleogroundwater, whereas meteoric groundwater close to shore, especially observed as submarine discharge, is probably related to an active coas flow system.

The geological conditions of the coast and continental shelf in Suriname are by n means unique. This, in combination with the fact that other occurrences are found all o the world, strongly suggests that offshore meteoric groundwater is a very common phe menon that may well be rule rather than exception.

The offshore extension of meteoric groundwater (Chapter 9)

The question, whether offshore meteoric groundwater is part of an active topography-driven flow system or paleogroundwater, has been addressed with an analytical model. The Sharp Interface Model (SIM) determines the length of the offshore extension of fresh groundwater in a semi-confined aquifer with onshore recharge and submarine groundwater seepage. The New Approximate Model (NAM) uses the SIM model but takes into account the downward diffusive salt transport through the aquitard, which counteracts the upward seepage. The approximate offshore extension of fresh water is, according to the NAM model, equal to the distance offshore where the diffusive transition layer becomes large enough to create convective density currents in the aquifer (Figure 9.1). The coastal flow domain may extend somewhat beyond this point, but groundwater is brackish. The SIM model approximates the outer limit of this zone.

Sensitivity analyses with the NAM model demonstrated that fresh groundwater generally does not extend more than 5 km offshore, except when extreme values for model parameters are adopted. Sensitivity analyses with the SIM model indicated that the offshore extension of the brackish groundwater tongue will not exceed 50 km. Applying the characteristics of the coasts of Suriname and New Jersey to these models, learns that meteoric groundwater found offshore must be paleogroundwater.

Flow and salt transport in submarine groundwater (Chapter 10).

In coastal and offshore sediments, inverse groundwater density stratifications may arise, where (i) there is offshore outflow of fresh groundwater in steady state coastal flow systems or (ii) where fresh sediments become inundated by the sea during a transgression, which creates an unsteady-state situation. The dynamics of these situations have been studied in three numerical models, simulating variable density flow and solute transport by advection, dispersion and diffusion.

Model 1 served to investigate the offshore salinity patterns for the situation of steady-state offshore outflow. On the basis of model experiments three zones can be distinguished (Figure 10.3):

- a proximal stable zone of fresh groundwater, where high upward seepage rates prevent downward salinization by diffusion and convective density currents;
- an intermediate zone with moderately brackish to brackish groundwater, where convective density currents arise continuously; although groundwater is brackish, there is still a net seaward topography-driven flow of groundwater; in the landward part of the intermediate zone fresh groundwater can still be found at the bottom of the aquifer;
- a distal stable zone with brackish water, where density differences are too small to trigger convective density currents; here topography driven flow and upward seepage have become very small.

The length of the proximal stable zone corresponds with the length of the fresh groundwater tongue calculated by the New Approximate Model in Chapter 8.

The changing salinity patterns following a marine transgression have been investigated with two different models. Experiments with Model 2, simulating the effects of a sea, encroaching on a slightly inclined continental shelf, showed four different modes of salinization:

- Mode 1: "Horizontal" seawater intrusion in the form of the slow landward migration of the fresh/saline transition zone or "interface" (Figure 10.5). Referring to the recent Holocene transgression this intrusion mode was not the dominant process in most of the offshore aquifers. The transgression speeds during the Early Holocene for many continental margins were far higher (> 100 m/a) than the critical transgression speed at which the interface could keep pace.
- Mode 2: Vertical seawater intrusion by convective density currents (Figure 10.6). This mode occurs for supra-critical transgression rates and relatively high-permeability substrate sediments (sand/silt). A wide high-salinity transition zone develops. This rapid intrusion mode can keep up even with rapidly advancing shorelines.
- Mode 3: Vertical seawater intrusion by diffusion (Figure 10.7). This mode occurs for supra-critical transgression rates and low-permeability substrate sediments (silt/clay) up to great depth. An extensive seaward dipping fresh-water wedge develops below a thick, almost vertically layered, transition zone. Salinization is mainly controlled by downward diffusion. This intrusion mode is restricted to shelf sediments with very thick clayey sediments below the sea floor.
- Mode 4: Vertical seawater intrusion by convective density currents of low-salinity fingers (Figure 10.8). This mode occurs for supra-critical transgression rates and a layer of low-permeability sea-floor sediments (silt/clay) overlying a relatively high-permeability aquifer. A wide, low-salinity transition zone develops in the aquifer resulting from convective density currents, while a relatively sharp diffusive boundary layer is present in the overlying low-permeability layer.

The second intrusion mode explains the presence of high-salinity groundwater in the exposed sandy aquifers in the western part of the Netherlands, which was inundated during the Early Holocene. Modes 3 and 4 explain the temporary preservation of offshore meteoric groundwater. Although the dimensions of the model are small, the same process explains the presence of vast bodies of meteoric groundwater far offshore along the coast of Suriname, the Netherlands, Indonesia (Java Sea) and the eastern USA (Chapter 8).

Experiments with Model 3 simulated the transgression of the sea over a hilly terrain with a substrate of an aquifer covered by a clay layer. This terrain represents the dissected landscape of the exposed continental shelf off Suriname during the last glacial (Chapter 4). During the transgression the valleys become submersed and form estuaries. Salinization only starts when sea level in a valley has risen to certain level and fresh groundwater seepage in the valley has diminished (Figures 10.9 and 10.10). As soon as the entire landscape becomes submerged, the flow system reverses. The remaining fresh and moderately brackish groundwater is slowly expelled via seepage from the former hills or plateaus, either as diffuse seepage or seepage through a permeable zone (10.11).

The experiments with Model 2 and 3 show that meteoric submarine groundwater can be preserved as paleogroundwater for thousands of years after the submersion of the landscape. The waning of the paleogroundwaters is an ongoing process. Some observations of groundwater discharge far offshore may be related to this process.

Concluding remarks

The overall methodology of this study is a typical example of an associative approach, where data and methodologies from various earth sciences needed to be combined in order

to understand more about coastal and offshore groundwater. This associative approach is essential to the science of hydrology, as the characteristics of water are continuously changing, while it circulates through - and interacts with - all compartments of the atmosphere, lithosphere and biosphere.

During the last years, this study has triggered new ideas for research in related subjects. In this thesis, variable density flow and transport modelling focus on salinization processes. However, much still needs to be learned from modelling of freshening processes on geological time scales. Also salinization mechanisms in more complex layered sedimentary environments require further research both by field studies using chemical and isotopic tracers and modelling experiments.

As for the exploration of offshore meteoric groundwater, application of rapid geophysical surveying techniques, based on Transient Domain Electromagnetics (TDEM) and Shallow High Resolution Seismics (SHRS), is under investigation.

More insight into the submarine discharge of offshore meteoric groundwater may become relevant in understanding processes related to gas hydrates underneath the sea floor, marine ecology and thermo-haline circulation in the seas.

One of the reasons for choosing the coastal plain of Suriname as a case study was the occurrence of meteoric groundwater extending 90 km into the offshore sediments. The work in this thesis shows that this phenomenon can no longer be considered an oddity, but may be the rule rather rule than exception on a global scale. This offshore meteoric groundwater may become a valuable water-supply source for densely populated coastal areas, where water resources are being overexploited or polluted. Treatment of meteoric groundwater may involve desalination, but is still much cheaper than desalination of seawater. This idea is currently being marketed at the moment by a consortium of commercial companies and the Vrije Universiteit. One could argue that this resource is non-renewable and that its exploitation is unsustainable. But in m opinion this principle is not valid here, as these bodies of offshore paleogroundwater are so large, that they could sustain coastal populations for hundreds to thousands of years. In addition, these meteoric waters would gradually disappear anyway by natural salinization processes.

References

Airey, P. L., Calf, G. E., Campbell, B. L., Hartley, P. E., Roman, D. and Habermehl, M. A., 1979. Aspects of the isotope hydrology of the Great Artesian Basin, Australia. In: Isotope Hydrology 1978, IAEA/UNESCO, Vienna, 205-219.

Appelo, C. A. J. and Postma, D., 1993. Geochemistry, groundwater and pollution. Balkema, Rotterdam, 536 pp.

Appelo, C. A. J., 1994. Cation and proton exchange, pH variations, and carbonate reactions in a fre ning aquifer. Water Resources Research 30, 2793-2805.

Arad, A., 1983. A summary of the artesian coastal basin of Guyana. Journal of Hydrology 63, 299-

Augustinus, P. G. E. F., 1978. The changing shoreline of Surinam. Ph.D. thesis, Rijksuniversiteit Utrecht, 232 pp.

Augustinus, P. G. E. F., Hazelhoff, L. and Kroon, A., 1989. The chenier coast of Suriname moder and geological development. In P. G. E. F. Augustinus (Ed.), Cheniers and chenier plains Marine Geology 90, 269-281.

Badon Ghijben, W., 1888. Nota in verband met de voorgenomen putboring nabij Amsterdam. Tijdschrift Koninklijk Instituut voor Ingenieurs, Verh. 1888-1889, 8-22.

Bear, J. and Dagan, G., 1964. Some exact solutions of interface problems by means of the hydro method. Journal of Geophysical Research 69, 1563-1572.

Beekman, H.E., 1991. Ion chromatography of fresh- and seawater intrusion: multicomponent disp ve and diffusive transport in groundwater. Ph.D. thesis, Vrije Universiteit, Amsterdam, pp.

Berger, A.L. et al (Eds.) Milankovitch and Climate. Part 1., 269-305.

Berner, R. A., 1980. Early Diagenesis: A Theoretical Approach. Princeton University Press, 241 p

Bethke, C. M., Harrison, W. J., Upson, C. and Altaner, S. P., 1988. Supercomputer analysis of sec mentary basins. Science 239, 261-267.

Bierman, P. R., Albrecht, A., Bothner, M. H., Brown, E. T., Bullen, T. D., Gray, L. B. and Turpin 1998. Erosion, weathering, and sedimentation. In: C. Kendall and J. McDonnell (Eds) Isotope tracers in catchment hydrology. Elsevier, Amsterdam. 647-678.

Bosma, W., Kroonenberg, S. B., Maas, K. and De Roever, E. W. F., 1983. Igneous and metamor complexes of the Guiana Shield in Suriname. Geologie en Mijnbouw 62, 241-254.

Brinkman, R. and Pons, L. J., 1968. A pedomorphological classification and map of the Holocer ments in the coastal plain of the three Guianas. Netherlands Soil Survey Institute, Wageningen, The Netherlands. Soil Survey Papers No. 4, 40 pp.

Brinkmann, R., Eichler, R., Ehhalt, D. and Münnich, K. O., 1963. Über den Deuteriumgehalt vo Niederschlag- und Grundwasser. Naturwissenschaften 50, 611-612.

Brook, G.A., Folkoff, M.E. and Box, E.O., 1983. A world model of soil carbon dioxide. Earth S Processes 8. 79-88.

Brouwer, L. C., 1996. Nutrient cycling in pristine and logged rain forest. A study in Guyana. Ph thesis, University of Utrecht, 224 pp.

Bruijnzeel, L.A., 1990. Hydrology of moist tropical forests and effects of conversion: a state of ledge review. UNESCO/IAHS. Netherlands IHP Committee, 224 pp.

Burke, W.H., Denison, R.E., Hetherington, E.A., Koepnick, R.B., Nelson, N.F. and Otto., J.B., 1982. Variation of seawater $^{87}Sr/^{86}Sr$ throughout Phanerozoic time. Geology 10, 516-519.

Cable, J. E., Bugna, G. C., Burnett, W. C. and Chanton, J. P., 1996a. Application of ^{222}Rn and CH_4 for assessment of groundwater discharge to the coastal ocean. Limnology and Oceanography 4, 1347-1353.

Cable, J. E., Burnett, W. C., Chanton, J. P. and Weatherly, G. L., 1996b. Estimating groundwater discharge into northeastern Gulf of Mexico using radon-222. Earth and Planetary Science Letters 144, 591-604.

Cable, J. E., Burnett, W. C. and Chanton, J. P., 1997. Magnitude and variations of groundwater seepage along a Florida marine shoreline. Biogeochemistry 38, 189-205.

Carslaw, H.S. and Jaeger J.C., 1959. Conduction of heat in solids. Oxford University Press, London, 520 pp.

Cerling, T. E., 1984. The stable isotope composition of modern soil carbonate and its relationship to climate. Earth and Planetary Science Letters 71, 229-240.

Cerling, T. E., Solomon, D. K., Quade, J. and Bowman, J. R., 1991. On the isotopic composition of carbon in soil carbon dioxide. Geochimica et Cosmochimica Acta 55, 3403-3405.

Clapperton, C. M., 1993. Nature of environmental changes in South America at the last glacial maximum. Palaeogeography, Palaeoclimatology, Palaeoecology 101, 189-208.

Clark, I. D. and Fritz, P., 1997. Environmental isotopes in hydrogeology. Lewis Publishers, New York, 328 pp.

Clark, J. F., Stute, M., Schlosser, P. and Drenkard, S., 1997. A tracer study of the Floridan aquifer in southeastern Georgia: implications for groundwater flow and paleoclimate. Water Resources Research 33, 281-289.

Clark, J. F., Davisson, M. L., Hudson, G. B. and Macfarlane, P. A., 1998. Noble gases, stable isotopes, and radiocarbon as tracers of flow in the Dakota aquifer, Colorado and Kansas. Journal of Hydrology 211, 151-167.

Cohen, A. and Van der Eyk, J., 1953. Klassificatie en ontstaan van savannen in Suriname. Geologie en Mijnbouw 15, 202-214.

Cole, D. R. and Monger, H. C., 1994. Influence of atmospheric CO_2 on the decline of C4 plants during the last deglaciation. Nature 368, 533-536.

Cook, P. and Herczeg, A.L. (Eds.), 2000. Environmental Tracers in Subsurface Hydrology. Kluwer Academic Publishers, 529 pp.

Cooper, H. H., 1964. A hypothesis concerning the dynamic balance of fresh and salt water in a coastal aquifer. In: Sea water in coastal aquifers. US Geological Survey, Water Supply Paper 1613-C, 1-11.

Cronin, T. M., 1983. Rapid sea level and climate change: evidence from continental and island margins. Quaternary Science Reviews 1, 177-214.

Crutzen, P. J. and Andreae, M. O., 1990. Biomass Burning in the Tropics: Impact on Atmospheric Chemistry and Biogeochemical Cycles. Science 250, 1669-1678.

Custodio, E., 1987. Groundwater problems in coastal areas. Studies in hydrology Nr 45. IHP-UNESCO, 645 pp.

Dallwitz, M. J., 1980. A general system for coding taxonomic descriptions. Taxon 29, 41–46.

Dallwitz, M. J., Paine, T. A. and Zurcher, E. J., 1993 and onwards. User's Guide to the DELTA System: a General System for Processing Taxonomic Descriptions (4th ed.). CSIRO Division of Entomology, Canberra. http://biodiversity.uno.edu/delta/

Dansgaard, W., 1964. Stable isotopes in precipitation. Tellus 16, 436-468.

D'Audretsch, F. C., 1953. Recente Waterboringen in Suriname. Mededeling Geologische Mijnbouwkundige Dienst Suriname No 10, 1-12.

Davidson, E. A. and Trumbore, S. E., 1995. Gas diffusivity and production of CO_2 in deep soils of the eastern Amazon. Tellus 47B, 1-16.

Desaulniers, D. E., Cherry, J. A. and Fritz, P., 1981. Origin, age, and movement of pore waters in argillaceous Quaternary deposits at four sites in southwestern Ontario. Journal of Hydrology 50, 231-257.

Domenico, P.A. and Robbins G.A., 1985. The displacement of connate waters from aquifers. Geol. Soc. Amer. Bull. 96, 328-335

De Josselin de Jong, G. and Van Duijn, C. J., 1986. Transverse dispersion from an originally sharp fresh-salt interface caused by shear flow. Journal of Hydrology 84, 55-79.

De Vletter, D. R., Aleva, G. J. J. and Kroonenberg, S. B., 1998. Research into the Precambrium of Suriname. In: T. E. Wong, D. R. De Vletter, L. Krook, J. I. S. Zonneveld, and A. Van Loon J. (Eds.), The history of earth sciences in Suriname. Royal Netherlands Academy of Arts and Sciences Netherlands, Institute of Applied Geoscience TNO, 15-64.

De Vries, J.J., 1974. Groundwater flow systems and stream nets in the Netherlands. Ph.D. thesis, Vrije Universiteit, Amsterdam.

Diodato, D.M., 1997. Software spotlight. Groundwater 35, 922-923.

Dixon, V. R., 1971. Some aspects of the coastal artesian basin near Paramaribo. Mededeling Geologische Mijnbouwkundige Dienst Suriname 21, 167-175.

Dutton, A. R., 1995. Groundwater isotopic evidence for paleorecharge in U. S. High Plains aquifers. Quaternary Research 43, 221-231.

Edelman, J. H., 1972. Groundwater hydraulics of extensive aquifers. International Institute for Land Reclamation and Drainage Bulletin, Wageningen, 216 pp.

Edmunds, W.M. and Walton, N.R.G., 1983. The Lincolnshire limestone – Hydrogeochemical evolution over a ten-year period. Journal of Hydrology 61, 201-211.

Eggenkamp, H.G.M., 1994. The geochemistry of chlorine isotopes. Ph.D. thesis, Geologica Ultraiectina, Universiteit van Utrecht, Mededelingen van de Faculteit Aardwetenschappen, No 116, 150 pp.

Eggenkamp, H. G. M., Middelburg, J. J. and Kreulen, R., 1994. Preferential diffusion of ^{35}Cl relative to ^{37}Cl in sediments of Kau Bay, Halmahera, Indonesia. Chemical Geology 116, 317-325.

Ehleringer, J. R., Cerling, T. E. and Helliker, B. R., 1997. C4 photosynthesis, atmospheric CO_2, and climate. Oecologia 112, 285-299.

Eisma, D. and van der Marel, H. W., 1971. Marine muds along the Guyana coast and their origin from the Amazon basin. Contr. Mineralogy and Petrology 31, 321-334.

Elder, J.W., 1968. The unstable thermal interface. Journal of Fluid Mechanics, 32, 69-96.

Engelen, G. B. and Kloosterman, F. H., 1996. Hydrological systems analysis. Kluwer, Dordrecht, 152 pp.

Essaid, H. I., 1986. A comparison of the coupled fresh water-salt water flow and the Ghijben-Herzberg sharp interface approaches to modeling of transient behavior in coastal aquifer systems. Journal of Hydrology 86, 169-193.

Essaid, H. I., 1990. A multilayered sharp interface model of coupled freshwater and saltwater flow in coastal systems: model development and application. Water Resources Research 26, 1431-1454.

Fairbanks, R. G., 1989. A 17,000-year glacio-eustatic sea level record: influence of glacial melting rates on the Younger Dryas event and deep-ocean circulation. Nature 342, 637-642.

Faure, G., 1986. Stable Isotope Geology (2nd ed.). Springer Verlag, Berlin, 589 pp.

Forti, M. C. and Neal, C., 1992. Hydrochemical cycles in tropical rainforests: an overview with

emphasis on Central America. Journal of Hydrology 134, 103-115.
Frappa, M. and Pujos, M., 1994. Late Quaternary evolution of the French Guiana continental shelf: Evidence from 3.5 kHz data. Marine Geology, 121, 231-245.
Geirnaert, W., 1969. Preliminary report on hydrochemical investigations in the Western Netherlands. Geologie en Mijnbouw 48, 249-254.
Geyh, M. A. and Söfner, B., 1989. Groundwater analysis of environmental carbon and other isotopes from the Jakarta basin aquifer, Indonesia. Radiocarbon 31, 919-925.
Gibbs R.J., 1967. The Geochemistry of the Amazon river system. Part I. The factors that control the salinity and the composition and the concentration of the suspended solids. Geol. Soc. Am. Bull. 78, 1203-1232.
Gieske, J. M. J., 1991. De oorsprong van het brakke grondwater in het IJsselmeergebied: diffusie, dispersie of dichtheidsstroming. H_2O 24, 188-193.
Glover, R.E., 1959. The pattern of freshwater flow in a coastal aquifer. Journal of Geophysical Research 64, 439-475.
Grathwohl, P., 1998. Diffusion in natural porous media: contaminant transport, sorption/desorption and dissolution kinetics. Kluwer, Dordrecht, 224 pp.
Grimaldi, C., 1988. Origine de la composition chimique des eaux superficielles en milieu tropical humide: exemple de deux petits bassins versants sous foret en Guyane Francaise. Sci. Geol. Bull. 41, 247-262.
Groen, J., 1998. Hydrogeological investigations in Suriname. In T. E. Wong, D. R. De Vletter, L. Krook, J. I. S. Zonneveld, and A. J. Van Loon (Eds.). The history of earth sciences in Suriname. Royal Netherlands Academy of Arts and Sciences, Netherlands Institute of Applied Geoscience TNO, 129-174.
Groen, J., Velstra, J. and Meesters, A.G.C.A., 2000a. Salinization processes in paleowaters in coastal sediments of Suriname: evidence from $d^{37}Cl$ analysis and diffusion modeling. Journal of Hydrology 234, 1-20.
Groen, J., Post, V. E. A., Kooi, H. and Hemker, C.J., 2000b. Palaeohydrogeology of the sedimentary plain of Suriname. In: Proceedings TraM'2000 Conference on Tracers and Modelling in Hydrogeology, Liege Belgium. IAHS Publication No 262, 417- 424.
Guglielmi, Y. and Prieur, L., 1997. Locating and estimating submarine freshwater discharge from an interstitial confined coastal aquifer by measurements at sea: example from the lower Var valley, France. Journal of Hydrology 190, 111-122.
Hanou, M. J., 1981. Geologie and petroleum analysis of the Suriname coastal region. Staatsolie Maatschappij Suriname N.V, Paramaribo, Suriname.
Harrington, P. K., 1985. Formation of pockmarks by pore-water escape. Marine Letters 5, 193-197.
Harrison, W. J. and Summa, L. L., 1991. Paleohydrology of the Gulf of Mexico Basin. America Journal of Science 291, 109-176.
Hartman, P., 1969. The clay minerals from the boring Alliance-28. Surinam. Geologie en Mijnbouw 48, 121-124.
Hathaway, J.C., Poag, C.W. Valentine, P.C., Miller, R.E., Schultz, D.M., Manheim, F.T., Kohout, F.A., Bothner M.H. and Sangrey, D.A., 1979. U.S. Geological Survey. Core drilling on the Atlantic shelf. Science 206, 515-527.
Heaton, T. H. E., Talma, A. S. and Vogel, J. C., 1986. Dissolved gas paleotemperatures and $d^{18}O$ variations derived from groundwater near Uitenhage, South Africa. Quaternary Research 25, 79-88.
Henry, H. R., 1964. Effects of dispersion on salt encroachment in coastal aquifers. In: Sea water in coastal aquifers. US Geological Survey, Water-Supply Paper 1613-C, 70-84.
Herzberg, B., 1901. Die Waserverzorgung einiger Noordseebader. Zeitschrift Gasbeleuchtung und Wasserverzorgung 44, 815-819 and 842-844.
Heyligers, P.C., 1963. Vegetation and soil of a white-sand savanne in Suriname. The Vegetation of Suriname III. Ph.D. thesis. Verhandelingen Koninklijke Nederlandse Akademie van Wetenschappen, Serie 2, deel 54, 148 pp.
Ho Len Fat, A. G., 1986. Water influence on heavy crude oil production. A qualitative assessment. I O/86/3). Staatsolie Maatschappij Suriname N.V.
Hua Aibing, 1998. The impact of historical sea level changes to groundwater in Shangbai, China. Geological Review 44, 220-224 (Chinese).
Hubbert, M. K., 1940. The theory of ground-water motion. Journal of Geology 48, Part I., 785-94
Hutchinson, C. B., 1990. Analysis of groundwater flow in the A-sand aquifer at Paramaribo, Surina South-America. U.S. Geological Survey, Water-Resources Investigation Report 90-4036, pp.
Huyacorn, P.S., Anderson, P.F., Mercer, J.W. and White Jr., H.O., 1987. Saltwater intrusion in aquif development and testing of a three-dimensional finite element model. Water Resources Research 23, 293-312.
IAEA, 1981. Stable isotope hydrology: deuterium and oxygen-18 in the water cycle. Technical rep series no 210. International Atomic Energy Agency, Vienna, 337 pp.
IAEA, 1983. Paleoclimates and paleowaters: a collection of environmental isotope studies. Panel ceedings series. International Atomic Energy Agency, Vienna, 207 pp.
Imbrie, J., Hays, J. D., Martinson, D.G., McIntyre, A., Mix., A.C., Morley, J.J., Pisias, N.G., Prell, W.L. and Shackleton, N.J., 1984. The orbital theory of Pleistocene climate: support for a revised chronology of the marine oxygen isotope record. In:
IWACO, 1983. Winplaatsonderzoek en uitbreiding van het drinkwatervoorzieningsysteem van Paramaribo. Surinaamsche Waterleiding Maatschappij, Paramaribo.
IWACO, 1987. Projet hydraulique villageoise Volta-Noire, Programme des forages. Rapport final travaux de forages. Ministere de leau, Office national des puits et forages, Burkina Faso.
IWACO/E.R. Harris, 1991. Expansion of the water supply system of the city of Paramaribo and it' metropolitan area, final report. Surinaamsche Waterleiding Maatschappij, Paramaribo.
Jansma, R., 1994. Ecology of some Northern Suriname savannas. Koeltz, Koenigstein, 199 pp.
Johnson, D. W., 1939b. Origin of submarine canyons. Journal of Geomorphology II, 213-236.
Johnson, D. W., 1939a. Origin of submarine canyons. Journal of Geomorphology II, 133-158.
Johnson, T. M. and Depaolo, D. J., 1996. Reaction-transport models for radiocarbon in groundwat the effects of longitudinal dispersion and the use of Sr-isotope ratios to correct for wate interaction. Water Resources Research 32, 2203-2212.
Jouzel, J., Koster, R. D., Suozzo, R. J. and Russell, G. L., 1994. Stable water isotope behavior du the last glacial maximum: A general circulation model analysis. Journal of Geophysical Research 99(D12), 25791-25801.
Jouzel, J., Frochlich, K. and Schotterer, U., 1997. Deuterium and oxygen-18 in present day precip tion: data and modelling. Hydrological Sciences Journal 42, 747-763.
Kendall C. and McDonnell J. J. (Eds.), 1998. Isotope tracers in catchment hydrology. Elsevier, Amsterdam, 839 pp.
Kimmelman, A. A., Da Cunha Reboucas, S. A. and Freitas Santiago, M. M., 1989. ^{14}C analyses o groundwater from the Botucatu aquifer system in Brazil. In: A. Long, R. S. Kra and D. (Eds). Proceedings of the 13th international radiocarbon conference. Radiocarbon 31, 9 935.
Kohout, F. A., 1964. The flow of fresh water and salt water in the Biscayne aquifer of the Miami

Florida. In: Sea water in coastal aquifers. US Geological Survey, Washington, 12-32.

Kohout, F. A., 1966. Submarine springs: a neglected phenomenon of coastal hydrology. In: Proceedings Hydrology and Water Resources Development Symposium, Ankara, 391-413.

Kohout, F. A., Hathaway, J. C., Folger, D. W., Bothner, M. H., Walker, E. H., Delaney, D. F., Frimpter, M. H., Weed, E. G. A. and Rhodehamel, E. C., 1977. Fresh groundwater stored in aquifers under the continental shelf: implications from a deep test, Nantucket Island, Massachusetts. Water Resources Bulletin 13, 373-386.

Kohout, F. A., Meisler, H., Meyer, F. W., Johnston, R. H., Leve, G. W. and Wait, R. L., 1988 Hydrogeology of the Atlantic continental margin. In: R. E. Sheridan and J. A. Grow (Eds.), The Atlantic continental margin, Geological Society of America, 463-480.

Kolditz, O., Ratke, R., Diersch, H.-J. G. and Zielke, W., 1998. Coupled groundwater flow and transport: 1. Verification of variable density flow and transport models. Advances in Water Resources 21, 27-46.

Kooi, H., 1999. Competition between topography- and compaction-driven flow in a confined aquifer: some analytical results. Hydrogeology Journal 7, 245-250.

Kooi, H., Groen, J. and Leijnse, A., 2000. Modes of seawater intrusion during transgressions. Water Resources Research 36, 3581-3589.

Kooi, H. and Groen, J., 2001. Offshore continuation of coastal groundwater systems: predictions using sharp-interface approximations and variable-density flow modelling. Journal of Hydrology 246, 19-35.

Krook, L., 1979. Sediment petrographical studies in northern Suriname. Ph.D. thesis, Vrije Universiteit Amsterdam. Also published in Krook, L., 1984. Mededeling Geologische en Mijnbouwkundige Dienst Suriname No 28, 143 pp.

Krook, L., 1994. De geologische en geomorfologische ontwikkeling van Noord Suriname. In: L.J. Van der Steen (Ed), Recente geologische en mijnhouwkundige ontwikkelingen in Suriname. Publication Found. Sci. Res. Carribean Region, Amsterdam, 23-40.

Kutzbach, J., Gallimore, R., Harrison, S., Behling, P., Selin, R. and Laarif, F., 1998. Climate and biome simulations for the past 21000 years. Quaternary Science Reviews 17, 473-506.

Laeyendecker-Roosenburg, D.M., 1966. A palynological investigation of some archaeologically interesting sections in northwest Surinam. Leidse Geologische Mededelingen 38, 31-36.

Lee, D.R., 1977. A device for measuring seepage flux in lakes and estuaries. Limnology and Oceanography 22, 155-163.

Leijnse, A., 1992. Three-dimensional modeling of coupled flow and transport in porous media. Ph.D. thesis, Notre Dame University, Indiana, 251 pp.

Leijnse, A., and Hassanisadeh, S.M., 1989a. Verification of the METROPOL code for density dependent flow in porous media. Hydrocoin project level 2 case 2, RIVM Report 728528002, Bilthoven, The Netherlands.

Leijnse, A., and Hassanisadeh, S.M., 1989b. Verification of the METROPOL code for density dependent flow in porous media, Hydrocoin project level 1 case 5 and level 3 case 4, RIVM Report 728528004, Bilthoven.

Leijnse, A. and Oostrom, M., 1994. The onset of instabilities in the numerical simulation of density-driven flow in porous media. In: A. Peters et al.(Eds), Computational methods in water resources X, 1011-1018.

Lerman, A., 1979. Geochemical processes. Wiley, New York, 480 pp.

Levelt, T.W.M. and Quakernaat, J., 1968. Some results of profile drilling along the railroad between Onverwacht and Zanderij, Surinam. Geologie en Mijnbouw 47, 340-345.

Li, Y.H. and Gregory, S., 1974. Diffusion of ions in seawater and in deep-sea sediments. Geochimica et Cosmochimica Acta 38, 703-714.

Lindeman, J. C. and Moolenaar, S. P., 1959. The vegetation of Suriname. In: I.A. de Halster and J. Lanjouw (Eds), A series of papers on plant communities and their origin, distribution and relation to climate and habitat, Volume I, Part 2, Van Eedenfonds, 's Lands Bosbeheer, Suriname, 45 pp.

Linsley, B. K., 1996. Oxygen isotope record of sea level and climate variations in the Sulu Sea over the past 150,000 years. Nature 380, 234-237.

Love, A. J., Herczeg, A. L., Leaney, F. W., Stadter, M. F., Dighton, J. C. and Armstrong, D., 1994. Groundwater residence time and palaeohydrology in the Otway Basin, South Australia: ^{2}H, ^{18}O and ^{14}C data. Journal of Hydrology 153, 157-187.

Luszczynski, N. S. and Swarzenski, W. V., 1966. Salt water encroachment in southern Nassau and southeastern Queens counties, Long Island, New York. U.S. Geological Survey, Water Supply Paper 1613-F.

Maathuis, H., Yong, R. N., Adi, S. and Prawiradisastra, S., 1996. Development of groundwater management strategies in the coastal region of Jakarta, Indonesia. Final report No. SRC Publ. R-1250-1-E-96). International Development Research Centre (IDRC), Environment and Natural Resources Division Ottawa, Canada, 61 pp.

Manheim, F. T. and Horn, M. K., 1968. Composition of deeper subsurface waters along the Atlantic continental margin, Southeastern Geology 9, 215-236.

Manheim, F. T. and Pauli, C. K., 1981. Patterns of groundwater salinity changes in a deep continental-oceanic transect off the southeastern Atlantic coast of the U.S.A. Journal of Hydrology 54, 95-105.

Manheim, F. T., 1967. Evidence for submarine discharge of water on the Atlantic Continental slope of the southern United States, and suggestions for further research. Transactions of the New York Academy of Science, Series II 29, 839-854.

Markgraf, V., 1989. Palaeoclimates in Central and South America since 18,000 yr BP based on pollen and lake level records. Quaternary Science Reviews 8, 1-24.

Markgraf, V., 1993. Climatic history of Central and South America since 18,000 yr B.P.: Comparison of pollen records and model simulations. In: H. E. Wright (Ed.), Global climates since the last glacial maximum, University of Minnesota Press, 357-385.

Martinelli, L. A., Pessenda, L. C. R., Espinoza, E., Camargo, P. B., Telles, E. C., Victoria, R. L., Aravena, R., Richey, J. and Trumbore, S., 1996. Carbon-13 variation with depth in soils of Brazil and climate change during the Quaternary. Oecologia 106, 376-381.

Matsui, E., Salati, E., Ribeiro, M. N. G., Reis, C. M., Tancredi, A. C. S. N. and Gat, J. R., 1983. Precipitation in the central Amazon basin: the isotopic composition of rain and atmospheric moisture at Belem and Manaus. Acta Amazonica 13, 307-369.

McKnight, D. M., Thurman, E. M., Wershaw, R. L. and Hemond, H., 1985. Biogeochemistry of aquatic humic substances in Thoreau's bog, Concord, Massachusetts. Ecology 66, 1339-1352.

Meinardi, C. R., 1991. The origin of brackish groundwater in the lower parts of the Netherlands. In: De Breuck W. (Ed.), Hydrogeology of salt water intrusion: a selection of SWIM papers, International Association of Hydrogeologists, Heise, Hannover, 271-289.

Meisler, H., Leahy, P. P. and Knobel, L. L., 1984. Effect of eustatic sea-level changes on saltwater-freshwater relations in the northern Atlantic coastal plain. U.S. Geological Survey, Water Supply Paper 2255.

Mente, A., 1990a. Mission report on hydrogeological field investigation at Rijsdijk - Suriname. Surinaamsche Waterleiding Maatschappij, Organization of American States.

Mente, A., 1990b. Mission report on hydrogeological investigation for water supply expansion at

Meerzorg area - Suriname. Government of Suriname, Organization of American States.

Merlivat, L. and Jouzel, J., 1983. Deuterium and _^{18}O in precipitation: a global model from oceans to ice caps. In: Palaeoclimates and palaeowaters: a collection of environmental isotope studies. Internation Atomic Energy Agency. Vienna, Austria. 65-66.

Mook, W.G. (Ed), 2000a. Environmental isotopes in the hydrological cycle. Principles and applications. International Hydrology Programme, UNESCO/IAEA. Technical Documents in Hydrology No 39. 280 pp.

Mook, W.G., 2000b. Introduction: theory, methods, review (Volume I). In: W.G. Mook (Ed). Environmental isotopes in the hydrological cycle. Principles and applications. International Hydrology Programme, UNESCO/IAEA. Technical Documents in Hydrology No 39. 280 pp.

Moore, W. S., 1996. Large groundwater inputs to coastal waters revealed by 226-Ra enrichments. Nature 380, 612-614.

Mualem, Y. and Bear, J., 1974. The shape of the interface in steady flow in a stratified aquifer. Water Resources Research 10, 1207-1215.

Negrel, P., Lachassagne, P. and Laporte, P., 1997. Caracterisation chimique et isotopique des pluies de Cayenne (Guyane francaise). Academie des Sciences 324(serie IIa), 379-386.

Noorthoorn van der Kruijff, J. F., 1970. Suriname onshore exploration 1968/1969. Petroleum engineering and geology. Internal report Shell Suriname Exploratie- and Productiemaatschappij. 37 pp.

Nota, D. J. G., 1958. Sediments of the western Guiana shelf. Reports on the Orinoco shelf expedition. Volume II. Mededelingen van de Landbouwhogeschool te Wageningen 58, 1-98.

Nota, D. J. G., 1969. Geomorphology and sediments of western Surinam shelf: a preliminary note. Geologie en Mijnbouw 48, 185-188.

Nota, D. J. G., 1971. Morphology and sediments off the Marowijne River, eastern Surinam shelf. In: Scientific investigations on the shelf of Surinam. H.M. M. S. Luymes, 1969. Royal Netherlands Navy. Hydrogaphic Newsletter, Spec. Publ. No. 6, 31-36.

Ogata, A. and Banks, R.B., 1961. A solution of the differential equation of longitudinal dispersion in porous media. U.S.Geological Survey Professional Paper 411-A.

O'Leary, M. H., 1988. Carbon isotopes in photosynthesis. Bioscience 38, 328-335.

Oostrom, M., Leijnse, A. and Roberson, K.R., 1994. Simulation of two- and three-dimensional dense solute plume behavior with the METROPOL-3 code. In: A. Peters et al. (Eds), Computational methods in water resources X. Kluwer Academic Publ., Netherlands, 975-982.

Oude Essink, G.H.P., 1996. Impact of sea level rise on groundwater flow regimes: a sensitivity analysis for the Netherlands. Ph.D. thesis. Technische Universiteit Delft. 428 pp.

Parkhurst, D. L. and Appelo, C. A. J., 1999. User's guide to PHREEQC (version 2) - a computer program for speciation, batch reaction, one-dimensional transport and inverse geochemical calculations. Water-Resources Investigations Report 99-4259. US Geological Survey.

Paschke, N. W. and Hoopes, J. A., 1984. Buoyant contaminant plumes in groundwater. Water Resources Research, 20 1183-1192.

Piekarek-Jankowska, H., 1996. Hydrochemical effects of submarine groundwater discharge to the Puck Bay (Southern Baltic Sea, Poland). Geographia Polonica 67, 103-119.

Planning and Research Corporation, 1988. Feasibility study and preliminary design for the improvements and expansion of the potable water supply for Paramaribo and its metropolitan area. Surinaamsche Waterleiding Maatschappij, Paramaribo.

Plummer, L. N., 1993. Stable isotope enrichment in paleowaters of the southeast Atlantic Coastal Plain, United States. Science 262, 2016-2020.

Poels, R. L. H., 1987. Soils, water and nutrients in a forest ecosystem in Suriname. Ph.D. thesis. Agricultural University Wageningen. 253 pp.

Post, V. E. A., 1996. Modelling of the paleohydrological situation in the coastal plain of Surinam. M.Sc. thesis, Vrije Universiteit Amsterdam. 35 pp.

Post, V.E.A., Hooijhoer, A.E.J., Groen, J., Gieske, J.M.J. and Kooi, H., 2000. Pore water chemistry c clay layers in the southern North Sea: clues to the hydrogeological evolution of coastal are Proceedings 16th SWIM Conference, Miedzydroje-Wollin Island, 127-132.

Priem, H. N. A., De Roever, E.W.F. and Bosma, W., 1980. A note on the age of the Paramaka metav canics in northeastern Suriname. Geologie en Mijnbouw 59, 171-173.

Prospero, J. M., Glaccum, R. A. and Nees, R. T., 1981. Atmospheric transport of soil dust from Afri to South America. Nature 289, 570-572.

Ramsahoye, L. E., 1959. The groundwater potential of the coastal areas of British Guiana. In: Fifth Inter-Guiana Geological Conference, Georgetown. Geological Survey Department, British Gniana, 303-309.

Ramsahoye, L. E., 1959. The groundwater potential of the coastal areas of British Guiana. Proceedi Fifth Inter-Guiana Geological Conference, Georgetown, Geological Survey Department, British Guiana, 303-309.

Ranganathan, V. and Hanor, J. S., 1987. A numerical model for the formation of saline waters due t diffusion of dissolved NaCl in subsiding sedimentary basins with evaporites. Journal of Hydrology 92, 97-120.

Reilly, T. E. and Goodman, A. S., 1985. Quantitative analysis of saltwater-freshwater relationships groundwater systems - a historical perspective. Journal of Hydrology 80, 125-160.

Remenda, V. H., Van der Kamp, G. and Cherry, J. A., 1996. Use of vertical profiles of d^{18}O to con strain estimates of hydraulic conductivity in a thick, unfractured aquitard. Water Resourc Research 32, 2979-2987.

Robb, J. M., 1990. Groundwater processes in the submarine environment. In C. G. Higgins and D. Coates (Eds.), Groundwater geomorphology: The role of subsurface water in earth-surfa processes and landforms. Geological Society of America, Boulder, Colorado, 267-281.

Robinson, R.A. and Stokes, R.H., 1965. Electrolyte solutions. Butterworth, London.

Roeleveld, W. and Van Loon, A. J., 1979. The Holocene development of the young coastal plain c Suriname. Geologie en Mijnbouw 58, 21-28.

Rona, P. A., 1969. Middle Atlantic continental slope of United States: deposition and erosion. AA Bulletin 53, 1453-1465.

Rozanski, K., Araguas-Araguas, L. and Gonfiantini, R., 1992. Relation between long-term trends oxygen-18 isotope composition of precipitation and climate. Science 258, 981-985.

Rozanski, K., Araguas-Araguas, L. and Gonfiantini, R., 1993. Isotopic patterns in modern global pitation. In: P. K. Swart, K. C. Lohmann, J. McKenzie and S. Savin (Eds.), Climate cha in continental isotopic records. American Geophysical Union, 1-36.

Rozanski, K., Johnsen, S. J., Schotterer, U. and Thompson, L. G., 1998. Reconstruction of past e tes from stable isotope records of palaeo-precipitation preserved in continental archive Hydrological Sciences Journal 42, 725-744.

Salati, E., Dall'Olio, A., Matsui, E. and Gat, J. R., 1979. Recycling of Water in the Amazon Basi Isotopic Study. Water Resources Research 15, 1250-1258.

Sanford, W. E., 1997. Correcting for diffusion in carbon-14 dating of ground water. Ground Wat 357-361.

Sanford, W. E. and Buapeng, S., 1996. Assessment of a groundwater flow model of the Bangkol basin, Thailand, using carbon-14-based ages and paleohydrology. Hydrogeology journ

26-40.

Sauter, F.J., Leijnse, A. and Beusen, A.H.W., 1993. Metropol's user's guide. National Institute of Public Health and Environmental Protection. RIVM, Bilthoven.

Schincariol, R. A. and Schwartz, F. W., 1990. An experimental investigation of variable density flow and mixing in homogeneous and heterogeneous media. Water Resources Research 26, 2317-2329.

Shackleton, N. J., 1987. Oxygen isotopes, ice volume and sea level. Quaternary Science Reviews 6, 183-190.

Shaw, T. J., Moore, W. S., Kloepfer, J. and Sochaski, M. A., 1998. The flux of barium to the coastal waters of the southeastern USA: The importance of submarine groundwater discharge. Geochimica et Cosmochimica Acta 62, 3047-3054.

Simmons, C.T., Narayan, K.A. and Wooding, R.A., 1999. On a test case for density-dependent groundwater flow and solute transport models: The salt lake problem. Water Resources Research 35, 3607-3620.

Simmons, G.M.J., 1992. Importance of submarine groundwater discharge (SGWD) and sweater cycling to material flux across sediment / water interfaces in marine environments. Marine Ecology Progress Series 84, 173-184.

Souza, W.R. and Voss, C.I., 1987. Analysis of an anisotropic coastal aquifer system using variable-density flow and solute transport simulation. Journal of Hydrology 92, 17-41.

Stigter, T. Y., 1996. Analysing the hydrochemistry of groundwater in Surinam. M.Sc. thesis. Vrije Universiteit, Amsterdam, 43 pp.

Stringfield, V.T., 1966. Artesian water in Tertiary limestone in the Southeastern States. U. S. Geological Survey Professional Paper, 226 pp.

Stringfield, V. T. and LeGrand, H. E., 1969. Relation of sea water to fresh water in carbonate rocks in coastal areas with special reference to Florida, USA and Cephalonia (Kephallinia), Greece. Journal of Hydrology 9, 387-404.

Stringfield, V. T. and LeGrand, H. E., 1971. Effects of karst features of circulation of water in carbonate rocks in coastal areas. Journal of Hydrology 14, 139-157.

Stuiver, M., Reimer, P.J., Bard, E., Beck, J.W., Burr, G.S., Hughen, K.A., Kromer, B., McCormac, G., Van der Plicht, J. and Spurk, M., 1998. INTCAL98 Radiocarbon age calibration, 24000 – 0 cal BP. Radiocarbon 40, 1041-1083.

Stute, M. and Bonani, G., 1995. A 30000 yr continental paleotemperature record derived from noble gas dissolved in groundwater from the San Juan Basin, New Mexico. Quaternary Research. 43, 209-220.

Stute, M. and Talma, A. S., 1998. Glacial temperatures and moisture transport regimes reconstructed from noble gases and O-18, Stampriet aquifer, Namibia. In: Isotope techniques in the study of environmental change, IAEA, Vienna, 307-318.

Stute, M., Schlosser, P., Clark, J. F. and Broecker, W.S., 1992. Paleotemperatures in the southwestern United States derived from noble gas measurements in groundwater. Science 256, 1000-1003.

Stute, M., Forster, M., Frischkorn, H., Serejo, A., Clark, J. F., Schlosser, P., Broecker, W. S., and Bonani, G., 1995. Cooling of Tropical Brazil (5°C) during the Last Glacial Maximum. Science, 269, 379-383.

Stuyfzand, P.J., 1993. Hydrochemistry and hydrology of the coastal dune area of the western Netherlands. Ph.D. thesis, Vrije Universiteit Amsterdam.

Terracon Anguilla Ltd., 1994. Hydrogeology and dewatering study for Lelydorp III. Final report, Client N.V. Billiton Mining Company Suriname.

Teunissen, P.A. 1978. Reconnaissance map of Surinam Lowland Ecosystems. 1:200.000. STINASU. Paramaribo, Suriname.

Thomas, M. F. and Thorp, M. B., 1996. The response of geomorphic systems to climatic and hydrological change during the Late Glacial and early Holocene in the humid and sub-humid tropics. In: J. E. A. Branson (Ed.), Global changes: the context of palaeohydrology, Geological Society Publication. 139-153.

Toth, J., 1963. A theoretical analysis of groundwater flow in small drainage basins. Journal of Geophysical Research 68, 4795-4812.

Toth, J., 1995. Hydraulic continuity in large sedimentary basins. Hydrogeology Journal 3, 4-16.

Tricart, T., 1985. Evidence of Upper Pleistocene dry climates in northern South America. In: I. Douglas and T. Spencer (Eds), Environmental change and tropical geomorphology. Allen and Unwin, London. 197-217.

UNDP/WHO, 1972. Public water supplies and sewerage project, Volume III: Water Resources (Hydrogeological and Hydrological Studies). United Nations Development Programme and World Health Organization. 128 pp.

Valentin, H., 1954. Die Kusten der Erde : Beitrage zur allgemeinen und regionalen Kustenmorphologie. Erganzungsheft zu Petermanns Geographischen Mitteilungen, Nr. 246, Gotha, Haack.

Van der Eyk, J. J., 1954. De landschappen van Suriname. Centraal Bureau Luchtfotokartering Paramaribo, Suriname. Publicatie no 15, 22 pp.

Van der Eyk, J. J., 1957. Reconnaissance soil survey in Northern Surinam. Ph.D. thesis, Landbouwhogeschool te Wageningen. 99 pp.

Van der Hammen, T., 1963. A palynological study on the Quaternary of British Guiana. Leidse Geologische Mededelingen No 29, 125-180.

Van der Hammen, T., 1974. The Pleistocene changes of vegetation and climate in tropical South America. Journal of Biogeography 1, 3-26.

Van der Hammen, T. and Absy, M. L., 1994. Amazonia during the last glacial. Palaeogeography, Palaeoclimatology, Palaeoecology 109, 247-261.

Van der Molen, W. H., 1958. Over de zouthuishouding in de Noordoostpolder, Tjeenk Willink, Zwolle, 70 pp.

Van der Molen, W. H., 1989. Het zoute grondwater in West Nederland; een gevolg van dichtheidsstromingen ? H2O, 22, 330 –331 and 346.

Van der Straaten, C. M. and Mook, W. G., 1983. Stable isotopic composition of precipitation and climatic variability. In: Palaeoclimates and palaeowaters; a collection of environmental isotope studies. Internation Atomic Energy Agency, Vienna, 53-64.

Van Donselaar, J., 1965. An ecological and phytogeographic study of northern Surinam savannas. The Vegetation of Suriname IV. Mededelingen Bot. Mus. Herb. Utrecht, Wentia 14, 163 pp.

Van Vliet, K., 1998. Isotopic survey of the Tertiary and Quaternary aquifers of the coastal plain of Surinam. M.Sc. thesis, Vrije Universiteit Amsterdam, 90 pp.

Van Voorthuyzen, J. H., 1969. Introduction and summary of the stratigraphical and sedimentological results of boring Alliance-28 in the coastal plain of Surinam (Dutch Guiana). Geologie en Mijnbouw 48, 111-116.

Veen, A. W. L., 1970. On geogenesis and pedogenesis in the Old Coastal Plain of Surinam (South America). Ph.D. thesis, Universiteit van Amsterdam, 176 pp.

Velstra, J., 1996. The salinity distribution and hydrogeology in the coastal plain of Surinam. M.Sc. thesis, Vrije Universiteit Amsterdam, 59 pp.

Velstra, J., 1997. Study and modeling of the pore water chemistry in the Quaternary clays of Surinam.

M.Sc. thesis, Vrije Universiteit Amsterdam, 53 pp.

Verleur, H., 1991. Hydrogeological survey of the coastal plain of Surinam. M.Sc. thesis, Vrije Universiteit Amsterdam, 69 pp.

Verruijt, A., 1971. Steady dispersion across an interface in a porous medium. Journal of Hydrology 14, 337-347.

Vogel, J.C., 1993. Variability of carbon isotope fractionation during photosynthesis. In: J.R. Ehleringer, A.E. Hall and G.D. Farquhar (Eds), Stable isotopes and plant carbon - water relations. Academic Press, San Diego, 29-38.

Vogel, J. C. and Van Urk, H., 1975. Isotopic composition of groundwater in semi-arid regions of Southern Africa. Journal of Hydrology 25, 23-36.

Volker, A. and Van der Molen, W.H., 1991. The influence of groundwater on diffusion processes in a lake bottom: an old report reviewed. Journal of Hydrology 126, 159-169.

Vonhof, H. B., Wesselingh, F. P. and Ganssen, G. M., 1998. Reconstruction of the Miocene Western Amazonian aquatic system using molluscan isotopic signatures. Paleogeography, Paleoclimatology and Paleoecology 141, 85-93.

Voss, C.I., and Souza, W.R., 1987. Variable density flow and solute transport simulation of regional aquifers containing a narrow freshwater-saltwater transition zone. Water Resources Research 23, 1851-1866.

Walraevens, K., 1990. Natural-isotope research on groundwater from the semi-confined Ledo-Paniselian aquifer in Belgium: application of ^{14}C-correction methods. Natuurwetenschappelijk Tijdschrift, 72, 79-89.

Walraevens, K. and Lehhe, L., 1989. Groundwater quality in the Tertiary Ledo-Paniselian aquifer in Belgium as a result of fresh-water intrusion into sediments in chemical equilibrium with the sea. In: W. De Breuck and L. Walschot (Eds), 10th Salt Water Intrusion Meeting (SWIM) Conference, Ghent. Natuurwetenschappelijk Tijdschrift 70, 30-44.

Wang, J.H., Robinson, C.V. and Edelman, I.S., 1953. Self diffusion and structure of liquid water with ^{2}H, ^{3}H and ^{18}O as tracers. Journal of the American Chemical Society 75, 466-470.

Wang, R., 1994. Survey of a fresh water aquifer in Shengsi sea area. Hydrogeology and Engineering sGeology 3, 5-10.

Weyerman, J.W.J., 1930. Twee rapporten over den aanleg ener waterleiding te Paramaribo uitgebracht aan den Gouverneur van Suriname. 199 pp.

Wijmstra, T. A. and Van der Hammen, T., 1966. Palynological data on the history of tropical savannas in northern South America. Leidse Geologische Mededelingen 38, 71-90.

Williams, M. O., 1946. Bahrein: Port of pearls and petroleum. National Geographic 89, 194-210.

Wong, Th. E., 1976. Tertiary stratigraphy and micropaleontology of the Guiana basin. Ph.D. thesis, Universiteit van Utrecht. Also published in: Mededeling Geologische Mijnbouwkundige Dienst Suriname No 25, 13-107.

Wong, Th. E., 1984. Stratigraphy and sedimentary history of the Guiana Basin. Mededeling Geologische en Mijnbouwkundige Dienst Suriname No 27, 83-90.

Wong, Th. E., 1986. Outline of the stratigraphy and geological history of the Suriname coastal plain. Geologie en Mijnhouw 65, 223-241.

Wong, Th. E., 1989. Revision of the stratigraphy of the coastal plain of Suriname. Mededeling Natuurwetenschappelijke Studiekring voor Suriname en de Nederlandse Antillen No 123, 64 pp.

Wong, Th. E., 1998. Hydrocarbon exploration and exploitation in Suriname. In: Th.W. Wong, D.R. de Vletter, L. Krook, J.I.S. Zonneveld and A.J. van Loon (Eds), The history of earth sciences in Suriname, Netherlands Institute of Applied Geoscience TNO, Royal Netherlands Academy of Arts and Sciences, 377-396.

Wong, Th. E., De Vletter, D. R., Krook, L., Zonneveld, J. I. S. and Van Loon, A. J. (Eds), 1998a. Th history of earth sciences in Suriname. Netherlands Institute of Applied Geoscience TNO, Royal Netherlands Academy of Arts and Sciences, Amsterdam, 479 pp.

Wong, Th. E., Krook, L. and Zonneveld, J.I.S., 1998b. Investigations in the coastal plain and offsh area of Suriname. In: Th.W. Wong, D.R. de Vletter, L. Krook, J.I.S. Zonneveld and A.J. v Loon (Eds), The history of earth sciences in Suriname. Netherlands Institute of Applied Geoscience TNO, Royal Netherlands Academy of Arts and Sciences, 73-100.

Wooding, R. A., Tyler, S. W. and White, I., 1997. Convection in groundwater below an evaporatin salt lake. 1. Onset of instability. Water Resources Research 33, 1199-1217.

Wooding, R. A., Tyler, S. W., White, I. and Anderson, P. A., 1997b. Convection in groundwater be an evaporating salt lake: 2. Evolution of fingers or plumes. Water Resources Research 3 1219-1228.

Worch, E., 1993. Eine neue Gleichung zur Berechnung von Diffusionskoeffizienten geloschter Sto Vom Wasser 81, 289-297.

Wymstra, T. A., 1969. Palynology of the Alliance Well. Geologie en Mijnbouw 48, 125-134.

Zektser, I. S. and Loaiciga, H. A., 1993. Groundwater fluxes in the global hydrologic cycle: past, ent and future. Journal of Hydrology 144, 405-427.

Zektzer, I. S., Ivanov, V. A. and Meskheteli, A. V., 1973. The problem of direct groundwater disch to the seas. Journal of Hydrology 20, 1-36.

Zonneveld, J.I.S., 1955. Over de geologische en paleogeografische ontwikkeling van de Surinaam kustvlakte. Leidse Geologische Mededelingen No 20, 214-224.

Annex I.

Sediments and aquifers in the Suriname coastal plain

I.1. The Guiana shield

The Proterozoic crystalline basement of Suriname is part of the Guiana shield (Figure 3.3) and consists mainly of granitoid rocks with numerous elongated dolerite intrusions (De Vletter et al., 1998). In the northeastern part of Suriname a region of metamorphic rocks occur consisting of metamorphosed volcano-sedimentary rocks (Marowijne Group) and gneisses and amphibolites (Coeroeni Group). Metamorphic rocks (metabasalts and greenstones) underlie the northern part of the catchments of the Saramacca and Suriname rivers (Figure 3.3)and are also encountered in boreholes in the coastal sedimentary zone (Figure 3.5). The top is strongly weathered, which could be detected in vertical electrical soundings (Velstra, 1996): the weathered layer appeared to have a very low resistivity of around 10 Wm, which was also observed in similar vulcano-sedimentary deposits in West Africa (IWACO, 1987).

I.2. The sedimentary coastal plain

The clastic Mesozoic and Cenozoic sediments in the coastal zone form the southern part of the Guiana Basin, which extends roughly from the Waini River in Guyana to Cayenne in French Guiana (Figure 3.3). The following descriptions of the sedimentary history and of the stratigraphy of the coastal plain are derived mainly from Wong (1984, 1989), Krook (1979), Hanou (1981), Veen (1970) and Brinkman and Pons (1968).

The depositional center is located at the mouth of the Corantijn River, where the formations attain their maximum thickness. Sedimentation in the Guiana Basin started in Late Jurassic to Early Cretaceous times, when the African and South American shields began to drift away (Wong, 1976). The coastal plain is underlain with various formations increasing in thickness and depth towards the North and onlapping older sediments or the basement rocks (Figures 3.4 and 3.5). The thickness of the sediment wedge increases from a few meters in the savannah belt to 750 m along the coastline and finally to some 10,000 m about 150 km offshore (Wong et al., 1998b). The Suriname coast is located on the hinge between the subsiding Guiana Basin and the rising Guiana Shield (Krook, 1994). Subsidence was accompanied by faulting and resulted in several horst and graben structures. Structurally the study area around Paramaribo is located on the lower blocks on the eastern flank of the Bakhuis horst. The faults remained active until Early Tertiary times (Wong, 1994, Hanou, 1981). The material for the subsiding basin was derived from the continuously rising crystalline basement directly south of the basin. After the Early Miocene, the Amazon River became a more important source of supply (Krook, 1979). Earlier, when the Andes Mountains were not yet formed, drainage on the South American continent was directed towards the west (Krook, 1979).

I.3. Cretaceous

The Late Cretaceous sediments in the coastal zone consist of terrestrial unconsolidated and consolidated fine sands and kaolinitic claystones, classified as the *Nickerie Formation*. The Cretaceous contain a high percentage of feldspar, which implies that the weathered top has been eroded (Krook, 1979). Apparently during the Cenozoic the impermeable Cretaceous material impeded flushing by aggressive meteoric groundwater, which leached most of non-quarts minerals from the overlying Tertiary sediments. Near Paramariho the *Nickerie Formation* is found at a depth of around -300 m (below sea level). The top of the Cretaceous dips to about –3,000 m at the shelf slope 150 km offshore (Figure 3.6). The top of the Cretaceous is recognized by a conspicuous density shift in geophysical well logs and seismic surveys for oil exploration.

I.4. Paleogene

During the Paleocene and Eocene mainly shallow marine sediments were deposited during several transgressive phases. Three formations are distinguished with different facies (Wong, 1986, 1989): the continental *Onverdacht Formation* is characterized by coarse kaolinitic sands and kaolinitic clays deposited in alluvial fans and braided rivers in the Paleocene and floodplains and coastal swamps in the more humid tropical Eocene. The 10 to 40 m thick formation is locally found as "buried hills" capped with bauxite and laterite in a 10 km wide small zone around Onverdacht and further eastward. The top of the formation is found close to the surface around Onverdacht until depths of 30 m below the surface near Lelydorp. Bauxite is the result of intensive weathering and leaching during the long Oligocene regression. The original sands were probably arkoses according to Krook (1979). Almost all bauxite in the study area has been excavated in open mines.

The *Onverdacht Formation* passes northward into the marine *Saramacca Formation*, though the transition is not clear due to faulting (UNDP/WHO, 1972). In the study area the formation is found between the line Groningen-Lelydorp and the coastline (Hanou, 1981). The formation consists of alternating quartz sands and kaolinitic clays forming series of depositional cycles, beginning with shallow-marine deposits, grading into beach and deltaic deposits and finally ending with fluvial (pointbar and channel) deposits. The formation contains thick and continuous sand units, which enabled deep groundwater circulation. Oil in the Tambaredjo oil field is recovered from one of the lower sand units (T-sands), which is confined by an impermeable clay layer. The source rocks of the oil are the offshore Lower Cretaceous marine shales (Wong, 1998).

The top of the formation is found at a depth of about -140 m (below sea level) just north of Lelydorp and slopes to - 220 m along the coastline west of Paramaribo.

Further North, the *Saramacca Formation* changes into the *Alliance Formation*, which consists of silty marls, clays, calcareous sands and lignites, deposited in a shallow-marine environment, and in coastal lagoons. Sand layers are not as massive as in the *Saramacca formation* and therefore the formation as a whole is much less permeable.

During the Oligocene the sea withdrew (10 million years), while climate changed from humid tropical to semi-arid. Weathering during this long period led to bauxite formation on Paleogene sediments and crystalline basement rocks. Erosion products were deposited as braided-river and alluvial-fan deposits forming the *Burnside Formation*. In the Holocene coastal plain, the formation is restricted to several northeast-southwest oriented tectonic basins along the coast (Hanou, 1981). The study area is located on one of the basins betw Groningen and Paramaribo. East of the Suriname River the formation is absent. The *Burnside Formation* has been encountered just North of Lelydorp at - 130 m. North of Paramaribo, near the coastline the top of the formation is found at -180 m. The thickness varies from 5 m to 80 m in the depositional center west of Paramaribo.

Low feldspar contents and the absence of calcite and aragonite in the Paleogene sed ments are signs of prolonged leaching by groundwater flow (Krook, 1979). Krook also believes that the mostly kaolinitic Tertiary clays (of marine origin) originally had a highe content of smectites and illites and that they were later transformed as a result of weathe and leaching. Magnetite and hematite appear to be the dominant iron(hydr)oxide minera

Thin aquifers with fresh water are found in the *Onverdacht Formation* below the bauxite caps, though they are discontinuous and of little importance to the regional grou water flow. The massive sand units in the *Saramacca Formation* form aquifers of regio extent. Around Paramaribo, the aquifers of this formation are moderately brackish and n suitable for water supply. Well known is the T-sand unit at the base of the formation, wh hosts the oil of the Tambaredjo oil field, 35 km west of Paramaribo. Though groundwat this oil-bearing layer is highly brackish, fresh groundwater is found just above the clay sealing the T-sands. UNDP/WHO (1972) reports hydraulic conduetivities varying from 40 m/day, derived from stem tests. The total thickness of the sand units is about 50 to 7

The coarse sands of the *Burnside Formation* vary in thickness from 10 to 60 m an form a good aquifer, also called *A-sand aquifer*. Around Paramaribo, hydraulic conduct ties and transmissivities vary from 30 to 80 m/day and 900 to 3200 m²/day respectively (UNDP/WHO, 1972). The high transmissivity for the Leysweg well field is related to t relatively large thickness and gravely nature of the aquifer near the depositional center *Burnside Formation* West of Paramaribo. In the southern part of the Holocene coastal p the aquifer contains fresh groundwater. A tongue of fresh water protrudes to the city of Paramaribo (Figure 3.7), where the aquifer is heavily exploited for the drinking water s ply.

Clays below the *Burnside Formation* probably have a high hydraulic resistance a as the salinity of pumped water in the well fields only slowly increases due to lateral a tion rather than by upward flow from the more saline deeper strata.

I.5. Neogene

During the Early Miocene transgression, clays, sandy clays and sands with glauc and lignite layers were deposited as beach sands and swamp clays with mangrove veg (*Coesewijne Formation*). Compared to the older formations, the deposits of this forma contain much more clay (40 to 80 %), originating from the proto-Amazon catchment. continental sbelf, the facies of the *Coesewijne Formation* changes into a shallow-mari bonate platform (Figure 3.6). After a regression lasting 2 to 3 million years, sediment resumed during the mid Early Miocene. More sands (beach and fluvial deposits) were deposited. In the study area, tbe lower, more clayey part of the *Coesewijne Formation* only found in the Holocene coastal plain at a depth of around -95 m. The upper, more part extends as far south as the Rijsdijk Road in the Pleistocene coastal plain, though absent on the buried bauxite hills around Onverdacht. The depth of the top of the

Coesewijne formation varies from -65 m to -75 m along the coastline.

After a long regression of about 5 million years during the Late Miocene, the Pliocene started with a transgression reaching as far as Republiek (Krook, 1979). The transgressive deposits have been removed largely during the subsequent Pliocene regression. Mainly coarse, white and brown, kaolinitic sands with interbedded kaolinite clays, were then deposited in braided streams and on alluvial fans under semi-arid conditions (Krook, 1979, Van Voorthuysen, 1969). These deposits, comprising the *Zanderij Formation*, crop out in the savannah belt. Intensive weathering and leaching gave the savannah sands their characteristic bright-white appearance. In the coastal plain, the *Zanderij Formation* dips below Quaternary sediments. At the coastline, the formation is found at a depth of -35 m.

Just as the Paleogene sediments, the Neogene sediments contain hardly any weatherable minerals like calcite and the more unstable silicates (Krook, 1979). Unpublished mineralogical analyses by Krook (related to Krook 1979) show that limonite (amorphous iron hydroxide) is the most abundant iron(hydr)oxide in the Pliocene and Miocene formations. He also found authigenic siderite in the top of the Pliocene formation. Pyrite appeared to be present in all Tertiary formations. The mostly kaolinitic clays in the marine Coesewijne Formation may have been transformed from clays with a higher smectite and illite content through weathering, as Krook (1979) suggested for the Paleogene clays.

Despite the large clay percentage of the *Coesewijne Formation* the individual sand layers are permeable and are generally grouped into two aquifers (IWACO/F.R. Harris, 1991). Sand units below a depth of -110 m comprise the *Lower Coesewijne aquifer* and are only present in the Holocene coastal plain. The *Upper Coesewijne Formation* contains thicker sand units and forms a better aquifer than the Lower Coesewijne aquifer. The top is found at a depth of -65 m, near Lelydorp, to -75 m along the coast. The total thickness of the sand units in both aquifers varies between 5 and 15 m, while hydraulic conductivities vary between 40 and 70 m/day (UNDP/WHO, 1972). South of Lelydorp the aquifer is hydraulically connected with the *Zanderij aquifer*. Though the *Upper Coesewijne aquifer* extends almost to Republiek in the South, it is absent on the bauxite hills around Onverdacht. North of the main coastal East-West road and along the Suriname and Saramacca rivers, groundwater in the *Coesewijne aquifers* is brackish (Figure 3.7). There are several pumping stations the Holocene coastal plain, which recover water form these aquifers (Table 3.2 and Figure 3.1). The clays and lignite layers in the lower part of the *Coesewijne Formation* form an effective aquitard, as indicated by the originally artesian groundwater heads in the *Burnside aquifer* (Section 3.6.3.).

The *Zanderij Formation* forms a continuous aquifer with a thickness of several meters in the savannah belt to 40 m along the coast. The Zanderij aquifer is absent on some of the more elevated bauxite hills. Various pumping tests carried out in the Pleistocene coastal plain report transmissivities varying from 300 m^2/day at Republiek to 1400 m^2/day at Lelydorp (IWACO/F.R. Harris, 1991; Terracon Anguilla Ltd, 1994; Mente, 1990a). The average hydraulic conductivity of the sands is 50 m/day. In the Holocene and part of the Pleistocene coastal plain, the aquifer contains brackish groundwater (Figure 3.7). Fresh groundwater is present in the area around Lelydorp (below the *Lelydorp sands*) and, further South, in the savannah belt and the adjacent coastal plain. The aquifer is exploited for the drinking-water supply of Paramaribo (Table 3.2 and Figure 3.1) and also for the SURALCO bauxite refinery at Paranam.

I.6. Pleistocene

In the Pleistocene coastal plain between Republiek and Lelydorp, marine deposits are found related to one or more Pleistocene transgressions. The deposits classified as the *Coropina Formation* consist mainly of clays (mudflats) interspersed with sand barriers. At the base of the formation also fluvial sands are found in some places, marking a continental sedimentary environment during the Early Pleistocene. Two members are distinguished (Brinkman and Pons, 1968; Veen, 1970). The *Para Member* dates from the Early Eemian or Yarmouthian (Holsteinian) interglacial and consist mainly of marine clays. The top of the Para Member is characterized by strong mottling (paleosol). The Lelydorp Member, which contains more sandy deposits than the Para Member, is probably formed during the Late Eemian interglacial. The *Lelydorp Member* is found in the northern part of the Pleistocene coastal plain. Characteristics is the elevated complex (up to 11+ msl) of sand barriers around Lelydorp. These *Lelydorp sands* form a more or less continuous shallow aquifer. According to Van der Eyk (1957), Eemian sea level reached a maximum of 8 m above present sea level. Brinkman and Pons (1968) distinguish two phases for the Lelydorp Member: the Onoribo phase characterized by deposition of clays rich in organic material and pyrite during a rising sea level, and the Santigron phase, during which clays with less pyrite and sand barriers were deposited after sea level had reached a stable level.

Weathering during the Wisconsinan affected the Pleistocene sediments consisting mainly of clays. Carbonates have largely disappeared (< 0.3 %). Also organic matter content is generally low (< 0.4 %), though Veen (1970) and Levelt and Quakernaat (1968) occasionally found high organic carbon contents in the lower part (up to 12 %). Oxidation can be recognized by the intense yellow and red mottling of iron oxides formed after breakdown of siderite and pyrite. XRF analyses of a few Koewarasan samples showed that sulfur has almost entirely disappeared. According to Veen (1970) and Levelt and Quakernaat (1968), weathering also transformed the clay minerals. Data of Levelt and Quakernaat (1968) show that kaolinite contents have increased at the expense of illite contents in comparison with the composition of Holocene clays. The content of smectite is comparable to that of the Holocene clays (0 – 20 %). Finally it is worth noting that the Pleistocene clays in the South contain acid and very dilute pore water and have a low base saturation (Levelt and Quakernaat, 1968; Veen, 1970).

The *Lelydorp sands* act as a local aquifer with a thickness of 2 to 8 m and contain fresh groundwater. This groundwater is recovered in open dug wells in remote places not connected to the public water-supply system. Long-duration tests with several piezometers, carried out only in the Pliocene *Zanderij aquifer* (IWACO/F.R. Harris, 1991; Terracon Anguilla Ltd, 1994; Mente, 1990a) showed that the clays of the *Coropina Formation* have a very high hydraulic resistance varying from 5×10^4 to more then 2×10^5 days. Given the thickness of the clays, the vertical hydraulic conductivity is about 10^{-4} m/day.

I.7. Holocene

During the Early Holocene (12 ka to 6 ka BP), sea level rose from a depth of 100 m to its present level (Roelevеld and Van Loon, 1979; Fairbanks, 1989). In the course of the sea-level rise, the large sediment load of the Amazon River could no longer be discharged in the deep sea far offshore. The sediment was taken northward with the Guiana Current and depo-

sited along the coast. The Holocene sediments obliterated most of the Pleistocene erosion topography. Because the Holocene transgression did not reach the level of the previous Sangamonian transgression, the Pleistocene coastal plain in the south was spared, though the gullies were filled with the peaty clays of the *Mara Formation* and can still be recognized as swamps. After sea-level rise slowed down between 7 and 6 ka BP, coastal aggradation began and extensive tidal-flat clays alternating with beach barriers with sands and shells were deposited in the Holocene coastal plain (*Coronie Formation*). Brinkman and Pons (1968) discerned three distinctive phases in the coastal aggradation: the Wanica phase from 6 to 3 ka BP, the Moleson phase from 2.5 to 1.3 ka BP and the Commewijne phase from 1 ka BP to present. The main part of the Holocene coastal plain in the study area dates from the Wanica phase. Only North of the Paramaribo-Groningen road and the Commewijne River, recent deposits of the Commewijne phase are found. In the littoral zone sedimentation and coastal aggradation continues (Augustinus, 1978; Augustinus et al., 1989). A series of mud banks, where suspended load from the Guiana current precipitates, is continuously moving westward, while between the mud banks energy-rich environments create elongated beach barriers. Oceanographic surveys show that these mud deposits are present on the sea floor to a distance of 30 km offshore and have a maximum thickness of 20 m (Nota, 1958, 1969). Further North, sandy, deposits are found on the sea floor. Just as in the coastal plain, the Holocene deposits have obliterated the Pleistocene topography apart from Pleistocene paleo-channels of the major rivers like the Marowijne (Nota, 1971). Other submarine morphological features are old coastlines and coral reefs, which indicate interruptions of the Holocene transgression. A coastline at a depth of 21 to 25 m was found dating from 8 to 9 ka BP (Nota, 1958;Van der Hammen, 1963). A coral reef at 80 to 90 m depth has an age of 12 to 17 ka BP (Nota, 1958, 1971).

The clays of the *Coronie Formation* have high smectite and illite (30 to 60 %) and low kaolinite (< 30 %) contents (Eisma and Van der Marel, 1971). The smectites and illites originate from the Andean mountains and were transported to the Suriname coast by the Amazon River and its tributaries and, subsequently, the Guyana current (Gibbs, 1967). According to analyses by Eisma and Van der Marel (1971) and samples from the Koewarasan and Tourtonne boreholes (Chapter 5), carbonate and organic matter content are about 2 – 6 % and 1-2 % respectively. The clays are also rich in pyrite, formed after deposition (Brinkman and Pons, 1968), as can be derived from the XRF analyses of Koewarasan and Tourtonne samples (sulfur contents from 0.2 to 0.8 %). However, after regression in the Late Holocene (after 4 ka BP), soil forming processes in the upper few meters of the Holocene clays led to pyrite oxidation and acidification (Brinkman and Pons, 1968).

The sands and shells layers in the Holocene beach-barrier deposits form local aquifers, from which groundwater was recovered by open dug wells before the construction of the city water-supply system in 1933.

Annex II.

Map of the Suriname coastal plain around Paramaribo with sam pled wells

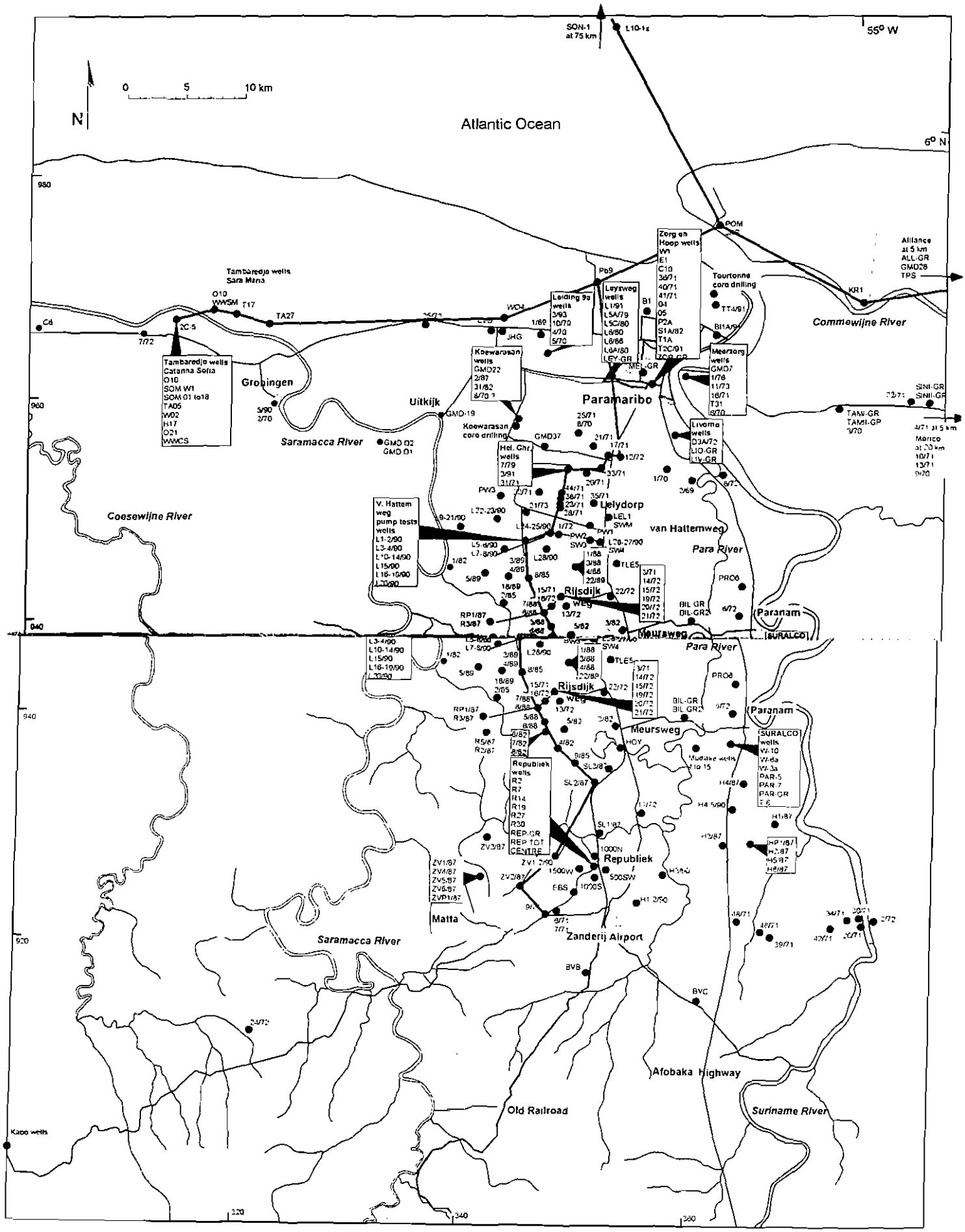

Map of the Suriname coastal plain around Paramaribo with sampled wells

Annex III.

Chemical and isotopic analysis of groundwater in the Suriname coastal plain (for locations see Annex II)

Chemical and isotopic analysis of groundwater in the Suriname coastal plain (for locations see Annex II)

Well	Location	Screen	Formation	Depth m	Date	Temp °C	pH-Lab	pH-Fld	EC-Lab µS/cm	Ec-Veld µS/cm	Cl⁻ mmol/l	Br⁻ mmol/l	CO_3^{2-} mmol/l	HCO_3^- mmol/l	SO_4^{2-} mmol/l	NO_3^- mmol/l	PO4-orth mmol/l	Na^+ mmol/l	K^+ mmol/l
Samples with analyses of all macroions and electro-neutrality error < 10 %																			
0/200O	Kabo	1	2	-7.5	17-08-83		6.23		61		0.077			0.032		0.357		0.107	0.048
0/200O	Kabo	1	2	-7.5	01-06-83		6.26		24		0.121			0.045	0.009			0.120	
0/200W	Kabo	1	2	-7.5	17-08-83		5.84		25		0.133			0.008				0.114	
0/200W	Kabo	1	2	-7.5	17-08-83		6.13		26		0.149			0.014	0.010			0.133	0.002
0/280O	Kabo	1	2	-7.5	01-06-83		6.38		24		0.124			0.067	0.004			0.141	
0/280O	Kabo	1	2	-7.5	01-06-83		6.38		24		0.124			0.067	0.004			0.141	
0/400O	Kabo	1	2	-7.5	17-08-83		5.35		27		0.130			0.004	0.015	0.015		0.123	0.009
0/400W	Kabo	1	2	-7.5	01-06-83		5.25		57		0.465			0.004				0.350	
0/400W	Kabo	1	2	-7.5	17-08-83		4.63		55		0.338			0.001		0.023		0.232	0.001
0/600O	Kabo	1	2	-7.5	17-08-83		6.35		24		0.098			0.051	0.011			0.097	0.003
0/600O	Kabo	1	2	-7.5	01-06-83		6.27		35		0.194			0.052	0.015	0.025		0.204	0.011
0/700W	Kabo	1	2	-7.5	17-08-83		6.52		34		0.122			0.078	0.010	0.022		0.189	0.006
0/700W	Kabo	1	2	-7.5	01-06-83		5.93		24		0.090			0.016	0.010	0.044		0.112	
0/900W	Kabo	1	2	-7.5	17-08-83		5.94		37		0.250			0.005				0.207	0.003
0/900W	Kabo	1	2	-7.5	01-06-83		6.07		63		0.421			0.029	0.021	0.024		0.357	0.018
1/72	Van Hattemweg	1	2	-40.2	11-09-72		7.4				0.451			1.700	0.104			1.217	0.102
1/76	Meerzorg	1	5	-151.1	05-12-80	30	7.1		400		3.385			1.344	0.166			3.740	0.230
1/82	Haarlem	2	3	-76.0	31-12-82	28	6.6		330		1.015			1.721	0.468	0.001	0.052	2.827	0.125
1/82	Haarlem	2	3	-76.0	14-07-95	33.8	7.27	6.7	2173	1450	16.107			2.508	1.197	0.006		14.049	0.260
1/88	Rijdijk	1	2	-49.2	31-12-90	24.3	6.05		291		1.692			1.100	0.032		0.004	1.652	0.066
10/70	Leiding 9a	1	5	-183.5	29-01-71		6.7				9.393		0.049	1.900				9.656	0.212
10/71	Morico II	1	3	-82.3	21-05-71		8.3				4.936		0.049	2.200	0.551			5.959	0.102
10/71	Morico II	1	3	-82.3	29-01-70		6.7				9.393		0.049	1.900				9.656	0.212
11	Mudlake SURALCO	1	2	-34.4	15-03-95	26.6	5.9		946		6.854			1.349				6.394	0.130
11/73	Meerzorg	1	5	-151.1	05-12-80	30	7.16		460		3.949			1.442	0.166			4.219	0.230
12	Mudlake SURALCO	1	2	-25.1	15-03-95	26.7	6.6		2810		18.645			4.939				17.833	0.439
12/72	Mon Plaisirweg	1	4	-125.0	10-05-72		6.9				1.382			1.200	1.770			5.480	0.102
13	Mudlake SURALCO	1	2	-29.0	05-05-95	26.6	6.73		5750		37.179			21.819				43.932	0.987
13/72	Rijsdijk South	1	2	-30.3	31-12-90	22.9	5.89		180		1.100			1.119	0.083		0.005	1.043	0.040
14	Mudlake SURALCO	1	2	-29.0	05-05-95	26.8	6.31		2420		17.827			8.172				20.530	0.506
14/72	Rijsdijk	1	2	-34.5	31-12-90	27.3	7.72		330		1.297			2.721	0.034		0.004	0.869	0.069

→ analyses of other parameters are continued on page 179 to 189

Well	Location	Screen	Formation	Depth m	Date	Temp °C	pH-Lab	pH-Fld	EC-Lab µS/cm	Ec-Veld µS/cm	Cl⁻ mmol/l	Br⁻ mmol/l	CO_3^{2-} mmol/l	HCO_3^- mmol/l	SO_4^{2-} mmol/l	NO_3^- mmol/l	PO4-orth mmol/l	Na^+ mmol/l	K^+ mmol/l
15	Mudlake SURALCO	1	2	-29.0	05-05-95	26	6.45		3970		27.447			10.790				32.187	0.639
16/71	Meerzorg	1	5	-151.1	07-07-71		6				5.416			1.000	0.145			5.176	0.179
17/71	Pad van Wanica	1	2	-38.8	04-08-71		6				17.235			0.500	1.218			7.872	0.294
18/69	Rijsdijk	1	2	-59.8	31-12-90	23.3	6.05		376		2.200			0.260	0.584		0.001	2.914	0.053
2/69	Houttuin	1	4	-126.2	02-06-71		8.3				3.977		0.349	0.900	0.468			4.393	0.153
2/87	Koewarasan	1	3	-84.0	07-07-95	28.2	6.76	5.99	845	834	4.372			1.573	1.249			2.474	0.143
21/71	Welgedacht B	1	3	-68.7	22-02-72		6.4				0.761			1.500	1.207			1.870	0.104
21/73	Landsboerd.(Javaweg)	1	2	-30.0	31-12-90	25.4	6.21		623		4.062			1.080	0.762		0.002	2.522	0.086
22/71	Commewijne km24	1	3	-67.0	27-07-71		5.4				51.622		0.299	0.100				35.798	0.409
22/72	Rijsdijk	1	2	-16.9	01-08-72		8.5				0.366		0.049	1.604				0.782	0.102
23/71	De Craneweg	1	3	-63.1	02-09-71		5.7				1.015			1.000	0.645			1.913	0.051
25/71	Magenta/Welgedacht C	1	3	-59.8	27-08-71		6.9				1.128			0.900	0.156			1.522	0.040
25/72	Gamizoenspad	1	5	-172.7	08-08-95	28	6.33	6.32	404	330	1.861			1.934	0.014	0.001		2.492	0.136
25/72	Gamizoenspad	1	5	-172.7	20-09-72		8.1				2.256			1.700				2.218	0.102
26/71	Carolina	1	2	0.0	31-08-71		4.7				1.128			0.080	0.322			1.043	0.051
29/71	Helena Christinaweg	1	2	-62.5	15-09-71		7.3				1.523			0.800	0.728			1.696	0.153
3/71	Rijsdijk	2	2	-52.3	08-04-71		7.2				1.354		0.149	0.800	0.135			1.739	0.063
3/71	Rijsdijk	3	2	-29.0	31-12-71	28	6.5		145		0.816			1.327	0.031	0.001	0.007	1.000	0.074
3/71	Rijsdijk	1	3	-78.1	09-03-71		6.3				3.413		0.199	1.100	1.082			5.785	0.158
3/82	Meursweg	3	2	-30.0	04-08-95	26.9	6.42	6.01	343	268	2.039	0.0035		0.836	0.093	0.004		1.513	0.059
3/82	Meursweg	1	3	-68.0	04-08-95	27.9	6.27	6.65	5581	4780	51.791	0.0826		1.163	2.884	0.006		35.232	0.521
3/91	Helena Christinaweg	1	5	-134.0	12-12-96	28.8	6.77	5.6	541	530	1.829			1.030	1.099	0.002	0.003	3.239	0.163
3/91	Helena Christinaweg	1	5	-134.0	07-07-95	29.5	6.75	5.76	565	520	1.695			1.229	1.322			3.392	0.167
3/93	Leiding 9a	1	3	-74.0	16-07-95	29.7	6.9	6.05	1264	1187	6.093			2.737	2.311	0.048		3.692	0.301
31/71	Helena Christinaweg	1	3	-87.2	31-01-72		7.3				1.974			1.000	0.780			2.435	0.191
31/71	Helena Christinaweg	1	3	-87.2	12-12-96	27.2	6.19	5.7	1286	1213	6.420			0.206	1.399	0.004	0.005	4.579	0.270
31/71	Helena Christinaweg	1	3	-87.2	07-07-95	27.7	5.85	5.6	1326	1260	9.365			0.524	1.405	0.020		4.784	0.224
31/82	Koewarasan	1	3	-66.0	07-07-95	27.1	6.77	6.18	1021	1036	5.669			1.508	1.468	0.024		2.857	0.160
31/82	Koewarasan	1	3	-66.0	13-12-96	27.1	6.64	6	965	931	5.440			1.520	1.609	0.001	0.006	2.649	0.207
33/71	Helena Christinaweg	1	2	-37.7	30-09-71		6.1				13.737			0.300	0.801			5.611	0.230
35/71	Tawajarweg	1	2	-43.0	18-10-71		6.4				2.059			1.100	0.520			1.522	0.102
36/71	Zorg en Hoop (Cor.str.)	1	5	-156.8	15-10-71	.	6.8				5.359			1.400				4.828	0.179
38/71	Sidodadleweg	1	2	-46.5	09-11-69		7				0.535			1.300	0.593			1.435	0.104

Well	Location	Screen	Formation	Depth m	Date	Temp °C	pH-Lab	pH-Fld	EC-Lab µS/cm	Ec-Veld µS/cm	Cl mmol/l	Br mmol/l	CO_3^{2-} mmol/l	HCO_3^- mmol/l	SO_4^{2-} mmol/l	NO_3^- mmol/l	PO4-orth mmol/l	Na^+ mmol/l	K^+ mmol/l
4	Mudlake SURALCO	1	6	-32.7	15-03-95	26.6	6.3		18160		153.653			21.780				145.280	2.225
4/670W	Kabo	1	2	-7.5	17-08-83		6.53		30		0.117			0.078				0.109	0.001
4/670W	Kabo	1	2	-7.5	01-06-83		6.52		33		0.098			0.074	0.004	0.089		0.098	0.030
4/70	Lelding 9a	1	3	-77.6	01-06-72		7.9				2.877			3.100	1.749			2.435	0.191
4/71	Commetewane Kreek	1	2	-97.6	08-03-71		6.7				7.765		0.349	2.800	1.530			9.612	0.358
4/82	Rijsdijk South	2	2	-38.3	31-12-82	28	4.4		810		7.616			0.044	0.197	0.001	0.005	4.784	0.179
4/82	Rijsdijk South	1	2	-54.3	31-12-82	28	6.7		1100		9.732			1.213	0.583	0.001	0.003	8.916	0.237
4/82	Rijsdijk South	3	2	-15.3	31-12-82	28	6.5		570		4.836			0.983	0.083	0.001	0.004	3.436	0.163
4/88	Rijsdijk	1	2	-27.2	31-12-82	24.4	6.39		303		0.959			2.131	0.042		0.048	1.217	0.046
4/89	Rijsdijk	1	2	-38.8	31-12-82	27.5	5.95		392		3.554			1.039	0.216		0.002	2.957	0.048
40/71	Zorg en Hoop (Postoff.)	1	5	-157.3	05-11-71		6.9				4.710			1.500				4.480	0.168
41/71	Zorg en Hoop (SWCC9)	1	5	-154.7	11-11-71		6.8				3.921			1.400				3.871	0.148
42/71	Carolina	1	2	-9.7	23-11-70		6.4				0.253			0.400				0.185	0.102
5	Mudlake SURALCO	1	1	-14.8	15-03-95	26.6	7.1		10450		70.296			36.498				90.474	2.301
5/82	Rijsdijk	3	2	-16.2	31-12-82		5.9				1.805			0.754		0.001	0.200	1.565	0.204
5/82	Rijsdijk	1	2	-57.2	31-12-82		6.1				2.990			0.852		0.017	0.007	2.783	0.153
5/89	Rijsdijk	1	3	-93.9	31-12-82	22.9	5.76		520		4.259			1.319	0.975		0.003	3.697	0.117
5/90	Groningen	1	4	-136.0	26-07-95		6.52	6.85	759	685	2.039			2.000	1.624	0.222		4.480	0.217
6/200W	Kabo	1	2	-7.5	01-06-83		7.76		145		0.120			1.364	0.012	0.050		0.543	0.045
6/400O	Kabo	1	2	-7.5	17-08-83		6.13		31		0.118			0.022	0.019	0.021		0.077	0.029
6/400O	Kabo	1	2	-7.5	01-06-83		6.27		25		0.125			0.039	0.002	0.009		0.090	0.018
6/400W	Kabo	1	2	-7.5	17-08-83		6.47		36		0.153			0.085		0.018		0.172	0.005
6/400W	Kabo	1	2	-7.5	01-06-83		4.84		45		0.062			0.002	0.006	0.231		0.176	0.008
6/600W	Kabo	1	2	-7.5	17-08-83		6.03		41		0.210			0.024		0.023		0.219	0.017
6/600W	Kabo	1	2	-7.5	01-06-83		6.61		43		0.198			0.080	0.002	0.041		0.222	0.013
6/72	La Vigilantia	1	2	-23.4	01-03-72		5.5				15.796			2.200	0.197			15.963	0.230
6/82	Rijsdijk	1	2	-43.1	31-12-82	26	4.7		800		7.616			0.129	0.114	0.006	0.007	4.219	0.204
6/89	Rijsdijk	1	2	-36.9	31-12-90	27.2	5.61		1256		10.126			0.719	0.653		0.001	8.655	0.099
6/CENT	Kabo	1	2	-7.5	17-08-83		6.91		39		0.126			0.149	0.020			0.160	0.001
6/CENT	Kabo	1	2	-7.5	01-06-83		6.88		30		0.117			0.147	0.006			0.127	
6A	Mudlake SURALCO	1	6	-39.8	15-03-95	26.7	5.6		10090		108.716			3.372				73.945	1.432
7/72	Tijgerkreek	1	4	-130.0	15-07-72		7				2.877			4.800	2.915			11.570	0.161
7/79	Helena Christinaweg	1	2	-51.5	20-07-95	27.2	6.53	6.34	797	698	4.400			0.721	1.239	0.012		3.736	0.184

Well	Location	Screen	Formation	Depth m	Date	Temp °C	pH-Lab	pH-Fld	EC-Lab µS/cm	Ec-Veld µS/cm	Cl mmol/l	Br mmol/l	CO_3^{2-} mmol/l	HCO_3^- mmol/l	SO_4^{2-} mmol/l	NO_3^- mmol/l	PO4-orth mmol/l	Na^+ mmol/l	K^+ mmol/l
7/82	Rijsdijk	2	2	-22.4	31-12-82	28	6.5		760		6.629			0.688	0.218	0.001	0.005	3.871	0.184
7/82	Rijsdijk	1	2	-32.4	31-12-82	28	5.8		820		7.616			0.311	0.093	0.001	0.005	4.219	0.191
7A	Mudlake SURALCO	1	2	-39.5	15-03-95	26.9	6.2		17000		133.765			2.637				109.612	1.483
8	Mudlake SURALCO	1	1	-17.2	15-03-95	26.7	6.7		13570		112.496			25.786		0.008		113.092	2.058
8/72	Adhinweg	1	4	-114.0	11-04-72		6.7				8.603			0.800	0.270			6.263	0.148
8/82	Rijsdijk	1	2	-21.0	31-12-82	28	6.3		570		4.936			0.573	0.177	0.011	0.002	3.001	0.171
B1	Beni Park	1	5	-174.2	16-07-95	31.5	7.13	8.56	1975	1677	14.753			2.655	0.622	0.001		10.874	0.312
BL1A/91	Blauwgrond	1	5	-177.2	27-06-95	34	6.95	6.4	1375	1368	9.506	0.0150		2.918	0.170	0.006		10.265	0.204
C10	Zorg en Hoop	1	5	-157.5	06-12-80	30.5	6.88		440		4.785			1.196	0.104			4.219	0.230
D3A/72	Livorno	1	5	-169.8	30-06-95	29.6	6.95	6.09	607	613	2.877			1.639	0.583	0.009		4.158	0.150
E1	Zorg en Hoop	1	5	-157.5	06-12-80	31	7.01		840		9.224			1.344	0.052			7.525	0.306
EBS	Zanderij	1	2	-5.0		27.7	7.08	5.9	134	136	0.248			1.049	0.008	0.006	0.000	0.181	0.016
GMD 22	Koewarasan	1	4	-126.5	20-07-71		5.9				4.598		0.099	0.800	1.301			2.957	1.943
GMD 28	Alliance	1	4	-103.5	11-05-71		7.7				5.557		0.199	6.600	1.863			10.308	0.434
GMD 7	Meerzorg	1	5	-144.5	23-07-71		6.7				5.190		0.099	1.100	0.145			5.176	0.194
GMD D1	Kampong Barde	1	4	-126.5	22-03-71		6.5				2.708		0.049	1.000	1.228			4.523	0.253
H1/87	Highway (S. of Paranam	1	2	-14.3	31-12-90	27.1	5.5		66		0.366			0.329					0.007
H1-2/90	airport Zanderij	2	2	-14.3	31-12-90	23.8	5.83		54		0.112			0.243	0.233		0.082	0.347	0.010
HOY	Hoy Kreek	1	2	-0.5	18-12-96	29.7	5.19	5.42	45	35	0.182			0.087	0.083	0.007		0.157	0.004
JHG	Kwatta weg	1	3	-76.0	26-07-95		6.3	6.2	3818	3530	33.229			2.147	2.436			15.963	0.465
KW1	Koewarasan	1	1	-1.2	20-02-97		7.21	8.1	5511		17.600			3.550	36.289	0.036		28.600	0.051
KW11	Koewarasan	1	1	-11.2	20-02-97		7.21	7.6			76.500			2.450	6.559	0.324	0.008	68.600	1.080
KW12	Koewarasan	1	1	-12.2	20-02-97		7.19	8.4	8320		82.000			3.390	2.339	0.026	0.002	55.600	0.961
KW16	Koewarasan	1	1	-16.2	20-02-97			8.7			89.900				5.229	0.212	0.002	66.000	1.130
KW17	Koewarasan	1	1	-17.2	20-02-97		7.16	8.2	6956		79.000			1.660	2.269	0.859	0.001	45.900	0.856
KW19	Koewarasan	1	1	-19.2	20-02-97		7.16	7.8			81.700			1.130	1.939	0.039	0.003	48.500	0.857
KW3	Koewarasan	1	0	-3.2	20-02-97		7.21	7.5	6875		30.600			6.260	41.500	0.025	0.020	41.500	0.860
KW9	Koewarasan	1	1	-9.2	20-02-97		7.12	8.2	7338		82.100			0.990	2.249	0.065		34.500	0.847
L1/91	Leysweg	1	3	-84.0	17-12-96	28.1	6.1	6	1495	1490	9.860			0.931	1.829	0.003	0.005	5.179	0.315
L10-14/0	Van Hattenweg west	3	3	-71.0	31-12-90	24.1	6.01		403		1.100			1.918	0.874		0.183	2.566	0.051
L1-2/90	Van Hattenweg west	1	3	-74.5	31-12-90	25.2	5.84		290		1.184			1.180	0.288		0.003	1.478	0.046
L15/90	Van Hattenweg west	1	2	-50.5	31-12-90	23.9	5.24		393		0.987			2.508	0.265		0.004	1.739	0.081
L16-19/0	Van Hattenweg west	4	1	-4.8	31-12-90	24.9	5.59		309		0.423			2.704	0.074			0.391	0.058

Well	Location	Screen	Formation	Depth m	Date	Temp °C	pH-Lab	pH-Fld	EC-Lab µS/cm	Ec-Veld µS/cm	Cl^- mmol/l	Br^- mmol/l	CO_3^{2-} mmol/l	HCO_3^- mmol/l	SO_4^{2-} mmol/l	NO_3^- mmol/l	PO_4-orth mmol/l	Na^+ mmol/l	K^+ mmol/l
																		1.565	0.092
L18-19/0	Van Hattemweg west	3	2	-33.8	31-12-90	24.2	5.73		515		0.761			3.983	0.100				
L16-19/0	Van Hattemweg west	2	2	-57.5	31-12-90	24.3	5.51		489		0.930			3.836	0.076		0.001	1.739	0.092
L20/90	Van Hattemweg west	1	1	-4.3	31-12-90	24.9	5.87		168		0.592			1.080	0.042			0.391	0.017
L22-23/0	Santigron	1	3	-76.0	31-12-90	25	6.16		350		1.212			1.180	0.703		0.011	2.000	0.100
L24-25/0	Van Hattemweg	1	3	-72.0	31-12-90	26.3	6.09		353		1.551			1.400	0.354		0.003	2.000	
L28/90	Spoil Area	1	2	-33.0	31-12-90	25.8	6.22		6		0.733			1.129	1.926		0.007	2.000	0.100
L3-4/90	Van Hattenweg west	2	2	-29.3	31-12-90	26.6	6.2		437		0.733			2.901	0.510		0.003	1.261	0.066
L5-6/90	Van Hattenweg west	1	2	-42.3	31-12-90	24.4	6.2		251		0.874			0.719	0.184		0.005	1.130	0.040
L5A/79	Leysweg	1	5	-162.8	27-06-95	31	6.46	5.85	1185	1150	9.337			1.344	0.010	0.004		6.785	0.204
L5C/80	Leysweg	1	3	-76.2	27-06-95	28.3	6.29	5.74	957	1003	4.654			1.278	1.749	0.022		3.179	0.224
L6/80	Leysweg	1	3	-74.5	17-12-96	28	6.46	5.7	899	888	4.320			1.350	1.779	0.008	0.006	3.179	0.245
L9-21/90	Santigron	2	2	-49.0	31-12-90	24.2	5.89		451		2.256			1.000	0.258		0.007	1.000	
L9-21/90	Santigron	1	3	-73.0	31-12-90	23.2	5.85		666		3.808			0.919	0.861		0.004	2.000	1.000
LEL1	Lelydorp	1	2	-40.5	17-12-96	26.9	7.09	6.13	303	283	0.662			1.450	0.500	0.003	0.009	1.239	0.104
LEY-GR	Leysweg	1	2	0.5	31-12-90	29	6.2		1030		7.249			1.098	1.082	0.004	0.001	5.872	0.383
LIO-GR	Livorno	1	5	0.5	31-12-90	30.5	6.3		520		2.284			1.114	0.624	0.037		3.827	0.186
LIV-GR	Livorno	1	5	-147.5	17-12-80	30	6.71		440		3.667			1.295	0.562			4.132	0.230
LVD	Kwattaweg	1	3	-85.0	08-08-95	28.5	6.03	6.37	1781	1600	11.875	0.0175		1.704	2.342			5.263	0.322
MEL-GR	Melkcentrale	1	4	-127.5	05-03-71						5.049		0.299	0.100	1.530			4.697	0.281
O10	Tambaredjo oil field	1	6	-288.5	03-01-97	35.7	7.15	6.5	1826	1911	11.500			5.590	0.414		0.001	14.700	0.281
O4	Zorg en Hoop	1	5	-157.5	31-12-80	30.5	7		820		8.744			1.360	0.010			7.394	0.332
O5	Zorg en Hoop	1	4	-122.0	15-02-72		6.2				2.313			1.500	0.708			3.523	0.179
P2A	Zorg en Hoop	1	5	-157.5	02-12-80	29	6.74		750		5.782			0.918	1.186			5.176	0.383
PAR-GR	Paramam	1	2	-27.5	07-10-71		5.5				0.366			0.500	0.052			0.304	0.102
POM	Jonkermanskreek	1	4	-100.0	22-07-95	30.3	7.24	6.79	1238	1112	6.741			6.000	0.123	0.020		7.785	0.281
PR06	Acaribo	1	2	-34.8	13-07-95	26.9	4.91	4.83	10660	10300	119.210			0.163	0.467	0.032		82.818	1.038
PW1	Javaweg	1	2	-50.0	31-12-90	23.9	5.34		330		1.212			1.619	0.437		0.005	1.000	
PW2	Van Hattemweg	1	2	-55.0	31-12-90	24.4	6.18		192		0.592			1.100	0.270		0.001	1.000	
PW3	Einde Javaweg	1	2	-60.0	31-12-90	23.6	6.53		410		1.551			1.439	0.918			1.000	
R2	Republiek	1	2	-22.0		27.1	5.93	5.2	68	66	0.335			0.097	0.031	0.003	0.001	0.223	0.014
R27	Republiek	1	2	-22.0		27.2	5.77	4.73	62	49	0.299			0.084	0.026	0.010	0.000	0.207	0.020
R30	Republiek	1	2	-22.0		26.7	6.48	5.11	69	62	0.335			0.197	0.020	0.001	0.001	0.340	0.024
R5/87	Rijsdijk	1	2	-19.0	15-06-87		6		160		0.400								

Well	Location	Screen	Formation	Depth m	Date	Temp °C	pH-Lab	pH-Fld	EC-Lab µS/cm	Ec-Veld µS/cm	Cl^- mmol/l	Br^- mmol/l	CO_3^{2-} mmol/l	HCO_3^- mmol/l	SO_4^{2-} mmol/l	NO_3^- mmol/l	PO_4-orth mmol/l	Na^+ mmol/l	K^+ mmol/l
S1A/82	Zorg en Hoop	1	5	-166.9	27-06-95	30.5	6.55	5.95	1266	1272	9.675			1.770	0.003	0.085		8.307	0.207
SINI-GR	Sinabo	1	0	-4.0	09-12-80	26.5	7.63		200		0.310			2.655	0.041			0.391	0.076
SINII-GR	Sinabo	1	0	-4.0	09-12-80	27	7.67		210		0.310			2.655	0.041			0.173	0.076
SOM01	Tambaredjo oil field	1	6	-296.5	25-01-85						53.145			6.229	0.385			52.936	
SOM01	Tambaredjo oil field	1	6	-296.5	24-07-95	32	7.56	6.48	4814	4630	40.818	0.0688		7.409	0.438	0.003		39.625	0.342
SOM01	Tambaredjo oil field	1	6	-296.5	01-03-97	34.8	7.52		4347		36.700			7.590	0.094		0.001	33.900	0.465
SOM02	Tambaredjo oil field	1	6	-298.2	19-11-84						35.825			6.639	0.317			40.974	
SOM03	Tambaredjo oil field	1	6	-294.1	19-11-84						23.977			6.229	0.159			29.317	
SOM04	Tambaredjo oil field	1	6	-299.0	28-11-84						37.940			6.245	0.052			45.933	
SOM04	Tambaredjo oil field	1	6	-299.0	21-12-84						37.545			8.049	0.551			36.972	
SOM05	Tambaredjo oil field	1	6	-298.7	12-02-85						36.614			5.573	0.333			32.187	
SOM06	Tambaredjo oil field	1	6	-300.0	28-11-84						50.803			6.819	0.593			54.371	
SOM06	Tambaredjo oil field	1	6	-300.0	25-01-85						49.506			6.311	0.217			52.196	
SOM09	Tambaredjo oil field	1	6	-299.4	12-02-85						6.205			3.950	4.268			12.222	
SOM10	Tambaredjo oil field	1	6	-296.5	28-02-85						34.894			6.459	0.020			31.361	
SOM11	Tambaredjo oil field	1	6	-297.8	28-02-85						40.507			6.885	0.343			37.625	
SOM12	Tambaredjo oil field	1	6	-299.9	19-11-84						27.785			6.295	0.508			35.319	
SOM13	Tambaredjo oil field	1	6	-295.6	19-11-84						36.853		0.033	5.819	0.066			41.017	
SOM16	Tambaredjo oil field	1	6	-298.8	28-11-84						11.311			4.885	0.370			13.614	
SOM16	Tambaredjo oil field	1	6	-298.8	25-01-85						11.678			6.409	0.304			12.483	
SOM18	Tambaredjo oil field	1	6	-301.7	28-11-84						32.891			6.442	0.348			38.668	
SOM22	Tambaredjo oil field	1	6	-296.1	28-02-85						12.270			5.491	2.800			15.745	
SOM-W1	Tambaredjo oil field	1	6	-294.2	28-02-85						4.795			3.950	4.695			11.135	
SWM	Lelydorp	1	2	-63.9	25-04-29		6				1.692				0.426				
T1A	Zorg en Hoop	1	5	-157.5	06-12-80	31	6.99		850		9.026			1.508	0.020			8.003	0.332
T2C/91	Zorg en Hoop	1	4	-122.0	28-06-95	28.9	5.95	5.95	1606	1793	11.706			0.737	1.363	0.001		6.568	0.268
T31	Meerzorg	1	5	-152.5	16-12-80	30	6.36		770		9.590			0.213	0.062			6.220	0.434
TA05	La Prevoyance	1	6	-307.5	28-11-84						81.833			9.098	0.496			72.509	
TAMI-GR	Tamenredjo	1	1	-4.0	09-12-80	29	7.48		310		0.959			2.393	0.406			0.869	0.358
TAMII-GR	Tamenredjo	1	1	-4.0	09-12-80	27.5	7.56		300		1.015			2.393	0.333			1.087	0.358
TLE5	Lelydorp	1	2	-37.5	16-07-95	27.1	5.08	6.03	1836	1818	16.163			0.131	0.148	0.001		8.264	0.204
TO1	Tourtonne	1	0	-1.2	13-02-97		7.25	7.7	15390		159.000			20.570	3.869	0.080	0.048	134.000	2.190
TO11	Tourtonne	1	0	-11.2	13-02-97		7.25	7.8	35000		457.000			20.030	0.701	0.079	0.061	368.000	7.250

Well	Location	Screen	Formation	Depth m	Date	Temp °C	pH-Lab	pH-Fld	EC-Lab µS/cm	Ec-Veld µS/cm	Cl⁻ mmol/l	Br⁻ mmol/l	CO_3^{2-} mmol/l	HCO_3^- mmol/l	SO_4^{2-} mmol/l	NO_3^- mmol/l	PO4-orth mmol/l	Na^+ mmol/l	K^+ mmol/l
TO13	Tourtonne	1	0	-13.2	13-02-97		7.25	7.6	34700		473.000			19.930	0.461	0.101	0.052	355.000	7.000
TO15	Tourtonne	1	0	-15.2	13-02-97		7.25	7.6	34050		443.000			18.210	0.568	0.097	0.031	306.000	5.980
TO17	Tourtonne	1	0	-17.2	13-02-97		7.25	7.7	32460		448.000			16.920	0.559	0.141	0.058	318.000	6.370
TO19	Tourtonne	1	0	-19.2	13-02-97		7.25	7.5	31020		405.000			15.160	0.989	0.131	0.056	324.000	5.450
TO21	Tourtonne	1	0	-21.2	13-02-97		7.25	7.6	29980		377.000			12.760	1.779	0.045	0.045	299.000	5.760
TO23	Tourtonne	1	0	-23.2	13-02-97		7.25	7.5	28700		347.000			14.570	0.625	0.026	0.117	305.000	4.490
TO25	Tourtonne	1	0	-25.2	13-02-97		7.25	7.6	27250		341.000			14.480	0.550	0.029	0.037	323.140	4.450
TO3	Tourtonne	1	0	-3.2	13-02-97		7.31	8.2	14980		143.000			17.120	4.379	0.079	0.160	138.000	3.070
TO5	Tourtonne	1	0	-5.2	13-02-97			8.6			136.000				8.439	0.048	0.026	136.000	3.990
TO7	Tourtonne	1	0	-7.2	13-02-97		7.24	7.6	33530		426.000			18.390	0.379	0.106	0.089	335.000	5.710
TO9	Tourtonne	1	0	-9.2	13-02-97		7.29	7.7	35380		498.000			18.510	1.019	0.067	0.075	349.000	7.420
TT4/91	Tourtonne	1	5	-184.5	17-12-96	32.9	7.07	6.2	1106	1120	7.029			2.720	0.089	0.009	0.003	8.279	0.218
TT4/91	Tourtonne	1	5	-184.5	30-06-95	31.3	7.33	6.37	1138	1236	7.559			3.000	0.058			8.046	0.187
W02	Tambaredjo oil field	1	6	-299.0	03-01-97	34	7.55	6.58	1437	1425	8.920			5.600	0.063		0.002	11.700	0.266
W1	Zorg en Hoop	1	5	-157.5	06-12-80	31	7.03		540		5.359			1.442	0.166			5.263	0.230
W-10	Paranam	1	2	-30.0	20-03-95	27.7	5.3		99		0.493			0.149		0.009		0.500	0.018
W-3A	Paranam	1	2	-30.0	20-03-95	26.9	5.1		117		0.699			0.237				0.643	0.020
W-5A	Paranam	1	2	-30.0	20-03-95	28.2	4.9		122		0.753			0.178				0.674	0.018
WWCS	Tambaredjo oil field	1	4	-107.0	24-07-95	30.5	6.97	6.5	1674	1610	4.541			3.737	4.779	0.604		10.265	0.416
WWSM	Tambaredjo oil field	1	5	-155.5	24-07-95	30.1	7.43	6.98	910	801	1.906			4.065	1.822	0.161		6.437	0.248
ZOR-GR	Zorg en Hoop	1	5	0.5	15-02-72		6.2				2.313			1.500	0.708			3.523	0.179
ZOR-GR	Zorg en Hoop	1	5	0.5	31-12-82	31	6.2		940		7.503			1.262	0.145	0.037		6.785	0.281
ZV1-2/90	Vierkinderen	1	2	-34.3	31-12-90	23.6	6.44		720		7.165			1.200	0.134		0.011	7.916	0.173
ZV1-2/90	Vierkinderen	2	2	-12.3	25-08-95	32.3	6.54	6.03	80	80	0.136	0.0003		0.644	0.016	0.003	0.004	0.170	0.017
ZV1-2/90	Vierkinderen	1	2	-34.3	25-08-95	32.1	7.14	7.05	1019	1017	6.420	0.0119		2.880	0.036	0.008	0.022	6.819	0.235
ZV5/87	Matta	1	2	-14.0	14-04-87	25	6		130		0.400								
Samples with incomplete analyses and electro-neutrality error > 10 %																			
0/150O	Kabo	1	2	-7.5	01-06-83		3.84		89		0.040				0.009	0.299		0.028	0.029
0/200W	Kabo	1	2	-7.5	01-06-83		6		16		0.032			0.022	0.015	0.021		0.037	0.009
0/400O	Kabo	1	2	-7.5	01-06-83		5.95		24		0.103			0.021	0.023	0.005		0.087	0.004
1/69	Stolkslust	1	3	-87.2	6/111971		8.1				4.231			0.100	2.019			3.740	2.838
1/69	Stolkslust	2	2	-62.5	6/111971						5.190				2.061				
1/69	Stolkslust	3	2	-43.7	6/111971						17.884				1.999				

Well	Location	Screen	Formation	Depth m	Date	Temp °C	pH-Lab	pH-Fld	EC-Lab µS/cm	Ec-Veld µS/cm	Cl⁻ mmol/l	Br⁻ mmol/l	CO_3^{2-} mmol/l	HCO_3^- mmol/l	SO_4^{2-} mmol/l	NO_3^- mmol/l	PO4-orth mmol/l	Na^+ mmol/l	K^+ mmol/l
1/70	Tout Lui Faut	1	5	-143.9	30-06-71						3.864								
1/82	Haarlem	1	4	-111.0	31-12-82	28	6.2		1500		0.705			3.278	0.187	0.001	0.007	22.183	0.332
1/82	Haarlem	3	2	-47.0	31-12-82	28	6.7		250		0.507			1.803	0.010	0.001	0.055	2.914	0.109
1000 N	Republiek	1	2	-11.6	28-02-30		5.5				0.169								
1000 S	Republiek	1	2	-8.6	19-03-30		5				0.169								
11/72	Mainroad/Coropina Cr.	1	2	-16.5	25-04-72		6							0.200				1.609	0.104
13/71	Morico West	1	3	-79.4	09-12-80	27	7.31		780		5.641			2.655	0.864			4.915	0.537
13/71	Morico West	1	3	-79.4	28-07-71						5.641			1.100	1.665				
14/72	Rijsdijk	1	2	-34.5	02-08-72		8.1				0.451		0.024	1.500				0.652	0.102
15/71	Rijsdijk	1	2	-19.9	09-07-71						0.789			0.800	0.083				
1500 W	Republiek	1	2	-15.7	03-02-30		5				0.143								
2/69	Houttuin	2	2	-27.1	02-06-71						35.937				0.708				
2/70	Groningen	1	4	-132.9	20-07-71		6.4				2.228		0.049	1.600				5.089	0.230
2/70	Groningen	2	3	-85.4	20-07-71						64.680								
2/72	Pierre Kondre	1	2	15.9	18-02-72		4.3							0.200				0.160	0.104
2/85	Rijsdijk	1	2	-42.8	31-12-90	27.3	6.05		125		1.410			0.560	0.121		0.002	0.739	0.020
22/89	Spoil Area	1	3	-66.8	31-12-90	27	6.5		950		2.002			2.295	0.056			1.522	0.145
24/72	Cobitie	1	2	-10.0	22-08-72		6						1.499					0.347	0.102
28/71	De Craneweg	1	2	-43.2	26-08-71		5.7				1.071			0.900	0.270			1.522	0.102
3	Mudlake SURALCO	1	1	-9.4	15-03-95	27.3	6.5		2510		6.713			5.316				13.049	0.654
3/70	Tamanredjo	1	2	-23.7	03-08-71		8.3				24.005				1.436				
3/71	Rijsdijk	3	2	-29.0	19-04-71		6				0.789		0.099	1.500	0.052			0.565	0.102
3/88	Rijsdijk	1	3	-68.2	31-12-90	23.9	6.52		492		1.438			1.409				2.696	0.076
30/71	Caroline	1	2	-0.9	27-09-71		6				0.620			0.300	0.270			5.654	0.281
32/71	De Craneweg	1	2	-49.0	08-10-71		6.9				0.761			1.500	0.697			1.478	0.102
34/71	Carolina	1	2	-0.1	22-10-71		5.4				0.112			0.100	0.104			0.130	0.102
39/71	Powakka	1	2	3.0	05-11-71		6.4				6.544			1.700	0.104				
4/670W	Kabo	1	2	-7.5	04-06-81		7.51		108		0.150			0.766	0.005			0.371	0.016
44/71	Siddosdleweg	1	2	-40.7	30-12-71		6.5				0.479			1.400	0.593			1.304	0.127
48/71	Powakka West	1	2	9.1	29-12-71		5.1				0.169			0.100				0.287	0.104
48/71	Powakka West	1	2	9.1	31-12-90	24.8	5.45		24		0.197			0.120			0.001		
5/70	Leiding 9a	1	3	-91.8	20-10-70						3.849								
5/70	Leiding 9a	2	3	-71.2	20-10-70		8.5				3.921				1.915				

Well	Location	Screen	Formation	Depth m	Date	Temp °C	pH-Lab	pH-Fld	EC-Lab µS/cm	Ec-Veld µS/cm	Cl⁻ mmol/l	Br⁻ mmol/l	CO_3^{2-} mmol/l	HCO_3^- mmol/l	SO_4^{2-} mmol/l	NO_3^- mmol/l	PO4-orth mmol/l	Na^+ mmol/l	K^+ mmol/l
							5.7				1.523			0.459		0.003	0.027	1.391	0.179
5/82	North of Coropina Cr.	2	2	-32.2	10-12-82		5.5				0.409								
500 SW	Republiek	1	2	-13.3	28-02-30		7				11.283				0.333				
6/70	Meerzorg	1	6	-228.9	09-10-70		5.4				0.211			0.400	0.031				
6/71	Zanderij Matta	1	2	-2.4	02-08-71		3.7				0.930			0.300				0.130	0.102
7/71	Zanderij Matta	1	2	5.9	02-08-71		6.5				2.905		0.199	1.200	0.218				
8/70	Magenta-Weigedacht C	1	5	-125.1	31-12-70		7.36	5.84	1011	860	6.375			3.196	0.017	0.006		4.201	0.147
8/70 7	Koewarasan	1	5	-125.1	07-07-95	29.6	6.9				5.782		0.199	3.900	1.239				
9/70	Morico	1	4	-108.2	31-12-70		5.02		35		0.310			0.550			0.001		
9/71	Matta	1	2	-6.3	31-12-90	25.8	6				0.535			0.200				0.521	0.102
BIL-GR	Billiton	1	2	-22.5	08-10-71		6.35	4.51	40	19	0.138				0.009	0.035	0.000	0.061	0.001
BVB	Berlijn (bron)	1	2	-0.5		26.1	4.53	3.87	40	23	0.096				0.053	0.008	0.000	0.080	0.006
BVC	Carolina (bron)	1	2	-0.5		28.7	8.7				2.905		0.199	5.000	0.031			1.478	0.191
C6	Calcutta	1	6	-197.5	15-01-72		5.6				0.169			0.100	0.156			0.260	0.102
CENTRE	Republiek	1	2	-10.6	13-10-71		6.9				1.974				0.728				
GMD 37	Santa Boma	1	4	-133.5	29-08-70		6		150		0.600								
H1/87	Highway (S. of Paranam	1	2	-14.3	07-07-87		5.4		44		0.141			0.280	0.232		0.037	1.652	0.012
H1-2/90	Airport Zanderij	1	2	-24.3	31-12-90	26.5	7.51	6.7	3337	3290	26.300			7.880	0.385		0.002	24.300	0.371
H17	Tamanredjo	1	6	-276.0	03-01-97	34.5	6		90		0.401								
H2/87	Highway (S. of Paranam	1	2	-16.5	15-04-87		6.59		213		0.592			0.890			0.007	2.218	0.033
H3/87	Highway (S. of Paranam	1	2	-12.8	31-12-90	26.8	6.3		220		0.600								
H3/87	Highway (S. of Paranam	1	2	-12.8	15-04-87		6.4		272		0.959			1.655	0.706		0.001	2.044	0.089
H3/90	Highway (S. of Paranam	1	2	-8.8	31-12-90	24.9	6		420		3.404								
H4/87	Highway (S. of Paranam	1	2	-40.0	12-05-87		4.55		80		0.225			0.419	0.106		0.001	1.000	
H4-5/90	Highway (S. of Paranam	1	2	-27.3	31-12-90	26.4	5.14		100		0.225			0.760	0.259		0.001		
H4-5/90	Highway (S. of Paranam	2	2	-12.3	31-12-90	26.3	6		40		0.400								
H5/87	Highway (S. of Paranam	1	2	-16.0	12-05-87		6		85		0.400								
H6/87	Highway (S. of Paranam	1	2	-16.0	15-04-87		6				0.400			0.300		0.002	0.004	0.542	0.369
HP1/87	Highway (S. of Paranam	1	2	-17.8	13-04-87	25.6	6				61.400			3.950	16.599	0.040	0.069	62.800	1.470
KW8	Koewarasan	1	0	-6.2	20-02-97		7.2	8.6			0.874			3.180	0.265		0.003	4.175	0.081
L10-14/0	Van Hattemweg West	1	4	-105.0	31-12-90	24.8	6.62		453		0.959			2.639	0.372		0.366	4.001	0.076
L10-14/0	Van Hattemweg West	2	3	-91.0	31-12-90	24.6	6.54		449		0.846			2.524	0.306		0.329	3.392	0.071
L10-14/0	Van Hattemweg West	4	2	-58.0	31-12-90	25.2	6.33		421		0.592			1.803	0.250		0.054	0.739	0.025
L10-14/0	Van Hattemweg West	5	2	-34.0	31-12-90	24.2	6.18		255										

Well	Location	Screen	Formation	Depth m	Date	Temp °C	pH-Lab	pH-Fld	EC-Lab µS/cm	Ec-Veld µS/cm	Cl⁻ mmol/l	Br⁻ mmol/l	CO_3^{2-} mmol/l	HCO_3^- mmol/l	SO_4^{2-} mmol/l	NO_3^- mmol/l	PO4-orth mmol/l	Na^+ mmol/l	K^+ mmol/l
L16-19/0	Van Hattemweg West	1	3	-78.0	31-12-90	24.8	5.67		900		0.169			0.557	0.142			1.000	0.200
L22-23/0	Santigron	2	2	-44.0	31-12-90	24.9	6.28		375		0.959			2.377	1.436		0.218	2.000	
L24-25/0	Van Hattemweg	2	2	-39.0	31-12-90	25.9	6.19		334		1.156			1.704	0.397		0.004	1.000	
L26-27/0	Indihra Ghandi weg	2	2	-36.0	31-12-90	23.1	6.39		183		1.410			0.071	2.519	0.005	0.001		
L26-27/0	Indihra Ghandi weg	1	2	-59.0	31-12-90	22.8	6.07		149		1.692			0.070	1.207	0.001	0.001		
L3-4/90	Van Hattemweg	1	2	-61.7	31-12-90	25.7	6.02		305		1.184			1.560	0.020		0.004	2.044	0.056
L7-8/90	Van Hattemweg West	2	2	-36.3	31-12-90	24.9	6.32		268		0.874			0.839	0.185		0.025		
O21	Tambaredjo oil field	1	6	-300.5	03-01-97	34.4	7.2	6.5	3903	4140	31.900			8.140	0.096		0.002	28.100	0.435
R14	Republiek	1	2	-22.0		27.1	5.05	4.61	54	48	0.146			0.034	0.049	0.003	0.001	0.167	0.013
R19	Republiek	1	2	-22.0		27.1	6.11	5.3	47	43	0.203			0.138	0.044	0.005	0.001	0.310	0.016
R2/87	Rijsdijk	1	2	-36.5	10-05-87		6		157		13.018								
R3/87	Rijsdijk	1	2	-32.5	10-05-87		6.1		185		0.400								
R7	Republiek	1	2	-22.5	18-12-96	26.7	6.51	5.3	44	26	0.198			0.241	0.057	0.007		0.145	
REP-GR	Republiek	1	2	0.5	31-12-82	26	5.6		44		0.112			0.144	0.052			0.287	0.030
RP1/87	Rijsdijk	1	2	-32.5	03-08-87	26.2	6.41				0.400			0.095		0.001	0.006	0.556	0.056
SL1/87	Railroad (N. of Republik	1	2	-13.0	13-05-87		6		100		1.001								
SL2/87	Railroad (N. of Republik	1	2	-16.0	13-05-87		6.1		480		2.803								
SL3/87	Railroad (N. of Republik	1	2	-24.0	31-12-90	25.2	6.46		295		1.297			1.770	0.032		0.010	1.913	0.061
SL3/87	Railroad (N. of Republik	1	2	-24.0	13-05-87		6		340		1.401								
SOM07	Tambaredjo oil field	1	6	-292.0	19-11-84						8.236			4.639	0.613			21.444	
SW3	Van Hattemweg	1	1	-4.5	31-12-90	23.8	5.4		108		0.338			0.390	0.105	0.301	0.001		0.100
SWM	Lelydorp	3	2	-30.3	06-04-29		6.5				0.220								
SWM	Lelydorp	2	2	-48.5	22-04-29		6.5				0.818				0.124				
T-6	Paranam	1	2	-29.5	20-03-95	26.6	5.9		480		0.163			1.309				2.392	0.071
ZV1/87	Matta	1	2	-18.0	14-04-87		6		85		0.400								
ZV1/87	Matta	1	2	-18.0	31-12-90	26.4	5.64		38		0.253			1.737					
ZV1-2/90	Vierkinderen	2	2	-12.3	31-12-90	26.6	5.28		60		0.338			0.380	1.301		0.024	0.695	0.017
ZV2/87	Matta East	1	2	-19.0	09-05-87		6		45		0.400								
ZV3/87	Matta	1	2	-18.0	31-12-90	26.8	5.41		68		0.535			0.239				0.347	0.023
ZV3/87	Matta	1	2	-18.0	08-07-87		6		95		0.600								
ZV4/87	Matta	1	2	-13.0	14-04-87		6		70		0.400								
ZV6/87	Matta	1	2	-30.0	14-04-87		6		90		0.400								
ZVP1/87	Matta	1	2	-18.3	19-08-87	25.5	5.22				0.200			0.213			0.001	0.034	0.186

Well	Location	Screen	Formation	Depth m	Date	Temp °C	pH-Lab	pH-Fld	EC-Lab µS/cm	Ec-Veld µS/cm	Cl⁻ mmol/l	Br⁻ mmol/l	CO_3^{2-} mmol/l	HCO_3^- mmol/l	SO_4^{2-} mmol/l	NO_3^- mmol/l	PO_4-orth mmol/l	Na^+ mmol/l	K^+ mmol/l
ZVP1/87	Matta	1	2	-18.3	22-04-87	25	6				0.400			0.200	0.095		0.001	0.177	0.014
Samples with only isotope analyses																			
15/72	Rijsdijk	1	2	-30.5	10-07-72														
1500 W	Republiek	1	2	-15.7	10-07-72														
16/72	Rijsdijk South	1	1	-22.0	27-07-72														
19/72	Rijsdijk East	1	2	-38.5	18-07-72														
20/72	Rijsdijk East	1	2	-31.5	18-07-72														
21/72	Rijsdijk East	1	1	-18.5	18-07-72														
3/82	Meursweg	1	3	-68.0	31-12-90														
3/89	Rijsdijk North	1	3	-66.0	31-12-90														
3/91	Helena Christinaweg	1	5	-134.0	31-12-90														
7/71	Zanderij Matta	1	2	5.9	14-07-72														
9/71	Matta	1	2	-6.3	14-07-72														
ALL-GR	Alliance	1	4	-105.5	11-05-71														
BIL-GR2	Onverdacht	1	2	-32.5	08-10-71														
BIL-GR2	Onverdacht	1	2	-32.5	29-03-72														
GMD-19	Uitvlugt	1	5	-159.2	22-03-72														
GMD-2	Kampong Baroe	1	4	-126.2	19-10-71														
KW7.5	Koewarasan	1	1	-7.7	15-12-96														
L19/90	Van Hattemweg West	1	1	-4.3	31-12-90														
L6/86	Leysweg	1	5	-163.0	31-12-90														
L6A/80	Leysweg	1	5	-163.0	31-12-90														
PAR-5	Paranam	1	2	-25.5	07-10-71														
PAR-7	Paranam	1	2	-25.5	07-10-71														
REP-GR	Republiek	1	2	0.5	07-10-71														
REP-TOT	Republiek	1	2	-20.0	13-10-71														
REP-TOT	Republiek	1	2	-20.0	12-07-72														
SW4	Van Hattemweg	1	1	-4.5	31-12-90														

Well	Ca^{2+} mmol/l	Mg^{2+} mmol/l	Sr^{2+} mmol/l	Fe-tot mmol/l	Mn-tot mmol/l	Al-tot mmol/l	NH_4^+ mmol/l	SiO_2 mmol/l	CO_2 mmol/l	TIC-Cal mmol/l	Σ-Anions mmol/l	Σ-Kations mmol/l	Error %	$\delta^{18}O$ ‰	$\delta^{2}H$ ‰	$\delta^{13}C$ ‰	^{14}C %(pmc)	^{3}H TU	$\delta^{37}Cl$ ‰	$^{87}Sr/^{86}Sr$
Samples with analyses of all macroions and electro-neutrality error < 10 %																				
0/200O	0.096	0.065		0.004	0.002			0.046		0.074	0.466	0.486	-2.10							
0/200O	0.012	0.016		0.002	0.001			0.011		0.100	0.183	0.179	1.10							
0/200W	0.011	0.013		0.003	0.002			0.053		0.039	0.141	0.170	-9.33							
0/280O	0.010	0.012		0.003	0.002					0.039	0.183	0.187	-1.08							
0/280O	0.008	0.008		0.002	0.001			0.008		0.129	0.199	0.178	5.57							
0/400O	0.012	0.017		0.004	0.002		0.002	0.113		0.092	0.179	0.203	-6.28							
0/400W	0.003	0.027		0.003	0.001			0.074		0.128	0.469	0.416	5.99							
0/400W	0.015	0.021		0.004	0.002			0.099		1.292	0.362	0.315	6.94							
0/500O	0.026	0.007		0.003	0.002		0.002	0.015		0.101	0.170	0.176	-1.73							
0/500O	0.015	0.011		0.002	0.001		0.001	0.052		0.114	0.300	0.272	4.90							
0/700W	0.015	0.012		0.005	0.002			0.206		0.129	0.242	0.262	-3.97							
0/700W	0.008	0.019		0.002	0.001			0.042		0.061	0.169	0.171	-0.59							
0/900W	0.010	0.008		0.004	0.002			0.050		0.021	0.255	0.258	-0.59							
0/900W	0.019	0.020		0.002	0.001			0.060		0.085	0.515	0.457	5.97							
1/72	0.149	0.329		0.071	0.003					1.832	2.359	2.423	-1.34							
1/76	0.148	0.411		0.078					0.204	1.548	5.061	5.246	-1.79							
1/82	0.192	0.246		0.062	0.005		0.017	0.199	0.136	2.585	3.673	3.979	-4.00	-2.55	-10.3					
1/82	1.120	1.893		0.200	0.018		0.034	0.470		3.362	21.015	20.805	0.50							
1/88	0.204	0.380		0.080	0.003		0.041	0.188	2.204	3.162	2.856	3.093	-3.98	-2.77			10.1			
10/70	0.374	0.905		0.180						2.731	11.391	12.786	-5.77							
10/71	0.299	1.358		0.268	0.003					2.204	8.336	9.917	-8.66							
10/71	0.374	0.905		0.180						2.749	11.391	12.786	-5.77	-2.80				1.7		
11	0.147	0.493		0.118	0.004	0.003		0.324		4.681	8.203	8.048	0.95							
11/73	0.149	0.534		0.084					0.136	1.630	5.723	5.983	-2.22							
12	0.471	1.810		0.358	0.003	0.003		0.214		7.183	23.584	23.556	0.06							
12/72	0.149	0.411		0.039	0.008					1.492	6.122	6.796	-5.22							
13	0.339	2.304				0.003				28.951	58.998	50.205	8.05							
13/72	0.189	0.177		0.076	0.007		0.016	0.267	2.022	4.243	2.385	1.997	8.85	-2.80				0.6		
14	0.955	1.316				0.003				15.533	25.999	25.578	0.82							
14/72	1.167	0.079		0.001	0.001		0.016	0.237	0.659	2.803	4.086	3.450	8.44	-2.37						

Well	Ca^{2+} mmol/l	Mg^{2+} mmol/l	Sr^{2+} mmol/l	Fe-tot mmol/l	Mn-tot mmol/l	Al-tot mmol/l	NH_4^+ mmol/l	SiO2 mmol/l	CO2 mmol/l	TIC-Cal mmol/l	Σ-Anions mmol/l	Σ-Kations mmol/l	Error %	$\delta^{18}O$ ‰	$\delta^{2}H$ ‰	$\delta^{13}C$ ‰	^{14}C %(pmc)	^{3}H TU	$\delta^{37}Cl$ ‰	$^{87}Sr/^{86}Sr$
15	0.818	2.469				0.003				17.661	38.237	39.400	-1.50							
16/71	0.149	0.576		0.256	0.007					2.904	6.706	7.331	-4.45							
17/71	1.472	4.238		0.089	0.040					1.408	20.171	19.844	0.82	-2.60		-18.10	16.8	2.3		
18/69	0.239	0.207		0.116	0.036		0.027	0.369	1.522	0.751	3.628	4.190	-7.19							
2/69	0.174	0.781		0.130	0.001					1.553	6.511	6.718	-1.56	-3.10		-21.60	9	1.5		
2/87	0.738	1.609		0.209	0.011	0.001	0.052			4.615	8.443	7.803	3.94	-2.54	-11.8	-15.43				
21/71	0.548	0.946		0.039						2.677	4.675	5.040	-3.76							
21/73	0.229	1.255		0.177	0.009		0.038	0.277	2.681	2.406	6.666	5.986	5.37							
22/71	2.844	6.090		0.537	0.058					5.235	52.320	55.265	-2.74							
22/72	0.299	0.370		0.039						1.652	2.068	2.300	-5.31							
23/71	0.299	0.452		0.119	0.001					5.000	3.305	3.706	-5.72	-2.70		-16.40	18.9			
25/71	0.174	0.288		0.053						1.130	2.340	2.592	-5.11							
25/72	0.105	0.251		0.023	0.001	0.002	0.072			3.747	3.824	3.460	5.00	-3.00	-13.6	-19.07	7.6			
25/72	0.149	0.370		0.012	0.001					1.704	3.956	3.384	7.79							
26/71	0.099	0.164		0.161	0.005					4.295	1.852	1.952	-2.63							
29/71	0.673	0.576		0.007	0.007					0.878	3.779	4.375	-7.31			-17.76	21.2			
3/71	0.159	0.246		0.044	0.001					1.237	2.722	2.702	0.37	-2.70						
3/71	0.129	0.197		0.096	0.003		0.003	0.216	0.840	2.180	2.208	1.927	6.80	-2.80		-19.20	57.9	2.3		
3/71	0.062	0.465		0.089	0.002					2.968	7.075	7.179	-0.73							
3/82	0.135	0.209		0.119	0.003		0.017	0.536		2.506	3.065	2.521	9.74	-2.90	-13.9	-16.10	55.4	0.1		
3/82	2.744	6.502		0.383	0.205	0.005	0.110	0.591		1.561	58.728	55.531	2.80	-2.93	-12.4	-15.25	19.2			
3/91	0.147	0.507	0.002	0.097	0.004	0.003	0.053			6.076	5.059	4.965	0.94	-2.37	-12.8	-19.68	20.5		-0.096	
3/91	0.144	0.440		0.078	0.002	0.001	0.047	0.536		5.375	5.568	4.934	6.04	-2.79	-14.3	-20.42	15.2			0.710757
3/93	0.596	3.139		0.216	0.019	0.001	0.088	0.680		7.161	13.500	12.021	5.80	-2.75	-12.6	-16.23	14.8			
31/71	0.087	1.028		0.032	0.007					1.096	4.534	4.934	-4.22	-2.60		-18.80	17			0.710358
31/71	0.610	2.570	0.006	0.443	0.028	0.010	0.089	0.793		0.893	11.428	12.240	-3.43	-2.58	-12.0	-10.85	20.82			
31/71	0.251	2.502		0.463	0.024	0.001	0.094			2.954	12.719	11.582	4.68	-2.62	-12.9	-18.09				
31/82	1.067	2.168		0.222	0.015	0.001	0.077			3.380	10.137	10.056	0.39	-2.43	-8.9	-14.00	16.9			0.709316
31/82	1.069	2.120	0.006	0.241	0.020	0.017	0.048	0.936		4.273	10.179	9.804	1.88	-2.20	-11.6	-13.95			-3.571	
33/71	1.122	3.662		0.048	0.005					0.742	15.639	15.515	0.40							
35/71	0.374	0.740		0.014	0.007					1.980	4.199	3.894	3.77	-3.20				1		
36/71	0.199	0.534		0.094	0.003					1.825	6.759	6.667	0.69	-3.30		-19.30	20.3	0.6		
38/71	0.232	0.473		0.005						1.563	3.021	2.959	1.04							

Well	Ca^{2+} mmol/l	Mg^{2+} mmol/l	Sr^{2+} mmol/l	Fe-tot mmol/l	Mn-tot mmol/l	Al-tot mmol/l	NH_4^+ mmol/l	SiO2 mmol/l	CO2 mmol/l	TIC-Cal mmol/l	Σ-Anions mmol/l	Σ-Kations mmol/l	Error %	$\delta^{18}O$ ‰	$\delta^{2}H$ ‰	$\delta^{13}C$ ‰	^{14}C %(pmc)	^{3}H TU	$\delta^{37}Cl$ ‰	$^{87}Sr/^{86}Sr$
4	1.571	13.168		0.150	0.002	0.003		0.819		37.860	175.433	177.287	-0.53							
4/670W	0.022	0.013		0.004	0.002		0.015	0.032		0.128	0.195	0.204	-2.26							
4/670W	0.022	0.022		0.002	0.001		0.016			0.123	0.269	0.236	6.53							
4/70	1.097	2.469		0.286	0.020					3.095	9.475	10.370	-4.51	-2.50		-17.60	17			
4/71	0.523	1.440		0.143	0.009					4.795	14.343	14.200	0.50							
4/82	0.424	0.905		0.137	0.012		0.045	0.019	3.272	6.828	8.055	7.964	0.57							
4/82	0.449	0.781		0.005	0.007		0.037	0.126	0.522	1.675	12.112	11.674	1.84							
4/82	0.399	0.699		0.017	0.004		0.002	0.151	0.590	1.594	6.086	5.839	2.07							
4/88	0.299	0.563		0.070	0.010		0.109	0.234	2.727	3.940	3.174	3.256	-1.28	-2.85						
4/89	0.339	0.261		0.097			0.019	0.033		3.365	5.025	4.418	6.43	-2.56						
40/71	0.214	0.493		0.047	0.001					1.864	6.210	6.146	0.52							
41/71	0.174	0.444		0.071	0.001					1.630	5.321	5.399	-0.73							
42/71	0.074	0.123		0.053						0.739	0.653	0.797	-9.93							
5	0.611	5.761		0.037		0.007		1.070		41.247	106.794	105.593	0.57							
5/82	0.239	0.329		0.034	0.002		0.007	0.166	2.272	2.713	2.560	2.984	-7.65							
5/82	0.299	0.362		0.014	0.004		0.008	0.149	1.590	2.219	3.859	4.302	-5.43							
5/89	0.548	0.868		0.186	0.009		0.045	0.264	2.931	6.019	7.528	7.081	3.06	-2.91						
5/90	0.264	0.765		0.001	0.002	0.001	0.210	0.488		2.537	7.509	6.971	3.72							
6/200W	0.263	0.173		0.002	0.001	0.002		0.843		1.392	1.558	1.465	3.08							
6/400O	0.031	0.018		0.003	0.002			0.051		0.059	0.198	0.212	-3.42							
6/400O	0.016	0.014		0.002	0.001	0.000	0.004	0.022		0.084	0.177	0.175	0.57							
6/400W	0.016	0.029		0.003	0.001		0.007	0.053		0.148	0.256	0.280	-4.48							
6/400W	0.016	0.054		0.002	0.001	0.005		0.054		0.436	0.307	0.329	-3.46							
6/600W	0.022	0.011		0.003	0.001			0.067		0.075	0.257	0.309	-9.19							
6/600W	0.009	0.015		0.002		0.000	0.008			0.121	0.323	0.292	5.04							
6/72	0.249	1.275		0.035	0.001					3.515	18.390	19.313	-2.45							
6/82	0.474	1.234		0.007	0.012		0.036	0.432	4.545	6.107	7.979	7.913	0.42							
6/89	0.618	1.176		0.207			0.031	0.056		4.068	12.151	12.787	-2.55							
6/CENT	0.034	0.044		0.003	0.002			0.151		0.188	0.314	0.326	-1.88							
6/CENT	0.022	0.029		0.001	0.001	0.001		0.153		0.185	0.276	0.231	8.88							
6A	3.193	9.465		1.217	0.036	0.014		0.264		15.970	112.088	103.199	4.13							
7/72	0.354	1.016		0.019	0.003					5.692	13.507	14.515	-3.60							
7/79	0.351	1.106		0.533	0.012	0.003	0.026	0.584		1.327	7.611	7.950	-2.18	-3.01	-15.7	-18.33	81.7	0.53		

Well	Ca^{2+} mmol/l	Mg^{2+} mmol/l	Sr^{2+} mmol/l	Fe-tot mmol/l	Mn-tot mmol/l	Al-tot mmol/l	$NH4^{+}$ mmol/l	SiO2 mmol/l	CO2 mmol/l	TIC-Cal mmol/l	Σ-Anions mmol/l	Σ-Kations mmol/l	Error %	$\delta^{18}O$ ‰	$\delta^{2}H$ ‰	$\delta^{13}C$ ‰	^{14}C %(pmc)	^{3}H TU	$\delta^{37}Cl$ ‰	$^{87}Sr/^{86}Sr$
7/82	0.573	1.687		0.028	0.012		0.036	0.183	0.386	1.105	7.754	8.691	-5.70							
7/82	0.548	1.234		0.196	0.015		0.038	0.199	0.954	1.256	8.114	8.434	-1.93							
7A	3.655	11.522		1.611	0.013	0.022		0.427		4.896	136.402	144.697	-2.95							
8	1.035	9.053		0.075		0.003		0.890		33.813	138.290	135.476	1.03							
8/72	0.124	0.740		0.071	0.004					1.106	9.943	8.289	9.07							
8/82	0.399	0.987		0.153	0.007		0.016	0.466	0.522	1.130	5.874	6.280	-3.34							
B1	0.481	2.226		0.032	0.013	0.004	0.121	0.353		3.936	16.653	16.811	5.19	-3.09	-17.4	-10.50	6.1			
BL1A/91	0.321	0.514				0.001	0.066	0.239		5.016	12.770	12.205	2.26	-3.00	-14.7					
C10	0.199	0.576		0.082					0.250	1.433	6.199	6.163	0.29							
D3A/72	0.106	0.322		0.072	0.001	0.001	0.050	0.243		4.225	5.691	5.360	3.00	-2.91	-14.4	-20.82	8.2		1.1895	
E1	0.249	0.823		0.098					0.250	1.585	10.672	10.171	2.40							
EBS	0.481	0.013		0.010	0.000	0.006	0.027	0.087		0.000	1.320	1.243	3.01							
GMD 22	0.424	1.769		0.019	0.018					3.385	8.198	9.360	-6.62							
GMD 28	0.673	1.769		0.007	0.002					7.209	16.281	15.644	2.00							
GMD 7	0.249	0.576		0.014	0.005					1.798	6.778	7.058	-2.02							
GMD D1	0.177	0.617		0.053	0.003					1.771	6.262	6.476	-1.68	-3.40				0.9		
H1/87	0.009	0.069		0.207			0.020		4.590	2.519	0.695	0.597	7.59							
H1-2/90	0.089	0.009		0.082	0.009		0.012	0.334	1.272	1.033	0.821	0.747	4.72	-1.74						
HOY	0.036	0.044		0.022		0.017	0.009	0.104		0.555	0.442	0.374	8.33	-1.36	-6.9					0.712877
JHG	1.307	7.777		0.350	0.040	0.001	0.110	0.947		4.419	40.248	35.486	6.29	-2.50	-10.1	-17.39	16.3			
KW1	11.600	16.300	0.105	0.230	0.202	0.313	0.239	0.832		4.064	93.784	85.554	4.59	-3.06	-17.0					0.709999
KW11	2.900	0.627	0.021	0.057	0.010	0.100	0.589	0.212		2.117	92.392	77.457	8.79	-2.55	-10.9	-15.96				
KW12	4.819	8.990	0.023	0.024	0.023	0.033	0.393	0.123		3.001	90.094	84.666	3.11	-2.35	-7.7				1.193	
KW16	5.619	7.880	0.034		0.030	0.061	0.373	0.064			100.570	94.561	3.08	-2.85	-9.9					
KW17	3.950	6.000	0.030	0.020	0.090	0.050	0.594	0.198		1.561	86.257	71.470	9.38	-4.79	-30.5				0.3675	
KW19	5.909	18.300	0.043	0.054	0.301	0.070	0.725	0.538		0.826	86.747	99.210	-6.70	-2.88	-10.9	-10.01				
KW3	8.309	22.900	0.248	0.537	0.061	0.209	0.219	3.770		5.636	120.085	106.393	6.05	-2.79	-13.2	-23.04				0.709496
KW9	4.419	15.300	0.084	0.084	0.718	0.386	0.597	0.477		0.000	87.653	78.986	5.20	-4.52	-32.6					
L1/91	0.916	3.690	0.005	0.001	0.002	0.005	0.077	0.276		2.612	14.452	14.789	-1.15	-2.32	-11.8	-17.88				
L10-14/0	0.329	0.296		0.088	0.036		0.017	0.379	1.818	5.814	4.766	4.132	7.13	-2.71		-16.80	45.5	3.8		
L1-2/90	0.209	0.325		0.087	0.005		0.078	0.271	2.090	4.729	2.940	2.854	1.48							
L15/90	0.738	0.355		0.207	0.025		0.006	0.266	3.772	32.349	4.025	4.476	-5.31							
L16-19/0	0.748	0.316		0.225	0.014		0.007	0.279	6.227	16.966	3.275	3.062	3.36							

Well	Ca^{2+} mmol/l	Mg^{2+} mmol/l	Sr^{2+} mmol/l	Fe-tot mmol/l	Mn-tot mmol/l	Al-tot mmol/l	$NH4^{+}$ mmol/l	SiO2 mmol/l	CO2 mmol/l	TIC-Cal mmol/l	Σ-Anions mmol/l	Σ-Kations mmol/l	Error %	$\delta^{18}O$ ‰	$\delta^{2}H$ ‰	$\delta^{13}C$ ‰	^{14}C %(pmc)	^{3}H TU	$\delta^{37}Cl$ ‰	$^{87}Sr/^{86}Sr$
L16-19/0	1.297	0.514		0.173	0.014		0.016	0.059	8.227	19.045	4.944	5.669	-6.83							
L16-19/0	1.117	0.514		0.205	0.016		0.017	0.316	7.772	27.909	4.918	5.552	-6.06							
L20/90	0.299	0.138		0.114	0.007		0.017	0.249	3.909	4.160	1.756	1.541	6.52	-1.98	-2.9					
L22-23/0	0.369	0.375		0.051	0.010		0.036	0.299	2.000	2.867	3.798	3.746	0.69							
L24-25/0	0.289	0.276		0.076	0.001		0.036	0.221	1.909	3.724	3.659	3.320	4.86							
L28/90	0.494	1.020		0.156	0.010		0.090	0.567	2.886	2.482	5.714	5.550	1.46							
L3-4/90	0.399	1.037		0.153	0.007		0.030	0.344	4.318	6.540	4.654	4.549	1.14							
L5-6/90	0.459			0.078	0.007		0.026	0.327	2.909	1.680	1.961	2.284	-7.61							
L5A/79	0.336	1.037		0.067	0.004	0.001	0.077	0.278		4.865	10.705	9.954	3.64							
L5C/80	0.536	2.185		0.254	0.018	0.001	0.077	0.613		5.629	9.452	9.466	-0.07	-2.66	-13.7	-18.26	15.4		-1.488	
L6/80	0.589	1.690	0.007	0.254	0.021	0.016	0.071	0.907		6.310	9.236	8.603	3.55	-2.23	-12.0	-16.72				
L9-21/90	0.459	0.592		0.155	0.003		0.034	0.412	2.318	3.667	3.772	3.452	4.43	-2.44	-7.1		21.4			
L9-21/90	0.578	0.860		0.213	0.003		0.041	0.388	2.977	3.577	6.449	6.349	0.78	-2.55	-11.4	-19.17	19.6			
LEL1	0.239	0.486	0.002	0.116	0.007	0.003	0.047	0.958		3.604	3.115	3.086	0.47	-2.52	-13.9	-17.02	18.06			0.709618
LEY-GR	0.598	2.222		0.270	0.021		0.002	0.221	1.386	2.371	10.515	12.479	-8.54							
LIO-GR	0.149	0.395		0.082	0.004		0.002	0.119	1.159	2.182	4.683	5.275	-5.94							
LIV-GR	0.099	0.823		0.062					0.500	1.778	6.086	6.370	-2.28							
LVD	1.112	4.444		0.427	0.042	0.001	0.083	0.897		2.980	18.263	17.718	1.51	-2.63	-10.4	-18.02	16.5			
MEL-GR	0.523	1.316		0.179	0.009					1.527	8.807	9.032	-1.26							
O10	0.240	0.570	0.009	0.004		0.009	0.225	0.263		8.646	17.918	16.834	3.12	-2.57	-14.5	-11.63	8			0.71032
O4	0.324	0.864		0.085					0.250	1.611	10.124	10.272	-0.73							
O5	0.249	0.864		0.035	0.007					3.343	5.229	6.012	-6.97							
P2A	0.449	1.769		0.286					0.318	1.226	9.072	10.567	-7.81							
PAR-GR	0.074	0.123		0.003						3.876	0.970	0.806	9.23							
POM	0.341	1.329		0.022	0.006	0.002	0.166	0.630		7.792	13.007	11.628	5.60	-2.86	-13.8		8.3	0.7	0.0445	
PR06	2.225	12.345		2.059	0.123	0.001	0.964	0.284		3.989	120.339	118.324	0.84	-2.47	-14.4	-19.18	29.9	0.43		
PW1	0.339	0.633		0.129	0.007		0.041	0.312		17.095	3.705	3.257	6.43	-2.88	-9.7					
PW2	0.178	0.306		0.064	0.003		0.022	0.374	1.500	2.639	2.232	2.126	2.43	-2.77		-19.46	116.2	1.3		
PW3	0.479	0.868		0.118	0.009		0.037	0.367	2.272	2.317	4.826	3.985	9.54							
R2	0.017	0.042		0.114	0.000	0.000	0.018	0.138		0.000	0.498	0.602	-9.48							
R27	0.010	0.039		0.021	0.000	0.000	0.012	0.138		0.000	0.444	0.378	8.02			-24.40				
R30	0.030	0.043		0.018	0.000	0.000	0.017	0.189		0.000	0.572	0.565	0.64			-23.87				

Well	Ca^{2+} mmol/l	Mg^{2+} mmol/l	Sr^{2+} mmol/l	Fe-tot mmol/l	Mn-tot mmol/l	Al-tot mmol/l	$NH4^+$ mmol/l	SiO2 mmol/l	CO2 mmol/l	TIC-Cal mmol/l	Σ-Anions mmol/l	Σ-Kations mmol/l	Error %	$\delta^{18}O$ ‰	$\delta^{2}H$ ‰	$\delta^{13}C$ ‰	^{14}C %(pmc)	^{3}H TU	$\delta^{37}Cl$ ‰	$^{87}Sr/^{86}Sr$
S1A/82	0.291	0.851		0.033	0.001	0.002	0.083	0.260		5.467	11.536	10.949	2.61	-2.92	-14.0	-12.84	4.3			
SINI-GR	1.097	0.209		0.030					0.136	2.763	3.047	3.139	-1.49							
SINII-GR	1.172	0.403		0.019					0.113	2.749	3.047	3.437	-6.01							
SOM01	1.846	1.893								9.405	60.144	60.414	-0.22							
SOM01	1.212	1.300		0.002		0.001	0.099	0.292		11.507	49.106	45.094	4.26	-2.90	-12.6	-0.19	0.9		1.317	
SOM01	1.020	1.130	0.022	0.003	0.002	0.018	0.239	0.325		1.292	44.478	38.915	0.06	-2.63	-13.0	0.61				
SOM02	1.322	1.234								10.128	43.098	46.086	-3.35							
SOM03	1.222	0.905								9.595	30.524	33.571	-4.75							
SOM04	0.823	1.769		0.001						9.508	44.289	51.119	-7.16							
SOM04	1.247	1.563								12.280	46.696	42.592	4.60							
SOM05	0.149	1.399								8.561	42.853	35.283	9.69							
SOM06	1.746	2.181		0.001						10.287	58.808	62.227	-2.82							
SOM06	0.873	2.057								9.557	56.251	58.056	-1.58							
SOM09	0.199	2.016								6.161	18.691	16.652	5.77							
SOM10	0.149	1.358								9.934	41.393	34.375	9.26							
SOM11	0.224	1.563								10.532	48.078	41.199	7.71							
SOM12	1.422	1.152								9.642	35.096	40.467	-7.11							
SOM13	1.347	1.316		0.001						8.977	42.970	46.345	-3.78							
SOM18	0.748	1.028								7.635	16.936	17.166	-0.67							
SOM16	0.623	0.823								10.032	18.695	15.375	9.74							
SOM18	1.197	1.563								9.835	40.029	44.188	-4.94							
SOM22	0.249	1.975								8.535	23.361	20.193	7.27							
SOM-W1	0.773	2.345								8.149	18.135	17.371	2.15							
SWM	0.399	0.617		0.286							2.544	2.604	-1.17							
T1A	0.299	0.823		0.059					2.090	1.792	10.574	10.697	-0.58							
T2C/91	0.653	2.810		0.553	0.029	0.001	0.053	0.908		2.207	15.170	14.979	0.63	-2.71	-15.3	-18.63	14.8		-1.255	0.709646
T31	0.324	0.699		0.075					0.181	0.389	9.927	8.850	5.74							
TA05	2.669	3.209								13.531	91.923	84.265	4.35							
TAMI-GR	1.447	0.378		0.010					0.159	2.534	4.164	4.897	-8.09							
TAMII-GR	1.222	0.390		0.005					0.136	2.510	4.074	4.679	-6.91							
TLE5	0.988	2.230		1.187	0.016	0.001	0.072	0.232		0.339	16.591	17.382	-2.33	-2.98	-12.9	-20.42	20.7			
TO1	1.739	22.400	0.037	0.060	0.060	0.071	0.379	0.690		20.644	187.388	185.087	0.62	-1.98	-14.2	-22.54	88.7			0.709290
TO11	0.743	49.300	0.045	0.021	0.005	0.063	6.019	0.425		19.787	478.511	481.407	-0.30	-1.15	-6.3					0.709187

Well	Ca^{2+} mmol/l	Mg^{2+} mmol/l	Sr^{2+} mmol/l	Fe-tot mmol/l	Mn-tot mmol/l	Al-tot mmol/l	$NH4^+$ mmol/l	SiO2 mmol/l	CO2 mmol/l	TIC-Cal mmol/l	Σ-Anions mmol/l	Σ-Kations mmol/l	Error %	$\delta^{18}O$ ‰	$\delta^{2}H$ ‰	$\delta^{13}C$ ‰	^{14}C %(pmc)	^{3}H TU	$\delta^{37}Cl$ ‰	$^{87}Sr/^{86}Sr$
TO13	0.677	47.600	0.049	0.044	0.005	0.054	6.300	0.725		20.248	493.953	464.952	3.02	-0.92	-8.1				0.0685	0.709178
TO15	0.690	41.800	0.060	0.072	0.004	0.067	4.779	1.040		18.438	462.443	401.891	7.01	-1.02	-7.6					0.709195
TO17	0.654	39.900	0.049	0.044	0.005	0.079	6.739	0.472		18.105	466.179	412.315	6.13	-1.02	-7.6	-6.60	52.6		-0.101	0.709162
TO19	1.269	37.200	0.053	0.073		0.047	6.539	0.273		15.543	422.269	413.073	1.10	-0.96	-3.5				-0.192	0.709163
TO21	1.129	36.100	0.042	0.049		0.070	7.879			12.745	393.363	387.195	0.79	-1.03	-6.3					0.709226
TO23	1.489	35.700	0.048	0.081		0.048	7.229	0.420		14.886	362.846	391.259	-3.77	-1.33	-9.7				-0.196	0.709217
TO25	1.209	31.600	0.426	0.357	0.036	0.173	8.939	4.390		14.054	356.609	402.933	-6.10	-1.14	-4.9	-2.71	43.5		-0.183	0.709259
TO3	1.589	15.300	0.025	0.032	0.004	0.048	2.109	0.339		16.241	168.957	177.029	-2.33	-1.25	-8.0	-20.25	91.6			0.709207
TO5	1.579	13.300	0.024	0.061	0.008	0.142	2.250	0.291			152.926	172.136	-5.91	-1.27	-11.4					
TO7	0.871	40.800	0.048	0.135	0.005	0.068	5.139	0.556		18.608	445.254	429.471	1.80	-1.31	-6.6					0.709201
TO9	1.139	46.000	0.051	0.055	0.008	0.064	6.059	0.653		18.534	518.615	456.883	6.33	-2.28	-12.7	-2.59	66.5		0.35	0.709198
TT4/91	0.267	0.498	0.004	0.001	0.001	0.004	0.051	0.233		5.866	9.936	10.092	-0.78	-2.71	-15.7	-14.74	5.28		-1.131	0.709371
TT4/91	0.279	0.440				0.001	0.054			5.392	10.675	9.725	4.66	-3.01	-15.9	-17.62	3.9			
W02	0.131	0.526	0.007	0.001		0.010	0.104	0.294		6.204	14.646	13.386	4.49	-2.52	-15.2	-9.63				
W1	0.174	0.576		0.057					0.250	1.695	7.133	7.107	0.18							
W-10	0.012	0.045		0.003		0.003		0.192		1.736	0.651	0.638	1.01							
W-3A	0.011	0.049		0.004		0.003		0.231		4.319	0.936	0.791	8.40							
W-6A	0.010	0.039		0.006		0.003		0.253		5.151	0.931	0.802	7.44							
WWCS	0.341	2.201		0.021	0.015	0.001	0.415	0.908		5.866	18.440	16.252	6.31	-3.01	-13.7	-18.66	6.6	0.2		
WWSM	0.351	0.534		0.103	0.002	0.001	0.060	0.694		4.656	9.776	8.725	5.68	-2.84	-11.8	-17.29	5.6			
ZOR-GR	0.249	0.864		0.035	0.007					3.403	5.229	6.012	-6.97							
ZOR-GR	0.324	0.864		0.175	0.009		0.002	0.164	1.613	2.739	9.092	9.812	-3.61							
ZV1-2/90	0.239	0.266		0.023	0.012		0.031	0.817	0.909	2.095	8.633	9.200	-3.18							
ZV1-2/90	0.272	0.011		0.038		0.007	0.004	0.173		1.791	0.815	0.833	-1.09	-3.24	-18.0	-11.76	104.3			
ZV1-2/90	0.610	0.400		0.098		0.021	0.076	0.658		3.251	9.380	9.346	0.18	-2.79	-14.5	-12.99	46.7	0.35		
ZV5/87				0.214							0.400	0.428	-3.38							
Samples with incomplete analyses and electro-neutrality error > 10 %																				
0/150O	0.006	0.014		0.057	0.001		0.055	0.026			0.356	0.267	14.27							
0/200W	0.017	0.012		0.007	0.001		0.015	0.001			0.104	0.133	-12.24							
0/400O	0.006	0.008		0.002	0.002			0.089			0.174	0.125	16.39							
1/69	0.848	2.757		0.017	0.020						8.369	13.862	-24.71	-2.80				1.3		
1/69													100.00							
1/69													100.00							

Well	Ca^{2+} mmol/l	Mg^{2+} mmol/l	Sr^{2+} mmol/l	Fe-tot mmol/l	Mn-tot mmol/l	Al-tot mmol/l	$NH4^{+}$ mmol/l	SiO2 mmol/l	CO2 mmol/l	TIC-Cal mmol/l	Σ-Anions mmol/l	Σ-Kations mmol/l	Error %	$\delta^{18}O$ ‰	$\delta^{2}H$ ‰	$\delta^{13}C$ ‰	^{14}C %(pmc)	^{3}H TU	$\delta^{37}Cl$ ‰	$^{87}Sr/^{86}Sr$
1/70													100.00							
1/82	0.237	0.308		0.179	0.006		0.015	0.029	3.522		4.358	23.990	-69.25							
1/82	0.089	0.065		0.039	0.002		0.013	0.094	0.659		2.331	3.426	-19.02							
1000 N	0.012	0.016		0.017							0.169	0.090	30.50							
1000 S	0.004	0.008									0.169	0.024	75.13							
11/72	0.089	0.123		0.007							0.200	2.151	-82.99	-2.90				2.4		
13/71	0.823	2.469		0.266					0.250		10.024	12.608	-11.42							
13/71				0.116							10.071	0.232	95.50							
14/72	0.099	0.197		0.012	0.001						1.999	1.372	18.60							
15/71														-2.20				0.6		
1500 W	0.007	0.008		0.001							0.143	0.032	63.43							
2/69													100.00							
2/70	0.099	0.699		0.016	0.005						3.926	6.957	-27.85	-3.30				0.3		
2/70													100.00							
2/72	0.107	0.123		0.010	0.005						0.200	0.754	-58.07							
2/85	0.109	0.138		0.052	0.007		0.017	0.033	1.340		2.212	1.388	22.89							
22/89	0.439	0.395		0.091					0.690		4.409	3.517	11.25							
24/72	0.087	0.041		0.001							2.996	0.707	61.84							
26/71	0.249	0.493		0.039	0.003						2.511	3.192	-11.94	-2.60		-17.40	18.5	2.3		
3	1.195	3.456		0.232	0.002	0.007					12.029	23.473	-32.23							
3/70													100.00							
3/71	0.873	0.493		0.073	0.030						2.591	3.805	-16.37	-2.60				0.6		
3/88	0.533	0.814		0.030	0.014				2.386		2.847	5.754	-33.80							
30/71	4.116	3.251		0.098	0.003						1.460	20.871	-86.82							
32/71	0.274	0.123		0.059	0.005						3.755	2.502	20.03	-2.80				0.4		
34/71	0.074	0.123		0.003							0.420	0.632	-20.15							
39/71				0.015	0.021	0.003					8.452	0.072	98.31							
4/670W	0.048	0.047		0.004	0.002		0.151	0.175			0.926	0.739	11.23							
44/71	0.087	0.617		0.537	0.003						3.065	3.919	-12.23							
48/71	0.087	0.123									0.269	0.811	-50.19							
48/71	0.024	0.030		0.024	0.003						0.317	0.162	32.36							
5/70													100.00							
5/70													100.00							

Well	Ca^{2+} mmol/l	Mg^{2+} mmol/l	Sr^{2+} mmol/l	Fe-tot mmol/l	Mn-tot mmol/l	Al-tot mmol/l	$NH4^{+}$ mmol/l	SiO2 mmol/l	CO2 mmol/l	TIC-Cal mmol/l	Σ-Anions mmol/l	Σ-Kations mmol/l	Error %	$\delta^{18}O$ ‰	$\delta^{2}H$ ‰	$\delta^{13}C$ ‰	^{14}C %(pmc)	^{3}H TU	$\delta^{37}Cl$ ‰	$^{87}Sr/^{86}Sr$
5/82	0.159	0.246		0.060	0.003		0.006	0.133	2.204		1.965	2.512	-11.72							
500 SW	0.019	0.012		0.007							0.409	0.076	68.66							
6/70													100.00							
6/71				0.017		0.007					0.873	0.034	90.38	-2.40				1		
7/71	0.087	0.123		0.017							1.230	0.686	28.39	-3.00				17.8		
8/70				0.148	0.020						4.939	0.336	87.26							
8/70 ?	0.339	0.901		0.109	0.004	0.001	0.036	0.349			9.611	7.090	15.09	-2.90	-12.5	-18.17	5.6		-0.497	
9/70				0.171	0.014						12.558	0.370	94.28							
9/71	0.029	0.580		0.013	0.005						0.860	1.254	-18.64							
BIL-GR	0.074	0.123		0.001							0.735	1.019	-16.19							
BVB	0.011	0.007		0.004	0.000	0.001	0.010	0.032			0.192	0.116	24.84	-3.26	-20.6	-25.03				
BVC	0.005	0.019		0.004	0.000	0.006	0.023	0.017			0.210	0.163	12.57							
C6	0.232	0.534		0.019							8.365	3.239	44.17							
CENTRE	0.074	0.123		0.003							0.581	0.762	-13.48							
GMD 37													100.00							
H1/87				0.402							0.600	0.604	-14.53							
H1-2/90	0.109			0.014			0.024	0.334	1.785		0.885	1.934	-37.21							0.710231
H17	0.859	0.437	0.018	0.001	0.001	0.016	0.216				34.950	27.483	11.96	-2.57	-14.4	-2.55				
H2/87				0.035							0.401	0.070	70.28							
H3/87	0.079	0.169		0.045	0.005		0.015		3.681		1.482	2.862	-31.77	-1.74						
H3/87				0.062	0.002						0.600	0.128	64.84							
H3/90	0.199	0.108		0.095	0.009			0.477			4.026	2.955	15.24	-3.25						
H4/87				0.017	0.001						3.404	0.038	97.91							
H4-5/90	0.109			0.111	0.005		0.005	0.114	3.113		0.856	1.455	-25.92	-2.94				-0.2		
H4-5/90	0.089	0.098		0.248	0.007		0.007	0.149			1.500	0.891	25.56							
H5/87				0.007							0.400	0.014	93.24							
H6/87				0.008							0.400	0.016	92.31							
HP1/87	0.005	0.016		0.011					1.620		0.702	0.975	-16.28							
KW6	1.579	5.160	0.285	0.558	0.190	0.330	0.439	0.023			98.588	79.683	10.60	-3.51	-14.6					
L10-14/0	0.548	0.316		0.013	0.010		0.020	0.407	2.363		4.584	6.050	-13.79	-2.63						
L10-14/0	0.479	0.248		0.022	0.010		0.019	0.339	2.454		4.342	5.610	-12.74							
L10-14/0	0.339	0.268		0.098			0.015	0.181	2.090		3.982	4.884	-10.17	-2.84	-10.8		48.6	0.7		

Well	Ca^{2+} mmol/l	Mg^{2+} mmol/l	Sr^{2+} mmol/l	Fe-tot mmol/l	Mn-tot mmol/l	Al-tot mmol/l	$NH4^{+}$ mmol/l	SiO2 mmol/l	CO2 mmol/l	TIC-Cal mmol/l	Σ-Anions mmol/l	Σ-Kations mmol/l	Error %	$\delta^{18}O$ ‰	$\delta^{2}H$ ‰	$\delta^{13}C$ ‰	^{14}C %(pmc)	^{3}H TU	$\delta^{37}Cl$ ‰	$^{87}Sr/^{86}Sr$
L18-19/0	2.495	2.164		0.160	0.036		0.114	0.257	4.272		1.010	11.024	-83.21	-2.54	-10.2			4.8		
L22-23/0	0.558	0.465		0.045			0.045	1.173	1.818		6.208	4.161	19.51							
L24-25/0	0.379	0.493		0.049	0.007		0.047	0.121	2.068		3.654	2.903	11.45							
L26-27/0	0.938	0.009		0.110	0.214		0.063	2.846			6.524	2.605	42.93	-2.90						
L26-27/0	0.249	0.128		0.100	0.178		0.021	1.531			4.177	1.331	51.67	-2.85	-13.5	-19.95	28.3			
L3-4/90	0.369	0.227		0.090	0.005		0.023	0.033	3.568		2.764	3.505	-11.48							
L7-8/90	0.289	0.389		0.092	0.009		0.034	0.527	2.727		2.083	1.552	14.61							
O21	0.943	0.475	0.019	0.001	0.001	0.018	0.136	0.277			40.232	31.511	12.16	-2.58	-14.1	1.32				
R14	0.010	0.037		0.087	0.000	0.001	0.018	0.133			0.282	0.469	-24.90			-23.91				
R19	0.012	0.040		0.076	0.000	0.001	0.048	0.141			0.433	0.631	-18.60							
R2/87				0.769	0.023						13.018	1.584	78.30							
R3/87				0.286	0.003						0.400	0.578	-18.20							
R7	0.006	0.024		0.012		0.012	0.008				0.560	0.237	40.53	-2.62	-13.6	-20.40	115.7	2.8		
REP-GR	0.034	0.041		0.033			0.002	0.104	0.840		0.360	0.535	-19.55							
RP1/87	0.072	0.119		0.252			0.020		0.886		0.496	1.518	-50.74							
SL1/87				0.035	0.001						1.001	0.072	86.58							
SL2/87				0.143	0.005						2.803	0.296	80.90							
SL3/87	0.239	0.813		0.092	0.018		0.019	0.282			3.131	3.817	-11.15	-2.95	-12.9					
SL3/87				0.112	0.003						1.401	0.230	71.80							
SOM07	0.848	0.817		0.003							14.101	24.380	-26.71							
SW3	0.219	0.079		0.006			0.007	0.059	1.545		1.239	0.715	26.82	-3.01						
SWM	0.336										0.220	0.672	-50.67							
SWM	0.274										1.068	0.546	32.09							
T-6	0.161	0.411		0.214	0.006	0.003					1.472	4.047	-46.66							
ZV1/87				0.021							0.400	0.042	81.00							
ZV1/87	0.019	0.019		0.031	0.005						1.990	0.148	86.16							
ZV1-2/90	0.029	0.088		0.031			0.027	0.678	1.772		3.320	1.035	52.47							
ZV2/87				0.035							0.400	0.070	70.21							
ZV3/87	0.029	0.029		0.019	0.014						0.774	0.552	16.74	-3.11				0.1		
ZV3/87				0.034							0.600	0.068	79.64							
ZV4/87				0.089							0.400	0.178	38.41							
ZV6/87				0.008							0.400	0.016	92.31							
ZVP1/87	0.002	0.012		0.016			0.004		1.477		0.413	0.284	18.51							

Well	Ca^{2+} mmol/l	Mg^{2+} mmol/l	Sr^{2+} mmol/l	Fe-tot mmol/l	Mn-tot mmol/l	Al-tot mmol/l	$NH4^{+}$ mmol/l	SiO2 mmol/l	CO2 mmol/l	TIC-Cal mmol/l	Σ-Anions mmol/l	Σ-Kations mmol/l	Error %	$\delta^{18}O$ ‰	$\delta^{2}H$ ‰	$\delta^{13}C$ ‰	^{14}C %(pmc)	^{3}H TU	$\delta^{37}Cl$ ‰	$^{87}Sr/^{86}Sr$
ZVP1/87		0.013		0.018			0.005	0.016	0.904		0.790	0.258	50.76							
	Samples with only isotope analyses																			
15/72														-2.60				1.5		
1500 W														-2.60				1.5		
18/72														-2.90				1.1		
19/72														-2.70				0.9		
20/72														-2.80				1.3		
21/72														-2.70				1.1		
3/82														-2.19			13.7			
3/89														-2.45		-13.02	53.6			
3/91														-2.45		-13.02	53.6			
7/71														-2.90				11.5		
9/71														-2.30				18		
ALL-GR														-2.80						
BIL-GR2														-3.50				1		
BIL-GR2														-3.30		-18.80	57.2			
GMD-19														-2.90		-12.70	8.5			
GMD-2														-3.40				0.9		
KW7.5														-3.74	-18.4					
L19/90														-2.54	-10.2			4.8		
L6/86														-2.84		-11.18	21.2			
L6A/80														-2.85		-21.97	8			
PAR-5														-3.30				1.1		
PAR-7														-3.20				3.5		
REP-GR														-3.20				3.5		
REP-TOT														-3.30				10.6		
REP-TOT														-2.90				10.1		
SW4														-2.42				3.4		

Annex IV.

Plant species and photosynthetic pathways in the savannah belt of Suriname

Species	Family	Savannah Type	Photos. pathway
Paspalum pulchellum	Poaceae	Zan,	C4
Panicum micranthum	Poaceae	Zan,	C4
Lagenocarpus tremulus	Cyperaceae	Zan, (Kas.)	?
Rhynchospora graminae	Cyperaceae	Zan	C4
Rhynchospora tenuis	Cyperaceae	Zan	C4
Paepalanthus polytrichoides	Eriocaulaceae	Zan	non-C4
Scleria pyramidalis	Cyperaceae	Kas	?
Abolboda americana	Xyridaceae	Zan	?
Xyris guianensis	Xyridaceae	Zan	?
Trachypogon plumosus	Poaceae	Kas, Coe	C4
Bulbostylis conifera	Cyperaceae	Zan, Kas, Coe	C4
Xyris surinamensis	Xyridaceae	Zan	?
Lagenacarpus weigeltii	Cyperaceae	Kas	?
Mesosetum loliiforme	Poaceae	Kas, Zan	C4
Bulbostylis fasciculata	Cyperaceae	Kas	C4
Mitracarpus discolor	Rubiaceae	Kas	C3
Axonopus pulcher	Poaceae	Kas, Wel, Coe	C4
Hypogonium virgatum	Poaceae	Wel	C4
Panicum stenodaides	Poaceae	Wel	C4
Axonopus chrysites	Poaceae	Wel	C4
Leptocoryphium lanatum	Poaceae	Zan, Kas, Wel, Coe	C4
Panicum nervosum	Poaceae	Zan	C4
Rhynchospora globosa	Cyperaceae	Wel	C4
Mesosetum cayennense	Poaceae	Coe	C4
Rhynchospora barbata	Cyperaceae	Zan, Wel, Coe	C4
Syngonanthus umbellatus	Eriocaulaceae	Zan	non-C4
Panicum polycanum	Poaceae	Zan	C4
Comolia vernicosa	Melastomataceae	Zan	non-C4
Axonopus flabelliformis	Poaceae	Kas	C4
Panicum rudgei	Poaceae	Coe	C4
Thrasya petrosa	Poaceae	Coe	C4
Sporobolus cubensis	Poaceae	Coe	C4
Bulbostylis junciformis	Cyperaceae	Coe	C4
Bulbostylis capillaris var. *tenuifolia*	Cyperaceae	Coe	C4
Davilla aspera	Dilleniaceae	Kas	non-C4

Table IV.1. Species of the open savannahs

Species	Family	Savannah type	Photos. pathway
Licania incana	Chrysobalanaceae	Kas, Zan	?
Clusia fockeana	Clusiaceae	Zan, (Kas)	non-C4
Humiria balsamifera var. *balssamifera*	Humiriaceae	Kas, Zan	?
Humiria balsamifera var.*floribunda*	Humiriaceae	Kas	?
Ternstroemia punctata	Theaceae	Kas, Zan	?
Swartzia bannia	Legum.-Caesalpinioideae	Kas	C3
Dimorphandra conjugata	Legum.-Caesalpinioideae	Kas	C3
Retiniphyllum schomburgkii	Rubiaceae	Zan	C3
Matayba opaca	Sapindaceae	Kas	non-C4
Myrcia sylvatica	Myrtaceae	Kas	C3
Bactris campestris	Palmae	Zan	C3
Conomorpha magnoliifolia	Myrsinaceae	Zan, Kas	non-C4
Ormasia costulata	Legum.-Papilionoideae	Zan	C3
Tibouchina aspera	Melastomataceae	Wel, Coe	non-C4
Imperata brasiliensis	Poaceae	Coe	C4
Byrsonima coccolobifolia	Malpighiaceae	Coe	non-C4
Byrsonima verbascifolio	Malpighiaceae	Coe	non-C4
Scleria pyramidalis	Cyperaceae	Zan	?
Scleria bracteata	Cyperaceae	Coe	?
Marliera montana	Myrtaceae	Zan	C3
Curatella americana	Dilleniaceae	Wel, Coe	non-C4

Table IV.2. Species of savannah bushes

Species	Family	Photos. pathway
Clusia fockeana	Clusiaceae	non-C4
Humiria balsamifera	Humiriaceae	?
Swartzia bannia	Legum.-Caesalpinioideae	C3
Ilex martiniana	Aquifoliaceae	C3
Ocatea schomburgkiano	Lauraceae	?
Dimorphandra conjugata	Legum.-Caesalpinioideae	non-C4
Isertia anceps	Rubiaceae	C3
Licania divaricata	Chrysobalanaceae	?
Protium heptaphyllum	Burseraceae	C3
Tapirara guianensis	Anacardiaceae	C3
Aspidosperma marcgravianum	Apocynaceae	C3 and CAM
Bombax flaviflorum	Bombacaceae	C3
Matayba opaca	Sapindaceae	non-C4
Licania incana	Chrysobalanaceae	?
Conomarpha magnoliifolio	Myrsinaceae	non-C4
Marlierea montana	Myrtaceae	C3

Table IV.3. Species of dryland forest

Legend: Zan = Savannahs of Zanderij type (poorly drained white sand savannahs); Kas = Savannahs of Kasipora type (extremely well drained white sand savannahs); Coe = Savannahs of Coesewijne type (well drained brown loamy sand to sandy loam savannahs); Wel = Savannahs of Welgelen type (well drained clay savannahs). Species are based on studies of Heyligers (1963), Van Donselaar (1965) and Jansma (1994). Photosynthetic pathways are derived form databases of Dallwitz (1980), Dallwitz et al. (1993) and onwards, and Ehleringer et al. (1997).